การเกิดพอลิเมอไรเซชันของเอทิลีนในวัฏภาคแก๊สและของเหลว ด้วยตัวเร่งปฏิกิริยาเมทัลโลซีนบิสนอมอลบิวทิลไซโคเพนตะไดอินิลเซอร์โคเนียมไดคลอไรด์ บนตัวรองรับเมโซพอรัสโมเลคิวลาร์ซีฟ

นาย พรยุทธ คำแก้ว

วิทยานิพนธ์นี้เป็นส่วนหนึ่งของการศึกษาตามหลักสูตรปริญญาวิศวกรรมศาสตรดุษฎีบัณฑิต
สาขาวิชาวิศวกรรมเคมี ภาควิชาวิศวกรรมเคมี
คณะวิศวกรรมศาสตร์ จุฬาลงกรณ์มหาวิทยาลัย
ปีการศึกษา 2545

ISBN 974-17-1981-7

ETHYLENE POLYMERIZATION IN GAS PHASE AND SLURRY PHASE WITH METALLOCENE $(n\text{-BuCp})_2\text{ZrCl}_2$ SUPPORTED ON MESOPOROUS MOLECULAR SIEVES

Mr. Pornyoot Kumkaew

A Dissertation Submitted in Partial Fulfillment of Requirements
for the Degree of Doctor of Engineering in Chemical Engineering
Department of Chemical Engineering
Faculty of Engineering
Chulalongkorn University
Academic year 2002

ISBN 974-17-1981-7

Thesis Title	ETHYLENE POLYMERIZATION IN GAS PHASE AND SLURRY PHASE WITH METALLOCENE ($(n\text{-BuCp})_2ZrCl_2$) SUPPORTED ON MESOPOROUS MOLECULAR SIEVES
By	Mr. Pornyoot Kumkaew
Field of Study	Chemical Engineering
Thesis Advisor	Professor Piyasan Praserthdam, Dr.Ing.
Thesis Co-advisor	Professor Sieghard E. Wanke, Ph.D.

Accepted by the Faculty of Engineering, Chulalongkorn University in Partial Fulfillment of the Requirements for the Doctor's Degree

………………………………………..……Dean of Faculty of Engineering
(Professor Somsak Panyakeow, D.Eng.)

THESIS COMMITTEE

……………………………………………….. Chairman
(Montree Wongsri, D.Sc.)
…………………………………………….…… Thesis Advisor
(Professor Piyasan Praserthdam, Dr.Ing.)
……………………………………………….. Thesis Co-advisor
(Professor Sieghard E. Wanke, Ph.D.)
……………………………………………….. Member
(Assistant Professor Siriporn Damrongsakkul, Ph.D.)
……………………………………………….. Member
(Suphot Phatanasri, D.Eng.)
……………………………………………….. Member
(Pailin Chuchottaworn, D.Eng.)

พรยุทธ คำแก้ว: การเกิดพอลิเมอไรเซชันของเอทิลีนในวัฏภาคแก๊สและของเหลวด้วย ตัวเร่งปฏิกิริยาเมทัลโลซีนบิสนอมอลบิวทิลไซโคเพนตะไดอินิลเซอร์โคเนียมไดคลอไรด์บนตัวรองรับเมโซพอรัสโมเลคิวลาร์ซีฟ (ETHYLENE POLYMERIZATION IN GAS PHASE AND SLURRY PHASE WITH METALLOCENE (n-BuCp)$_2$ZrCl$_2$ SUPPORTED ON MESOPOROUS MOLECULAR SIEVES) อ. ที่ปรึกษา: ศ.ดร. ปิยะสาร ประเสริฐธรรม, อาจารย์ที่ปรึกษาร่วม: Prof. Sieghard E. Wanke, 257 หน้า ISBN 974-17-1981-7.

งานวิจัยนี้ศึกษาการเกิดพอลิเมอไรเซชันของเอทิลีนและโคพอลิเมอไรเซชันของเอทิลีนกับแอลฟาโอเลฟินในระบบแก๊สและของเหลวด้วยการใช้ตัวรองรับเมโซพอรัสโมเลคิวลาร์ซีฟที่ผ่านการยึดจับกับสารประกอบเมทิลอะลูมินอกเซนและตัวเร่งปฏิกิริยาบิสนอมอลบิวทิลไซโคเพนตะไดอินิลเซอร์โคเนียมไดคลอไรด์ ตัวรองรับเมโซพอรัสโมเลคิวลาร์ซีฟที่ใช้ในการศึกษานี้มีขนาดเส้นผ่านศูนย์กลางของรูพรุน 2.5 ถึง 25 นาโนมิเตอร์ การวัดความว่องไวของตัวเร่งปฏิกิริยาเหล่านี้วัดที่ความดันของเอทิลีน 200 พีเอสไอเอ และที่อุณหภูมิ 50 ถึง 100 องศาเซลเซียสในระบบแก๊ส สำหรับระบบของเหลววัดที่ความดันรวม 115 พีเอสไอเอ และอุณหภูมิ 50 ถึง 80 องศาเซลเซียส โคพอลิเมอไรเซชันของเอทิลีนกับเฮกซีนในระบบแก๊สศึกษาที่ 70 องศาเซลเซียส และในระบบของเหลวการศึกษาโคพอลิเมอไรเซชันของเอทิลีน กับ เฮกซีน ออกทีน และเดกซีนทำโดยการเติมแอลฟาโอเลฟินปริมาณ 3 มิลลิลิตร ลงในเฮปเทนปริมาตร 30 มิลลิลิตร จากการทดลองพบว่าความว่องไวในการเกิดพอลิเมอไรเซชันและรูปร่างของโพรไฟล์ความว่องไวขึ้นอยู่กับขนาดรูพรุนของตัวรองรับทั้งระบบแก๊สและของเหลว ในระบบแก๊สขนาดเส้นผ่านศูนย์กลางรูพรุน 2.6 และ 5.8 นาโนมิเตอร์ มีความว่องไวในการพอลิเมอไรเซชันสูงที่สุด สำหรับในระบบของเหลวความว่องไวในการพอลิเมอไรเซชันมีค่าสูงสุดที่ขนาดเส้นผ่านศูนย์กลางรูพรุน 2.5 และ 2.6 นาโนมิเตอร์ นอกจากนี้ทำการศึกษาสมบัติของพอลิเมอร์ที่ผลิตขึ้นจากตัวเร่งปฏิกิริยาเหล่านี้โดยการใช้เทคนิคการแยกส่วนของพอลิเมอร์ด้วยการเพิ่มขึ้นของอุณหภูมิ เทคนิคดิฟเฟอเรนเชียลสแกนนิ่งแคลอริเมทรี เทคนิคสแกนนิ่งอิเล็กตรอนไมโครสโคปี และ เทคนิคของการแยกขนาดน้ำหนักโมเลกุลของพอลิเมอร์ พบว่าตัวเร่งปฏิกิริยามีองค์ประกอบของตำแหน่งความว่องไวหลายชนิด โดยชนิดและความเข้มข้นของตำแหน่งดังกล่าวขึ้นอยู่กับขนาดรูพรุนของตัวรองรับและเวลาในการทำปฏิกิริยา นอกจากนี้ยังพบว่าขนาดรูพรุนของตัวรองรับ ความเข้มข้นของเฮกซีนและอุณหภูมิในการพอลิเมอไรเซชันเป็นปัจจัยที่สำคัญต่ออัตราการพอลิเมอไรซ์ของเอทิลีนและอัตราการเข้าร่วมในปฏิกิริยาของเฮกซีน พอลิเมอไรเซชันในระบบแก๊สพบว่าตัวเร่งปฏิกิริยาที่มีขนาดรูพรุนใหญ่มีอัตราการเข้าร่วมของเฮกซีนสูงกว่าตัวเร่งปฏิกิริยาที่มีขนาดรูพรุนเล็ก และเวลาในพอลิเมอไรเซชันยังส่งผลต่ออัตราการเข้าร่วมในปฏิกิริยาของเฮกซีน สำหรับพอลิเมอไรเซชันในระบบของเหลวไม่พบแนวโน้มที่ชัดเจนของการเปลี่ยนแปลงขนาดรูพรุนต่อการเข้าร่วมในปฏิกิริยาของเฮกซีน

ภาควิชา……วิศวกรรมเคมี…….	ลายมือชื่อนิสิต………………….……..………
สาขาวิชา……วิศวกรรมเคมี……	ลายมือชื่ออาจารย์ที่ปรึกษา…………...……..….
ปีการศึกษา..…….2545…….…	ลายมือชื่ออาจารย์ที่ปรึกษาร่วม………..……..….

#4271810021: MAJOR CHEMICAL ENGINEERING
KEY WORD: Metallocene Catalyst / Support/ Polymerization / Methylaluminoxane

PORNYOOT KUMKAEW: ETHYLENE POLYMERIZATION IN GAS PHASE AND SLURRY PHASE WITH METALLOCENE (n-BuCp)$_2$ZrCl$_2$ SUPPORTED ON MESOPOROUS MOLECULAR SIEVES. THESIS ADVISOR: PROF. PIYASAN PRASERTHDAM, Dr.Ing., THESIS COADVISOR: PROF. SIEGHARD E. WANKE, Ph.D., 257 pp. ISBN 974-17-1981-7.

Ethylene homopolymerization and ethylene/α-olefin copolymerization were studied in the gas phase and in slurries using mesoporous molecular sieves impregnated with methylaluminoxane and (n-BuCp)$_2$ZrCl$_2$; the mesoporous molecular sieves had pore diameters of 2.5 to 25 nm. Activities were measured for these catalysts at ethylene pressures of 200 psia and 50 to 100°C for gas-phase operation and, at total pressures of 115 psia and 50 to 80°C for slurry operation. Gas-phase copolymerizations of ethylene/1-hexene at various 1-hexene concentrations were done at 70°C and slurry copolymerizations of ethylene and 1-hexene, 1-octene and 1-decene, were done by adding 3.0 mL of the α-olefin to 30 mL of the heptane reaction medium. Polymerization activities and the shape of the activity profiles were a function of the support pore size for both gas-phase and slurry systems. Maximum activities for gas-phase operation occurred for support pore sizes of 2.6 to 5.8 nm; the maximum activities for slurry operation occurred for support pore sizes of 2.5 and 2.6 nm. Temperature rising elution fractionation, differential scanning calorimetry, scanning electron microscopy and size exclusion chromatography were used to characterize the products. The results showed that the catalysts contained multiple types of catalytic sites; the types and concentration of these sites were a strong function of the support pore size and reaction time. Ethylene polymerization rates and 1-hexene incorporation rates were strong functions of support pore size, 1-hexene concentration and reaction temperature. Large-pored catalysts had higher 1-hexene incorporation rates than small-pored catalysts for gas-phase polymerization, and the 1-hexene incorporation rate was a function of reaction time. For slurry operation, no clear trends in α-olefin incorporation as a function of pore size was observed.

Department…..Chemical Engineering …. Student's signature…………………………
Field of Study..Chemical Engineering….. Advisor's signature………………………...
Academic year…………2002…………...Co-advisor's signature……………………...

ACKNOWLEDGEMENTS

I would like to give special recognition to Professor Dr. Piyasan Praserthdram, advisor, and Professor Dr. Sieghard E. Wanke, co-advisor, for their generosity in providing guidance and sharing their ideas on the interesting work, and for their academic and personal influence on me from which I will benefit in my lifetime.

Dr. Montri Wongsri, chairman of the committee, and all of members of examining committee including, Assosiate Professor Dr. Siriporn Damrongsakkul, Dr Pailin Chuchottaworn, and Dr. Suphot Phatanasri, are acknowledged for their spending time in reviewing my thesis, and for their criticism and advice on my work.

Thanks for the financial support are conveyed to The Thailand Research Fund (TRF) and Natural Sciences and Engineering Research Council of Canada (NSERC). I gratefully acknowledge the generous facilities provided by the Department of Chemical and Materials Engineering at the University of Alberta, Canada, and the Graduate School and Department of Chemical Engineering at Chulalongkorn University.

I wish to thank the department staffs of the Department of Chemical and Materials Engineering at the University of Alberta: Ms. Christina Baker for performing the scanning electron microscopy, Ms. Naiyu Bu for measuring the molar masses of polymers and copolymers, Dr. Jaimin Zhou for assistances in the gas-phase preliminary experiments, Mr. Mingqian Zhang and Dr. Long Wu for measuring temperature rising elution fractionation (TREF), differential scanning calorimetry (DSC), and giving me the valuable guidance and assistance on the experimental procedures. I also thank Professor Dr. Serge Kaliaguine and Dr. Nai Hong Li for the preparation of support materials.

I gratefully thank all group members, Thai student at the University of Alberta, and friends for giving me strength encouragement.

Finally, I am also very appreciative of my parents and sister for their tremendous support and overwhelming encouragement by their unending love.

CONTENTS

PAGE

CHAPTERS

CONTENTS(Cont.)

PAGE

CONTENTS(Cont.)

PAGE

CONTENTS(Cont.)

PAGE

LIST OF TABLES

TABLE **PAGE**

LIST OF TABLES (Cont.)

TABLE **PAGE**

LIST OF FIGURES

FIGURE **PAGE**

LIST OF FIGURES (Cont.)

FIGURE **PAGE**

LIST OF FIGURES (Cont.)

FIGURE **PAGE**

LIST OF FIGURES (Cont.)

FIGURE **PAGE**

LIST OF FIGURES (Cont.)

FIGURE **PAGE**

LIST OF FIGURES (Cont.)

FIGURE **PAGE**

LIST OF FIGURES (Cont.)

FIGURE **PAGE**

LIST OF FIGURES (Cont.)

FIGURE **PAGE**

LIST OF ABBREVIATIONS

ACHIEVE	Polypropylenes from Exxon Chemical
AFFINITY	Polyolefin plastomers from Dow Chemical
Al-NMR	Aluminum Nuclear Magnetic Resonance
ATREF	Analytical Temperature Rising Elution Fractionation
BAO	Butylaluminoxane
CD	Cyclodextrin
C-NMR	Carbon Nuclear Magnetic Resonance
CRYSTAF	Crystallization Analysis Fractionation
DA	Dehydroxylated Alumina
DSC	Differential Scanning Calorimetry
EBI	Ethylenebisindenyl Zirconiumdichloride Catalyst
ELITE	Enhanced Polyethylene from Dow Chemical
ENGAGE	Polyolefin Elastomers from DuPont Dow Elastomers
EXACT	Polyolefin Plastomers from Exxon Chemical
EXCEED	Gas Phase LLDPE from Exxon Chemical
HDPE	High Density Polyethylene
HMDS	Hexamethyl-disilazane
H-NMR	Proton Nuclear Magnetic Resonance
LCB	Long Chain Branches
LDPE	Linear Density Polyethylene
LLDPE	Linear Low Density Polyethylene
MAO	Methylaluminoxane
MLLDPE	Linear Low Density Polyethylene Produced with Metallocene Catalysts
MM	Molar Mass
MMD	Molar Mass Distribution
MMS	Mesoporous Molecular Sieves
MSF	Mesoporous Silica Fibers
MSL	Methylene Sequence Length

MWD	Molecular Weight Distribution
NIST	National Institute of Standards and Technology
PD	Polydispersities
PE	Polyethylene
PH	Polyhexene
PO	Polyoctadiene
PP	Polypropylene
PS	Polystyrene
PTREF	Preparative Temperature Rising Elution Fractionation
SCB	Short Chain Branches
SCBD	Short Chain Branching Distribution
SEC	Size Exclusion Chromatrography
SEM	Scanning Electron Microscopy
SMAO	Methylaluminoxane Treated Silica
SSA	Successive Self-Nucleation/Annealing
SSC	Single Site Catalyst
TEA	Triethylaluminum
TEOS	Tetraethyl Orthosilicate
TIBA	Triisobutylaluminum
TMA	Trimethylaluminum
TREF	Temperature Rising Elution Fractionation
ULDPE	Ultra Low Density Polyethylene
UNIPOL	Union Carbide Gas-Phase Process
VLDPE	Very Low Density Polyethylene

CHAPTER I

INTRODUCTION

Polyolefins are one of the largest businesses for catalyst in industry with worldwide production of 78 million tons a year, the majority of which are produced catalytically. Polyethylene (PE) alone is the most widely used synthetic polymer; world consumption exceeded 50 million tons in 2000 (Robinson, 2001), and again most of the polyethylene is produced by catalytic processes. Polyethylene has such large usage because its chemical stability and great range of physical properties make it suitable for a broad range of applications, from strong, flexible films and coatings to rigid containers. It is the variations in molecular structure that results in this range of physical properties. Major changes have occurred in the ability to control the molecular structure in the large-scale production of ethylene since the first commercial production of polyethylene in the 1930s (Bett et al, 1983). A major change occurred in the 1970s when the large-scale production of linear low-density polyethylene (LLDPE) was commercialized (Staub, 1983). The production of LLDPE experienced large growth rates, and it is, and continues to be, the most rapidly growing type of polyethylene (Phillip Townsend Assoc Newsletter Plast Chem Ind, 2001; and Buckalew and Schumacher, 2000). The newest type or polyethylene to be commercialized is LLDPE produced with metallocene or other single-site catalysts; the production of this type of polyethylene, frequently referred to as mLLDPE, is expected to increase by 15 to 20% a year in the next few years if production and processability problems are resolved (Chem Ind Newslett SRI Consult, 2000).

The discovery of metallocene catalysts by Sinn and Kaminsky has been considered as one of the major revolutionary steps in the history of polymer industry. Metallocene catalysts, based on zirconium, hafnium or titanium, show in contrast to Ziegler systems only one type of active site (single-site catalyst), which produces polymers with a narrow molar mass distribution ($M_w/M_n = 2$), and their structure can be easily changed. Metallocenes are soluble in hydrocarbons or liquid propene. These properties allow one to predict accurately the properties of the resulting polyolefins by knowing the structure of the catalyst used during their manufacture and to control the resulting molar mass and distribution, comonomer content and tacticity by careful selection of the appropriate reactor conditions. In addition, their catalytic activity is 10-100 times higher than that of the classical Ziegler-Natta systems. Metallocene catalysts are frequently referred to as single-site catalysts because the polymers produced with these catalysts frequently have narrow molar mass distributions, i.e. polydispersities close to 2 (Janiak and Rieger, 1994; and Galland et al., 1999). However, temperature rising elution fractionation (TREF) results of Soga et al. (1995) with ethylene/1-hexene copolymers produced by homogeneous Cp_2ZrCl_2-methylaluminoxane (MAO) catalysts suggested that these catalyst systems contained two different types of catalytic species. Estrada and Hamielec (1994) proposed a two-site model for ethylene homopolymerization with homogeneous Cp_2ZrCl_2-MAO catalyst based on activity profiles and size exclusion chromatography (SEC) results. Subsequently, Wang et al. (1991) made similar observations for homogeneous Cp_2ZrCl_2-MAO and Cp_2ZrCl_2- butylaluminoxane (BAO) catalysts; they proposed a two-site model for Cp_2ZrCl_2- MAO and a three-site model for Cp_2ZrCl_2-BAO. Crystallization analysis fractionation (CRYSTAF) results of Kim and Soares (1999) with ethylene/1-hexene copolymers produced during slurry operation with various silica supported metallocenes led to the conclusion that these supported catalysts contained two or more types of catalytic sites.

Metallocenes, in combination with the conventional aluminumalkyl cocatalyst used in Ziegler systems, are indeed capable of polymerizing ethylene, but only at a very low activity. Only with the discovery and application of methylaluminoxane (MAO) by Kaminsky, was it possible to enhance the activity, surprisingly, by factor of 10000. The enormous interest in the scientific community as well as in industry in metallocene catalysts is due to their high activity in the presence of MAO and the well-defined nature of the active sites (Scheirs and Kaminsky, 2000). However, despite their numerous advantages, several problems still need to be solved before metallocene catalysts can be used widely in industry for the commercial production of large amounts of polyolefins. There are two main problems which have delayed the use of metallocene catalysts for the large scale production of commodity polyolefins: One, reactor operating problems, that is, the difficulty in controlling polymer morphology with soluble homogeneous catalysts limits their use in slurry and gas-phase processes due to reactor fouling, and two, the very large amounts of a cocatalyst required with homogeneous metallocenes to achieve high activities. One route to overcome these problems is the development of supported metallocene catalysts suitable for use in gas and slurry-phase processes; supported metallocene would resolve the two main problems, which are reactor fouling and the requirement of large amounts of a cocatalyst. The majority of ethylene polymerization studies with metallocene catalysts have been done with homogeneous catalysts, and the vast majority of studies with supported metallocene have been done in the slurry mode. Several reviews dealing with supported (i.e. heterogenized) single-site catalysts and the properties required for commercial applications in slurry or gas-phase reactors have appeared in recent years (Ribeiro et al., 1997, Chien, 1999; and Hlatky, 2000). Very little has been published in the open literature on gas-phase polymerization over metallocene catalysts.

In the current study, polymerization was carried out in the slurry phase as well as in the gas phase because gas-phase polymerization is widely used commercially for the production of linear low density polyethylene (LLDPE). TREF, DSC and SEC characterization of polyethylenes produced with metallocene catalysts in slurry reactors have been reported by Lehmus et al. (1998) and Yoon et al. (2000). However, no such studies for polyethylenes produced with metallocene catalyst in gas-phase reactors have been reported, even though it has been predicted that gas-phase processes will be used for commercial production of LLDPE with metallocene catalysts (Foxley, 1998). Very little information is available about the effects of reaction temperature and comonomer concentration on the rate of polymerization and comonomer incorporation during gas-phase polymerization with supported metallocene catalysts. Therefore, the emphasis in the present study is to increase our understanding of the factors, which affect the performance of supported metallocene catalysts in gas- and slurry-phase polymerization, especially LLDPE production, in the gas-phase and slurry-phase polymerization. The specific catalysts studied are $(n\text{-BuCp})_2ZrCl_2$ – supported on MAO-treated mesoporous molecular sieves with different pore sizes. The properties of the products produced with different catalysts and at different operating conditions were determined by temperature rising elution fractionation (TREF), size exclusion chromatography (SEC) and differential scanning calorimetry (DSC).

The objectives of this investigation were to study the influences of the pore size of supports and polymerization conditions on the catalytic activity and polymer properties during gas- and slurry-phase polymerization of ethylene and ethylene/1-hexene using bis(butylcyclopentadienyl)zirconium dichloride $(n\text{-BuCp})_2ZrCl_2$ supported on MAO-treated mesoporous molecular sieves.

A review of the open literature dealing with metallocene catalysis for olefin polymerization is presented in Chapter II. Emphasis in this review is on metallocene catalyst system used for gas-phase and slurry-phase homo- and copolymerization of ethylene and α-olefins. The experimental procedures for preparing supported metallocene catalyst and performing homopolymerization and copolymerization in gas- and slurry-phase processes, as well as the techniques used for characterizing catalyst and the resulting polymers are described in Chapter III.

In Chapter IV, the results on gas-phase ethylene polymerization are presented. The influences of the pore size of supports and polymerization conditions on the catalytic activity and polymerization behavior are explained. Molar mass and scanning electron micrographs of support, catalyst, and produced polymer are provided.

To provide guidance for the development of supported metallocene catalyst for gas-phase copolymerization, since it is expected that the majority of mLLDPE will be produced in gas-phase processes, ethylene/1-hexene copolymerization was studied. These results are presented in Chapter V. The effects of polymerization temperature, 1-hexene concentration, and pore size of support on the average polymerization activities and polymer properties are presented. The polymer properties were determined by size exclusion chromatography (SEC), differential scanning calorimetry (DSC), and temperature rising elution fractionation (TREF).

In Chapter VI, results of slurry-phase ethylene polymerization and copolymerization of ethylene/α-olefins, i.e. 1-hexene, 1-octene, and 1-decene, using the supported metallocene catalyst with different pore size of mesoporous molecular sieves are presented and discussed. In Chapter VII, the gas-phase and slurry-phase results for homopolymerization and copolymerization are compared to determine the effects of support pore size on catalyst performance and product properties.

Finally, the observations and discussions presented in Chapter IV, V, VI and VII are summarized in Chapter VIII. Recommendations for future research work are also provided in Chapter VIII.

CHAPTER II

Literature Survey: Group IV Metallocene Catalysts for Olefin Polymerization

Two major classes of single-site catalyst (SSC) technology were recently developed for the polymerization of ethylene and α-olefins. These two catalyst systems are the metallocene catalyst and constrained geometry catalyst systems. The use of these catalyst technologies has allowed a very rapid development of olefin copolymers with a wide range of structures and related properties. This technology has initiated a major revolution for the polyolefin industry (Scheirs and Kaminsky, 1999). Several families of SSC technology-based polyolefin copolymers have been commercialized in the 1990s. These include polyolefin elastomers (ENGAGE from DuPont Dow Elastomers), polyolefin plastomers (AFFINITY from Dow Chemical; EXACT from Exxon Chemical), EPDM (NORDEL IP from DuPont Dow Elastomers), enhanced polyethylene (ELITE from Dow Chemical), gas phase LLDPE (EXCEED from Exxon Chemical) and polypropylenes (ACHIEVE from Exxon Chemical). In addition to these commercial activities, several other single-site catalyst-related technologies that allow the copolymerization of α-olefins with polar comonomers are also under industrial and academic development (Johnson et al, 1995,1996).

One of the biggest challenges for modern organometallic chemistry is to apply metallocene complexes with Group IV metals to new technologies and production of new materials. Metallocene compounds are becoming an important class of catalysts for the synthesis of organic molecules and polymers. Metallocene catalysts are operative in all existing industrial plants that are presently used for polyolefin manufacture revolutionize the technology for the production of these polymers (Imanishi and Naga, 2001).

Research in single-center metal-catalyzed polymerization has seen explosive growth over the past two decades, advancing from questions of academic interest to solving problems in the commercial field. The variation of the aromatic ligands, the bridging of ligands and the variation in the type of metal provides an enormous number of variations to control polymerization reactions in terms of stereospecificity, long chain and short chain branching and the generation of block copolymers.

Metallocene catalysts can produce tailored polyolefins for nearly every purpose and with these new materials they generate new markets, such as LLDPE (linear low density polyethylene) with new properties.

This great potential of the new technologies is reflected in the attention given to this area both in academic and industrial laboratories throughout the world. The explosion of interest in this area has already yielded a large number of research publications, reviews, and patents granted to major chemical industries. As we found in the open literature, there are many reviews on the nature of metallocene complexes, catalytic performance and its influence on polymer properties, cocatalyst for metal-catalyzed olefin polymerization, and polymerization reactions including reaction mechanisms of polymerization and chain transfer (Gupta et al., 1994; Brintzinger et al., 1995; Britovsek et al., 1999; Kaminsky, 1999; Hlatky, 1999; Chen and Marks, 2000; Bajgur and Sivaram, 2000; Alt and Koppl, 2000; Rappe et al., 2000; Kaminsky and Laban, 2001; and Imanishi and Naga, 2001).

In Sections 2.1 to 2.6 of this chapter, the important parameters in metallocene catalysts are summarized; this summary is largely based on the above cited reviews. The emphasis in the current review is on aspects related to the present work, i.e. it is focused on the catalytic performance of supported metallocene/methylaluminoxane catalyst in gas-phase and slurry-phase ethylene polymerization and copolymerization of ethylene/α-olefins and on the properties of polymers made with these catalysts.

2.1. Classification of Polyethylene

Polyethylene (PE) is the major commodity polymer worldwide; world demand exceeded 50 million tons in 2000. The consensus of numerous studies shows that the world production of polyethylene is estimated to be around 93 million tons; LDPE/LLDPE 55 million tons and HDPE 38 million tons in 2010 (Kaminsky and Laban, 2001). Such increase in production of this material is due to the outstanding versatile physical and chemical properties of PE. Conventionally polyethylene is classified into three types according to its density: high density polyethylene (HDPE), low density polyethylene (LDPE), and linear low density polyethylene (LLDPE).

Table 2.1 summarizes some characteristics of the three types of polyethylenes. It is evident that each type of PE is associated with the characteristic molecular structure, production process, density range, and applications. HDPE is a homopolymer of ethylene possessing a linear chain structure with no or very few branches, and up to 70% of the polymer can be in the crystalline phase, resulting in a high density of about 0.96 g/cm^3. LDPE is also a homopolymer of ethylene, but has a branched structure with long chain branches (LCB) and short chain branches (SCB) as depicted in Table 2.1. The branches disrupt the ordered arrangement of the macromolecular chains. A high SCB or LCB content means a large amount of crystal defects, which lead to a lower crystallinity with a lower density and melting temperature. In general, LCBs have a profound effect on solution viscosity and melt rheology because of molecular size reduction and entanglements, while SCBs are particularly critical in influencing the morphology and solid-state properties of polyethylene.

The polymer commonly known as LLDPE is a copolymer produced by copolymerizing ethylene with α-olefins such as propylene, 1-butene, 1-hexene, 1-octene, and 4-methyl-1-pentene. LLDPE possesses a linear molecular structure with SCBs distributed nonuniformly along the backbone of polyethylene chain. The amount and distribution of SCBs have a profound effect on the thermal, physical, and mechanical properties of LLDPE. The diversity of the various LLDPE grades is primarily a result of variations in distributions of molar mass and short chain branches.

Polyethylenes properties must meet customer needs and the appropriate technology must be used to produce products with the required properties. This requires detailed knowledge and know-how of relationships among processing conditions, polymer structure and polymer properties. For catalytic polymerization processes the catalyst, mostly in combination with a cocatalyst, and the polymerization process are regarded as the polymerization technology. This means that both the process and the catalyst are an integrated whole and must be well balanced in respect to each other (Xie et al., 1994). The catalyst or catalyst system plays the key role, as shown on Figure 2.1, in the choice of process and product properties. The catalyst determines the polymerization behavior, the polymer structure and for heterogeneous processes the polymer powder morphology. The catalyst system must fit the polymerization process.

Table 2.1. Density range, molecular structure, synthesis, and applications of various types of polyethylenes.

Type of PE	Density range (g/cm^3)	Molecular structure	Synthesis	Common uses
HDPE	0.945-0.965		Polymerization of ethylene on Phillips, Ziegler-Natta and metallocene catalysts.	Gas pipe, car gas tanks, bottles, rope, and fertilizer bags.
LDPE	0.890-0.940		Free radical polymerization of ethylene at high temperature and high pressure.	Packing film, bags, wire sheathing, pipes, and waterproof membranes.
LLDPE (VLDPE,ULDPE)*	0.910-0.925	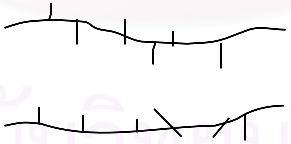	Copolymerization of ethylene with α-olefins on Ziegler-Natta metallocene catalyst.	Shopping bags, stretch wrap, greenhouse film.

* A family of LLDPE with density of 0.87-0.915 g/cm^3.

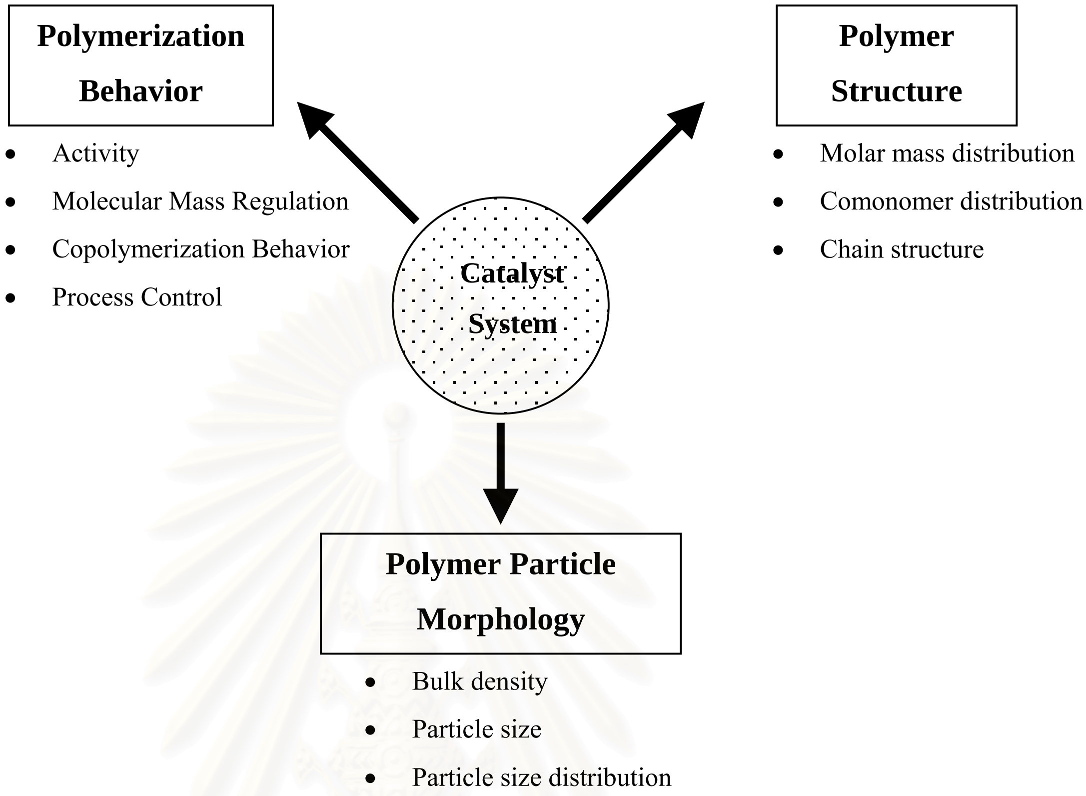

Figure 2.1. The key role of the catalyst system (Kaminsky, 1999)

In heterogeneous processes (slurry or gas-phase technology) the polymerization reaction only takes place inside the polymer particles. Each of these polymer particles is a small reactor (micro reactor) with its own energy and mass balance. The polymer particles grow from the catalyst particles by polymer formation around the catalyst fragments (primary particles) (Kaminsky, 1999).

2.2. Polymerization Process

Polymer, with single-site catalyst technology, can be produced by high-pressure, solution, gas-phase and slurry-phase processes. The gas-phase and slurry-phase processes are reviewed because they are closely related to the present study. Typical process conditions for making homopolymers and copolymers in these processes are the following: Slurry reactors, rather than gas-phase reactors, are used in the majority of laboratory studies of catalytic olefin polymerization. The results from slurry reactors are frequently used to predict the activity of catalysts for gas-phase reactors. Gas-phase processes are increasingly being used for commercial production of polyolefins since gas-phase operation has significant advantages over slurry and solution processes; these advantages include lower operating cost, safer operation, more environmentally friend, and wider range of product molar masses (Jejelowo et al., 1991). However, gas-phase processes have some disadvantage, these include temperature control problems, special catalyst requirements, and the limitations on the type and concentration of comonomer.

2.2.1. High-Pressure Process

Two types of commercial reactors, stirred autoclave or a tube reactor, are used for the polymerization of ethylene and ethylene/α-olefin copolymers at high pressure. Ethylene and an α-olefin comonomer are usually compressed to at least 10,000 psi when fed into the reactor. The polymerization temperature usually exceeds 100°C.

2.2.2. Solution Process

In the solution processes (Hamielec and Soares, 1996; Scheirs and Kaminsky, 1999), stirred reactors are usually used for the polymerization of ethylene and ethylene/α-olefin copolymers in a solution. In most cases, C_6-C_8 hydrocarbons are used as the solvent. The active centers and polymer chains are soluble in the solvent at reaction conditions. These processes are generally carried out at temperatures above the melting temperatures of the polymer product. The reactors are operated at about 500 psi pressure and the polymerization is carried out at > 140°C for LLDPE production. Solution processes are preferred for long chain branch synthesis for several reasons. Macromonomers with terminal vinyl unsaturation are formed at higher rates at elevated temperatures. These dissolved polymer chains, with concentrations usually less than 15 wt% in solvent, are mobile and have relatively large self-diffusion coefficients. Most importantly, at these higher temperatures the steric barrier for the addition of a macromonomer to the active center is relatively less important than at lower temperatures. A potential negative effect of these elevated temperatures is the reduced lifetime of the catalytically active centers. Short residence times can be used with a CSTR to overcome this problem. Shorter reactor residence times would also have the advantage of making product grade transitions more efficient.

Solution processes are especially adequate for the production of polyolefins containing long chain branches. Presently, two industrial solution processes are being used to produce polyethylene: Dow Chemical 's INSITE process and Exxon 's EXACT process. These processes can produce polyolefins with novel properties due to the controlled incorporation of long chain branches in a homo- or copolymer backbone.

2.2.3. Slurry-Phase Process

In slurry polymerization with soluble metallocene systems, the polymer molecules are insoluble in the solvent (also called the diluent) (Hamielec and Soares, 1996). When polymer chains precipitate from solution, there is the possibility of two-phase polymerization, one occurring in the solvent phase and the other occurring in the polymer phase. Active centers and monomers may partition between these two phases, giving rise to different polymerization rates and forming polymers with different molecular weight distributions in each of the two phases. The polymers are made in stirred reactors with an organic diluent (C_4-C_6 hydrocarbons). The polymerization process temperature is generally $< 90°C$ with a reactor pressure of $<$ 300 psi. Products made in this process are in powder form and can be converted into pellets using extrusion processes (Scheirs and Kaminsky, 1999).

In batch and semi-batch reactor operations, phase volume ratios would change with time, giving overall polymerization rates and molecular weight distributions, which would change with time. However, the slurry polymerization of ethylene with Cp_2ZrCl_2/MAO in toluene in a semi-batch reactor has a constant rate of polymerization and the polyethylene produced has a polydispersity of about two, suggesting that the active centers do not partition between the two phases. Although no conclusive evidence has been presented in the literature, it is generally accepted that the active sites remain in the solvent phase during the polymerization.

With supported metallocenes, which are insoluble in the solvent, active centers are encapsulated by polymer and the polymerization occurs almost exclusively in the polymer phase. Long chain branch formation should depend on the mobility of the macromonomers in the monomer/solvent swollen polymer particles. Self-diffusion coefficients of macromonomers depend on molecular weight and one therefore might expect that the rate of addition of a macromonomer to the active center is diffusion-controlled with preferential formation of shorter long chain branches. On the other hand, the steric barrier for addition of a macromonomer also increases with size of the reactant, retarding the addition process of the longer macromolecules and, as a result, diffusion resistances may not be as important for larger macromolecules as one might expect (the controlling step may be the overcoming of the steric barrier at the metal center).

2.2.4. Gas-Phase Process

In the gas phase (Scheirs and Kaminsky, 1999), ethylene and an α-olefin comonomer (1-butene or 1- hexane) are polymerized in the solid state in a fluidized bed reactor into a powder form. The polymer powder is then converted into pellet form by an extrusion process. The reactor is usually set at > 300 psi and the polymerization process is generally carried out at < 90°C.

The distinguishing characteristic of gas-phase polymerization is that the system does not involve any liquid phase in the polymerization zone. Polymerization occurs at the interface between the solid catalyst and the polymer matrix, which is swollen with monomers during polymerization. The gas phase plays a role in the supply of monomers, mixing of polymer particles, and removal of reaction heat (Xie et al., 1994). In this section, commercial gas-phase polymerization processes and experimental studies of gas-phase polymerization are discussed. The first commercial gas-phase polymerization plant using a fluidized bed reactor was constructed by Union Carbide in 1968 at Seadrift, TX. This process was developed initially for HDPE production. The success of this novel technology led to the extension of the process to LLDPE, the first commercial reactor was built in1975. The Union Carbide gas-phase process, commonly called UNIPOL, has been licensed worldwide with more than 25 licenses operating in 14 different countries. Production of LLDPE using gas-phase processes is more difficult than production of HDPE because the difference between the melting point and polymerization temperature is much smaller for LLDPE. The catalyst types and equipment design developed for

HDPE cannot be used to produce LLDPE because of the potential of agglomeration of polymer particles. Hence, significant engineering and chemistry research has been required to assure the success of gas-phase LLDPE production. According to Karol (1983), the keys to the success of the UNIPOL technology for LLDPE production are the proprietary catalysts that operate at low pressure and low temperature and which are suitable for use in gas-phase fluidized bed reactors.

In 1964 BASF first developed a gas-phase ethylene polymerization process using Phillips catalysts (Sailors and Hogan, 1981), and a commercial gas phase HDPE plant was built in Germany in 1976 (Choi and Ray, 1985a). BASF uses a continuous stirred-bed reactor for gas-phase ethylene polymerization. The reactor is equipped with an anchor agitator and is operated at higher pressure and temperature (35 atm, 100-110°C) than those employed in UNIPOL.

Despite the commercial success of gas-phase ethylene polymerization technology, the public literature contains no accounts of fundamental scale-up studies of gas-phase processes. There is a need, therefore, for a comprehensive understanding of detailed polymerization behavior in gas-phase polymerization. A challenge for academic researchers studying gas-phase polymerization of ethylene is how to scale down commercial processes for experimental laboratory studies.

With the development of commercial gas-phase polymerization processes, more university-based researchers have attempted to extend experimental studies of gas-phase polymerization in recent years. Choi and Ray (1985b) designed a 1 L gas-phase stirred bed reactor equipped with an anchor-type agitator. Mabilon and Spitz (1985) used a 675 cm^3 stainless steel reactor stirred by vertical oscillations for gas-phase polymerization. However, the detailed reactor configuration used in this investigation was not described. More recently, Lynch and Wanke (1990) constructed a 1 L stainless steel reactor with a specially designed paddle agitator. The reactor temperature is controlled using a 26 L oil bath. To improve reactor mixing and heat transfer, Dusseault and Hsu (1993) designed an 800 cm^3 horizontal stirred reactor with both internal cooling coil and external cooling/heating jacket. The agitator is designed in such a way so that the entire polymer bed can be turned over.

2.3. History of Catalyst Systems for Olefin Polymerization

The first polymerization of ethylene to form polyethylene was performed by a free radical initiation in a high-pressure process, and subsequently a low-pressure process was invented using metal alkyls as catalyst. The discovery of catalysts based on titanium trichloride and diethylaluminum chloride as cocatalyst was made by Karl Ziegler, who succeeded in polymerizing ethylene into high-density polyethylene (HDPE) at standard pressure and room temperature in 1953 at the Max-Planck-Institute in Mulheim. A little later, Natta, at the Polytechnical Institute of Milan, was able to demonstrate that Ziegler's catalyst system was capable of polymerizing propene into semi-crystalline polypropene. Ziegler and Natta shared a Nobel Prize for Chemistry in 1963 for their work on olefin polymerization (Reddy and Sivaram, 1995). With this so-called Ziegler-Natta catalyst, ethylene can be polymerized at low pressure (< 2 MPa) and low temperature (60-110°C), compared with free radical ethylene polymerization, which requires high pressure (~ 300 MPa) and high temperature (~ 300°C). The first generation Ziegler-Natta catalyst consisted of a transition metal compound, as an active component, and an alkyl or hydride of a main group element, as a cocatalyst. The most often used active component was $TiCl_3$, and the most common cocatalyst was triethylaluminum ($AlEt_3$). The development of new generations of Ziegler-Natta catalysts is based on these two components. The second-generation Ziegler-Natta catalysts, which were at least 100 times more active than the first generation catalysts consisted of $MgCl_2$ supported $TiCl_4$, with or without the addition of an electron donor, and triethylaluminum as the cocatalyst. Initially, the improvements of catalysts were to increase their activity for producing HDPE (to increase both their activity and stereoregularity for producing polypropylene) by adding a third component, i.e., an electron donor (Lewis base). The development of the third-generation Ziegler-Natta catalysts had copolymerization activity which made the production of LLDPE possible. However, the third-generation catalysts produced polyolefin copolymers in which the comonomer incorporation was very heterogenous, i.e. the comonomer content differed significantly among molecules, and the amount of comonomer incorporation was relatively low. Based on the third-generation Ziegler-Natta catalysts, the fourth-generation catalysts were developed to produce polyolefins with improved properties, such as heteroplastic olefin copolymers, reactor blends, multiphase alloys, and non-olefin grafted polyolefin alloys in a production process (Galli, 1994). The molecular structure of the polymers cannot be controlled well for conventional Ziegler-Natta catalysts because these catalysts are heterogenous with different types of catalytic sites.

The discovery of metallocene/MAO catalysts by Sinn and Kaminsky has been considered as one of the major revolutionary steps in the history of polymer industry. Metallocene catalysts, based on zirconium, hafnium or titanium, show in contrast to conventional Ziegler-Natta catalytic systems, only one type of active site (single site catalyst), which produces polymers with a narrow molar mass distribution (M_w/M_n = 2). The molecular structure of the metallocene catalysts can be easily changed which allows control of the structure of polyolefin produced with these catalysts. Many metallocenes are soluble in hydrocarbons or liquid propene. These properties allow one to predict accurately the properties of the resulting polyolefins by knowing the structure of the catalyst used during their manufacture and to control the resulting molar mass and distribution, comonomer content and tacticity by careful selection of the appropriate reactor conditions. In addition, their catalytic activity is 10-100 times higher than that of the classical Ziegler-Natta systems. The structure of metallocenes, so called “sandwich compounds”, in which a π-bonded metal atom is situated between two aromatic ring systems, was discovered by Fischer (1952) and Wilkinson and Birmingham (1954).

Metallocenes, in combination with the conventional aluminum alkyl cocatalyst used in Ziegler systems, are indeed capable of polymerizing ethylene, but only at a very low activity. Only with the discovery and application of methylaluminoxane (MAO) by Sinn et al., 1980, was it possible to enhance the activity, surprisingly, by a factor of 10000. Therefore, MAO played a crucial part in the catalysis with metallocenes. The high activity and the well-defined active species for olefin polymerization are responsible for the enormous interest in these systems by the scientific community as well as in industry (Scheirs and Kaminsky, 1999). Since this discovery of effective zirconocene-MAO catalyst systems for ethylene polymerization, improvement of the catalyst system has been conducted to achieve higher activity and to obtain higher molecular weight polyethylene. Modifications of metallocene ligand were investigated in non-bridged and bridged zirconocene catalysts (Alt and Koppl, 2000). The results of ethylene polymerization with various group IV metallocene catalysts were previously reviewed (Hlatky, 1999).

Copolymerization of ethylene with α-olefin is an industrially important process: the length of the side chain in the copolymer can be controlled by the introduced commonomer and this allows the manufacture of linear low-density polyethylene (LLDPE). Metallocene catalysts show high activity for ethylene/ α-olefin copolymerization, and exhibit higher reactivity for α-olefins than conventional Ziegler-Natta catalysts. The copolymers produced are characterized by narrow molecular weight distribution and short chain branching with a random distribution. The characteristic structures affect the properties of LLDPE prepared by metallocene catalyst. For example, the film made of the LLDPE shows superior mechanical properties and heat-sealing properties to that prepared with conventional Ziegler-Natta catalysts.

Metallocene catalysts have been used to polymerize ethylene, propylene and higher α-olefins to produce polymers with narrow molar mass distributions (Kaminsky, 1996; Hlatky, 1999; Imanishi and Naga, 2001), but metallocenes have also been used in styrene and other olefin polymerizations such as, syndiotactic polystyrene (Riccardo and Nicoletta, 1996; Schwecke and Kaminsky, 2001) and cyclopolymerization of 1,7-octadiene (Naga et al., 1999).

However, extensive research has been devoted towards metallocene catalyst studying modifications of the catalyst system, which leads to specific changes in catalytic activity and product characteristics (Scheirs and Kaminsky, 1999; Alt and Koppl, 2000). The development of metallocene catalysts has not yet been concluded and studies are required to increase the understanding of several important factors which affect catalytic performance, such as transition metal-olefin interaction, metal-alkyl bond stability, influence of other ligands, and steric effects of the other ligands.

2.4. Metallocene Catalysts

Metallocene catalysts are organometallic coordination compounds in which one or two π-carbocylic ligands such as cyclopentadienyl ring, substituted cyclopentadienyl ring, or derivative of cyclopentadienyl ring (such as fluorenyl, indenyl etc.) are bonded to a central transition metal atom. The cyclopentadienyl ring of metallocene individually bonded to the ring-metal bond is not centered on any one of the five carbon atoms in the ring but equally on all of them. The typical chemical structure of a metallocene catalyst is represented by Figure 2.2 where Mt is a Group 4, 5, or 6 transition metal, normally from Group 4 (e.g. Zr, Ti or Hf); A is an optional bridging unit consisting of 1-3 atoms in the backbone; R is hydrocarbyl substituents or fused ring systems (indenyl, fluorenyl and substituted derivatives); and X is chlorine or other halogens from group 17 or an alkyl group. The cyclopentadienyl ligands, halides and hydrocabyls substituents or fused ring systems represent the three classes of ligands of the metallocene catalysts and variation of, and/or substitutions within, some of these ligands could result in variation of the catalytic activity, polymer stereoregularity, and average molecular mass.

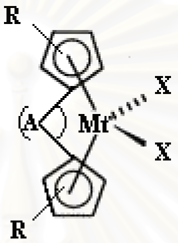

Fig 2.2. Typical chemical structure of a metallocene catalyst (Alt, 1999)

Single site catalysts can be divided into five main symmetry categories, which influence on the polymer architectures as shown in Figure 2.3. It is assumed that the polymer rapidly equilibrates with the available coordination site for the purposes of assigning symmetry. Catalysts exhibiting C_{2v} symmetry typically produce atactic polymers or moderately stereoregular polymers by chain-end control mechanisms. C_s-symmetric catalysts that have mirror planes containing the two-diastereotopic coordination sites behave similarly. However, C_s-symmetric catalysts that have a mirror plane reflecting two enantiotopic coordination sites frequently produce syndiotactic polymers. C_2-symmetric complexes, both racemic mixtures and enantiomerically pure ones, typically produce isotactic polymers via a site-control mechanism. Stereoselectivities of asymmetric (C_1) complexes are unpredictable and have been reported to produce polymer architectures ranging from highly isotactic, to atactic, including isotactic-atactic stereoblock and hemiisotactic. Polymer architectures relevant to this modification of ligands are shown in Figure 2.4.

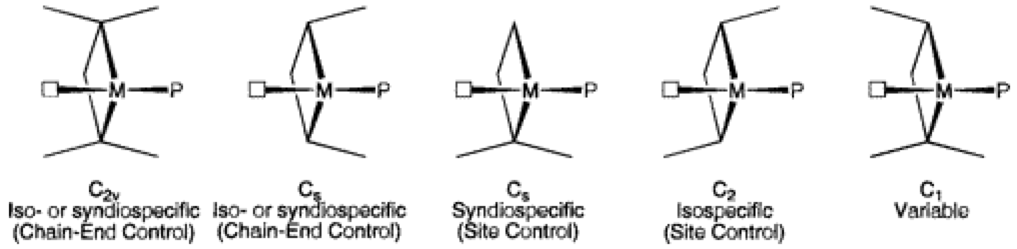

Figure 2.3. General symmetry classifications, based on ligand geometries, of catalysts and their stereoselectivities for polyolefin synthesis (Coates, 2000)

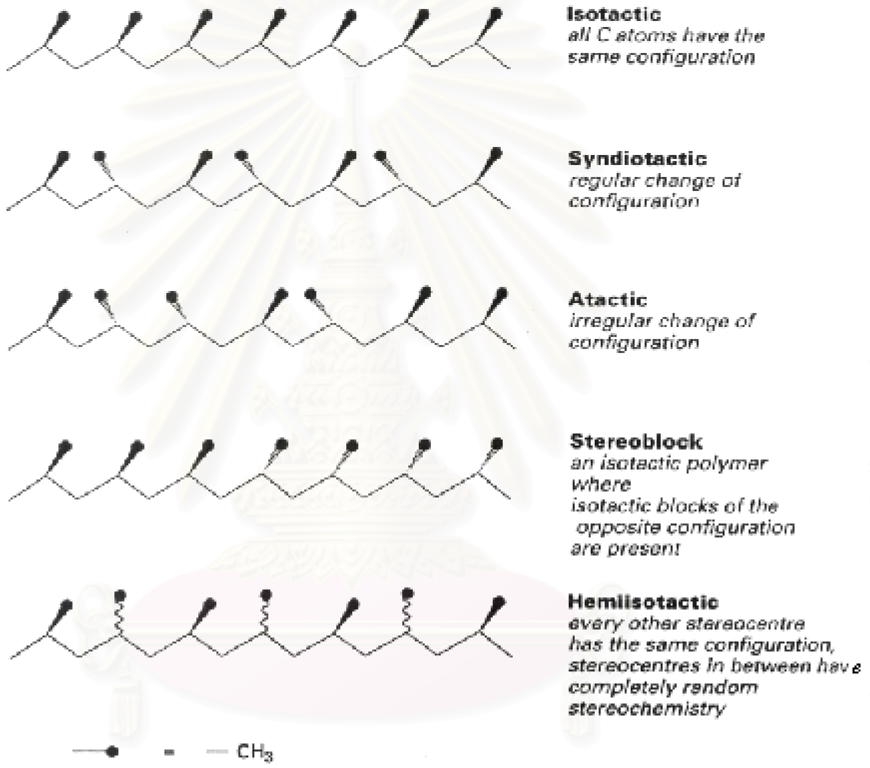

Figure 2.4. Common polymer tacticities (Long, 1998)

The synthesis of metallocene structures modified by the variation of ligands, substituted derivatives, metal atoms or bridging units are generally described in the open literature. By tailoring of the coordination environment of the metal center, single-site catalysts are now available that can control the molecular weight, molecular weight distribution, and comonomer incorporation.

Low catalytic activity in the polymerization of α-olefins with metallocene and half-sandwich complexes can be due to many reasons; however, the central metal plays the most important part. Zirconium and in some cases titanium provide the highest polymerization activities. Hafnium exhibits unattractive activities due to kinetic reason (slow olefin coordination and insertion step). However, most hafnium complexes provide polymers with higher molecular weights than the analogous zirconium and titanium complexes due to the dramatically stronger Hf-C bonds. Steric effects, such as the bite angle between the two η^5-coordinated aromatic ligands or bulky substituents at these ligands, dramatically influence the catalytic performance.

In addition, the electronic structure, mainly determined by the central metal and Lewis-basic or Lewis-acidic substituents at the ligands, is an important factor in the polymerization activity of metallocene and half-sandwich complexes. Complexes with sterically accessible oxygen or a nitrogen atom (Lewis bases) coordinated to the central metal are not useful for a good catalytic performance. Generally, hafnium metallocene and half-sandwich complexes exhibit lower polymerization activities due to a more stable halfnium-carbon bond, which lowers the insertion rate of the coordinated monomer into the growing polymer chain. Another aspect for low activity is the limited lifetime of the catalytic species due to decomposition processes such as the reduction of the metal atom in the catalyst. The evidence of electronic structure affecting the activity has been reported by Wang et al. (2001). Polyethylene was made using a (n-BuCp)$_2$ZrCl$_2$/MAO catalytic system. It is believed the (n-BuCp)$_2$ZrCl$_2$/MAO catalytic system yield higher polymerization activity mainly as a result of the electronic effects, since the size of substituent groups are larger than 0.25 nm, (Wang et al., 2001).

The nature of the ligand in complexes of the $(L^1)(L^2)$ $ZrCl_2$ (L^1, L^2 = Cp, Ind, and Flu) has also been studied. Unbridged metallocene dichloride complexes exhibit maximum activities when cyclopentadienyl (1500 kg of PE/g of Zr·h) or indenyl ligands (3200 kg of PE/g of Zr·h) are used. As soon as fluorenyl ligands are involved, the catalyst activity drops (423 kg of PE/g of Zr·h). This behavior could be due to the potential of fluorenyl ligands for ring-slippage reactions, forming unstable complexes. This instability is already obvious in the case of the unactivated metallocene dichloride complexes; whereas Cp_2ZrCl_2 can be stored at air, Flu_2ZrCl_2 decomposes easily. Also, substituted indenyl ligands in metallocene complexes of the type (Ind′)(Cp)ZrCl$_2$; (Ind′ = substituted indenyl) were studied. The maximum activities exceed those with substituted cyclopentadienyl ligands. However, no obvious trend in the molecular weights of the obtained polymer was found. From the bridged metallocene complexes, the variations of the bridging unit in metallocene complexes of the (Flu-bridging unit-Cp)$ZrCl_2$ were studied. Several substituents were introduced into the bridging unit of that type of complexes, known to have a great influence on the activity and stereospecifity. Indeed, bulky phenyl or cyclohexyl groups at the bridging unit increase the catalyst performance and the molecular weight of the produced polypropylene. More details on the modifications of ligands in both unbridged and bridged metallocene complexes have already been reported (Alt and Koppl, 2000).

2.5. Methylaluminoxane Cocatalyst

Cocatalysts, often in the form of main-group organometallic compounds in traditional two-component Ziegler-Natta catalytic systems, have also played a very important role in the single-site polymerization revolution. The discoveries of new and more effective cocatalysts have contributed significantly to fundamental understanding as well as technology developments in this field. From an economic point of view, the cost of the cocatalyst is frequently more than that of the precatalyst, especially for Group 4 metal-catalyzed olefin polymerization systems. Thus, the potential value of developing a new catalyst system or rendering a current system more efficient by discovering high-performance and low-cost cocatalysts and understanding their role in the polymerization process is compelling. Furthermore, it is likely that, in solution, slurry, and gas phase polymerizations, some process may have to rely on cocatalyst screening and anion engineering to afford better control of catalyst solubility and stability, the polymerization kinetic profiles, as well as morphological behavior of resulting polymer.

The importance of cocatalysts in metal-catalyzed polymerization processes can be appreciated as follows. First, to form active catalysts, catalyst precursors must be transformed into active catalysts by an effective and appropriate activating species. Second, a successful activation process requires cocatalysts which retain the nature of the catalytic site and do not have adverse effects on the polymerization kinetics and polymer properties. Finally, the cocatalyst, which becomes an anion after the activation process, is the vital part of catalytically active cation-anion pair and may significantly influence polymerization characteristics and polymer properties.

The emergence of numerous studies suggesting a significant influence of cocatalyst on catalytic activity, stability, polymerization kinetic profile, and stereoregularlity in cationic processes has gradually changed the view of the function of activators in single-site olefin polymerization. Several types of cocatalysts, formed by organometallic compounds, have been studied such as aluminum alkyl, alkylaluminoxane, perfluoroaryl boranes, fluoroarylalanes and cocatalysts containing non-group 13 elements (Chen and Marks, 2000). This section presents the current understanding of alkylalumoxanes, their synthesis and their structure. However, this review should not be taken to be conclusive due to the rapidly evolving nature of our knowledge of alkylalumoxanes.

Aluminoxanes were prepared by controlled hydrolysis of alkylaluminums (Scheirs and Kaminsky, 1999). The reaction of alkylaluminum compounds with water is a violent highly exothermic reaction and is best carried out at low temperature in an inert solvent; however, syntheses have been reported at temperature from –78 to 110°C. Those employing the direct addition of water or ice are carried out below room temperature. These products are obtained by different method of synthesis (Kaminsky, 1999), for example by using a water-saturated nitrogen flow, direct reaction of AlR_3 and water in organic solvents, and using hydrate metal salts as water sources. In an effort to control the rate at which the water reacts with the trialkylaluminum, different inorganic hydrated salts, such as $Al_2(SO_4)_3.14(H_2O)$ or $CuSO_4.5H_2O$, have been used as an indirect water source for hydrolysis in the preparation of aluminoxane from alkylaluminum (Giannett et al., 1985). The hydrolysis of AlR_3 (R = Me, Et, iBu) has been shown to proceed via the formation of an alkylaluminum water complex shown in Equation 2.1 (Barron, 1993), which subsequently eliminates an alkane to form a dialkylaluminum hydroxide complex. This rapidly associates to give dimers or larger oligomers in solution as shown in Equation 2.2.

$$AlR_3 + H_2O \longrightarrow AlR_3(H_2O) \qquad \text{--------(2.1)}$$

$$AlR_3(H_2O) \longrightarrow 1/n[R_2Al\,(OH)]_n + RH \qquad \text{--------(2.2)}$$

Alkylaluminoxanes, oligomeric compounds consisting of –Al(R)-O- subunits, have been known to be active for the polymerization of monomers. Before the discovery of the MAO cocatalyst, the homogeneous Ziegler-Natta catalyst Cp_2TiCl_2 was activated with alkylaluminum chloride, which yielded catalysts with low activity. The use of MAO cocatalyst raised the catalyst activity by several orders of magnitude. There are other aluminoxanes which can also activate metallocenes, such as ethylaluminoxane (EAO) and isobutylaluminoxane (iBAO), but methylaluminoxane (MAO) is much more effective than its ethyl and isobutyl analogues and is most preferred in practice (Pasynkiewicz, 1990; Barron, 1993).

Methylaluminoxane (MAO), i.e. $[\text{-Al(Me)-O-}]_n$, prepared by controlled hydrolysis of $AlMe_3$ and typically having $n \sim 5\text{-}20$, is the most common cocatalyst and yields highly very active catalysts for polymerizing ethylene, propylene, and higher α-olefins when combined with Group 4 metallocenes. Although various physicochemical data, such as compositional analysis, molecular weight determination, mass spectra, X-ray powder diffraction, infrared, NMR spectroscopy, UV spectroscopy, and other methods have been used and investigated for the characterization, the structure of MAO remains too complex and still not entirely clear or well-understood (Resconi et al., 1990; Siedle et al., 1990; Cam and Giannini, 1992; Barron et al., 1993; Harlan et al., 1994; and Reddy and Sivaram, 1995; Bryant et al, 2001). MAO can be described as a mixture of linear and cyclic oligomers that coexist in a dynamic equilibrium (Sangokoya, 1993 and Graefe et al., 1995). The proposed structures for MAO in the open literature shown in Figure 2.5 include: (1) one-dimensional linear chains; (2) cyclic rings, which contain three-coordinate Al centers; (3) two-dimensional structures, and (4) three-dimensional clusters. The three-dimensional structure (4) proposed by Sinn, 1995 is based on structural similarities with *tert*-butylaluminoxanes, which form isoluable and X-ray crystallographically characterizable cage structures (5). Barron characterized tert-butylaluminoxane as a $[^tBuAlO]_6$ cage with four coordinated aluminum atoms (Barron, 1993). This may be an indication for a similar MAO structure as also suggested by Sinn (1995). This aluminoxane has been shown to form a three-dimensional oxo-bridged structure (cage structure). Structure (4) has the basic formula $[Al_4O_3(CH_3)_6]_4$ with a CH_3:Al ratio of ~ 1.5, which is in agreement with the general formula $[AlO_{0.8\text{-}0.75}(CH_3)_{1.4\text{-}1.5}]_n$, recently reported by Albemarle researchers from ^1H-NMR measurements (Imhoff et al., 1998). Sinn (1995) presented additional evidence for hexamethyl-tetraaluminoxane,

$[Al_4O_3(CH_3)_6]_4$, as a major component of MAO, and have proposed an alternative structure model (similar to (4) but having a more rigid structure with four-, six-, and eight-membered rings). Multinuclear NMR investigations of MAO also indicate a possible cage structure under ambient conditions (Babushkin et al., 1997). Most aluminum centers in structure (4), except for the peripheral ones, are tetracoordinated. Characterization of MAO by ^{27}Al-NMR spectroscopy has shown that four-coordinate Al centers predominate in MAO solutions (Sugano et al., 1993), although three-coordinate Al sites are also presented (Siedle et al., 1993).

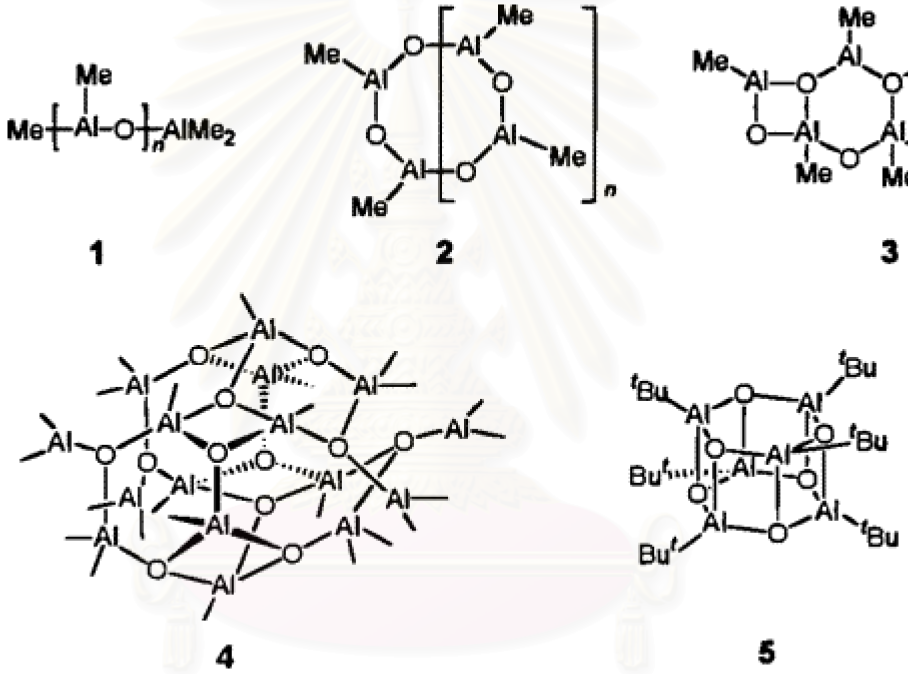

Figure 2.5. The general proposed structure of MAO (Chen and Marks, 2000)

Recently, the first information on the structure and reactive sites of MAO obtained via DFT quantum-chemical studies have been presented by Zakharov et al. (1999). It has been found that the three-dimensional oxo-bridged (cage structure) of MAO is more stable than the cycle structure and the Lewis acidity of Al atoms in MAO depends on size of MAO and increases with increasing MAO size.

Despite its unique effectiveness as a cocatalyst, MAO still remains a “black box”. Depending on the nature of the hydrated salt (the H_2O source) used for the MAO synthesis and the exact MAO synthetic reaction conditions, MAO-activated metallocenes may exhibit widely differing activities in olefin polymerization. The MAO structure can hardly be elucidated directly because of the multiple equilibria present in MAO solutions, and residual trimethylaluminum in MAO solutions appears to participate in equilibria that interconvert various MAO oligomers (Giannetti et al., 1985; Resconi et al., 1990; and Pasynkiewicz, 1990). There are two types of TMA present in typical MAO solutions: "free" TMA and "associated" TMA shown in Equation 2.3. It is difficult to reduce the CH_3:Al ratio to less than 1.5 by evaporating of volatile components because vacuum-drying removes only the free TMA, while the

$$[\!-\text{Al(Me)O}-\!]_n \cdot x\,\text{AlMe}_3 \rightleftharpoons [\!-\text{Al(Me)O}-\!]_n \cdot \underset{\text{"Associated"}}{(x\text{-}y)\,\text{AlMe}_3} + \underset{\text{"Free"}}{y\,\text{AlMe}_3} \qquad \text{-----(2.3)}$$

associated TMA can only be removed chemically. Tritto et al. (1997) found that cryoscopic MAO molecular weight decrease after $AlMe_3$ addition according to a linear relationship, which is caused by disproportionation reactions. However, recent in-situ FTIR spectroscopy investigations do not indicate any obvious reaction between TMA and MAO (Kaminsky, 1999). Nevertheless, in light of its complicated, unresolved structural features, MAO is usually represented for the sake of simplicity as having linear chain or cyclic ring structures $[\text{-Al(Me)-O-}]_n$, containing three-coordinate aluminum centers. Recently, Ystenes et al. (2000) investigated the structure of MAO by Raman and in situ IR spectroscopy. With bis(pentamethylcyclopentadieny) zirconium dichloride ($Cp^*_2ZrCl_2$), MAO and TMA seem to influence chain termination independently. A strong dependence of Mw of the polymer on the TMA concentration was found for the polymerization of ethylene with $Cp^*_2ZrCl_2$/MAO/TMA in toluene, indicating chain transfer to TMA.

Up to now the most favorable proposal for the active MAO species is to assume a cage built from six-membered rings, which consist of MeAlO building blocks. In such cages there are monomeric $AlMe_3$ molecules that have the following functionalities: alkylation of the metallocene dichloride complex and the formal abstraction of a methyl anion from the transition metal to give a metallocene monomethyl cation that is stabilized by a bulky MAO anion Figure 2.6 (Alt and Koppl, 2000).

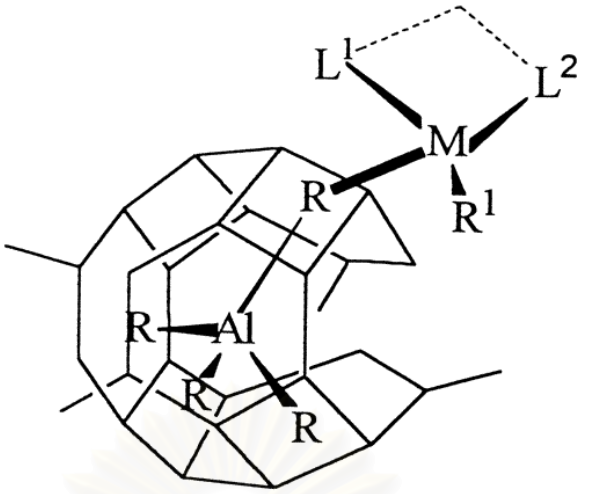

Figure 2.6. Model for an MAO cage stabilizing an activated metallocene complex (Alt and Koppl, 2000)

Quite recently, the modification by evacuated MAO was studied. Ioku et al. (2002); they found that dried methylaluminoxane (MAO) which was free of Me_3Al, was more active than the standard MAO system, resulting in a steady polymerization rate and giving higher Mw polypropylenes. Additive effects of trialkylaluminum on the dried MAO system showed that the polymer yield was increased by the addition of $i\text{-}Bu_3Al$ and Oct_3Al and decrease by Me_3Al and Et_3Al.

Wilmes et al. (2002) showed that the nature of the cocatalyst have a significant influence on the productivity and stereoselectivity of the unbridged 2-arylindenyl metallocene complexes. The type of MAO influences the stereoselectivity of propylene polymerization: MAOs containing isobutylaluminum groups yielded higher tacticity polypropylenes than those with only methylaluminum groups.

2.6. General Aspects of Metallocene/MAO Catalyst Systems

The science of homogeneous metallocene polymerization catalysis has proved to be very popular because it is both curiousity-driven and application-driven. The turning point from purely academic to applied research came 30 years after their discovery with the realization that changing the structures of the catalyst's cyclopentadienyl (Cp) ligands had favorable and exceptionally powerful effects on the catalyst's activities and, more importantly, on the polymer's structures and chain lengths. The following properties of metallocene catalysts indicate why there is so much interest in metallocenes (Alt and Koppl, 2000).

(1) The homogeneous nature of these catalysts provides active sites for every molecule in solution and explains their enormous activity. They can be a 100 times more active than conventional Ziegler-Natta or Phillips catalysts. For instance, the ansa bis(fluorenyl) complex. $(C_{13}H_{18}\text{-}C_2H_4\text{-}C_{13}H_{18})ZrCl_2$, can produces as much as 300 t of PE/g of Zr·h at 70°C after activation with a cocatalyst
(2) Metallocenes have the potential to polymerize prochiral olefins, such as propylene, to give stereospecific polymers (isotactic, syndiotactic, hemitactic polypropylene). Their variety opens the door to polyolefin elastomers.
(3) Metallocenes due to their "single site" nature can produce polyolefins with narrow molecular weight distributions ($Mw/Mn \approx 2$).
(4) Metallocene catalysts can produce polyolefins with relatively homogeneous inter- and intramolecular distribution of short- and long-chain branches. These parameters determine the properties of new materials for new applications, i.e. mLLDPE, and thus generate new markets.
(5) The heterogenization of metallocene catalysts provides different active sites than those in solution and can have an enormous effect on the catalyst activity and the properties of the produced polyolefins in terms of molecular weights, branching, and stereospecificity.

2.6.1. Activation of the Metallocene Catalyst and Mechanism of Polymerization

To understand the nearly unlimited versatility of metallocene complexes, it is necessary to take a closer look at the catalyst precursor and its activation process with the cocatalyst methylaluminoxane as illustrated in Figure 2.7.

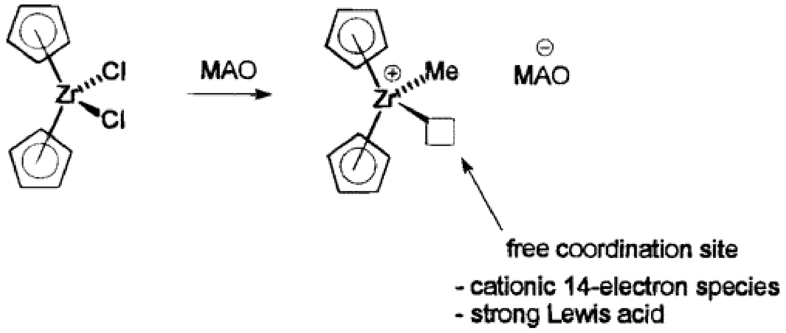

Figure 2.7. Activation of the metallocene complex Cp_2ZrCl_2 (Alt and Koppl, 2000)

The mechanism of olefin polymerization catalyzed by a highly active metallocene-aluminoxane system has been the subject of many experimental and theoretical investigations, i.e. the Cossee mechanism and the Trigger mechanism, (Castonguay and Rappe, 1992; Ystenes, 1993). In the cationic metallocene species, the metal atom is coordinated with the π-ligands and alkyl group (growing polymer chain). During polymerization, the monomer is coordinated with a highly electrophillic and coordinatively unsaturated cationic complex. It is followed by insertion of a monomer in the metal-carbon bond to produce a polymer chain. The migration of the polymer chain and the formation of the metal-carbon bond occur in concert through a four-center transition state. These results in the reaction of a vacant coordination site at the site originally occupied by the polymer chain. This process involving shifting of the growing chain to the position previously occupied by a coordinated monomer continues until termination of the polymer chain. The mechanism of metallocene-catalyzed polymerization is illustrated in Figure 2.8.

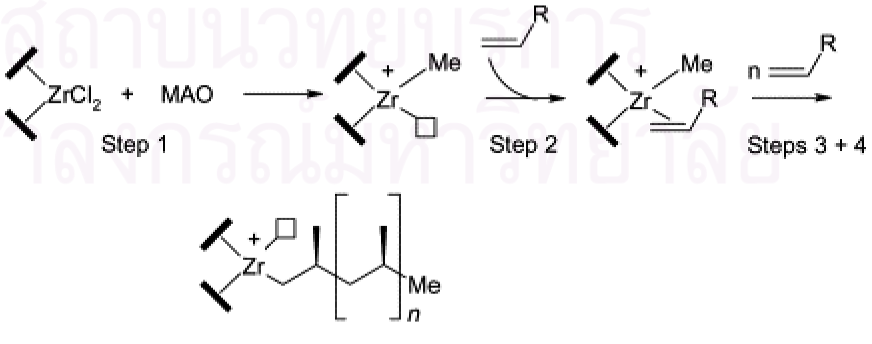

Figure 2.8. Mechanism of olefin polymerization using metallocene catalyst (Kaminsky and Laban, 2000)

The accepted mechanism for the polymerization of olefins by zirconocene catalysts, as shown in Figure 2.8, consists of the following steps: Step 1, the cocatalyst (MAO) converts the catalyst after complexation into the active species that has a free coordination position for the monomer and stabilizes the latter; Step 2, the monomer (alkene) becomes part of the complex; Step 3, insertion of the alkene into the zirconiumalkyl bond and provision of a new free coordination position; Step 4, repetition of step 3 in a very short period of time (about 2000 propene molecules per catalyst molecule per second), thus, rendering a polymer chain.

2.6.2. Chain Termination and Transfer

Chain termination and transfer mechanisms can have tremendous influences on the nature of the polymer. In metallocene-catalyzed olefin polymerization (Gupta et al., 1994), the termination of polymer chain occurs through a chain transfer involving β-H elimination (Figure 2.9) and β-Me elimination (Figure 2.10). The termination of a polymer chain may also occur due to chain transfer to aluminum (Figure 2.11), monomer (Figure 2.12), or hydrogen (Figure 2.13). All of the mechanisms proposed above are dependent on the nature of the metallocene, aluminoxane, and the polymerization conditions. Resconi et al. (1992) studied the contribution of various chain transfer processes in the propylene polymerization reaction due to the different metallocenes and reaction conditions. $Cp_2^*MCl_2$/MAO (Cp^* = pentamethylcyclopentadienyl; M = Zr, Hf) gives atactic propylene oligomers and low molecular weight polymer. The GC-MS and ^{1}H-and ^{13}C-NMR analyses of the products show the presence of unsaturated and saturated end groups. The unsaturated end groups contain vinylidine and alkyl groups. Product analysis shows that both M-CH_3 and M-H bonded active species are involved in the chain termination step involving β-CH_3 and β-H elimination.

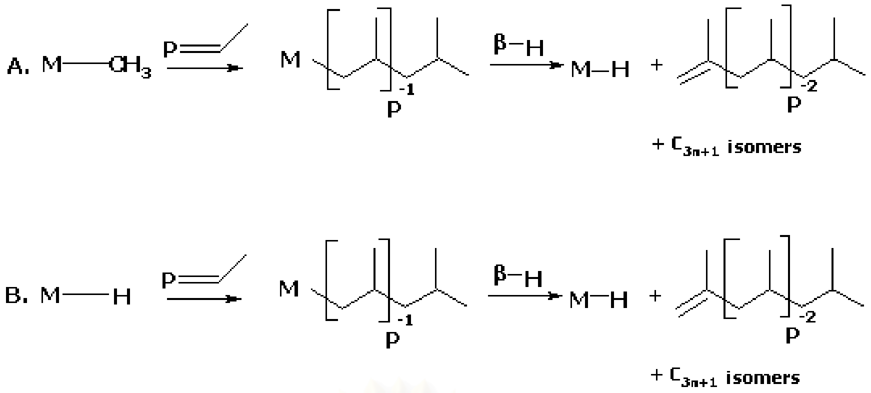

Figure 2.9. Chain transfer via β-H elimination (Resconi et al., 1992)

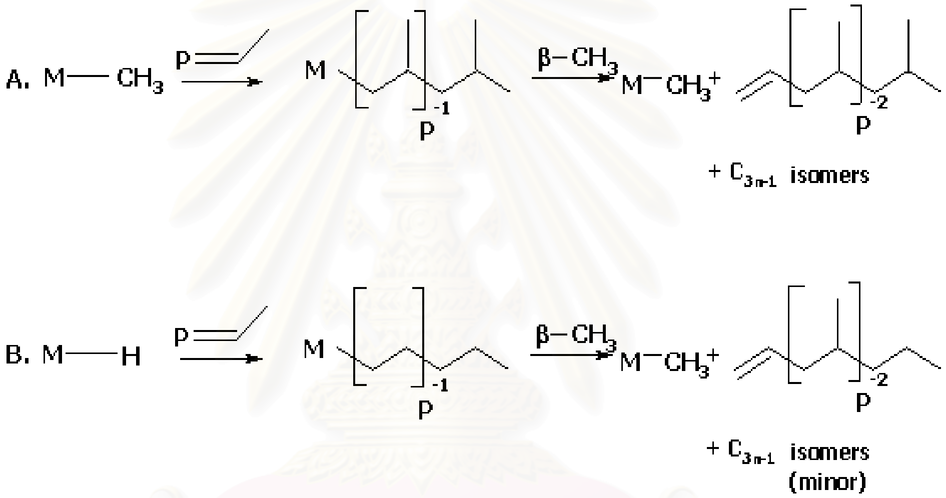

Figure 2.10. Chain transfer via β-Me elimination (Resconi et al., 1992)

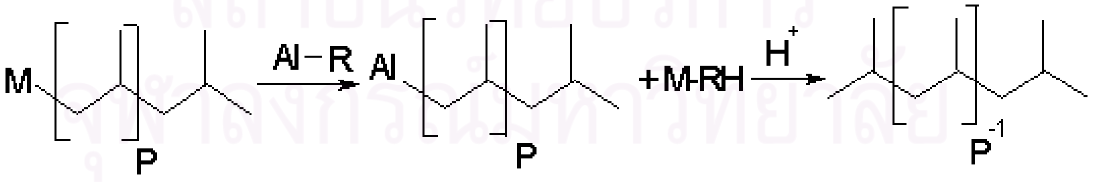

Figure 2.11. Chain transfer to aluminum (Resconi et al., 1992)

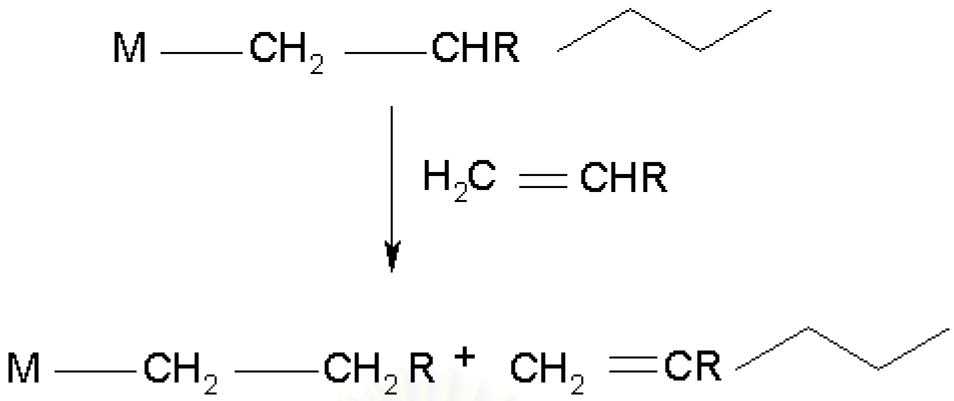

Figure 2.12. Chain transfer to monomer (Gupta et al., 1994)

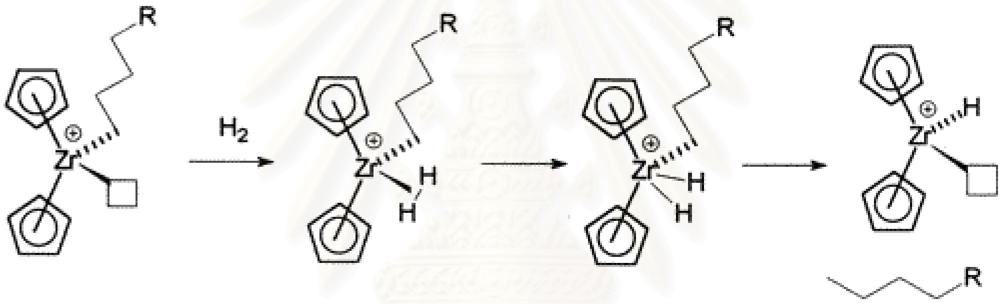

Figure 2.13. Chain transfer to hydrogen (Alt and Koppl, 2000)

2.6.3. Deactivation Processes

An important deactivation process for MAO-activated catalytic systems is α-hydrogen transfer, which leads to the production of methane (Kaminsky, 1996). The condensation reaction of the metallocenium alkyl + MAO forms Zr-CH_2-Al or Zr-CH_2-Zr structures in Equation 2.4 and these species are considered to be catalytically inactive. The condensation rate depends on the zirconocene structure, temperature, Al/Zr ratio, and concentration. The methane production is much more rapid with MAO than with less Lewis acidic TMA. It was observed in ^{1}H NMR studies that the inactive Zr-CH_2-Al structures can be reactivated with excess MAO, forming $L_2Zr(CH_3)^+$ and Al-CH_2-Al structures. That is, these deactivated species are reactivated according to Equation 2.5

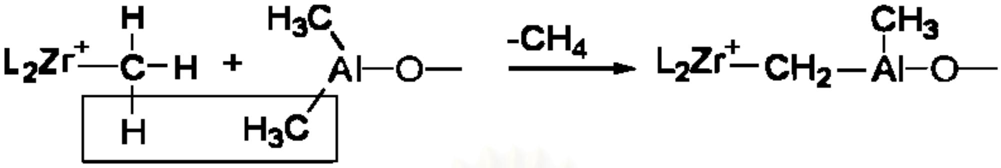

----(2.4)

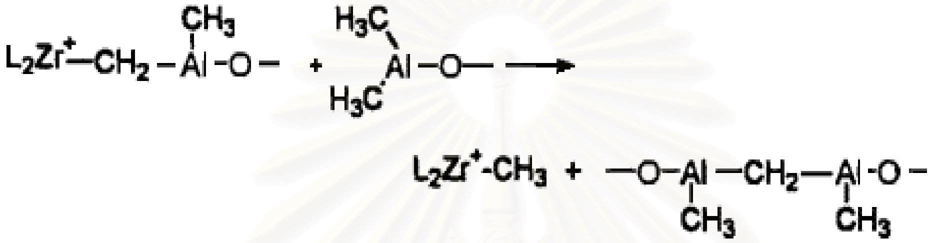

----(2.5)

Fischer et al. (1993) studied the kinetics of propylene oligomerization catalyzed by Cp_2ZrCl_2/MAO in toluene and subsequently proposed a reversible + irreversible deactivation process kinetic scheme to fit the decay of the polymerization rate as a function of time (Equation 2.6). The reversible deactivation is second-order relative to the zirconium active site concentration, which may involve interactions between active as well as inactive Zr sites (binuclear processes), for example dimerization and disproportionation. At low temperatures deactivation is predominantly reversible.

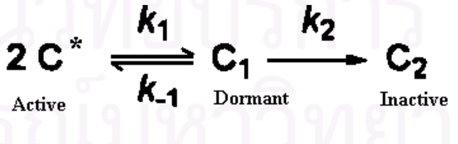

$$\underset{\text{Active}}{2\,C^*} \underset{k_{-1}}{\overset{k_1}{\rightleftharpoons}} \underset{\text{Dormant}}{C_1} \xrightarrow{k_2} \underset{\text{Inactive}}{C_2}$$

----(2.6)

Reduction of the Group 4 (IV)M metal center by MAO or trialkylaluminum to lower-valent species is a common phenomenon, especially for titanium complexes and sometimes for zirconium complexes as well (Cam et al., 1994; Yu et al., 1998; and Huang et al., 1999). These reductive processes are not considered to be deactivation but rather part of generating the true catalytically active species in the case mono-Cp titanium complexes for syndiospecific styrene polymerization. Addition of a monomer to an active catalytic system often surprisingly increases the quantity of Ti (III) or Zr (III) present, leading to the hypothesis that either the M-R insertion product is more easily reduced than the initial M-CH_3 species and/or that most of M (III) species initially existed as bimetallic or polynuclear structures before addition of monomers or Lewis bases. A number of deactivation and irreversible decomposition processes have been documented for the catalytic systems involved in borane/borate/aluminate activation. The most commonly observed decomposition mode is C_6F_5-group transfer to the electron-deficient transition metal (Chen and Marks, 2000).

2.7. Heterogeneous Metallocene Catalyst

The homogeneous metallocene systems are able to polymerize several olefins with high activities into high-molecular weight polymers and copolymers, characterized by a narrow molecular weight distribution ($Mw/Mn \approx 2$) and homogeneous chemical composition. However, despite their numerous advantages, several problems still need to be solved before the metallocene catalysts can be used widely in industry for the commercial production of large amounts of polyolefins. There are two main problems which have delayed the use of metallocene catalysts of large scale production of commodity polyolefins: One, reactor operating problems, e.g. the difficulty in controlling polymer morphology with soluble homogeneous catalysts limits their use in slurry and gas-phase processes due to reactor fouling, and two, the very large amounts of a cocatalyst required with homogeneous metallocenes to achieve high activities, i.e. Al to metallocene molar ratios >1000. The high levels of MAO as cocatalyst are a problem commercially, due to relatively high cost of MAO. In addition, the very high level of MAO can result in large amount of aluminum-containing ash in the polymer, which can effect on the production properties (Ribeiro et al., 1997; Fink et al., 2000; and Tait et al., 2000). Supported (heterogenized) catalysts provide possible solutions to these problems. However, improvements in supported catalysts need to be achieved in order to be acceptable for in existing polyolefin manufacturing facilities; the improvements required according the Chien (1999) are the following:

- Homogeneous metallocene catalysts can have a maximum activity in ethylene polymerization reactions in excess of 10^{10} g PE/(mol Zr·[C_2H_4]·h) and exceeding 10^9 g PE/(mol Zr·[C_3H_6]·h) for propylene polymerization reactions. The supported versions should have activity approaching those of the homogeneous catalysts.

- The activity of some homogeneous metallocene catalysts suffers a significant loss in the course of a polymerization reaction. The supported system needs to be more stable.

- A very large quantity of methylaluminoxane (MAO) cocatalyst is required to achieve high activity. This amount has to be greatly reduced for economic viability of the supported catalysts.

- Most metallocene catalysts in solution produce polyolefins of a very low molecular weight (M_W) especially at high polymerization temperatures (T_p). The supported catalyst should produce higher M_W polymers at high T_p.

- Polyolefins obtained in homogeneous processes have a very low particle size, as well as a broad size distribution and low bulk density. Supported catalysts must be able to control the polymer morphology.

- Metallocene catalysts in solution give polymers with narrow molecular weight distribution (MWD) and consequently with a poor processability-physicomechanical property balance. The supported systems should have the capability of producing polymers having a desired broad or bimodal MWD for good rheological and physical properties.

- Some supported metallocene catalysts have been reported to cause fouling of gas phase reactors. Corrective measures must be found.

- The steric control of metallocene catalysts is determined by molecular structure. It would be advantageous if this can be controlled or even altered by the support.

A large number of studies have been devoted to the transformation of soluble metallocene complexes into heterogeneous catalysts by supporting them on inorganic or organic carriers (Ribeiro et al., 1997; Ciardelli et al., 1998; Kristen, 1999; and Hlatky, 2000). Surface modification of the support can also be applied to improve the catalyst's performances. Modifications may include reactions of the support with organometallic compounds as well as thermal treatments; the nature of support and the technique used for supporting the metallocene have a crucial influence on the resulting catalytic behavior and polymer properties. Hence, the type of carriers, the procedures for supporting the metallocene, and preparation conditions are reviewed below.

In the following sections, the present state of art of supported metallocene catalyst preparation with respect to the type and nature of supports, especially silicas and mesoporous molecular sieves and the supporting procedures including conditions of preparation, are reviewed. The effects of polymerization conditions on the catalytic performances in gas-phase and slurry-phase ethylene homopolymerization and copolymerization of ethylene/1-hexene and polymer properties are included in the review.

2.7.1. Types of Supports

Many materials have been used as catalyst support to improve the catalytic efficiency and product morphology. The supports used include silica, alumina, magnesium chloride, starch, zeolites, cyclodextrin, polymers, and mesoporous molecular sieves. The most commonly used supports are spherical amorphous silica, alumina, and magnesium chloride. Since most of these supports have been widely discussed in the open literature, the emphasis in this review will be closely related to the use of silica and meosporous molecular sieves as supports. Mesoporous molecular sieves have recently been used for olefin polymerization and proposed as support for metallocene catalyst to synthesize the polymers having controlled molecular weight and narrow polydispersity. These characteristics of these catalysts are of both fundamental interest and practical importance.

2.7.1.1. Silica and Mesoporous Molecular Sieves as Supporting Materials

The right choices of supporting material as well as the choice of suitable properties (pore size, specific surface area, chemical surface composition) are important factors influencing the immobilization of the metallocene catalyst and the fragmentation of the support during polymerization. Commercially used porous silica gels are prepared by neutralization of aqueous alkali metal silicate with acid. The pore structure and pore size distribution can be controlled by the type of chemical reaction and experimental conditions. The pore size distribution is relatively narrow; pore diameters range from 1 to 20 nm; i.e. the silicas contain micropores (pore diameter ≤2 nm) and mesopores (pore diameters 2 to 50 nm). These small pores are responsible for the high specific surface area, which ranges from 250 to 1000 m^2/g, depending on whether micro- or mesopores are dominant.

The chemical properties of amorphous silica widely used as supporting materials for metallocene catalysts are mostly governed by the chemistry of its surface, especially by the presence of silanol groups (Soga and Kaminaka, 1992; Kaminsky and Renner, 1993; Soga et al., 1994; Sacchi et al., 1995; Quijada et al., 1997; Jenny and Maddox, 1998). A change in structure due to thermal or subsequent chemical treatment can strongly alter the properties. Therefore, it is possible to broaden the field of application for metallocene supporting materials. The concentration of silanol groups on the inner and outer surface of the silica gels has been analyzed by electron paramagnetic resonance, infrared spectroscopy, and tritation. Figure 2.14 shows the thermally induced change of silica gel surface from silanol to siloxane. The surface of pure silica gel is covered with silanol groups, at a maximum concentration of 8 OH groups per nm^2. They are mostly found as geminal or isolated pairs and are neither very acidic nor very basic. The hydroxylated surface is hydrophilic and easily adsorbs moisture from the air. This physically adsorbed water can be desorbs by raising the temperature to 100-200°C. In the course of this heating a partial dehydroxylation of the silica gel takes place, reducing the number of OH groups per nm^2 to approximately 5.5. One-half of these OH groups are geminal pairs; the other halves are vicinal ones. The number of hydroxyl groups decreases continuously as the temperature is raised, until at a temperature of 600-800°C an almost completely dehydroxylated silica with approximately 1 OH group per nm^2 is left. At this silanol concentration, or lower, the surface is hydrophobic.

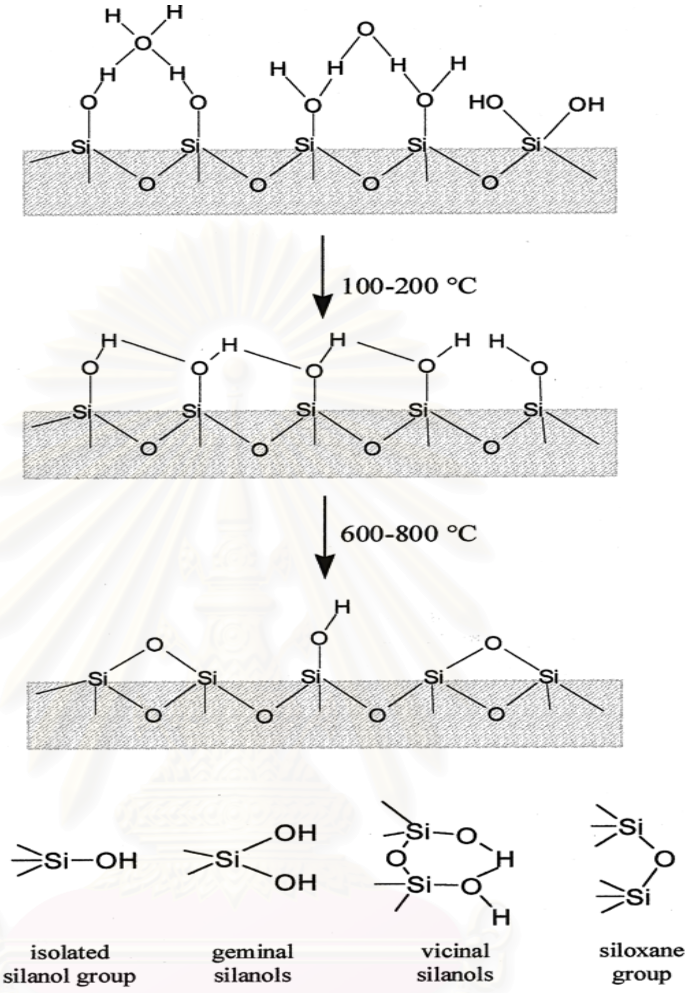

Figure 2.14. Schematic representation of the dehydration of a silica gel surface (Fink et al., 2000)

The interaction of surface silica and cocatalyst, especially with MAO, has been investigated and is a topic of interest to the current study. Panchenko et al. (1999) used IR spectroscopy to study the interaction of silica with TMA and with two methylaluminoxane (MAO) samples different trimethylaluminum (TMA) contents. Whereas TMA interacts with terminal hydroxyl groups of silica via the protolysis reaction, MAO mainly adsorbs on the surface hydroxyl groups of silica without noticeable protolytic reaction with them. When silica is treated with commercial grade MAO with significant TMA content, the silica surface hydroxyl groups mainly interacts with TMA and MAO adsorbs on the surface of the SiO_2/TMA. Recently, Ferreira et al. (2000) examined the MAO-silica interaction experimentally and theoretically by studying CH_4 evolution. The conclusion of this work is that OH from a silica surface reacts with MAO and probably with TMA during the MAO treatment. The most probable final species is where the MAO molecule is fixed to the surface by several points, mainly in a linear form. When MAO*TMA is supported, TMA would be associated to MAO on the surface and the reaction of TMA with the surface would be possible.

Recently, mesoporous molecular sieves were proposed as catalyst supports for the synthesis of the polymers with controlled molecular weight and narrow polydispersity (Trong et al., 2001). The mesoporous molecular sieves (MMS) have been designed to be used as catalytic materials. Any chemical composition based classification of mesostructured materials must begin with mesostructured silicas which have been studied extensively due to their easier synthesis and stable structures. A large variety of materials have been prepared using various of inclusion chemistry to introduce catalytically active species in mesoporous silica as guest materials. These include co-condensation of active species during the MMS synthesis or post-synthesis methods such as ion-exchange, impregnation, adsorption, grafting of reactive metal complexes (alkoxides, carbonyls, chlorides, metallocenes). Obviously, in all these synthesis, the mesostructured pore lattice yields a clear advantage by providing enough space for the insertion of bulky active complexes. It is of potential interest for catalytic applications that ordered mesoporous materials, and in particular SBA-15 type silica may be prepared in a variety of morphologies and textures such as spheres, hollow spheres, or fibers.

Metallocene complexes of various metals, including Zr and Ti which are known to be very active catalysts for olefin polymerizations, can be attached onto the inner surface of mesoporous molecular sieves (Hamielec and Soares, 1996; and Yasuga, 2000). Mesoporous molecular sieves may play a key role in accommodating the larger metallocenes and polymerizing larger monomers such as propylene due to their controllable pore size, pore volume and high surface areas. These new materials allow the anchoring of more active complexes and the co-catalyst species (MAO). The larger pores, compared to microporous zeolites, allow better access to the active sites by bulky monomers during polymerization. For example, mesoporous silica MCM-41 materials supported metallocene

[$Me_2C(Cp)(Flu)]ZrCl_2$ were indeed used by Kaminsky et al. (2000) for syndiospecific propene polymerization with higher syndiotacticity and higher melting point than achieved when using homogeneous systems or supported systems based on ordinary silica.

The efficiency of supported metallocene or metallocene amides catalysts activated with methylaluminoxane species (MAO) as co-catalysts was reported by many authors for olefins polymerization (Sano et al., 1999a, 1999b, 2000; Hlatky, 2000; Licht et al., 2000, and Sano et al., 2001a). Most of the time, large amounts of these activated species (e.g. MAO) are required and the large surface areas of mesoporous molecular sieves provide for their high dispersion onto the inner walls in addition to the high surface coverage of the metallocenes used. Hence, the application of these supports will be discussed in scope of the catalytic activity and product properties.

Propene polymerization catalyzed over MCM-41 and VPI-5 supported $Et(Ind)_2ZrCl_2$ catalysts was studied by Ko et al. (1996). They concluded that rac- $Et(Ind)_2ZrCl_2$ supported on these molecular sieves having small and regular cylindrical pores polymerized propene with high activity. Stereoregularity, melting point and molecular weight of obtained PP were increased and its polymerization behaviors were quite different from that of homogeneous $Et(Ind)_2ZrCl_2$. The characteristic structures of the pore of MCM-41 and VPI-5 should not allow the active sites to form binuclear complexes between metallocenes, or between metallocene and MAO, resulting in stable active sites and high activity in propene polymerization. $Et(Ind)_2ZrCl_2$ confined in the small regular cylindrical pores also could be more stereoselective than unsupported $Et(Ind)_2ZrCl_2$ in propene polymerization.

Little later, Tudor and Hare (1997) demonstrated the effectiveness of MCM-41 in providing a solid support for the homogeneous chiral catalyst *rac*-$Et(Ind)_2ZrCl_2$ and its application toward controlling polymer morphology. Hence, polypropene produced by the MCM-41 derived catalyst consists entirely of spherulite particles, with a distinct shell and core morphology. The polymer is highly isotactic and exhibits higher melting points than the corresponding homogeneous and clay supported system.

Van Looveren et al. (1998a) reported the syndiospecific propene polymerization and the co-oligomerization of ethylene using methylaluminoxane (MAO) MCM-41 supported metallocene catalysts [$\{C_2H_4(1\text{-indenyl})_2\}Zr(CH_3)_2$] and described a new heterogeneous aluminoxane derivative generated by in situ hydrolysis of TMA in the mesoporous of the siliceous molecular sieve MCM-41. The spectroscopic and physicochemical features of the solids obtained point to the formation of an MAO phase chemically linked to the pore walls of the support. This MAO phase is accessible for interaction with zirconocene and does not require supplementary MAO for co-oligomerization of ethene and propene. Especially at low concentrations the MAO-MCM-41 is chemically more active than the corresponding silica-based MAO derivative or the homogeneous system. The molecular weight and physical properties of the co-oligomers are dependent on the pore size of MCM-41, which suggests shape-selective oligomerization. The main advantage of in situ alumoxane synthesis over physisorption is that cluster aggregation is prevented. The author also prepared those synthesis with $Cp_2Zr(CH_3)_2$ (Van Looveren et al., 1998b). The regioselective preference of the immobilized metallocene is preserved and a typical Flory-Schulz molar mass distribution for the propene oligomers is obtained. Koppl et al. (1999) provided more information on the hydrolysis of trimethylaluminium to form MAO species. They demonstrated that the silanol groups on the mesoporous materials surface can be used to modify the properties of the solid support and ultimately its catalytic performance via in situ hydrolysis of trimethylaluminum species ($AlMe_3$) into MAO species. This process followed by reaction of the MAO species with metallocene complexes had been proposed earlier to design microporous silica supported polymerization catalysts. These MAO species can also be used to provide chirality to attached metallocene active species. The chirality can be derived from appropiate control of channels size, which may impose a specific environment sometimes in conjunction with the various kinds of silanol groups (geminal, vicinal, isolated silanol group) on the inner surface of the mesoporous materials including those associated with heteroatoms present in their framework.

Commercial Grace silica, mesoporous silicate, MCM-41, and aluminum-modified MCM-41 were used as support for catalyst activity in ethylene slurry polymerization. The effect of the structure and surface properties of support material on metallocene (zirconocene chloride) adsorption and catalyst activity was studied. Rahiala et al. (1999) reported that the highest amount of zirconocene dichloride was adsorbed on Al-modified MCM-41 (Si/Al = 32), providing the most reactive sites for attachment of the active component on the support surface. The ^{13}C-CPMAS NMR studies proved that the Cp_2ZrCl_2 is bound to the support surface. Also the highest in ethane polymerization was obtained using this support.

Schneider et al. (2001) also reported ethylene and propylene polymerization using η^5-cyclopentadienyltris(dimethylamido) zirconium [$CpZr(NMe_2)_3$] catalyst immobilized on a chlorosilane- and hexamethyl-disilazane (HMDS)-modified mesoporous silica surface. This heterogenization process is absolutely necessary to make the homogeneous metallocene catalysts useful for industrial applications in order to avoid the fouling generated by polymer precipitation onto internal reactor surfaces, as the polymer precipitates instead onto the catalyst surface or to reduce side reactions.

Sano et al., (1999a, 1999b, 2000, 2001a) used mesoporous silicas and silica gels with various pore sizes to fractionate methylaluminoxane (MAO). They used the MAO left in solution as well the MAO/support solids to prepare supported Cp_2ZrCl_2 catalysts. They observed that the activities of these catalysts for ethylene and propylene polymerization were a strong function of the pore sizes of the supports used to fractionate the MAO. All the polymerization studies by Sano and co-workers were done using toluene slurries. Sano et al. (2001b) also prepared AlMCM-41 by a post synthesis alumination of MCM-41 and used these for propylene polymerization with *rac*-ethylene(bisindenyl)zirconium dichloride and triisobutylaluminum. The resulting catalyst system gave selectively isotactic polypropylene and the polymer yield was strongly dependent upon the evacuation temperature in the pretreatment of the AlMCM-41 before use. From the linear relationship between the polymer yield and the number of Lewis acid sites on the AlMCM-41 evaluated by pyridine adsorption, it was found that Lewis acid sites on AlMCM-41 are able to activate effectively the metallocene compound, resulting in the formation of active species.

The catalytic activity of Cp_2ZrCl_2 supported on three types of molecular sieves (MCM-41, VPI-5, and Y Zeolites) was evaluated by Paulino et al. (2000) in slurry-phase polymerization of ethylene. The supports were dehydrated, pretreated with MAO then reacted with Cp_2ZrCl_2. MCM-41 proved to be the best support for Cp_2ZrCl_2, showing the highest values for activity and productivity.

Additionally, polyethylene obtained with this catalytic system presented better properties such as larger molecular weight and higher melting point.

Gas-phase and slurry-phase ethylene polymerizations with chromium complexes grafted onto MCM-41 and modified MCM-41 were done by Weckhuysen et al. (2000); they showed that chromium acetyl acetone [$Cr(acac)_3$] complexes grafted onto the surface of either pure silica MCM-41 or Al-containing silica (Si/Al ratio of 27) were effective catalysts for gas-phase and slurry-phase polymerization of ethylene at 100°C. The formation of polyethylene nanofibers took place within the hexagonal channels of the mesoporous crystalline aluminosilicates. Optimal activity was observed at 1 wt.% Cr over the Al containing MCM-41. Increasing the calcinations temperature from 550 to 720°C further enhanced the activity. The author also demonstrated that aluminum atoms incorporated in the framework of mesoporous molecular sieves provide more thermal stability to deposited chromium acetyl acetonate complexes compared to aluminum free mesoporous molecular sieves.

It is interesting to note that in the above discussed work of Kaminsky and coworkers, a higher activity in syndiotactic polypropylene polymerization over supported zirconocene [$Me_2C(Cp)(Flu)$]$ZrCl_2$/MAO was obtained when the MCM-41 support contained no framework Al. It is therefore clear that the Lewis acid sites generated by this aluminum species affects the nature of the grafted complex. In this particular work it is shown that the introduction of Al in the framework converts the catalytic site from one, which yields syndiotactic polypropylene to an isotactic polymer-producing site.

Kageyama et al. (1999) made especially interesting observations using hexagonal mesoporous molecular sieves (MMS) in the form of mesoporous silica fibers (MSF) as support for ethylene polymerization catalysts. Dichlorotitanocene (Cp_2TiCl_2) and MAO were grafted on an MSF support having a mesopore diameter of 2.7 nm. In order to explain the observed formation of crystalline polyethylene fibers with a diameter of 30-50 nm, they proposed that linear nanofibers of polyethylene with ultrahigh molecular weight are produced through an “extrusion polymerization mechanism”. This new concept of using the morphology of mesoporous molecular sieve to provide oriented nano molds for the synthesis of crystalline polymer fibers is likely to have broad general applications. Et(Ind)$_2$ZrCl$_2$ confined into the pore of MCM-41 can polymerize ethylene-propylene copolymer with a higher content of propylene and a high comonomer enhancement effect. Ko and Woo (2001) did not observe the comonomer effect on the polymerization rate for ethylene/1-octadecene copolymerization, and the resulting copolymer had a low content of 1-octadecene. These results show the effect of steric hinderance in regular and small pore structure of MCM-41 on the stereoregularity and polymerization.

Recently, Ye et al. (2003) supported a nickel-diimine on mesoporous particles having a parallel hexagonal nanotube pore structure (MCM-41 and MSF) and used these catalysts for ethylene polymerization. Pretreating the supports with methylaluminoxane (MAO) followed by nickel diimine catalyst impregnation gave much higher catalyst loading and higher catalytic activity than the direct impregnation of with nickel diimine catalyst. The mesoporous supports exerted steric effects on unleached active sites, lowering chain walking ability, and producing polymers having lower short chain branch density. Replication of the particle morphology was observed in some polymer product.

2.7.1.2. Other Supported Catalysts

Amorphous and porous silica at present constitute the best support for metallocenes and MAO as cocatalyst because they possess high surface area and high porosity, have good mechanical properties, and are stable and inert under reaction and processing conditions (Fink et al., 2000). In addition to the classic MgCl$_2$ and Al$_2$O$_3$, less common supporting materials have been used as support materials; examples are zeolites and polymeric aluminoxanes. Attempts have also been made to imitate the surface of silica by using cyclodextrin (Lee and Yoon, 1999), chitosan (Eberhart et al., 2001) and polysiloxane derivertives. Most recent experiments employ cross-linked polystyrene as supporting material for metallocene catalysts. Many of these supports yield good polymer morphologies but had lower activities than the silica supported catalysts. Some findings with these non-silica supports are reviewed below.

Magnesium chloride (MgCl$_2$), a widely used support in conventional Ziegler-Natta catalysts (Jaber and Ray, 1993a, 1993b, 1993c, and

1993d), but it has been studied far less extensively than silica as a carrier for single-site catalysts (Sensarma and Sivaram, 1999). The surface chemistry of γ-alumina has also been studied in terms of dehydroxylated alumina (DA) and partially dehydroxylated alumina (PDA) and used as supports for polymerization.

Soga and Kaminaka (1994) copolymerized ethylene and propylene with SiO_2-, Al_2O_3-, $MgCl_2$- supported metallocene catalysts. Random copolymers were obtained ($r_1*r_2 \leq 1$). The content of comonomer incorporated was in the order of $SiO_2 \sim Al_2O_3 > MgCl_2$. Harrison et al. (1998) compared silica and alumina as supports with methyl- aluminoxane and a variety of metallocene dichloride complexes. Aluminas derived from calcinations of sol-gel precursors feature high degrees of surface hydroxylation in comparison with commercially available silica of similar surface area and total porosity so that they provide a mechanism for increasing the amount of aluminoxane on the supports and result in higher activities.

The polymerization of ethylene performed in hexane using supported zirconocene catalysts with varying support compositions SiO_2-MAO-$Me_2Si(Ind)_2ZrCl_2$ + TIBA (I), $MgCl_2$-MAO-$Me_2Si(Ind)_2ZrCl_2$ + TIBA (II) and a homogeneous $Me_2Si(Ind)_2ZrCl_2$ + MAO was investigated by Echevskaya et al. (2001). Molecular structure of the resulting PE, studied by IR and ^{13}C NMR spectroscopy was investigated. The examined catalytic systems differ in their activity and ability to control the molecular mass of the resulting polymer. The homogeneous catalyst and catalyst (I) produced PE containing ethyl branches along with the end methyl groups in the low molecular mass fractions. On the other hand, PE prepared with supported catalyst (II) was devoid of ethyl branches but contained vinyl groups as the main type of unsaturation.

Chien and Hsieh (1996) prepared a series of catalyst systems containing R_4Ti, R_3TiCl (R = benzyl, *p*-methylbenzyl) and $Cp_2M_{tr}(CH_3)_2$ (M_{tr} = Ti, Zr, Hf) supported on alumina, zeolite, silica, Mg(OH)Cl, $Ca(OH)_2$ and polyvinylalcohol and used them to polymerize ethylene as well as propylene, the latter to isotactic polypropylene.

Crystalline zeolites have a large surface area, a well-defined pore structure and a very narrow pore size distribution, Woo et al. (1995) investigated the suitability of this group of materials as supports. In one catalyst, NaY (pore diameter 5 Å) was first modified with MAO, filtered, dried, and then impregnated with Cp_2ZrCl_2. It was tested using an additional amount of MAO in slurry-phase ethylene polymerization. Without the additional MAO injection there was virtually no polymerization. At an optimum amount of MAO, the catalyst shows 0.016 of the activity of Cp_2ZrCl_2-MAO mixture in solution (zeolite support: 200 kg polymer/[mol Zr·atm·h]; homogeneous: 12500 kg polymer/[mol Zr·atm·h]). The low activity may be due to a small number of cages capable of accommodating both catalyst components, or to a smaller rate constant of propagation, or a limitation of the monomer diffusion to active sites. There is virtually no activity decay at 50°C indicating no migration of active species from one cage to another. Polymerization at 70°C has a four times greater initial activity but suffers a factor of two loss of activity within 30 min, which was attributed to intercage diffusion and deactivation at this temperature. NaY pretreated with TMA instead of MAO was not an active support material.

Y zeolites with different sodium contents and a sodium mordenite were evaluated as support for Cp_2ZrCl_2 as catalysts for ethylene polymerization in toluene medium. Marques et al. (1997) found that, although the activities of the supported catalysts were much lower than those of the homogeneous system, the average molecular weight of the polyethylene produced from the former was in general much higher than that of the polymer produced in solution. Contrary to the expected trend that the specific area was the dominant factor for catalytic activity, the best catalyst was the one supported on NaM zeolite sodium mordenite. Thus, the results indicate that the concentration of framework aluminum atoms was the dominant factor, but that the contribution of the external surface was also important. Simone et al. (2001) evaluated this zeolite for further work. They observed that high amounts of zirconium incorporated on the support lead to catalysts with lower activity, but these supported catalyst was able to produce polymer with high molecular weights.

Meshkova et al. (2000) fixed aluminoxanes on the Na-form of ZSM-5 (Si/Al = 42) by partial hydrolysis of trimethylaluminum (TMA) with water which was present inside the zeolite. It was shown that aluminoxanes synthesized on zeolite surface form the heterogenized complexes with Cp_2ZrCl_2 and $Et[Ind]_2ZrCl_2$ which have long-term activity for ethylene polymerization without addition of other aluminiumorganic cocatalyst. The activation energy of ethylene polymerization in the presence of ZSM-5(H_2O)/TMA-Et[Ind]$_2$ZrCl$_2$ was equal to 32 kJ/mol. Molecular weight and melting point of polyethylene obtained with such zeolite supported zirconocene catalysts were higher than those formed with appropiate homogeneous metallocene systems.

Cyclodextrins are a family of oligosaccharides derived from starch. Lee and Yoon (1994) used organic supported as α-cyclodextrin (CD) for preparing supported catalysts in order to perform ethylene polymerization. The cyclodextrin was previously treated with modified methylaluminoxanes (PMAO; Al=7.56 wt% or MMAO; Al=12.5 wt%) or trimethylaluminum (TMA), and then Cp_2ZrCl_2 was supported on the modified cyclodextrin by using triethylaluminum (TEA), trimethylaluminum (TMA) or MMAO as cocatalyst. When Cp_2ZrCl_2 was anchored on CD/PMAO, CD/MMAO or CD/TMA, polymerization could be initiated with the ordinary trialkylaluminum, such as TMA and TEA. From this study, it was found that the molecular weight (Mw) of polyethylene (PE) obtained with CD-supported catalysts were 30 times greather than with unsupported catalyst and molecular weight distribution (MWD) presented a narrow polydispersity index (2.3-2.5). They also treated CD with either MAO or TMA. The former contained 9.1% Al, while the latter had 2.6% Al. The treated supports were both impregnated with Cp_2ZrCl_2. Activation with AlR_3 resulted in modest ethylene polymerization activities, 5 to 9 x 10^5 g PE/(mol Zr·h·bar).

Clays such as montmorillonite, hectorite, and mica have also been employed as carriers for single-site catalysts. The alkylaluminum acts only as an alkylating agent for the metal component; active catalysts were obtained when Cp_2ZrMe_2 was contacted with clays impregnated with tertiary ammonium cations without further recourse to alkylating agents or scavengers (Hlatky, 2000).

Several kinds of polystyrene-supported metallocene catalysts were prepared and used in the polymerization of propylene and ethylene with methylaluminoxane (MAO) as cocatalyst by Nishida et al. (1995). It was found that these catalysts are stable even at 70°C. They display fairly high activities when the polymerizations are conducted at high temperature. A novel polymer supported metallocene catalyst with crosslinked poly (styrene-co-acrylamide) (PSAm) as the support has been prepared and characterized by Liu et al. (1999). Ethylene/α-octene copolymerization was carried out and found that the catalytic activity is not markedly affected by adding α-octene. ^{13}C NMR analysis of the ethylene/ α-octene copolymer indicated that the composition distribution of the copolymer is uniform. Recently, Zhou et al. (2003) investigated the gas-phase homopolymerization of ethylene and the copolymerization of ethylene/1-hexene $(n\text{-BuCp})_2ZrCl_2$ supported on MAO-treated spherical polystyrene-divinyl benzene particles. The catalysts had high activity and produced product with excellent morphology (Zhou et al., 2003).

Poly (styrene-co-divinylbenzene) beads supported *rac*-$Ph_2Si(Ind)_2ZrCl_2$ was prepared and tested as a catalyst for ethylene polymerization using methylaluminoxane (MAO) in toluene medium by Hong et al. (1998). The catalyst showed resonably high activity to give polyethylene beads replicating the shape of carrier at polymerization temperature below 100°C. With increasing polymerization temperature up to 150°C, the catalyst activity increased drastically but the spherical shape of polyethylene disappeared due to the melting. Meng et al. (1999) investigated the effect of several factors (time, temperature, Al/Zr and the mode of feeding) on the activity of the catalysts using poly(styrene-co-4-vinylpyridine) as the supports for zirconocene catalyst in slurry-phase ethylene polymerization. The activity of the catalysts sharply increased with either the degree of crosslinking or the content of 4-vinylpyridiene in the support.

2.7.2. Supported Metallocene Catalyst Procedures

Recent developments concerning the preparation, structure and nature of active sites in supported metallocene-based catalysts have been reviewed in several papers (Ribeiro et al., 1997; Kristen, 1999; Hlatky, 2000; and Kaminsky and Laban, 2001) The performance for ethylene and propylene polymerizations of various supported metallocene systems and final polymer properties are compared and discussed on the basis of the different catalyst preparations and polymerization conditions. According to these comprehensive reviews, the different methods of heterogenization are possible and can be mainly divided into three general methods according to Kaminsky and Laban (2001). These three methods are conceptually described and illustrated in Figure 2.15.

(I). In the method of direct heterogenization, the metallocene or a mixture of the metallocene and MAO is anchored via physisorption or chemisorption onto the support. In this first class, the metallocene must be activated by external MAO.

(II). The metallocene can be supported by covalent bonding of its ligand environment to the support followed by activation with external MAO. The metallocene can be synthesized gradually as a covalent bonded species direct on the supporting material.

(III). Initial impregnation of MAO onto supports followed by adsorption and simultaneous activation of the metallocene (indirect heterogenization). In analogy to the homogeneous metallocene catalysis, the bonding between the active species $[Cp_2ZrCH_3]^+$ and the supported MAO is ionic. When performing the method indirect heterogenization, no further MAO has to be added.

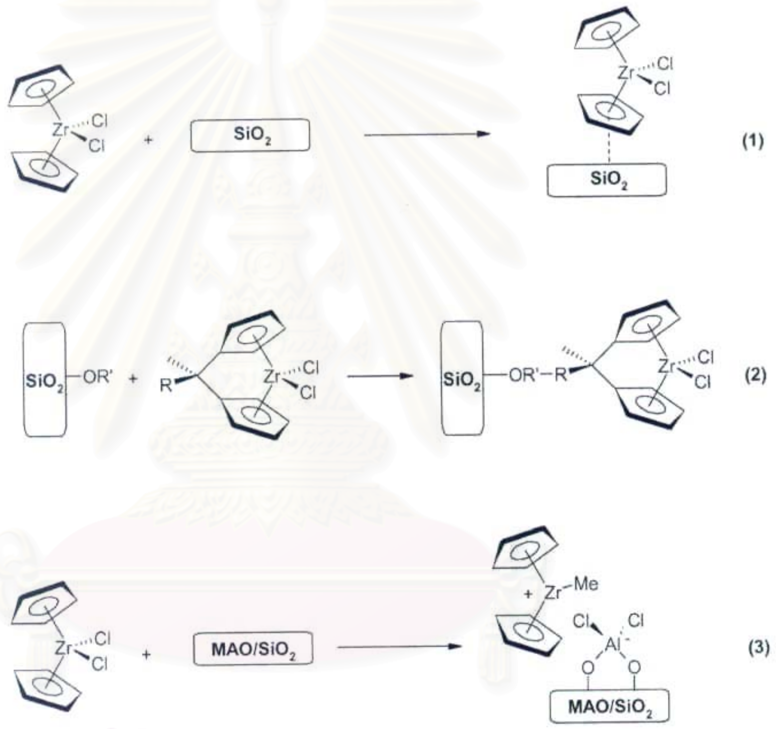

Figure 2.15. Supporting methods of metallocenes: (1) direct heterogenization, (2) covalent bonding on the support, (3) indirect heterogenization (Kaminsky and Laban, 2001)

Metallocenes supported according to the method of direct heterogenization (1) have been known to produce polymers with higher molecular weight than those obtained with homogeneous catalysts. However, direct heterogenization (2) has also been known to change the polymerization characteristics of the metallocene, possibly by the interaction with surface hydroxyl groups.

Difficulties can also be encountered in the covalent bonding of metallocene complexes. A mixture of different active species can be obtained if the metallocene complexes are successively synthesized on the support on chemically non-uniform anchor groups, such as vicinal and geminal silanol groups. The most promising method of supporting is indirect heterogenization (3) since the chemical nature of the metallocene is changed only to a small degree, if at all. The polymers obtained by the method of indirect heterogenization are very similar to those obtained by the homogeneous system. Each metallocene on the support forms an active center and the starting point for the growth of a polymer chain (Kaminsky and Laban, 2001). The preparation of supported catalysts by modifications of the surface of the support for the three basic methods have been widely investigated. The resulting catalysts have usually been evaluated slurry-phase polymerization with various modified silicas as the support. Another method to produce highly active polymerization catalysts consists of a one-step immobilization of a preactivated MAO/metallocene complex on a porous SiO_2 support. The activities and the polymer growth can be influenced by concentration and the viscosity of the organic solvent/diluent (Steinmetz et al., 1997).

Tait et al. (2000) reported part of a comparative investigation into the essential characteristic of some model soluble and supported metallocene catalyst systems when used along with MAO as cocatalyst for the slurry-phase polymerization of ethylene and propylene. The effect of preparation procedures on the catalyst activities was investigated and found that the temperature of dehydration, affecting the concentration of surface hydroxyl and siloxane groups, has a significant effect on the activities of silica supported metallocene catalyst. The use of lower dehydration temperature, 260°C, favors the formation of more active catalysts. These results suggest that a certain optimum concentration of hydroxyl groups, controlled by dehydration temperature, is needed to anchor the necessary layer of adsorbed MAO on the surface of the silica. It has been established that the order of reaction of silica, metallocene, and MAO affects the kinetic behavior and activity of supported metallocene catalysts. The results of a series of propylene polymerizations using $SiO_2/Et(Ind)_2ZrCl_2$, $SiO_2/Et(Ind)_2ZrCl_2/MAO$, $SiO_2/MAO/Et(Ind)_2ZrCl_2$, and $SiO_2/MAO/Et(Ind)_2ZrCl_2/MAO$ supported catalysts containing similar zirconium contents are presented by Tait (2000). The $SiO_2/MAO/Et(Ind)_2ZrCl_2$ had the highest activities at the conditions studied. Similar experiments with the variation of the MAO addition with Cp_2ZrCl_2 catalysts was performed. For this case as well, the

MAO addition to the SiO_2 before the Cp_2ZrCl_2 addition resulted in the highest activities.

The optimization of a silica supported bis(butylcyclopentadienyl)-zirconium dichloride catalyst for ethylene polymerization in slurry phase was studied by Santos et al. (1999a). The preparation parameters, namely silica activation temperature, grafting temperature, and grafting time were evaluated in terms of metal content on silica and ethylene homopolymerization activity. In the activation temperature range between 373 and 723 K, silica surface saturation in Zr was found to be around 0.34 wt.% for Zr/SiO_2. Silica pretreated at higher temperatures led to higher activity, producing polymers with higher M_v and lower polydispersity, probably due to the existence of isolated and very stable catalyst centers. The grafting reaction on the surface of silica was seen to be immediate, since the minimum contact time was already enough to immobilize some zirconocene. Grafting times longer than 6 h led to higher metal contents, but reduced the extent of active sites. A similar trend was observed with respect to the grafting temperature.

Supported metallocene catalysts prepared by a conventional adsorption method produced a polyethylene with a wide particle size distribution and an undesirable amount of fine particles. Lin (2000) found that the preparation of supported metallocene catalyst by a pre-mixing method produced a polyethylene of larger granular size with fewer fine particles than that prepared by the conventional adsorption of metallocene on a MAO-coated SiO_2 surface.

A series of heterogeneous catalyst systems was prepared by the immobilization of $(n\text{-BuCp})_2ZrCl_2$ on silica supports activated at different temperatures; the catalysts were evaluated in terms of retained metal loading and activity in ethylene slurry homopolymerization (Santos et al., 1999b). The highest metal loading (0.48 wt.% Zr/SiO_2) was achieved with silica treated under vacuum at room temperature (298K), but the catalyst showed very low polymerization activity, which may be attributed to a large number of inactive Zr-support bidentate species formed at a high surface density of OH in silica. The presence of bulky ligands in the catalyst molecule seems to prevent the remaining OH groups from reacting with additional metallocene complexes, keeping the metal loading around 0.35 wt.% Zr/SiO_2 for silica activated between 373 and 723 K. Practically all the prepared systems presented activity in ethylene polymerization with MAO as cocatalyst. The highest activity [5.1×10^5 g PE/(molZr·h)] having been obtained with silica dehydroxylated at 723 K.

The heterogenization of biscyclopentadienyl-zirconium dichloride (Cp_2ZrCl_2) on thermally and chemically treated silica surface was studied by Brandao et al. (2000). The sequence used for treating the silica support, thermally treated and untreated, by the addition of silica to TMA solution and the addition of TMA to silica was investigated. In term of activity, the addition of thermally treated silica to TMA gave the best supported catalyst. This is in agreement with the assumption that residual silanol groups on the silica surface cause activity loss. In addition, the supported catalysts when activated with a cocatalyst composed of equal parts of TMA and methylaluminoxane (MAO) had activity about twice that of the pure MAO as cocatalyst. On the other hand, TMA alone, at any concentration, always had a deleterious effect on the metallocene activity.

Ferreira and Damiani (2001) described several methods of preparing supported $Et[Ind]_2ZrCl_2$ (EBI) on SiO_2/MAO, varying the washing step durations and washing step temperatures. The activity of the supported catalysts EBI/MAO/SiO_2 decreases to one third of the soluble catalyst EBI/MAO with the same Al/Zr molar ratio. Zr contents higher than 0.7% produce catalysts with lower productivities and MAO coverage and SiO_2 that is higher than a monolayer is probably not useful for stabilizing the zirconocene on the SiO_2/MAO support.

The influence of the preparation conditions of MAO treated SiO_2 supported Cp_2ZrCl_2 catalyst on ethylene polymerization was investigated by Marques and Conte (2002). Temperature of catalyst preparation, washing method of the catalytic solid, MAO and metallocene concentration in the support treatment, time of MAO, and metallocene immobilization on the support, type of alkylaluminum used in the support pretreatment, and calcination temperatures of the support were investigated. Enhancing the temperature of MAO support pretreatment from room temperature to 70°C, and evaporating the Cp_2ZrCl_2 solution after its immobilization prior to washing, resulted in a significant enhancement of the catalyst activity. According to the results, the activity of some supported catalysts were far higher than with the homogeneous system. Moreover, polyethylene with high molecular weights and broader molecular weight distribution than those produced with the homogeneous precursors was obtained.

In addition to the three basic methods, some researchers have reported a new immobilization method by modification of the support by introducing a spacer group between the support and metallocene such as $(CH_3)_3SiCl$, $Cl_2Si(CH_3)_2$, polysiloxane (Arai et al., 1997).

Supported catalysts for ethylene polymerization have been prepared by interaction of Cp_2ZrX_2 (Cp = η^5-C_2H_5, X = Cl or CH_3) with silica chemically modified by $(CH_3)_3SiCl$ (TMCS) or trialkylaluminum compounds (TEA and TIBA) (Moroz et al., 1998). The $Cp_2Zr(CH_3)_2/SiO_2$-TMCS catalyst showed a fairly high activity in ethylene polymerization (30-300 kg PE(mol Zr·h·bar)$^{-1}$) even in the absence of addition of any cocatalysts. The addition of the cocatalyst (MAO or TIBA) led to a further increase in the activity of the supported catalysts. Polyethylene obtained with the $Cp_2Zr(CH_3)_2/SiO_2$-TMCS catalyst without any cocatalyst consisted of uniform polymer particles of a shape replicating that of the silica particles, whereas the shapeless aggregates of finely dispersed polymer particles similar to those usually obtained with homogeneous systems were produced with the same supported catalyst in the presence of the MAO cocatalyst.

New supported ($CpIndZrCl_2$) catalyst anchored on silica with trisiloxane spacer (ZATS) and a pentamethylene spacer (ZAPM) were prepared and used for ethylene polymerization in toluene with modified methylaluminoxane (MAO) as cocatalyst. ZATS and ZAPM produce polyethylene with lower molecular weight but showed higher activity than silica-supported $CpIndZrCl_2$, which was prepared by reacting zirconocene directly with silica. Introducing a spacer between silica surface and metallocene species enhances the activity of silica-supported $CpIndZrCl_2$ (Lee and Yoon, 1997).

Soga et al. (1993) prepared modified SiO_2 by reacting SiO_2 with $Cl_2Si(CH_3)_2$ in toluene, on which MAO was supported to obtain a catalyst precursor. The MAO-free catalyst system composed of the modified SiO_2 and Cp_2ZrCl_2 surprisingly was found to be activated by common trialkylaluminums. Silica supported (n-BuCp)$_2$ZrCl$_2$/MAO catalysts were synthesized by Kamfjord et al. (1998) according to the incipient wetness method from a solution of metallocene in a liquid monomer. The monomer was allowed to polymerize yielding a catalyst containing polyhexene (PH), polystyrene (PS) or polyoctadiene (PO). The catalysts were used to polymerize ethene in heptane at 70°C and 4 bar total pressure. The highest average activities were 8600 kg PE/(mol·Zr·h) for (n-BuCp)$_2$ZrCl$_2$/MAO/PS/SiO$_2$ using TEAL as activator. TIBAL, at the same Al/Zr ratio, resulted activities, which were 3 times higher than those with TEAL. The PH, PS, and PO in the catalyst form a protective layer around the active sites. Even after exposure to air for five hours these catalysts retain some polymerization activity.

In order to overcome the preparation complexities of traditionally supported metallocene catalysts, Chu et al. (2000) have developed a novel in situ supported Et[Ind]$_2$ZrCl$_2$ catalyst, which eliminates the need for a supporting step before polymerization. This catalyst has good catalytic activity, produces polymer with good morphology and high bulk density and does not cause reactor fouling. In situ supported catalysts are made by contacting a soluble metallocene with MAO-treated silica (SMAO) directly in the polymerization reactor just before pressurizing with monomer. Notice that polymerization starts immediately after adding the metallocene to SMAO i.e., there is no separate step for metallocene supporting, which make this polymerization technique very easy for use in laboratory scale reactors. No additional MAO is required, since in situ supported catalysts can be activated with common alkyl aluminum, trimethyl aluminum. They found that in the absence of TMA, in-situ-supported Et[Ind]$_2$ZrCl$_2$ was not active, but the addition of TMA during polymerization activated the catalyst. Et[Ind]$_2$Zr(CH$_3$)$_2$ was active even in the absence of TMA, whereas the addition of TMA during polymerization enhanced the catalytic activity. The polymerization rate profiles of the in situ supported metallocene catalysts did not show rate decay as a function of time. A polymerization mechanism of this system was proposed. The in situ supported metallocene catalysts may deactivate, but homogeneous metallocene species present in the reactor may form new active sites and compensate for deactivated sites. As the Al/Zr ratio (Al present in SMAO) increases, the catalytic activity increases. At high Al/Zr ratios, the ethylene feed rate decrease with time because there are less soluble metallocene species in the reaction medium. The Al/Zr molar ratio did not affect Mw and MWD of the polymer. The catalytic active sites are uniform and only one type of active species exists in the reaction system with in situ supported metallocene catalyst. The catalytic activity of the in situ supported Et[Ind]$_2$ZrCl$_2$ was less sensitive to TMA/SMAO mole ratio.

Chu et al. (1999) carried out the copolymerization of ethylene and 1-hexene with different catalysts (homogeneous Et[Ind]$_2$ZrCl$_2$, supported Et[Ind]$_2$ZrCl$_2$, and in situ supported Et[Ind]$_2$ZrCl$_2$). The in-situ supported metallocene catalyst showed higher activity than the corresponding supported metallocene catalyst. At the same polymerization conditions, the relative reactivity of 1-hexene increases in the following order: supported metallocene ~ in situ supported metallocene < homogeneous metallocene. The molecular weights of the produced copolymers with the three different catalysts were similar, but the MWD of the copolymer made with the in situ supported metallocene was broader than that of those made with the other catalysts. The short chain branching distribution indicated that there were at least two different active species present in the in-situ supported metallocene catalyst for the copolymerization of ethylene and 1- hexene.

Fink et al. (2000) have developed a technique, which immobilizes the active compounds on a spray-dried silica support by utilizing a fluidized bed reactor. They claimed to produce supported metallocene catalysts with a controllable distribution of active centers by using three different supporting methods. A new method for the preparation of heterogeneous catalysts was proposed with this approach of self-immobilizing metallocene catalysts. The metallocenes containing alkenyl substituents are incorporated as comonomers into the formed polyolefin chain (Alt, 1999).

2.8. Ethylene Polymerization and Copolymerization with Supported Metallocene Catalyst Systems in Slurry Phase and Gas Phase

The above review has shown that supported metallocene catalysts have been widely studied. The main aim of many of these studies was to make metallocene catalysts suitable for slurry-phase and gas-phase polymerization and copolymerization. It is very important to consider the details of both processes with supported metallocene catalysts. Factors affecting polymerization in slurry and gas phase will be described in this section. Most of the ethylene polymerization studies with metallocene catalysts have been performed with homogeneous catalysts, and the vast majority of the studies with supported metallocene have been performed in the slurry mode. Gas-phase polymerization is a common ethylene polymerization process due to its relative simplicity, flexibility, as well as low cost, in addition, it is predicted that the majority of mLLDPE will be produced with gas-phase processes. However, there is a lack of information in the open literature that can be used for the design of gas-phase polymerization with supported metallocene. Hence, it is important to provide more investigations dealing with gas-phase polymerizations with supported metallocene catalysts.

Gas-phase polymerizations of propylene with a solid complex catalyst obtained from Et(Ind)$_2$ZrCl$_2$ and methylaluminoxane without support have been carried out by Tsutsui and Kashiwa (1991). The resulting polymer had structurally similar features to that obtained in toluene liquid-phase polymerization with a soluble Zr catalyst. They suggested that this observations implies that the solid Zr complex catalyst in gas-phase polymerization has the same type of active centers as the soluble Zr catalyst system. Roos et al. (1997) were among the first to report detailed gas-phase ethylene polymerization results, including activity profiles, for silica supported metallocene (*rac*-Me$_2$Si[Ind]$_2$ZrCl$_2$)/MAO catalyst. Triethylaluminium (TEA) and NaCl were used as scarvenger and seedbed, respectively. The variation of polymerization temperature in the range of 40-80°C was reported. They found that the polymerization rate and the rate of deactivation increase with increasing temperature and the deactivation could be modeled using a first order dependence with respect to the polymerization rate. The reproducibility of the average catalyst activity was rather good within 10 % for low polymerization temperature. More studies of ethylene homopolymerization and copolymerization of ethylene/1-hexene for gas- and slurry-phase process over alumina- and silica-supported metallocene catalysts were carried out but no detailed gas-phase results were reported (Harrison et al., 1998).

Metallocene catalyst applications in manufacture of polyethylenes and high-impact polypropylenes in gas phase polymerization processes were discussed by Hamielec and Shouli (2000) on the topic of impact properties (bulk density, powder flowability and impact strength). Results on the polymerization of 1,3-butadiene with supported half sandwich-titanium-complexes in the gas-phase polymerization were also presented by Kaminsky and Strubel (2000). A novel molecularly hybridized polyethylene/silica composite thin film was obtained by the gas-phase polymerization of ethylene with a titanocene-mounted mesoporous silica layer on a mica plate with mesoscopic pores arranged on the film surface. However, when a glass plate with an islanded mesoporous silica on its surface was used, the resulting polyethylene/silica composite material was also islanded. These are two examples of a potential a new strategy of template-assisted polymerization for the processing and fabrication of molecularly hybridized organic/inorganic polymer composite materials (Tajima et al., 2000). Recently Ray and co-workers (Chakravarti et al., 2001a and 2001b; Xu et al.,

2001) published detailed kinetic results for ethylene/propylene and ethylene/1-hexene copolymerization in the gas phase over silica / methylaluminoxane (MAO) supported metallocene catalysts, but no details about the catalyst used nor the properties of PE produced were provided. Both temperature and comonomer effects on the kinetics ethylene-propylene copolymerization were investigated. With increasing temperatures, the magnitude of the reaction rate peak increased for both homopolymerization and copolymerization. The presence of the comonomer had a positive effect on the intrinsic reaction rate of ethylene. The comonomer and temperature effects observed in ethylene/1-hexene kinetics were found to be qualitatively similar to that observed for ethylene/propylene. The reaction rate order with respect to ethylene was found to be close to 1 in the presence of 1-hexene.

A new method was used to study the effect of light on the activity using metallocene catalysts supported on silica in the gas-phase polymerization of ethylene with video microscopic in the presence of visible light. Kallio et al. (2001) observed that halogen light has a significant effect on the polymerization activity of silica-supported metallocene catalysts. Three different metallocene catalysts have been tested in the gas-phase polymerization of ethylene. Surprisingly, the effect of activation depends not only on the type of transition metal, but also on the wavelength and intensity of the light. The activation by light was found to be a reversible process.

Tannous and Soares (2002) investigated the influence of polymerization conditions on the gas-phase polymerization of ethylene using a supported metallocene catalyst (Cp_2ZrCl_2/SiO_2); they used both 1 L semi batch autoclave reactor and 0.6 L glass reactor in their studies. The results demonstrated that several factors [pre-contacting time of the catalyst and cocatalyst (both MAO and TMA), catalyst injection, agitator design, hydrogen volume, polymerization temperature as well as pressure] were crucial to obtain well-controlled gas-phase polymerization. SEM analysis showed that irregular growth of polymer within shells often produced polymer particles of irregular shape. The molecular weight distributions were broad and sometimes multimodal. The use of hydroxyalted chloromethylated-styrene/divinylbenzene copolymers as a support for metallocene catalyst was examined for the polymerization of ethylene in gas phase using a horizontal reactor. The results presented by Chung et al., 2002 indicated that the temperature is the most important factor affecting the polymerization for three different types of metallocene catalyst (Cp_2ZrCl_2, $[Ind]_2ZrCl_2$, and $(CH_3)_2Si[Ind]_2ZrCl_2$). The pressure seems to show a negative effect and the kinetic studies reveals that the catalysts probably contain two types of active sites.

Quijada et al. (1998) studied the influence of reaction parameters on catalytic activity in the slurry polymerization of ethylene using supported and unsupported metallocene catalysts (Et[Ind]$_2$ZrCl$_2$ and [Ind]$_2$ZrCl$_2$). The catalytic activities of two metallocene compounds in homogeneous polymerization system depend heavily on certain parameters, such as Zr concentration, type of the reactor, and stirring speed. In the case of heterogeneous catalysts of the same metallcoenes, the most pronounced influence is related to the type of support and its porous nature. For good morphology control, the shapes of the final polymer particles are replicas of shapes of the original catalyst (supports) particles. Junior et al. (2002) carried out ethylene polymerization with homogeneous Cp$_2$ZrCl$_2$/MAO systems. They obtained the highest value of catalyst activity at 60^{o}C when a [Al]/[Zr] molar ratio = 500 was employed. Further increase of this ratio did not show a significant increase in the activity. Bianchini et al. (2002) evaluated the effect of Al content on MAO-modified silicas on catalyst activity, on polymer properties, and on residual metal content in the resulting polyethylenes. MAO-modified silicas were prepared by impregnating MAO toluene solutions in concentration range between 0.5 and 20.0 wt% Al/SiO$_2$. Using external MAO as cocatalyst (Al/Zr = 2000), no difference in catalyst activity was observed by Junior and co-workers. Nevertheless, for Al/Zr = 500, catalyst activities were shown to be higher for supported zirconocene systems containing 0.0-2.0 wt% Al/SiO$_2$ range. Polymers with two Tm peaks were obtained with catalysts prepared with 10.0 wt% Al/SiO$_2$ and 20.0 wt% Al/SiO$_2$.

Liu and Rytter (2001) used the dual site Cp$_2$*ZrCl$_2$/ Et[IndH$_4$]$_2$ZrCl$_2$ metallocene catalyst system with a mixture of MAO and TMA as the cocatalyst in slurry polymerization mode. Polymer properties can be controlled by the amount of TMA added, monomer pressure, polymerization temperature, and the addition of hexane or hydrogen. TMA is suggested to be partly coordinated to the active sites, thereby enhancing termination, increasing comonomer incorporation, but also partially blocking coordination and chain transfer to hydrogen.

Santos et al. (1999) evaluated the effects of slurry phase ethylene polymerization conditions i.e. Al/Zr molar ratio, reaction temperature, monomer pressure, the age and concentration of the catalyst, on the production of polyethylene by silica supported (*n*-BuCp)$_2$ZrCl$_2$ grafted under optimized conditions and cocatalyzed by methylaluminoxane. The best polymerization conditions include an Al:Zr mole ratio of 2000, 60°C, and 4 atm of ethylene pressure. Comparing properties of PEs produced by the supported catalyst and those obtained with the homogeneous system, it seems that the immobilized zirconocene remains attached to the silica surface during the polymerization reactions. Catalyst leaching by MAO, if present at all, seems to be minor. For aging catalyst results, the developed catalyst system remained active 6 months after preparation, but was sensitive to the air. Although showing lower activities than those observed in toluene, polymerization reactions in aliphatic milieu were successful after adding TIBA to MAO. For the supported system, a 1:1 optimum ratio was observed, while $(n\text{-BuCp})_2\text{ZrCl}_2$ in homogeneous milieu required a 3:1 ratio of MAO:TIBA for the best performance.

The effect of polymerization medium on the activity and kinetics of ethylene polymerization was studied by Tait et al. (2000) using a number of catalysts. Typical results for catalyst system SiO_2/MAO/Cp_2ZrCl_2-MAO are reported for polymerization in toluene, pentamethylheptane, and mixtures of both. It is evident that the nature of the polymerization medium can have a significant effect on the activity of the metallocene catalyst system, the more polar medium the higher the polymerization activity. For supported catalyst systems the effect is not limited only to activity since the nature of the polymerization medium also affects the stability of the catalyst system, the more active systems (in more polar solvents) being less stable. The effect of variation of MAO concentration using supported metallocene catalyst systems on ethylene polymerization was also reported. It is evident that both the average rate and the maximum rate of polymerization increase initially with an increase in the concentration of external MAO. It was also found that significant amount of leaching of zirconium took place in the presence of MAO when a supported metallocene catalyst was used in slurry polymerization. The schematic representation proposed for the leaching when using SiO_2/MAO toluene-MAO catalyst systems is shown in Figure 2.16. Similar behavior of catalyst leaching with supported catalyst systems was also observed. Semikolenova and Zakharov (1997); they found that the interaction of supported metallocene catalysts with methylaluminoxane leads to desorption of the metallocene compound from the surface of the support and the formation of highly active homogeneous complexes.

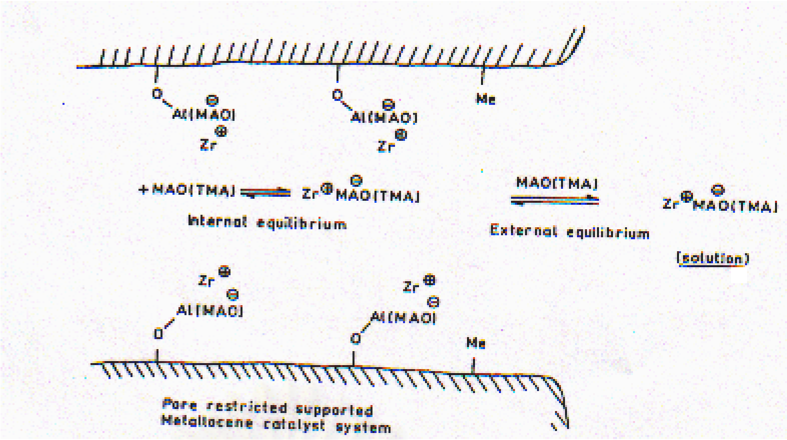

Figure 2.16. Schematic representation of the leaching behavior (Tait et al., 2000)

When heterogeneous catalysts are considered, it is important to consider the interactions of the metallocene catalyst and the cocatalyst with the support structure and its effect on the morphology of the polyolefin particles. Thus, while considering modeling of the particle growth and morphology development during polyolefin synthesis by supported metallocenes, it is necessary to incorporate the effects of metal extraction (Naik and Ray, 2001). The state of the art of particle models for olefin polymerization has been reviewed by many authors (Ha et al., 2001; Mckenna and Soares, 2001; and Yiagopoulos et al., 2001). The particle growth, polymerization rates, concentration and temperature radial profiles, polymer microstructure, and morphology are addressed in these models.

Haag et al. (2001) evaluated the effects of heterogenization parameters on compositional and catalytic properties of $Et[Ind]_2ZrCl_2$ supported on silica modified with MAO. Both MAO and $Et[Ind]_2ZrCl_2$ concentrations during preparation affected the final Al/Zr ratio on silica. The catalyst systems were tested for ethylene/propylene copolymerization using external MAO as cocatalyst. The Al/Zr ratio on silica influenced the average ethylene incorporation. Catalyst systems with given Al/Zr ratios yielded different crystallites, suggesting a plural distribution of chemical composition. This observation provided some insight into the nature of the active sites, which frequently are referred to as a single-site catalysts. Frauenrath et al. (2001) also found more than one active site. They investigated the nature of the active species in zirconocene/MAO catalyzed polymerizations. Varying monomer concentration and monomer conversion did not result in any unexpected behavior.

However, changing catalyst and cocatalyst concentration lead to broadened, or even bimodal MWD under certain reaction conditions. These results may be interpreted in terms of a coexistence of two active species with different rates of propagation and of termination.

Britto et al. (2001) tested copolymerization ethylene/1-hexene in hexane with Et[Ind]$_2$ZrCl$_2$/MAO in the presence of TIBA. Increasing the TIBA concentration, increases the MAO solubility in the polymerization milieu; this results in increased catalyst activity and comonomer incorporation. They provided additional suggestions that the presence of the comonomer may result in more amorphous product which results in increases in monomer solubility in the products. These factors increase the accessibility of monomers to the catalytic sites. Additional similar evidence is provided in the next section.

Shan et al. (2000) observed that the in situ supported Et[Ind]$_2$ZrCl$_2$ can be used with different alkylaluminum activators to produce poly(ethylene/1-hexene) with narrow MWD, yet broad and bimodal short chain branch distribution (SCBD). These findings are different from the ones observed with homogeneous systems and have not been previously reported for supported systems. It has been shown that, with the use of individual and mixed activator systems, it is possible to manipulate the SCBDs of the resulting copolymers while maintaining similar MWDs. Attempts to make predictions of the resulting SCBDs for a mixed activated system is difficult to quantify, since the behavior of the sites can be altered in the presence of mixtures of activators.

2.9. Polymer Characterization

There are two major aspects in which metallocene catalyst differs from conventional heterogeneous Ziegler-Natta catalysts (Reddy and Sivaram, 1995; Hamielec and Soares, 1996; Morse, 1998). For instance, all transition metal atoms are active in homogeneous metallocene systems and only a one type of catalytic site is present in a homogeneous system under proper conditions. Due to the single-site nature, metallocene catalysts can produce polymers with a sharp melting temperature, and narrow molar mass distribution which approaches the theoretical polydispersity value of 2.0 predicted by the Schultz-Flory mechanism. For copolymerization, metallocene catalyst can produce copolymers with an almost random incorporation of comonomers, which results in a maximum decrease in polymer crystallinity for a given amount of comonomer incorporation (Reddy and Sivaram, 1995; Hamielec and Soares, 1996).

Another primary advantage of metallocene catalysts is that it is possible to "tailor" the molecular architecture of the LLDPE by varying ligands in catalyst or polymerization conditions to provide the properties that are required for a particular application. This represents a major advance in capability for the polymer production, from a situation with Ziegler-Natta and Phillips catalyst. Although the metallocene LLDPE suffers from processability problems due to the narrower MWD, it is likely that blending such polymers with LDPE, developing supported system or incorporating long chain branching in the polymer backbone will overcome this problem. It is predicted that metallocene LLDPE with much improved product performance will gradually replace high pressure low density polyethylene and Ziegler-Natta linear low density polyethylene, particularly in film applications (Richard, 1998).

The properties of a polymer in the solid state and also in the molten state depend on its molecular structure. A variety of LLDPEs, which differ in properties are being produced worldwide and the end-use properties of these commercial LLDPEs depend upon not only average molar mass and chemical composition but also upon molar mass distribution and chemical composition distribution, i.e. short chain branch distribution. For an example, the high flexibility of a LLDPE stems from its short chain branches. For a given average SCB content, a broad SCBD indicates a greater amount of low SCB molecules with low flexibility. Therefore, the metallocene LLDPE with narrow SCBD has higher flexibility than Ziegler-Natta LLDPE.

As a consequence, it is interesting to take a closer look at the molecular structure of LLDPE in terms of average comonomer content, monomer sequence distribution along a polymer chain (intramolecular distribution of comonomer), and distribution of comonomer among polymer molecules (intermolecular distribution of SCB) besides average molar mass and molar mass distribution. It comes as no surprise that the development of fast and reliable techniques for the characterization of LLDPE in terms of molar mass (MM) and short chain branches (SCB) is of great interest in both industry and academia. Table 2.2 lists techniques most-commonly used for LLDPE characterization. For the characterization of short chain branches, techniques such as ^{13}C-NMR and FTIR are available, but they are only capable of determinating of average SCB content. Carbon-13 NMR, although frequently used for sequence distribution analysis of LLDPE, cannot distinguish the distribution of ethylene block length in runs longer than three ethylene units (Keating et al., 1996).

Table 2.2. Techniques for the characterization of "LLDPE" polymer

Molecular parameter	Characterization technique
Molar mass (MM)	SEC, viscometry, colligative properties
Molar mass distribution (MMD)	SEC
Short chain branching (SCB)	FTIR, ^{13}C NMR, TREF, CRYSTAF
Short chain branching distribution (SCBD)	TREF, DSC, CRYSTAF

Fractionation of LLDPE in terms of molar mass and short chain branch has been identified to be the best way to characterize the molecular structure of LLDPE (Francuskiewicz, 1994). Size exclusion chromatography (SEC) has long been employed and become a mature and routine technique to measure molar masses and molar mass distributions of polymer, although some other techniques are available. However, the reliability (accuracy and reproducibility) of SEC still requires improvement (Penlides et al., 2002). Temperature rising elution fractionation (TREF), a technique, which fractionates semicrystalline polymer according to crystallinity, has been widely used for the characterization of LLDPE with respect to SCB. Although TREF has been considered as the most reliable technique available for the characterization of LLDPE in terms of SCB, it suffers from being solvent-involved and time-consuming. A new technique to measure the SCBD in ethylene copolymers has been developed and applied to metallocene copolymers. Lehtinen et al. (1997) and Monrabal et al. (1994), (1996) and (1999) proposed a technique called crystallization analysis fractionation (CRYSTAF), based on a stepwise precipitation. This technique makes use of the different crystallizabilities of semicrystalline polymer as TREF does. Instead of physically fractionating a LLDPE sample, the CRYSTAF extracts information directly during the crystallization process by monitoring the solution concentration depression. The method dispenses with the elution step of TREF but is much more time-consuming compared to the off-column crystallization of TREF. In the past decade, thermally fractionated differential scanning calorimetry (DSC) has been emerged as an alternative technique for the compositional characterization. Since DSC apparatus is much more widely available than TREF equipment, and DSC analysis is solvent-free and much faster. LLDPE can be very heterogeneous on the molecular level in terms of SCBD, the thermal segregation process, which occurs during isothermal and dynamic crystallization of polymer from melt, can segregate LLDPE molecules according to the crystal size or the methylene sequence distribution. Although the thermally fractionated DSC is solvent-free and faster compared with TREF technique, the results are debatable, for the melting behaviors of LLDPE strongly depend on its thermal history. Furthermore, it is very difficult to obtain quantitative results from the thermally fractionated DSC reported in the open literature. The fractionation information of TREF and thermally fractionated DSC, primary techniques employed to characterize these LLDPEs with respect to SCB, is of interest to the current work; therefore, the results reported with these techniques are reviewed below.

2.9.1. Size Exclusion Chromatography (SEC)

Size exclusion chromatography (SEC) is also known as the gel permeation chromatography (GPC). In this method, the polymer chains are fractionated based on their hydrodynamic volume in solution as they flow through column(s) packed with particles of varying porosity and pore size (Xu et al., 1998). In general, polymers produced by supported metallocenes have narrow molecular weight distributions, with polydispersity indexes close to two or slightly higher. These MWDs can be well represented by Flory's most probable distribution, indicating that there is only one active site type as long as MWDs are concerned. However, Estrada and Hamielec (1994) proposed a two-site model for ethylene homopolymerization with homogeneous Cp_2ZrCl_2-MAO catalyst based on activity profiles and size exclusion chromatography (SEC) results. Subsequently, Wang et al. (1991) made similar observations for homogeneous Cp_2ZrCl_2-MAO and Cp_2ZrCl_2-butylaluminoxane (BAO) catalysts; they proposed a two-site model for Cp_2ZrCl_2 -

MAO and a three-site model for Cp_2ZrCl_2-BAO. Some supporting techniques can also lead to polyolefins with broad MWDs, which has been associated with the formation of several active site types and/or mass transfer resistances during polymerization. Therefore, by deconvoluting broad MWDs into narrower theoretical distributions, such as Flory's most probable distribution, information on active center types can be obtained in addition to the information on polymer chain length (Maschico et al., 1998). For the case of copolymers, besides MWD determination it is necessary to measure the chemical composition distribution to have a more complete understanding of active site types and polymer properties (Kim and Soares, 1999).

2.9.2 Temperature Rising Elution Fractionation (TREF)

TREF is a fractionation technique, which fractionates semi-crystalline polymer based on the difference in crystallinity of macromolecules due to the variation in short chain branching level. TREF was first used to fractionate low density polyethylene (LDPE) and linear low density polyethylene (LLDPE). The wide application of TREF in polyolefins is related to the following features of polyolefins:

(1) Most polyolefins are crystallisable (polyolefins are semi-crystalline materials)

(2) Polyolefins dissolve in solvents such as xylene, trichlorobenzene, and *o*-dichlorobenzene at high temperature. The fractionation can be performed without any special cooling equipment and the temperature is easy to control.

(3) Inhomogeneous structures including broad molecular weight distribution, composition distribution, and tacticity distribution of polyolefins prepared with conventional Ziegler-Natta catalysts permit that polymer fractions be eluted over a wide temperature range and make them suitable for TREF analysis. When polymer fractions obtained with TREF are analyzed with ^{13}C-NMR and other methods, it is possible to obtain very detailed information about polymer microstructure and nature of catalytic active site types.

The experimental separation mechanism of TREF can be depicted as fractionation mechanism shown in Figure 2.17. The operation of TREF is divided into two steps. In the first step, the dilute mixture of a polymer in a solvent is mixed with inert support (for instance, sea sand, glass beads, silica gel, etc.); this mixture is heated until the polymer is dissolved and then this mixture is slowly cooled to room temperature or below. Since the decreased crystallinity will be reflected in a lower dissolution temperature, the polymer fractions precipitate from the solution and coat the support layers of different crystallinity when temperature decreases gradually. The most easily crystallizable fraction precipitates first and deposits on the innermost layer. The fraction with the least crystallinity precipitates last and deposits on the outermost layer. This process is of great importance and a slow cooling rate is key, since it ensures that polymer fractions precipitate orderly according to crystallinity. A fast cooling rate may lead to cocrystallization of fractions with different crystallinity.

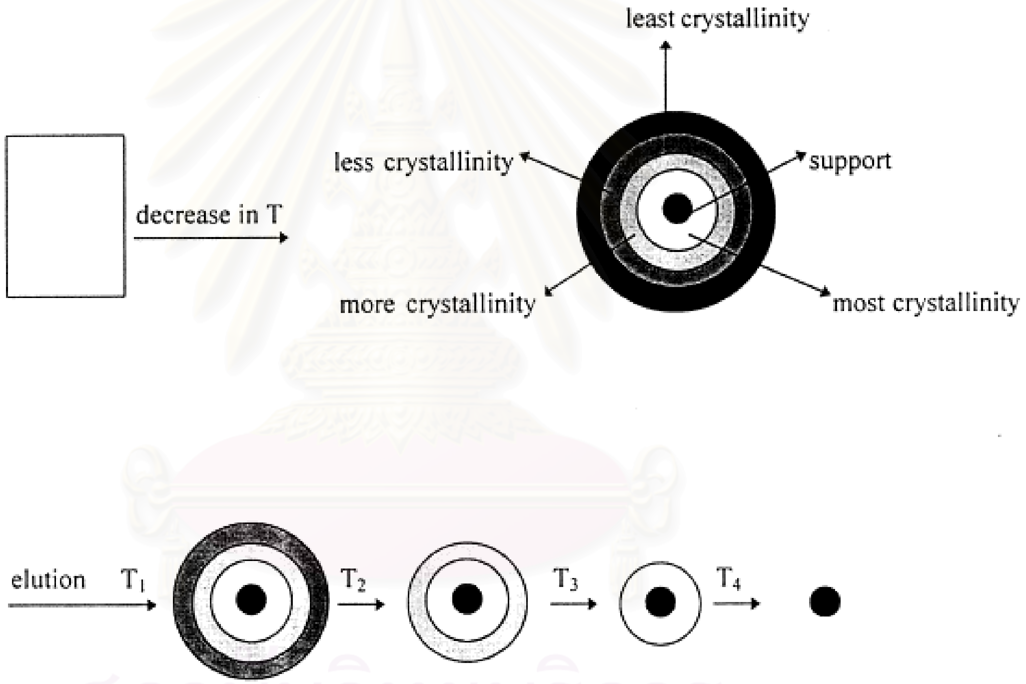

Figure 2.17. Schematic separation mechanism of TREF (Xu and Feng, 2000)

The slow cooling rate also provides optimal crystallizability separation, which is free from significant influence of molecular weight. In the second step, the precipitated polymer is eluted with solvent at increasing temperatures (continuously or stepwise). At lower temperatures, the fractions with low crystallinity (outermost layer) dissolve. With increasing elution temperature, the fractions of higher crystallinity dissolve. From the separation mechanism of TREF, one can see that TREF has two features compared with other fractionation methods. Firstly, the polymer is pretreated (crystallizing slowly from the solution) and the effect of the previous crystallization history of the polymer on fractionation is eliminated. In other fractionation methods such as extraction with solvents, badly crystallized samples may be extracted out at a lower temperature than the same well-crystallized sample, thus supermolecular structure also exerts an effect on extraction result. Secondly, the polymer fractions have been arranged regularly before fractionation. This reduces the effect of entanglement among polymer chains and facilitates the following separation.

In the past decade, TREF has been recognized as the most powerful and reliable technique for the structural analysis of LLDPEs and their blends (Kelusky et al., 1987; Soares et al., 1995a). Several reviews devoted to various aspects of TREF analysis have been published (Soares et al., 1995b). Although the TREF technique has been refined by a number of researchers by using data acquisition automation and off-line crystallization, the TREF procedure has been essentially similar to those summarized by Francuskiewicz (1994). Other than the characterization of LLDPEs and their blends, TREF has been also expanded recently to the characterization of other olefin copolymers such as polypropylene (PP), polyolefin alloys, ethylene/styrene copolymer (Thomann et al., 1997) and propylene/1-butene copolymer (Abiru et al., 1998).

The superior properties of metallocene LLDPE to conventional Ziegler-Natta LLDPE are probably a due to the different SCB distributions. The Ziegler-Natta catalyst possesses multiple active sites, which produce LLDPE molecules of different molar mass (MM) and short chain branches content (SCB), and MM increases with decreasing SCB. Metallocene are single-sited and produce LLDPE molecules with the same average SCB content. The difference in the molecular structure between Ziegler-Natta and metallocene LLDPE results in the remarkable difference in blown film properties.

There are two kinds of experimental TREF apparatus: analytical and preparative TREF. Analytical TREF is usually connected with other analytical instruments such as IR for continuous detection of eluted polymer concentration and even structure if absorbance at different IR frequencies is recorded simultaneously. Preparative TREF is used to collect larger amounts of polymer fractions eluted at different tempearatures, and the polymer fractions can be characterized off-line by

SEC, NMR and/or DSC. Preparative TREF is time-consuming, but it usually provides more information than analytical TREF and is frequently used for polypropylene. A calibration curve for structure versus elution temperature is usually employed when TREF is performed on an analytical scale. This calibration curve can be obtained by comparison with other standards or with the results of preparative TREF. A linear relationship between SCB content and elution temperature has frequently been used (Glockner, 1990; Soares et al., 1995a). The biggest challenge TREF is facing may be that the mechanism of TREF separation is not fully understood. This, to larger extent, will hamper the interpretation of different calibrations (Karbashewski et al., 1993; Bonner et al., 1993; Mathot 1994; Borrajo et al., 1995; Elicabe et al., 1996). It is generally accepted that TREF fractionates semi-crystalline polymers based on the difference in crystallizability due to various chemical composition of the polymeric chains (molecules), thus high SCB or increasing comonomer content results in an almost linear depression of the melting or elution temperature (Glockner, 1990; Soares et al., 1995a). However, the results from some LLDPEs have indicated otherwise. Karbashewski et al. (1993) investigated the effect of comonomer sequence distribution on TREF branching distribution. They suggested that it is not the average branch content but rather the effective branch content that determines the crystallinity distribution of a linear low density polyethylene. Pigeon and Rudin (1993 and 1994) employed dual IR detectors, one measuring a C-H stretching band of methyl groups and the other a C-H stretching band of methyl groups, and found that curves for two different LLDPEs are indeed slightly different.

On the other hand, there have been suggestions that TREF fractionates semi-crystalline polymer based on the length of crystallizable sequence between SCB points, commonly referred to as methylene sequence length (MSL). Based on this assumption and a modified Flory equation, Bonner et al. (1993) proposed a novel method of constructing the TREF calibration curve using five standard linear polyethylene samples. Borrajo et al. (1995) proposed a thermodynamic model for TREF based on the Flory-Huggins theory. They suggested that the TREF fractionation process is based essentially on crystallizable sequence lengths in addition to the degree of crystallinity attainable for the solid polymer after slow crystallization. Mathot (1994) indicated that there is a possibility that TREF may separate the polymer based on the longest sequence with in a molecule. This is based on the fact that a polymer molecule only elutes from TREF column and is detected at a temperature that is characteristic of the longest sequence in the molecule, suggesting that the calibration curve generated by Bonner et al. (1993) would be valid, and DSC can be a useful complementary tool, since at each temperature at which molecule parts dissolve, there is a measurable heat of fusion which is associated with sequences in molecules and between molecules. Recently, Xu et al. (2001) described a new and convenient method for the qualitative characterization of intramolecular composition heterogeneity. The metallocene-based and conventional ethylene/butene copolymers were fractionated with preparative temperature rising elution fractionation (TREF) technique, and some selected fractions were directly characterized with the differential scanning calorimetry (DSC) after stepwise crystallization. The observed multiple endotherms in the melting traces of some fractions were attributed to intramolecular composition heterogeneity after other possibilities were excluded. It is found that intramolecular composition heterogeneity is present in both metallocene-based and conventional ethylene/butene copolymers, but the metallocene-based copolymers may have a relatively narrower intramolecular composition distribution.

Perhaps one of the most important applications of TREF is its use for studying the nature of polymerization catalysts. Kim and Soares (1999) observed that the molecular weight distribution of all copolymers was narrow, indicating a uniform catalyst site. However, with respect to chemical composition distribution, some supported catalysts showed broad and sometimes bimodal distributions, which indicates the presence of two or more active site types. Previously, Usami et al. (1986) compared four LLDPE samples made with conventional Ziegler-Natta catalysts by different processes. The four LLDPEs show considerably broader and bimodal TREF profiles, which were ascribed to at least two different active sites present on the catalyst, one producing almost exclusively linear homopolyethylene and the other LLDPE with a broad composition distribution. Temperature rising elution fractionation (TREF) results of Soga et al. (1995) with ethylene/1-hexene copolymers produced by homogeneous Cp_2ZrCl_2-MAO catalysts suggested that these catalyst systems contained two different types of catalytic species. Crystallization analysis fractionation (CRYSTAF) results of Kim and Soares (1999) with ethylene/1-hexene copolymers produced during slurry operation with various silica supported metallocenes led to the conclusion that these supported catalysts contained two or more types of catalytic sites. Kakugo et al. (1988) used TREF to investigate the catalytic active sites for ethylene/propylene and propylene/1-butene copolymerization. The authors concluded that the lower isospecific catalytic sites were more active toward ethylene but that their activity did not change as much for 1-butene. Given the multiple-site nature of the metallocene catalyst, it has been shown that predicting the polymerization activity and the resulting microstructure of the polymer is a challenging task (Xu et al., 1999; and Shan et al., 2002).

2.9.3. Thermally Fractionated by (DSC)

DSC is a much faster technique than TREF, and it is solvent-free. Many studies have been devoted to utilizing DSC as a possible alternative to TREF. Various analytical methods have been used to determine the crystallinity of a polymer, but differential scanning calorimetry (DSC) is the most widely used technique. The usual procedure in measuring the degree of crystallinity by DSC involves drawing a linear baseline from the first onset of melting to the last trace of crystallinity and the determine the enthalpy of fusion from the area under this endotherm. (Kong and Hay, 2002).

The earlier studies done by Karbashewski et al. (1992) showed that DSC analyses of LLDPE samples, that had been crystallized slowly, gave much the same qualitative information as analytical TREF in terms of estimating the breadth of the SCBD, but the resolution of DSC was not as good as that of TREF. These studies also indicated that the quantitative analysis of DSC is difficult due to the fact the intensity of the DSC response is a product of the amount of material melted at a particular temperature and the enthalpy of fusion, ΔH_{melt}, of that material. In order to translate a DSC endotherm into a mass distribution, the ΔH_{melt} for each fraction has to be measured and the DSC response corrected for the differing enthalpies of melting. Evidently, the comonomer content will be the primary factor affecting to the final properties of ethylene copolymers. However, and for a given composition, the thermal history imposed on the sample may be also an important parameter. Cerrada et al. (2001) observed that the cooling treatment from the melt has a very significant effect, although its influence on the thermal properties is rather small, some structural parameters and the viscoelastic behavior are clearly dependent upon thermal history.

These parameters include the degree of crystallinity, lattice constants, relaxation processes, stiffness, and microhardness of the samples. The endotherms of nascent, i.e. as polymerized, polyolefins has been investigated as a function of the polymerization conditions used to make the polymers (Loos et al., 2002). They observed that the nascent polymer samples exhibit, in general, different behavior than thermally treated samples. They observed that the differential scanning calorimeter traces for most first heating scans (nascent polymer) have higher melting temperatures and higher enthalpy of fusion than for the second heating scans of the same, but now melt-crystallized, samples.

The resolution of DSC endotherms can be improved by thermal treatment of LLDPE. A thermal fractionation technique, first proposed by Adisson et al. (1992), consisted of a stepwise crystallization of the polyethylene chains from the melt by successive annealing at descending temperatures and the subsequent analysis of the melting behavior of the treated sample by DSC. The DSC thermograms of the semi-crystalline ethylene copolymers displayed multiple melting peaks. It was concluded that each peak is representative of a distinct family of macromolecules or block of monomeric units with different SCB content. Keating and McCord (1992) used a similar method to examine the distribution of ethylene block lengths and distinguish the structural subtleties of a variety of ethylene copolymers. They concluded that: (a) copolymers with high comonomer content are less crystalline and the ethylene sequences are shorter, (b) the comonomer type makes a difference in fractionation if H-bonding is involved, (c) the narrow comonomer distribution or ethylene segment length distribution has fewer DSC fractions, (d) fractionation by crystallinity is affected if the molar mass is very high, (e) branch content reduces the crystallinity and shortens the ethylene block length, and (f) there is no direct relation to molar mass distribution or comonomer content. Recently, the melting and crystallization behavior of random propene/higher linear α-olefin copolymers synthesized with metallocene catalyst were investigated. The melting point depression is linearly related to the amount of comonomer incorporated irrespective of the nature thereof according to Flory’s theory. The crystallization temperature decreased as well linearly with increasing comonomer content, but was independent of the comonomer type.

Starck (1996) conducted a comparative study on the comonomer distribution of a series of commercial LLDPEs produced with traditional high activity

Ziegler-Natta catalysts by using TREF and a segregation fractionation technique (SFT) based on a stepwise crystallization by DSC. The author concluded that the heterogeneity of the Ziegler-Natta type of commercial LLDPE and VLDPE copolymers can be evaluated in a much shorter time using DSC fractionation than using TREF, and the DSC method showed similar compositional information although the shapes of the curves were not the same. By applying the SFT, separation in different segregated species takes place, and smaller difference in the chemical composition distribution of the polymers can be identified.

A semi-quantitative study was done by Keating et al. (1996). They used thermal fractionation, i.e., step-crystallization method, to segregate very low density polyethylene (VLDPE) and ultra low density polyethylene (ULDPE). Both copolymers showed a DSC endotherm with multiple peaks, each of which represents a family of crystallizable ethylene sequences. A series of commercially-available hydrocarbons were treated under the same conditions as polymer samples, used to construct a calibration curve relating melting temperature to ethylene sequence length. The method gave rise to the semi-quantitative assessment of ethylene sequence length distribution of different LLDPEs.

Muller et al. (1997) applied the classical self-nucleation technique to segregate different types of polyethylenes. Based on a superposition of the self-nucleation and annealing cycles which are similar to those designed by Fillon et al. (1993) for the evaluation of the self-nucleation process in polypropylene (PP), a thermal treatment procedure referred to as successive self-nucleation/annealing (SSA) was developed for the segregation of various types of polyethylenes. The SSA procedure was compared with the step-crystallization (SC) method in the literature. It was concluded that the SSA generally produces better fractionation than the step-crystallization and that the chain branching distributions derived from the SSA-DSC can be qualitatively comparable to those obtained by TREF. Feng and Jin (1999) investigated the effect of the self-nucleation on the crystallization and melting behavior of low ethylene content propylene-ethylene copolymers. The results indicated that the crystallization temperature depends on the pre-selected annealing temperature and the self-nucleation can enhance the crystallization, suggesting that the self-nucleation can offer advantages of high resolution and sensitivity for the segregation of LLDPEs.

CHAPTER III

EXPERIMENTAL

A large number of scientific articles and several reviews dealing with metallocenes for the catalysis of olefin polymerization have been published in recent years (Ribeiro et al., 1997; Chien, 1999; and Hlatky, 2000). However, they are mostly focused on homogeneous systems, and despite the importance of supported metallocene catalyst for industrial olefin polymerization processes, very little research has been reported in the literature, especially gas-phase polymerization. Therefore, the effects of polymerization conditions in gas- and slurry-phase process on the activity and product properties of polymer made with mesoporous molecular sieves supported metallocene catalyst are presented in this work.

Experimental work in the present study on the influence of supported zirconocene catalyst on ethylene homopolymerization and ethylene/α-olefin copolymerization consisted of preparation of supported metallocene catalyst using $(n\text{-BuCp})_2ZrCl_2$ supported on silicalite, mesoporous molecular sieves and silica gel by the impregnation method, the polymerization of ethylene and ethylene/α-olefins in the gas phase and slurry phase, and the characterization of catalysts and the obtained polymer. The experiments in the gas and slurry mode were carried out at the University of Alberta and Chulalongkorn University, respectively.

3.1. Materials

3.1.1. Materials Used in Gas-Phase Experiments

Metallocene catalyst, bis(n-butylcyclopentadienyl) zirconium dichloride $(n\text{-BuCp})_2ZrCl_2$, used in both gas phase and slurry phase, was donated by NOVA Chemical Co. and used without further purification. Anhydrous toluene (99.8%), 10wt % of methylaluminoxane (MAO) in toluene solution, and neat triisobutyl aluminum (TIBA), were obtained from Aldrich and used without further purification. Sodium chloride (NaCl) used as a seed bed with an average particle size of about 0.5 mm was obtained from Fisher Scientific (Edmonton, Canada). Polymer-grade ethylene and ultra-high-purity nitrogen were obtained from Matheson and Praxair (Edmonton, Canada), respectively. They were each passed through a series of Altech high-pressure gas purifiers containing BASF R3-11 catalyst, Ascarite and 3-Å molecular sieves for the removal of oxygen, carbon dioxide, and moisture, respectively. The polymer-grade 1-hexene donated by NOVA Chemicals was used as received.

3.1.2. Materials Used in Slurry-Phase Experiments

Toluene (commercial grade) donated by Exxon Chemical Ltd., Thailand, decane (GC grade 98%), heptane (99.9%), purchased from Fluka and Fisher Scientific, respectively, were purified before use. Calcium chloride ($CaCl_2$) and sodium alloy 99% from Aldrich, benzophenone from Fluka, and methanol (commercial grade) from SR laboratories lab were purchased. Hydrochloric acid (fuming 37%) was purchased from Merck. Ethylene (polymerization grade) was donated by National Petrochemical Co., Ltd., Thailand. Ultra-high purity argon was purchased from Thai Industrial Gas Co., Ltd. and further purified by passing through columns packed with BASF R3-11 catalyst, sodium hydroxide (NaOH), phosphorus pentaoxide (P_2O_5), and 4-Å molecular sieves to remove the traces of oxygen and moisture. Methylaluminoxane (MAO) 2.598 *M* in toluene solution and neat triisobutyl aluminum (TIBA) were donated by Tosoh Akzo, Japan, and used without further purification. 1-hexene (99.98%), 1-octene (98%), and 1-decene (98%) were purchased from Aldrich and further purified before use.

3.1.3. Materials Used for Size Exclusion Chromatography

HPLC-grade 1,2,4-trichlobenzene, purchased from Fisher Scientific, was used for dissolving the polymer for characterization by size exclusion chromatography. Polystyrene, linear alkanes and polyethylene were used for molar mass calibration. TSK standard polystyrene samples of known molar masses ranging from 870 to 8,420,000 were obtained from Tosoh Corporation and Toyo Soda Manufacturing Co., Ltd. Linear alkanes $C_{20}H_{42}$, $C_{40}H_{82}$, and $C_{60}H_{122}$ were obtained from Fluka. Narrow polyethylene standard reference materials 1475, 1482, 1483, and 1484 were obtained from National Institute of Standards and Technology (NIST).

3.2. Experimental Equipment

Special care was taken in the handling of reagents and for loading the catalyst into the reactor because most of the reagents and catalyst were very sensitive to the oxygen and moisture. In this study, special techniques, so called Schlenk and glove box techniques, for handling oxygen/moisture-sensitive compounds were used to eliminate oxygen and moisture from the reagents and catalysts. The equipment used for these techniques were the following:

(a) Glove box (Vacuum Atmospheres) with oxygen and moisture analyzer for transferring solid powder and liquid reagents under inert atmosphere and for storing air-sensitive reagents.

(b) Schlenk line consisting of a vacuum line connected to a vacuum pump and an inert gas line for purging while reagents were transferred, and a Schlenk tube for keeping reagents under inert atmosphere outside the glove box.

3.3. Support Preparation

The supports used in this work are described in Table 3.1. The mesoporous molecular sieves (identified by the prefix MMS) were synthesized and characterized at Laval University (Ste-Foy, Canada) except for MMS2.5, which was prepared at the University of Alberta (Edmonton, Canada). These supports were used in gas-phase and slurry-phase polymerization.

Sample (MMS2.6) was prepared as follows: A solution (Solution 1) containing the inorganic precursors was prepared from a mixture of 400 g of a sodium silicate solution, 856 g of water and 24 g of H_2SO_4. The second one (Solution 2) containing the surfactant was obtained by dispersing 336 g of cetyltrimethylammonium bromide (C_{16}TABr; an ionic surfactant) in 1000 g of water. Then, Solution 1 was added slowly to Solution 2 under mechanical stirring for 3 h. The pH of the gel was then adjusted to 11 with a dilute sulfuric acid solution. The resulting gel was transferred into a nalgen bottle, in which crystallization was allowed to take place at 70 °C for 168 h. The hexagonal MCM-41 type solid product was cooled to room temperature, filtered and washed thoroughly with deionized water until a neutral pH was obtained. This solid product was then calcined at 550 °C for 12 h in air.

Sample MMS5.8, MMS6.4, MMS7.2, MMS10, MMS12.5, MMS15.2, MMS16, MMS20 and MMS25 (where the number designates the pore diameter in nanometers) were prepared according to a slight modification of the synthesis method reported by Luan et al. (1999). In a typical synthesis, the required amount of nonionic surfactant [2 g of Pluronic $EO_{20}PO_{70}EO_{20}$ (P123) or $EO_{106}PO_{70}EO_{106}$ (F127)] was dispersed in a stirred mixture containing 15 g of water and 60 g of 2 *M* HCl. This homogeneous solution was kept at 40 °C for 2-3 h before the addition of 4.25 g of tetraethyl orthosilicate TEOS. The gel obtained was allowed to crystallize in a round bottom flask or in a Teflon-lined autoclave for different times and different temperatures as reported in Table 3.1. After crystallization, the solid product was ambient air-cooled, filtered, washed with deionized water, and dried in air at room temperature. The dried material was calcined at 500 °C for 6 h. in static air to decompose the template and to obtain a white powder of MMS of SBA-15 type. On the basis of the variations of synthesis parameters such as the crystallization time, the crystallization temperature, the nonionic surfactant nature, and the amount of mesitylene added, MMS with different pore diameters were prepared (see Table 3.1).

Sample MMS2.5 was prepared at the University of Alberta by mixing 100 mL of an aqueous solution of cetyltrimethlammonium hydroxide (25 mass %) with 54 g of a 10 to 20 mass % solution of tetramethylammonimu silicate solution, purchased from Aldrich, and adding 35.9 g of colloidal silica (LUDOX® HS-40) into a 500 mL reactor. The sealed readctor was kept at 80ºC overnight and then at 95ºC for 3 days. The solid product was removed by filtration, dired at ambient temperature followed by heating in flowing nitrogen for 1 h at 540ºC for 1 h and in following air ar 540ºC for 6 h.

Support S0.54 is silicalite (Flanigen et al., 1978), an essentially aluminum-free pentasil-type zeolite formerly manufactured by Union Carbide (Tarrytown, NY). The Silicalite used in this study was an unpelletized sample obtained from Union Carbide and used in previous studies (Rangwala et al., 1988). Support S1 is a commercial silica gel.

Table 3.1. Description of Supports

Support designation	Pore diameter (nm)	Surface area (m^2/g)	Pore volume (cm^3/g)	Crystallization temperature (°C)	Crystallization time (h)	Surfactant
MMS2.5[a,b]	2.5	890	0.61	95	85	C$_{16}$TAOH
MMS2.6[a,b]	2.6	1130	1.3	70	168	C$_{16}$TABr
MMS5.8[a]	5.8	980	0.8	62	24	P123
MMS6.4[b]	6.4	1240	1.5	70	24	P123
MMS7.2[a,b]	7.2	870	1.1	90	24	P123[d]
MMS10[a]	10	412	1.3	100	48	P123[e]
MMS12.5[b]	12.5	296	1.2	130	48	P123
MMS15.2[a]	15.2	330	1.3	120	48	P123
MMS16[b]	16	371	1.5	150	48	P123
MMS20[a]	20	310	1.6	145	48	F127
MMS25[a]	25	300	1.7	150	72	F127
S0.54[a,b]	0.54	435	-	-	-	-
S1[c]	16	270	1.4	-	-	-

[a] supports were used in gas-phase polymerization.

[b] supports were used in slurry-phase polymerization.

[c] Silica gel was used in preliminary results.

[d] 2 g of mesitylene added.

[e] 1.5 g of mesitylene added.

3.4. Catalyst Preparation

Catalysts used in this study are described in Table 3.2A. and 3.2B. The calculation of catalyst compositions is shown in Appendix A. All catalysts, except CAT-SD, were prepared at the University of Alberta and Chulalongkorn University by impregnation of the supports with toluene solutions of MAO and (*n*-BuCp)$_2$ZrCl$_2$. CAT-SD were donated by NOVA Chemicals Corp. The following procedure, using Schlenk and glove box techniques under ultra-high-purity of inert gas (nitrogen or argon), was used to impregnated the supports with MAO and (*n*-BuCp)$_2$ZrCl$_2$

1. Due to the requirement of dehydrated support, each support for catalysts used in subsequent gas-phase polymerizations was treated at 500ºC for 7 hours under flowing ultra-high-purity nitrogen. Dehydrogenation of supports for catalysts, which were only used in slurry polymerizations, was done under vacuum at the same temperature and for the same length of time. The dehydrated supports were placed into a 250 mL flask equipped with a stirrer and containing 10 mL of toluene and inert gas. The amount of support placed into the flask is indicated in Table 3.2. (Small amounts of MMS were used in some of the preparations, i.e., less than 1 g, because of the lack of larger quantities of these materials).
2. MAO in toluene solution was added drop wise to the suspended support/toluene suspension. The amount of solution added is shown in Table 3.2A. and 3.2B. Gas evolution was observed during the MAO addition.
3. The suspension was stirred at room temperature for 12 h.
4. The desired amount of (*n*-BuCp)$_2$ZrCl$_2$ in toluene was added to the suspension.
5. The suspension was stirred at room temperature for 4 h.
6. All the toluene was removed from the flask by evacuation at room temperature. The evacuation was continued until free-flowing solids were obtained.
7. The catalysts were stored in a glove box until use.

Table 3.2A. Description of catalysts used in gas phase polymerization.

Catalyst	Support Pore Diameter (nm)	Support	Amount of Support Used (g)	Amount of MAO Added (mL)	Zr Content		Al/Zr ratio
					mass %	mmol/g	
CAT0.54	0.54	S0.54	0.66	4.4	0.33	0.037	170
CAT2.6-1	2.6	MMS2.6	1.00	6.6	0.34	0.037	170
CAT2.6-2	2.6	MMS2.6	1.00	6.6	0.38	0.042	150
CAT2.6-3	2.6	MMS2.6	1.00	3.3	0.36	0.039	100
CAT5.8	5.8	MMS5.8	0.60	4.0	0.34	0.037	170
CAT7.2	7.2	MMS7.2	0.52	3.4	0.33	0.037	170
CAT10	10	MMS10	0.33	4.2	0.25	0.027	330
CAT15	15	MMS15	0.29	1.9	0.34	0.037	170
CAT20	20	MMS20	0.75	5.0	0.34	0.037	170
CAT25	25	MMS25	0.25	1.6	0.34	0.037	170
CATS1-1	16	S1	2.00	6.6	0.33	0.036	110
CATS1-2	16	S1	2.00	13.3	0.29	0.032	200
CAT-SD	a donated, uncharacterized (n-BuCp)$_2$ZrCl$_2$ /MAO/SiO$_2$ catalyst used in preliminary experiments.						

Table 3.2B. Description of catalysts used in slurry phase polymerization

Catalyst	Support pore diameter (nm)	Support	Amount of support used (g)	Amount of MAO Added (mL)	Zr Content		Al/Zr ratio
					mass %	mmol/g	
CATBA0.54	0.54	S0.54	2.00	7.7	0.33	0.037	170
CATBA2.5	2.5	MMS2.5	0.90	3.5	0.33	0.037	170
CATBA2.6	2.6	MMS2.6	0.71	2.7	0.33	0.037	170
CATBA6.4	6.4	MMS6.4	0.75	2.9	0.33	0.037	170
CATBA7.2	7.2	MMS7.2	0.82	3.2	0.33	0.027	170
CATBA12.5	12.5	MMS12.5	0.48	1.8	0.33	0.037	170
CATBA16	16	MMS16	0.37	1.4	0.33	0.037	170
CATBA-S1	16	S1	2.00	7.7	0.33	0.037	170

3.5. Polymerization Procedures

3.5.1. Gas-Phase Polymerization

The gas-phase polymerizations were carried out at the University of Alberta. The few slurry runs done at the University of Alberta were done to confirm that the low Al/Zr ratio was the reason for the low activities of CATS1-2 and CAT2.6-3. The reactor system described by Lynch and Wanke (1991) was used for the polymerization studies. A schematic diagram of this reactor system is shown in Figure 3.1. The standard procedure for gas-phase polymerization experiments consisted of the following steps:

1. About 80 g of sodium chloride, from Fisher Scientific (Edmonton, Canada) with an average particle size of 0.5 mm, was placed in a clean, 1-L stainless steel reactor; the NaCl acted as the seedbed.
2. The reactor assembly was tested for leaks at 300 psi with nitrogen and then evacuated overnight at 90ºC.

3. The reactor was cooled to the desired reaction temperature by the oil-bath temperature being lowered to about 1 or 2ºC below the desired reaction temperature.
4. Ethylene was added to the reactor to a pressure of about 20 psi.
5. The desired amount of TIBA, usually 0.15 ml, was injected into the reactor, and the data acquisition system was started (the temperatures, flow rate, and reactor pressure were recorded at 10 s intervals). The ethylene flow rates, measured with a Matheson 8142 mass flow meter (East Rutherford, NJ), were used to compute the instantaneous ethylene consumption rates.
6. Ethylene was added to the reactor to a pressure of 80 psi, and the reactor was stirred for 30 min.
7. The catalyst, contained in a catalyst injection holder charged with the catalyst in the glove box, was injected into the reactor by high-pressure ethylene (i.e., dry catalyst injection).
8. Ethylene was fed at the rate required to maintain the reactor pressure at 200 psi.
9. The polymerization was terminated after 2 h by the ethylene feed being stopped, the reactor being vented and evacuated while cooling, and reactor then being filled with air.
10. The product was repeatedly washed with water to remove all salt, and the mass of PE made was measured; this mass was used to calculate the average rate of polymerization.

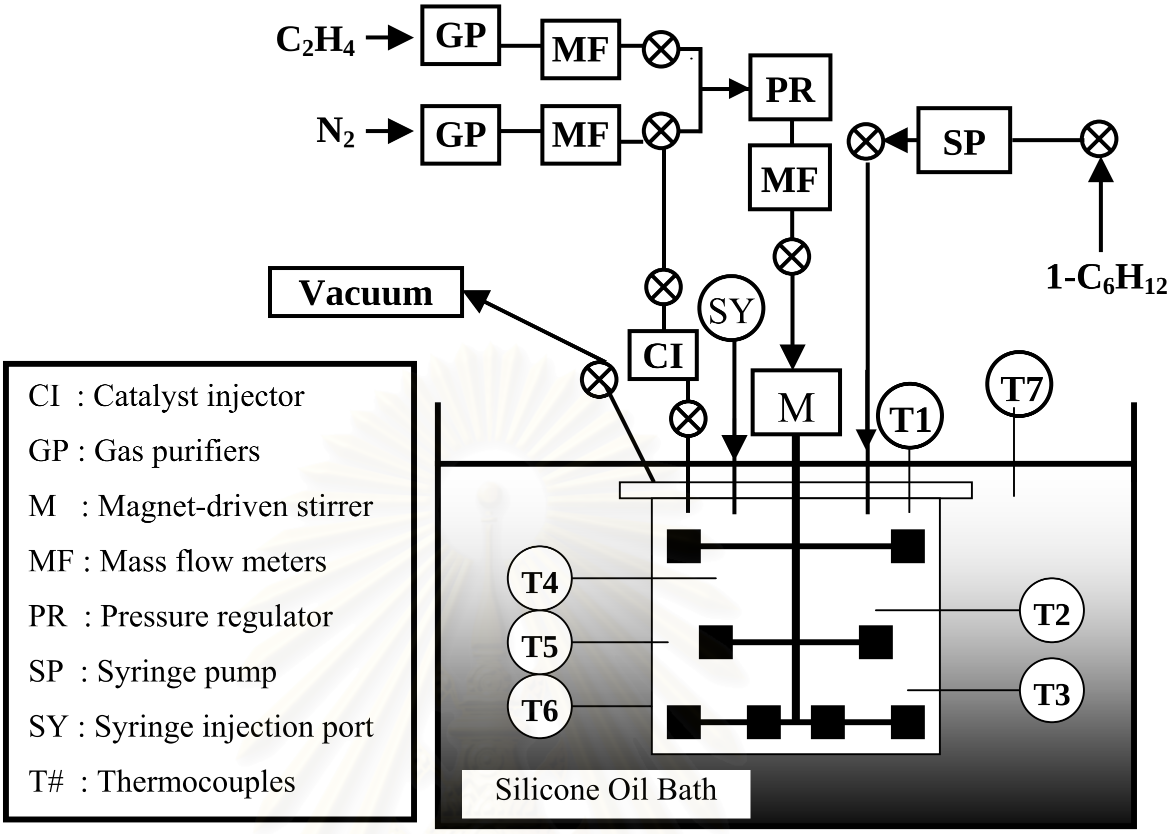

Fig 3.1. Schematic diagram of reactor system in gas phase polymerization

The ethylene was polymer-grade ethylene from Matheson purified by flowing through a series of three Alltech purifiers containing BASF R3-11, Ascarite and 3A molecular sieves, before entering the reactor. For gas-phase runs at a total ethylene pressure of 100 psi, no ethylene was added in Step 6; that is, the stirring for 30 min was done at a total pressure of 20 psi. For copolymerization runs, 1-hexene was injected after Step 4. No seed bed was used for the slurry runs (Step 1), and 300 mL of heptane were added to the reactor after the reactor had been cooled to the reaction temperature; MAO in toluene was added, ethylene was added to a pressure of 20 psi and the catalyst suspended in heptane was added with a syringe. The reactor pressure was then increased and maintained at the desired value by continuous addition of ethylene.

3.5.2. Slurry-Phase Polymerization

Ethylene polymerization and ethylene/α-olefin copolymerization in the slurry phase were carried out at Chulalongkorn University using a 100 mL semi-batch stainless steel autoclave reactor equipped with the mass flow meter (KOFLOC 3750) and magnetic stirrer. A schematic diagram of the system is shown in Figure 3.2. The loading of 30 mL of solvent, 50 mg of catalyst powder, and desired amount of cocatalyst or scavenger were performed inside a glove box. The loaded reactor was then cooled in liquid nitrogen for 15 min and the cooled reactor was attached to the ethylene feed line and the reactor was degassed. The reactor was immersed into the water bath controlled to the desired reaction temperature. The ethylene feed was started when the reactor reached the desired temperature; the ethylene feed was continued at the rate required to maintain the reactor pressure at 100 psi. The polymerization reaction was terminated after 15 min by venting and adding acidified methanol. The precipitated polymer was washed with methanol several times and dried under vacuum.

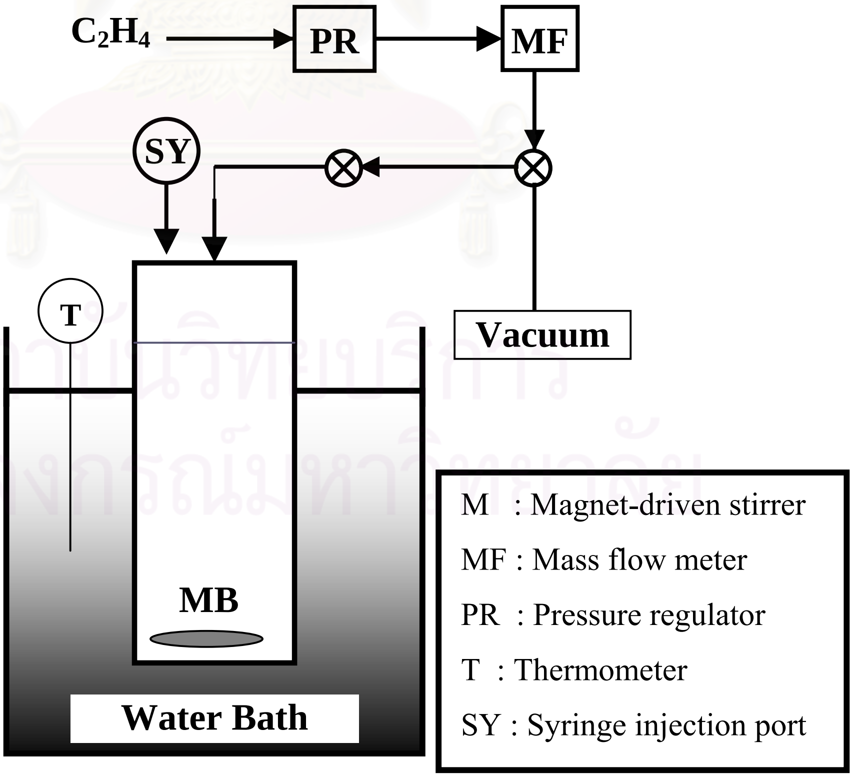

Fig 3.2. Schematic diagram of reactor system in slurry phase polymerization

For copolymerization, the desired amount of comonomer was injected into the reactor by the syringe before cooling the reactor in liquid nitrogen.

3.6. Characterization

3.6.1. BET Surface Area Analysis

The support surface areas were obtained from nitrogen sorption measurements at 77 K with an Omnisorp 100 or 360 sorptometer (Miami Lakes, FL); the Brunauer, Emmett and Teller (BET) method was used to calculate the surface area. The pore size distribution was obtained from desorption branch of the N_2 physisorption isotherm (with the Barrett-Joyner-Halenda formula). Before each adsorption experiment, the calcined samples (MMS) were outgassed at 573 K for at least 2 h in vacuo. The surface area of the silicalite was based on a single-point BET measurement. Pore sizes and pore volumes were obtained from nitrogen desorption curves.

3.6.2. Scanning Electron Microscopy (SEM)

The morphology of catalyst and polymers was examined by scanning electron microscopy (SEM) with a Hitachi S-2700 SEM at the University of Alberta, equipped with digital recording of images, and JSM-640 SEM at Technological Research Equipment Center, Chulalongkorn University using a camera and a Polaroid film. The specimens were coated with a thin layer of carbon before they were placed in the specimen chamber of the SEM. The accelerating voltage of electron beam used was 10 kV for most of SEM examinations. Application of specimen coating and low accelerating voltage operation can reduce the accumulation of electrons on the surface of the specimen. The accumulation of electrons will lead to serve distortions of the images (charging artefacts) for insulating materials, such as polyethylene.

3.6.3. Size Exclusion Chromatography (SEC)

The molar mass and polydispersity of polyethylene were measured be size exclusion chromatography (SEC) with an Alliance GPCV2000 equipped with a differential refractometer and series of three Waters HTGE columns. The columns and the detector were operated at 145ºC, and high performance liquid chromatography-grade 1,2,4-trichlorobenzene (from Fisher Scientific), containing 0.25 g/L of 2,6-tert-butyl-4-methyphenol as an antioxidant, was pumped through the columns at a rate of 1 cm^3/min. The molar masses were calibrated by polymer samples of known molar masses (Wu et al., 2000). These polymer samples included: TSK standard polystyrene samples with molar masses from 870 to 8,420,000 linear alkanes $C_{20}H_{42}$, $C_{40}H_{82}$, $C_{60}H_{122}$, and NIST narrow polyethylene standard reference materials 1482,1483,and 1484. For each sample measured, a solution of polyethylene concentrations of 0.035 to 0.07 mass % in 1,2,4-trichlorobenzene was prepared, and each solution was injected at least twice. Repeat analyses were done on all samples, and the reported values are the averages of two or more analyses.

3.6.4. Differential Scanning Calorimeter (DSC)

Differential scanning calorimetry (DSC) was used to investigate the melting properties of nascent polymer samples. A TA Instrument Model DSC2910 was used for the measurements; the endotherms of nascent polymers were obtained by scanning from an initial temperature of 0 or 25ºC to a final temperature of 160 ºC at a rate of 10 ºC/min. Repeat scans were done for most of the samples, but the first scans with the nascent polymers were of special interest. Percent crystallinity was computed from enthalpies of melting by Equation 3.1, using the reliable value of Wunderlich.

$$\chi\,(\%) = (\Delta H_m/\Delta H^\circ_m)\mathrm{x}100 \qquad \text{---- } \mathbf{(3.1)}$$

Where (ΔH_m) is the heat of fusion of sample and (ΔH°_m) is the heat of fusion of crystalline polyethylene[290 J/g] (Ottani and Porter, 1991).

3.6.5. Temperature Rising Elution Fractionation (TREF)

Temperature rising elution fraction, TREF, is a fractionation technique, which fractionates semi-crystalline polymer based on the difference in crystallinity of macromolecules. The TREF system used in this characterization was a custom-built apparatus and completed descriptions of the TREF procedure that have been described previously (Huang et al., 1997; Lacombe et al., 1997; and Zhang et al., 2000). A schematic representation of the TREF system is shown in Figure 3.3. Briefly, TREF analysis was used to obtain information on the branching structure. The analytic TREF procedure consisted of an off-column crystallization step in which the PE was dissolved in *o*-xylene at 125 ºC (1 mg PE/mL *o*-xylene) followed by cooling of the polymer solution at 1.5 ºC/min to –8 ºC. During the cooling the PE precipitated onto glass beads (80-100 mesh). The precipitated sample was transferred into a TREF column (9.5 mm in inside diameter and 63.5 mm in length), containing similar sized glass beads. The column was placed into the elution compartment of the custom-built TREF apparatus, and PE was eluted from the column by flowing *o*-dichlorobenzene (1.0 mL/min) by heating the column from 0 to 125 ºC at a constant rate of 1 ºC/min. The concentration of eluted PE was measured with an on-line IR detector tuned to 2860 cm-1. Linear paraffins (C_{40} and C_{60}), linear polyethylene reference materials (1475, 1482, 1483, and 1484 from NIST) and 17 linear polyethylene samples prepared in the laboratory at the University of Alberta by preparative TREF (polydispersities less than 1.3 and M_n of 1000 to 10,000) were used to obtain a correlation between TREF elution temperature and methyl group concentration. The obtained correlation, with $T_{elution}$ in ºC, is shown in Equation 3.2.

$$[\mathrm{CH_3}/1000\ \text{Carbons}] = 76.37 - 1.20T_{elution} + 0.0044T^{2}_{elution} \qquad \textbf{---- (3.2)}$$

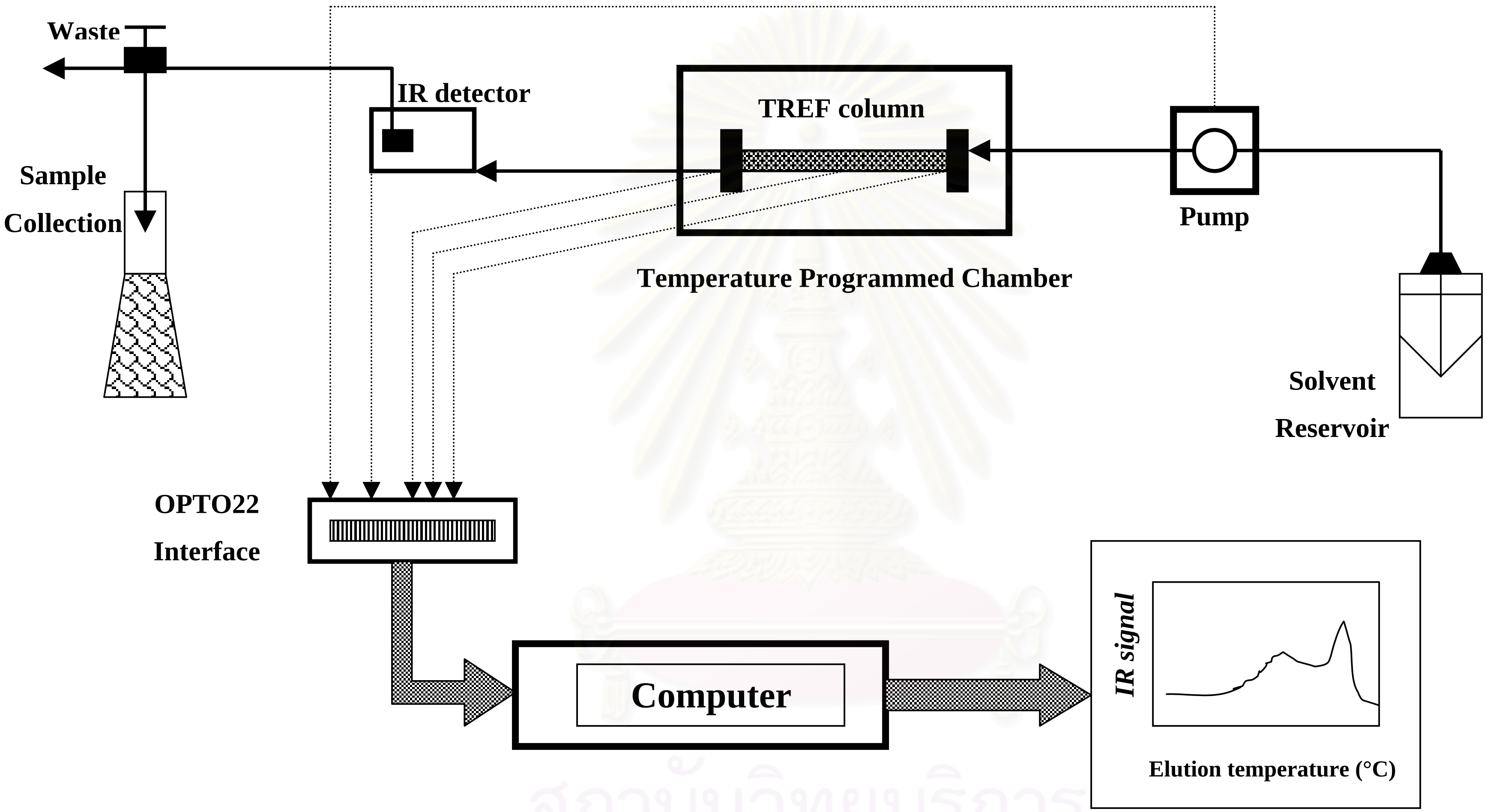

Figure 3.3. Schematic representation of TREF system (Zhang, 1999)

CHAPTER IV

Gas-Phase Polymerization of Ethylene and Ethylene/1-hexene

In this chapter, the catalytic performance of supported metallocene catalyst, using (n-BuCp)$_2$ZrCl$_2$ supported on silicalite, mesoporous molecular sieves and silica gel prepared by the impregnation method, is presented. The influence of the pore sizes of support and polymerization conditions on the gas-phase polymerization behavior of bis(butylcyclopentadienyl)zirconium dichloride (n-BuCp)$_2$ZrCl$_2$ supported on MAO-treated mesoporous molecular sieves with pore diameters of 2.6-25 nm was investigated. The properties of the catalysts and produced polymers are discussed. The supports and catalysts were described in the previous chapter (Tables 3.1 and 3.2A, respectively). The rate of ethylene polymerization and ethylene/1-hexene copolymerization in the gas-phase system is described. A version of this chapter has been published in the Journal of Applied Polymer Science, Vol. 87, 1161-1177 (2003).

4.1 Preliminary Results in Gas-Phase Polymerization

A number of preliminary experiments were done to determine suitable reactor conditions for gas-phase operation, to compare gas-phase activities with slurry activities, and to determine suitable Al/Zr ratios for the catalysts. The first set of experiments was performed with catalyst CAT-SD to determine the nature of the activity profiles for the homopolymerization and copolymerization and the effect of the amount of TIBA on polymerization activity. To minimize increases in bulk gas-phase temperatures due to the exothermic nature of the polymerization, small quantities of the catalyst were used in these experiments. The conditions for the experiments are described in Table 4.1, and activity profiles are shown in Figure 4.1. The bulk gas-phase temperature increases of 3.4ºC were observed for Run 2, the run with the highest activity; for other runs the bulk gas-phase temperature increases were less than 2ºC. The maximum rates listed in Table 4.1 were calculated from the measured ethylene feed rates, and they are an indication of the whether rises in the bulk temperature exceeding 1 or 2ºC are likely. Experience with the reactor described in Chapter III has shown that significant increases in the bulk gas-phase temperature occur if the instantaneous ethylene polymerization rate exceeds 25 to 30 g ethylene per hour.

Table 4.1. Results from Preliminary Experiments

		Amounts Charged to Reactor			C_2H_4		Activity (g PE/g cat·h)	
Catalyst	Run	Catalyst (mg)	TIBA (mmol)	1-hexene (mL)	pressure (psi)	Temp. (ºC)	Average	Maximum
CAT-SD	1	20	0.20	0	200	90	101	421
	2	20	0.40	0	200	90	464	2230
	3	20	0.60	0	200	90	451	1250
	4	10	0.20	1.42	200	90	145	410
	5	10	0.40	1.69	200	90	698	1240
CATS1-1	6	54	0.60	0	200	90	37	89
	7	53	1.00	0	200	90	22	35
	8	54	1.00	0	200	90	15	24
CATS1-2	9	53	0.60	0	200	50	20	--
CAT2.6-1	10	51	0.60	0	200	50	184	223
	11	52	0.60	0	200	70	377	761
CAT2.6-2	12	50	0.60	0	200	70	212	524
CAT2.6-3	13	50	0.60	0	200	70	60	--
CATS1-2	14	55	*	0	200	50	347	--
CAT2.6-3	15	50	*	0	100	50	481	--
CAT2.6-2	16	51	0.60	0	100	80	92	247
	17	50	0.60	0	200	80	241	880
CAT5.8	18	50	0.60	0	100	80	170	490
	19	54	0.60	0	200	80	293	556

* Slurry runs: no TIBA was added, but 14 mmol of Al as MAO was added to the slurry.

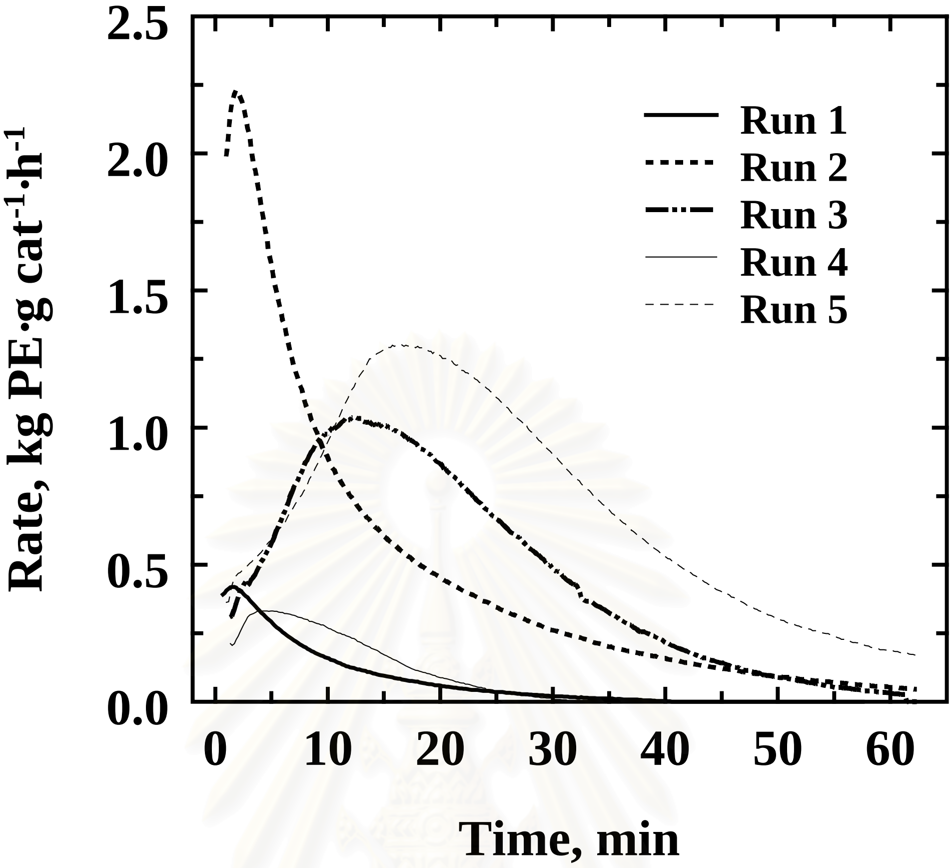

Figure 4.1. Activity profiles for CAT-SD (see Table 4.1 for the polymerization conditions)

From the results presented in Table 4.1 and Figure 4.1, it can be concluded that the amount of TIBA has a significant effect on the activity and the activity profile; too little TIBA resulted in low activities (cf. Runs 1 with Run 2 and Run 4 with Run 5); larger amounts of TIBA resulted in decreases in activity (cf. Runs 2 and 3). The low activities observed when only 0.2 mmol of TIBA was used (Runs 1 and 4) were probably due to incomplete scavenging of the impurities resulting in the subsequent deactivation of some of the catalyst. The amount of TIBA also has a marked effect on the shape of the activity profiles; larger amounts of TIBA broaden the activity profile with a decrease in the maximum activity; however, the average activity did not change significantly (cf. Runs 2 and 3). The activity profile for copolymerization was also broad (Run 4), similar to that for the homopolymerization with 0.6 mmol of TIBA. The comonomer effect, that is, activity enhancement due to the presence of a comonomer commonly observed for copolymerizations (Britto et al. 2001), was also observed for CAT-SD (cf. average rates for Runs 2 and 5).

Britto et al. (2001) investigated the effect of the TIBA concentration during 1-hexene/ethylelene copolymerization in a hexane slurry with a homogeneous Et(Ind)$_2$ZrCl$_2$-MAO/TIBA catalyst; they observed increases in the polymerization activity and amount of 1-hexene incorporation as the amount of TIBA was increased. They attributed the activity increase to an increase in MAO solubility in hexane with increasing TIBA concentrations. No studies on the effect of TIBA during gas-phase polymerizations were found in the open literature; such studies should be done because the aforementioned results indicate that TIBA plays a more complex role during gas-phase polymerization over supported metallocene catalysts than simply being a scavenger of impurities.

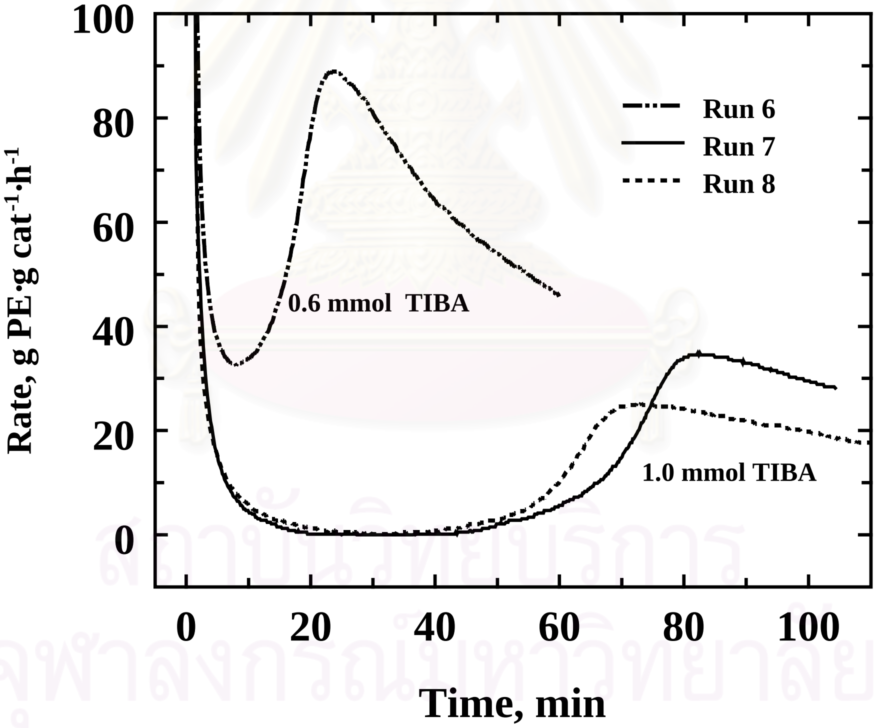

Figure 4.2. Effect of the amount of TIBA on the activity profile

A silica gel-supported catalyst (CATS1-1) with an Al/Zr ratio of 110 was prepared according to the procedure described previously and tested for activity (Runs 6 in Table 4.1); the activity was low, and increasing the amount of TIBA (Runs 7 and

8) did not improve the activity. However, the increased amounts of TIBA resulted in a large delay in the activation of the catalyst (see Figure 4.2). Another silica gel-supported catalyst (CATS1-2) with an Al/Zr ratio of 200 and an MMS2.6-supported catalyst (CAT2.6-1) with an Al/Zr ratio of 170 were prepared. The gas-phase polymerization activity for CATS1-2 was also low (Run 9, Table 4.1), but the activity of CAT2.6-1 was relatively high (Run 10). Two more MMS2.6-supported catalysts were prepared (CAT2.6-2; Al/Zr = 150 and CAT2.6-3; Al/Zr = 100) to determine whether the Al/Zr ratio had a large effect on the activity. The results for Runs 11-13 (Table 4.1) show that the activity was sensitive to the Al/Zr ratio; the activity increased by a factor of 3.5 when the Al/Zr ratio was increased for 100 to 150, and additional increase of about 80% occurred with an increase in the Al/Zr ratio from 150 to 170. On the basis of these observations, it was decided that all other catalyst preparations would have Al/Zr ratios of at least 170.

Slurry runs were done to confirm that the low Al/Zr ratio was the reason for the low activities of CATS1-2 and CAT2.6-3 (Runs 14 and 15); the Al/Zr ratio was increased to 8,800 for run 14 and to 7,000 for run 15 by the addition of MAO to the heptane. The activities for these slurry runs were much higher than the gas-phase activities; a greater than 15-fold increase in the activity occurred for CATS1-2 (cf. Runs 9 and 14). The activity profiles for the slurry runs were also markedly different than the gas-phase activity profiles (see Figure 4.3). The typical gas-phase activity profiles had an initial period of increasing activity followed by a decay in activity; the activity profiles for the slurry phased did not display deactivation behavior.

Finally, four experiments (Runs 16-19) were performed to determine the effect of ethylene pressure on the polymerization rates (Runs 16-19; Table 4.1). Doubling the ethylene pressure from 100 to 200 psi increased the average rates by a factor of 2.6 and 1.7 for catalysts CAT2.6-2 and CAT5.8, respectively. It is not expected that the average rates vary linearly with the gas-phase monomer concentration because the activity profiles for these catalysts, shown in Figure 4.4, have different activation-deactivation characteristics. The activity profile for Run 19 shows a delay in the activation similar to, but not as pronounced as, that observed for cases in which higher amounts of TIBA were used (see Runs 7 and 8 in Figure 4.2).

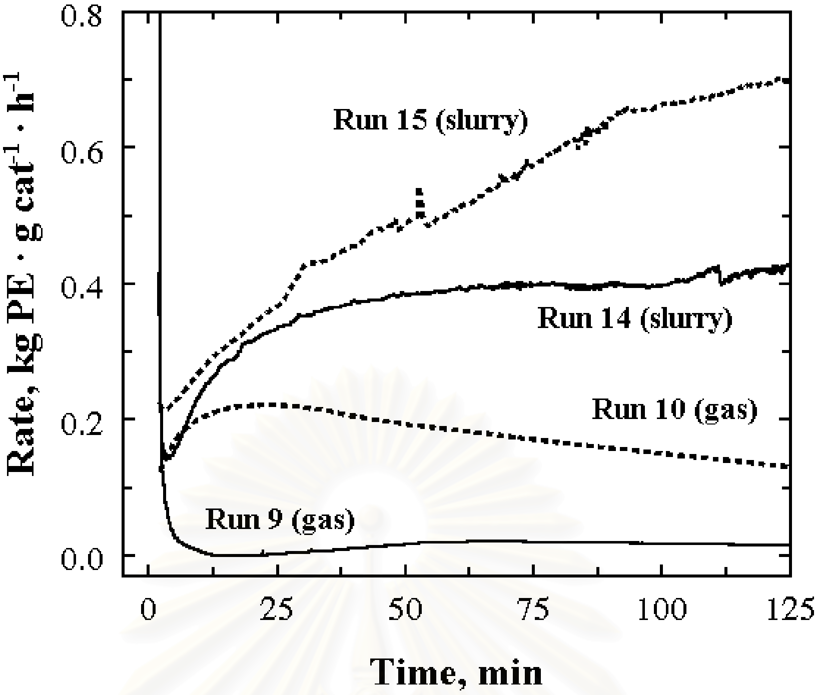

Figure 4.3. Comparison of the gas-phase and slurry-phase activity profiles (see Table 4.1 for the conditions)

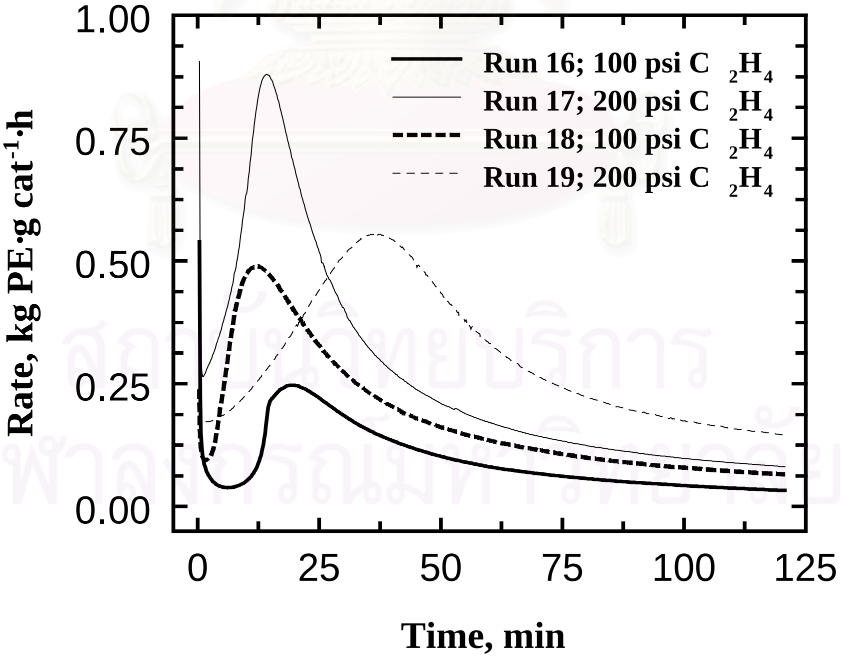

Figure 4.4. Effect of the ethylene pressure on the activity profiles

Therefore, it is likely that the concentration of TIBA was higher for Run 19 than for Run 18, possibly because of the lower consumption of TIBA for scavenging impurities. If overall polymerization rates for these types of hybrid activity profiles, such as those in Figure 4.4, are fit by power-law functions, an overall order between 1 and 2 usually results (Wu et al., 2000). At the end of the runs, that is, after 2 h of polymerization, the ratios of instantaneous specific polymerization rates for runs at 200 psi ethylene pressure to those at 100 psi were 2.2 and 2.4 for catalysts CAT2.6-2 and CAT5.8, respectively. It is likely that these ratios would approach 2.0, that is, first-order kinetics, at longer polymerization times when activation and deactivation rates are expected to become slow; for Run 19, the pseudo-steady state was not achieved after 2 h of reaction time (see Figure 4.4). It seems that the specific activity during the pseudo-steady state (at long reaction times) becomes relatively independent of the initial activation-deactivation behavior.

4.2. Influence of Support Pore Size and Polymerization Temperature on the Homopolymerization and Copolymerization Activities in Gas-Phase System

4.2.1. Homopolymerization Results

The homopolymerization activities for the various MMS-supported and silicalite-supported catalysts were measured at an ethylene pressure of 200 psi and at temperatures of 50-100ºC. The average activities are summarized in Table 4.2; these results show that the average polymerization rates were a function of the temperature and pore diameter of the support. Catalysts made with supports MMS2.6 and MMS5.8 had the maximum average rates; supports with larger pores yielded catalysts with lower activities, and the catalyst made with the small-pore silicalite had the lowest homopolymerization activities at all temperatures. The dependence of the activity on the pore size of the MMS supports appeared to decrease as the polymerization temperature increased, that is, at 100ºC, the variation in the average activities was a factor of three, whereas the activities at 90, 80, 70 and 50ºC varied by factors of about 4, 5, 6 and 7, respectively (Catalysts CAT2.6-1 and CAT25 are not included in this comparison because their activities were not measured at all the temperatures). The dependencies of the average rate on the pore diameter at 80 and 100ºC are illustrated in Figure 4.5. The variations in the activities with support type cannot be attributed to variations in the support surface areas or support pore volumes (see Table 3.1) because no trends in activity as a function of support surface area or pore volume could be detected.

The observed trends in activity as a function of the support pore size were very similar to those observed by Sano et al. (1999a and 1999b) for the slurry polymerization of ethylene using Cp_2ZrCl_2 supported on various silylated mesoporous molecular sieves, silica gels and silicalite that had been soaked in an MAO in toluene solution. The preparation techniques used by Sano and coworkers (1999a, 1999b, 2000, and 2001a) fractionated the MAO in the toluene solution, and the MAO left in the toluene yielded catalysts with different activities than the MAO retained by the supports. In our catalyst preparation techniques no macroscopic fractionation of the MAO occurred because all the MAO in the toluene was deposited onto or into the support (all the toluene was evaporated). However, some fractionation of the MAO must have occurred within the support particles; otherwise, it is difficult to explain the activity dependence on the support pore diameter.

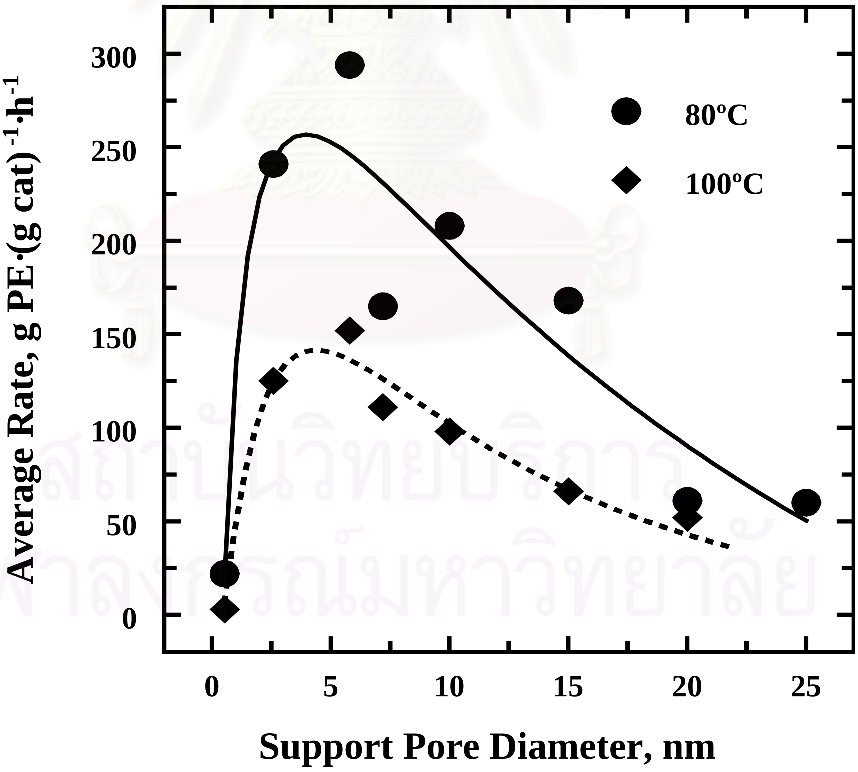

Figure 4.5. Effect of the support pore diameter on the average homopolymerization activity

Table 4.2. Average Ethylene Polymerization Activities as Function of Temperature and Support [**]

Catalyst	Support Pore Diameter (nm)	Al/Zr ratio	Average Polymerization Activities, g PE/(g cat·h)					
			50°C	70°C Homo-	70°C Co-*	80°C	90°C	100°C
CAT0.54	0.54	170	8	6	56	22	5	3
CAT2.6-1	2.6	170	249	339	330	---	---	---
CAT2.6-2	2.6	150	10	210	324	24	20	12
CAT5.8	5.8	170	47	172	136	29	13	15
CAT7.2	7.2	170	91	200	34	16	92	11
CAT10	10	330	14	186	0	20	15	98
CAT15	15	170	10	181	6	16	11	66
CAT20	20	170	19	37	63	61	55	52
CAT25	25	170	---	53	--	60	56	---

[*] 3.2 to 3.4 mL of 1-hexene added a beginning of each copolymerization run.

[**] Reaction Conditions: Ethylene Pressure = 200 psi
Amount of Catalyst = 52 (±2) mg
Amount of TIBA = 0.6 mmol
Polymerization Length = 2 h

MAO consists of a mixture of linear and cyclic oligomers of trimethylaluminum, which exist in dynamic equilibrium (Alt and Koppl, 2000). It has been proposed that the MAO species responsible for activating metallocenes consist of a cyclic cage structure made from CH_3AlO units (Sinn, 1995; Alt and Koppl, 2000). The higher activity of the catalysts made with MMS having pore diameters of 2.6 and 5.8 nm can be explained by assuming that the active MAO species are preferentially adsorbed by the MMS with small pores or possibly even stabilized by interaction with the surfaces of the small pores, such as a shift in the equilibrium from linear MAO to cyclic MAO. In larger pores, such segregation of MAO or favored formation of active MAO would not occur; it is even possible that absorption or formation of linear forms of MAO may be favored by some pore sizes. MAO cannot enter the very small pores of the silicalite-supported catalyst (CAT0.54) and this is the reason for its very low activity. Sano et al. (1999a and 1999b) also observed very low activities for silicalite-supported catalysts.

The pore size of the supports also had a significant effect on the shapes of the activity profiles; this is illustrated in Figures 4.6-4.8. All activity profiles showed a period of activation followed by deactivation, but the rates of activation and deactivation were functions not only of the temperature but also of the support pore diameter. Deactivation rates were more sensitive to temperature than activation rates; that is, there was a higher activation energy for the deactivation process(es) than for the activation process(es) of the catalytic sites. This behavior is well illustrated in Figure 4.6. The top panels in Figures 4.6-4.8 show the changes in the bulk gas-phase temperature as indicated by the average value measured with thermocouples T3 and T5 (Figure 3.1); the temperature increases at these locations were the highest because they were located where most of the reaction occurred. The tip of thermocouple T6 is located very close to the inside surface of the reactor wall and provided an indication of the inside wall temperature rather than the gas-phase temperature.

The activity profiles for CAT5.8 (Figure 4.7) were broader than those for CAT2.6-2, but the average activities for the two catalysts were about the same. The difference in the activity profiles for these two catalysts may be due to the size and shape of the catalyst (support) particles. CAT2.6-2 consisted of chunky particles 100-300 μm particles [see Figure 4.11 (a-d)], whereas CAT5.8 consisted of fibrous particles with diameters of about 20-50 μm [see Figure 4.12 (a-d)]. Therefore, temperature gradients inside the growing catalyst/polymer particles are likely to be larger for CAT2.6-2 than for CAT5.8, especially during the initial high-activity period. Temperatures inside the catalyst/polymer particles may be considerably higher than the bulk gas-phase temperature; such temperature gradients would lead to rapid activation followed by rapid deactivation, that is, profiles of the type observed for CAT2.6-2 (Figure 4.6). The activity profiles for CAT20, shown in Figure 4.8, are broad and there is no measurable increase in bulk gas-phase temperature because of the low activity of this catalyst. Therefore, it is unlikely that there were significant differences between gas-phase and catalyst-particle temperatures even though the catalyst particles were relatively large (see Figure 4.13). These observations indicate that the initial catalyst particle size as well as the support pore diameters can significantly affect the activity profiles.

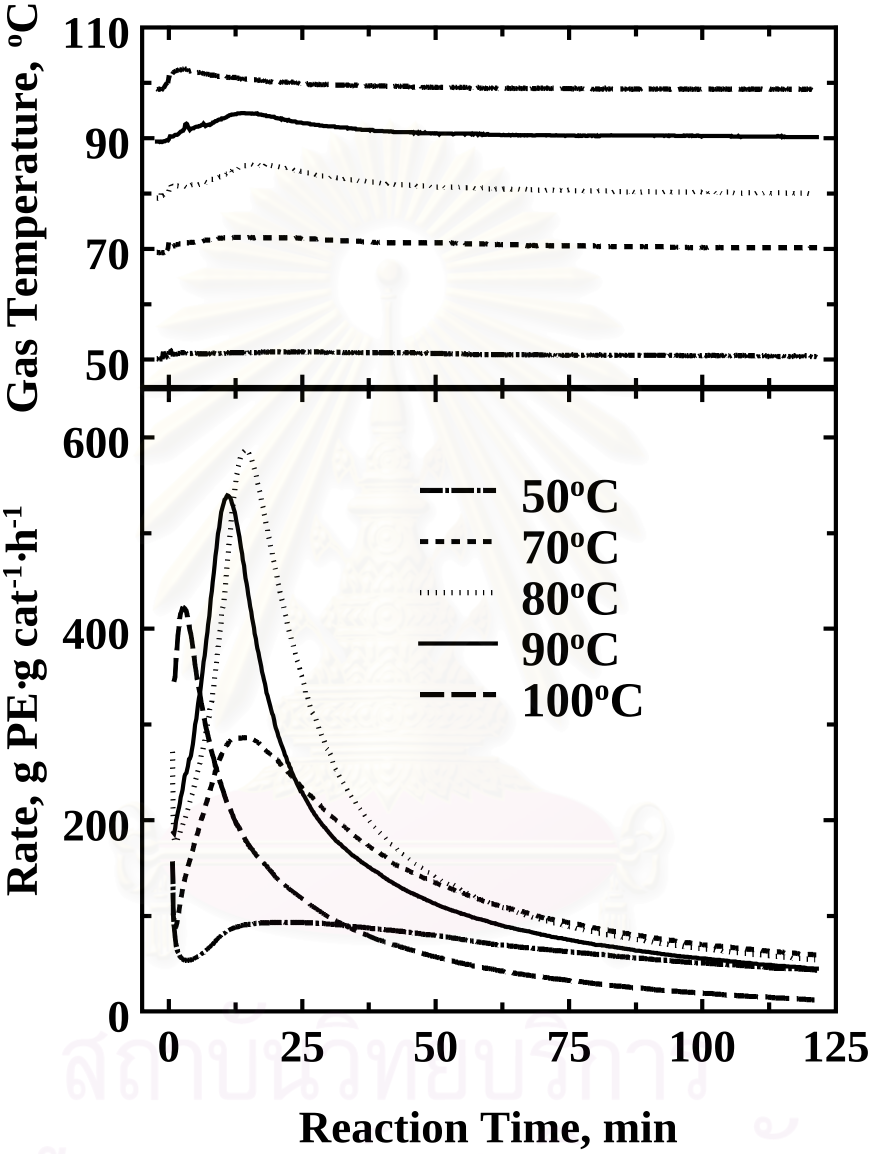

Figure 4.6. Activity and temperature profiles as a function of the reaction temperature for CAT2.6-2

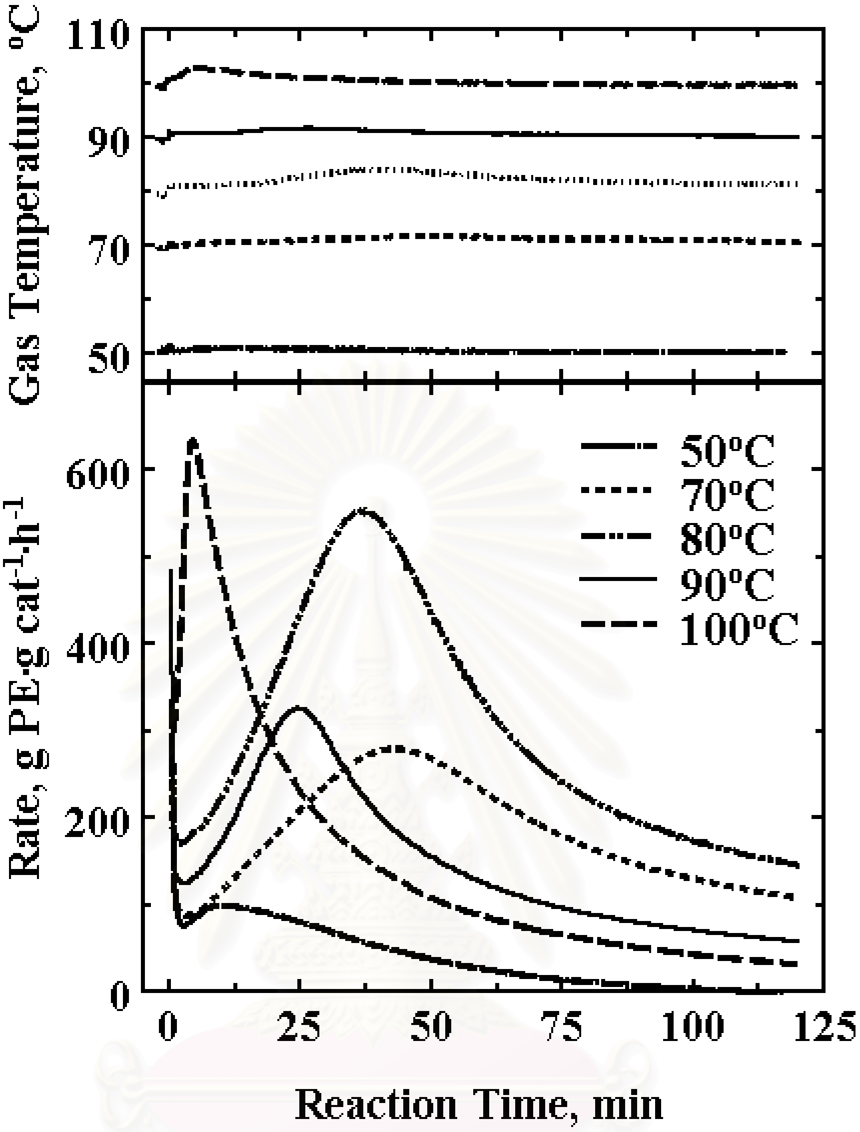

Figure 4.7. Activity and temperature profiles as a function of the reaction temperature for CAT5.8

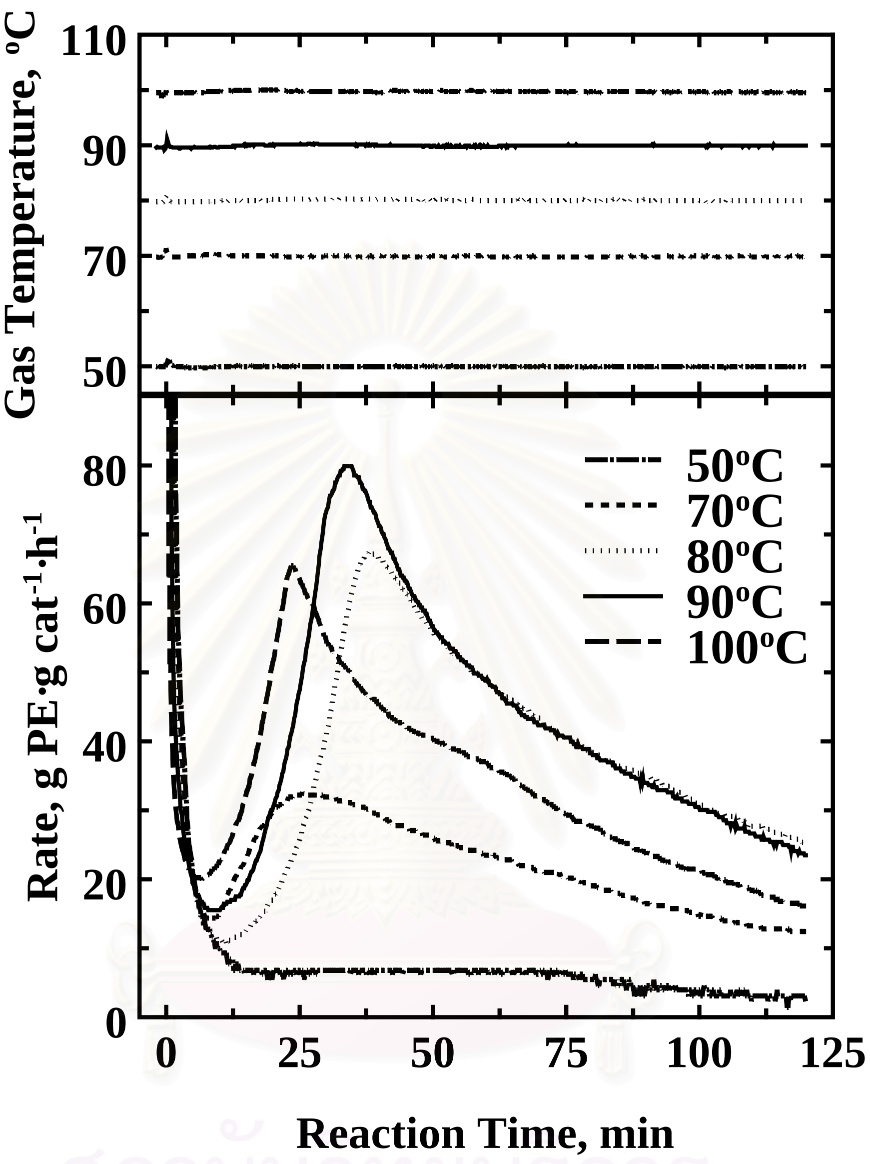

Figure 4.8. Activity and temperature profiles as a function of the reaction temperature for CAT20

4.2.2. Copolymerization Results

Copolymerization activities for 1-hexene/ethylene were measured at 70°C. 1-Hexene was injected only at the beginning of each copolymerization run; that is, the 1-hexene concentration was varied throughout the run. The amount of liquid 1-hexene injected into the reactor at the beginning of each copolymerization run was 3.3

(±0.1) mL. The initial 1-hexene partial pressure for 3.4 mL of 1-hexene was about 11 psi; the vapor pressure of 1-hexene at 70ºC is 18 psi. The average copolymerization activities, listed in Table 4.1, were much more support-dependent than the homopolymerization activities. The copolymerization and homopolymerization activities at 70ºC are compared in Figure 4.9. The copolymerization activities of catalysts made with support pore diameters of 7.2-15 nm were very low even though the homopolymerization activities were quite high. The reason for this unusual behavior is unknown. Unfortunately, insufficient amounts of the catalyst were available for repeat measurements; however, it is unlikely that all three copolymerization experiments with the catalysts made with the larger pore sizes were in error.

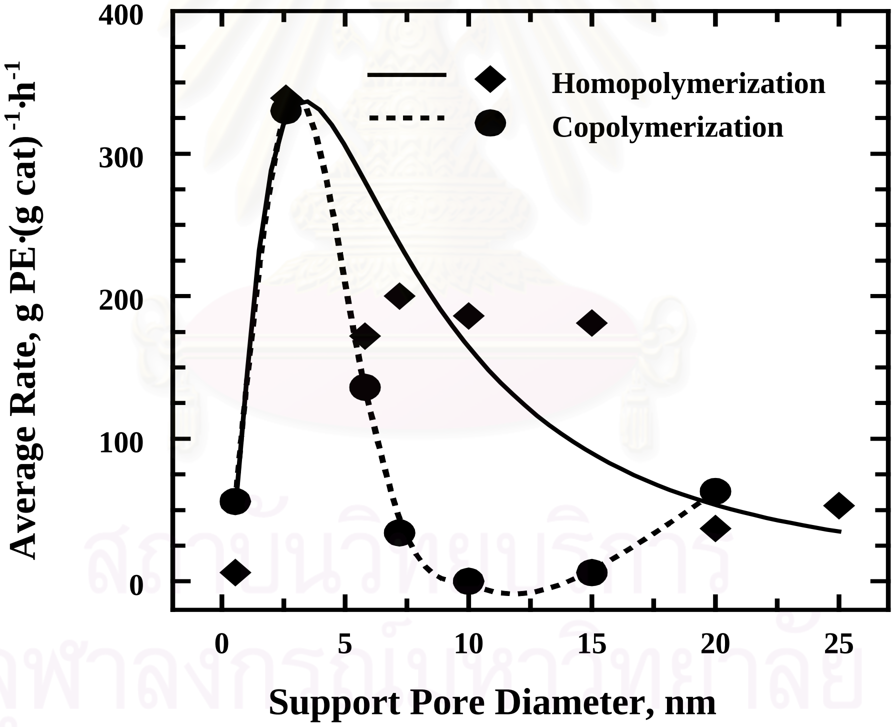

Figure 4.9. Comparison of the effects of the support pore diameter on the average homopolymerization and copolymerization activities at 70°C

The activity profiles for the copolymerizations are shown in Figure 4.10. All the profiles are broad, even those for the high-activity catalysts (CAT2.6-1 and CAT2.6-1). This indicates that the 1-hexene participated in the site activation processes, but the reason(s) for the very marked difference in homopolymerization and copolymerization activity profiles is not know. The degree of 1-hexene incorporation will be discussed in Chapter V, but the presence of 1-hexene does have a significant effect on the molar masses, as discussed later. Additional copolymerization experiments with freshly prepared catalysts and characterization of the polymers, including determination of 1-hexene incorporation, were done to obtain more insight into the copolymerization processes over mesoporous molecular sieve-supported ($(n\text{-BuCp})_2ZrCl_2$) catalysts. These experiments will be discussed next chapter.

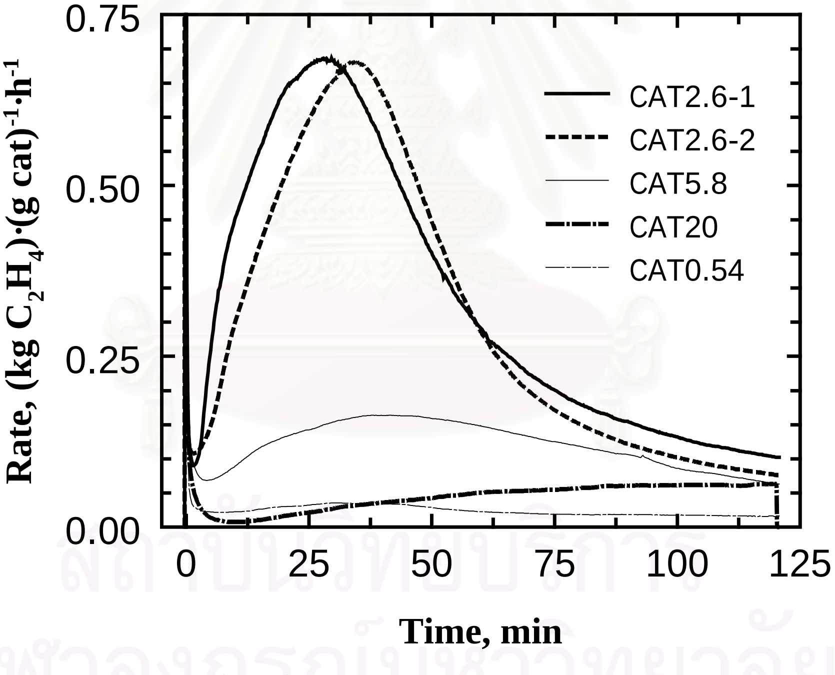

Figure 4.10. Activity profiles for 1-hexene/ethylene copolymerization with various catalysts

4.2.3. Comparison of Activity Profiles and Activities with those in the Literature

Activity profiles are only reported infrequently in the literature, and activity profiles for gas-phase polymerization over supported metallocene catalysts are even rarer. Only two studies that reported gas-phase activity profiles for ethylene polymerization were found in the literature: the 1997 study by Roos et al. (1997) and the recent study by Ray and coworkers (Xu et al., 2001, 2001b, and Chakravarti et al., 2001a). Roos and coworkers used 1 mass% $Me_2Si[Ind]_2ZrCl_2$ on an MAO-treated silica as a catalyst, and Ray and coworkers used bridged and unbridged metallocenes supported on MAO-containing silicas; the nature of the metallocenes was not specified. The activity profiles in both of these studies had similar shapes to those reported in this study, that is, an activation period followed by deactivation. The activation was very rapid in the study by Roos et al., and some oscillations are apparent in the ethylene feed rates in the initial 30 min of the runs because of temperature control problems.

The average normalized gas-phase polymerization activity at 70ºC (i.e. activity per mole of Zr and per atmosphere of ethylene pressure) of the supported $Me_2Si[Ind]_2ZrCl_2$ catalyst used by Roos et al. (1997) was essentially the same as that of CAT2.6-2 used in the current work. In Table 4.3, these average gas-phase activities are compared to some average activities obtained for slurry operations. Comparisons are made with slurry results because normalized activities, other than the study by Roos et al., are not available in the open literature for gas-phase studies with supported metallocene catalysts. Comparing activities, even normalized average activities, should be done with care because different polymerization conditions have been used by various investigators. In the absence of activity profiles, which is frequently the case, it is impossible to know whether the average activity for a short polymerization time is comparable to that for a longer polymerization time; therefore, the normalization of activities to a time period of one hour can be very misleading. Despite these difficulties, it is possible to draw the following general conclusions from the results in Table 4.3: First, average activities of silica-supported metallocenes in slurries are up to 10-fold higher than average gas-phase activities if the Al/Zr ratio is increased by the addition of MAO to the slurry; and second, if no additional MAO is added to the slurry then gas-phase and slurry activities appear to be approximately equal. Increases in gas-phase activities for supported metallocene catalysts may be attainable by the support surface being changed to improve interactions with MAO (Harrison et al., 1998).

Table 4.3. Comparison of Average Polymerization Rates Over Silica-Supported Metallocene Catalysts.

Catalyst	Support	Reactor Mode	Al/Zr Ratio[a]	Temperature °C	Pressure of C_2H_4 (psi)	Normalized Rate[b]	Comments	Ref.
$(n\text{-BuCp})_2ZrCl_2$	MMS/MAO	Gas	150	70	200	420	CAT2.6-2	[c]
$(n\text{-BuCp})_2ZrCl_2$	MMS/MAO	Gas	150	70	200	640	$1\text{-}C_6H_{12}$ copolymerization	[c]
$Me_2[Ind]_2ZrCl_2$	Silica/MAO	Gas	383	70	73	440	--	Roos et al. (1997)
$(n\text{-BuCp})_2ZrCl_2$	Silica/TMA	Slurry	--	70	560	63	Hydrated silica treated with TMA	Lee and Sinn (1995)
$(n\text{-BuCp})_2ZrCl_2$	Silica/MAO	Slurry	326	20	30	400	Activity from activity profile	Goretzki et al. (1999)
$(n\text{-BuCp})_2ZrCl_2$	Silica	Slurry	3000	70	15	510	No Al added to SiO_2	Dos Santos et al. (1999)
$en[Ind]_2ZrCl_2$	Silica/MAO	Slurry	1000	20	60	2,250	Added MAO to slurry	Harrison et al. (1998)
Cp_2ZrCl_2	MMS/MAO	Slurry	40	20	60	200	Activity after 10 min	Trong On et al. (2001)
Cp_2ZrCl_2	Silica/MAO	Slurry	1000	60	145	370	Added MAO to slurry	Alt and Koppl (2000)
Cp_2ZrCl_2	MMS/MAO	Slurry	2000	50	36	2,240	Added MAO to slurry	Rahiala et al. (1999)
Cp_2ZrCl_2	Silica/MAO	Slurry	2000	50	36	4,000	Added MAO to slurry	Rahiala et al. (1999)
Cp_2ZrCl_2	Silica/MAO	Slurry	2757	70	15	5,000	Added MAO to slurry	Tait and Monterio (2000)

[a] The Al/Zr ratio includes Al added to catalyst as well as Al added to slurry

[b] Normalized rate kg PE/(mol Zr·h·atm C_2H_4)

[c] Current work.

4.3. Molar Mass Properties and Characteristics of Catalyst and Polymer

Scanning electron micrographs of supports and catalysts prepared from MMS2.6, MMS5.8, MMS20, and S0.54 are shown in the top panels of Figure 4.11-4.14. Support MMS2.6 consisted of irregularly shaped particles that appeared to be agglomerates of short fibrous particles [see Figure 4.11(a,b)]. Support MMS5.8 consisted of macrofibers [Figure 4.12(a)] made up of smaller short fibers [Figure 4.12(b)]. The structure of supports MMS7.2 and MMS15.2 (see in Appendix A) was very similar to that of MMS5.8. MMS10 had a more globular, rather than fibrous structure, but was not as agglomerated as MMS20, as shown in the top panels of Figure 4.13. MMS25, like MMS20, consisted of agglomerated particles, but the agglomerates had a macroporous structure. The silicalite, shown in Figure 4.14(a-c), consisted of loosely agglomerated 1-3 μm crystals. The structures of the catalysts, as shown by scanning electron microscopy, were very similar to those of the starting supports (see the middle panels in Figures 4.11-4.14. In some cases, the catalyst preparation resulted in additional agglomeration [cf. Figure 4.14 (a,d)]. Information on the morphology of the polymers produced obtained by SEM and representative micrographs of the polymers produced are shown in the bottom panels of Figures 4.11-4.14. The homopolymer particles made with MMS-supported catalysts all consisted of agglomerates of fairly dense, plate-like polymer particles. The fiber morphology of CAT5.8, CAT7.2 and CAT15 was not replicated into the polymer particle morphology. The morphology of the polymer made with CAT0.54 (silicalite-supported) was different than the polymers made with MMS-supported catalysts (bottom panels of Figures 4.11-4.14). The structure of the polymer made with CAT0.54 was more open, and unfractured silicalite particles are clearly visible in the polymer matrix [Figure 4.14(h,i)]; that is, MAO and (n-BuCp)$_2$ZrCl$_2$ did not enter the pores of the silicalite, and MAO and (n-BuCp)$_2$ZrCl$_2$ in CAT0.54 were supported on the external surface of the silicalite crystals, similar to the catalyst prepared by Goretzki et al. (1999), except that the silicalite particles were much smaller than the silica gel particles that they used.

The structure of the copolymer particles made with CAT 2.6-2 and CAT5.8 were more porous [see Figures 4.11(h) and 4.12(h)] than those of the homopolymers. The micrograph for a copolymer made with CAT20 [Figure 4.13(h)] does not show a porous structure, but other regions of the particles shown in Figure 4.13(g) are porous.

The region shown in Figure 4.13(h) was chosen because it clearly shows unfractured catalyst (support) particles possibly indicated that some of the support particles were not active, because of a lack of impregnation with MAO and/or (n-BuCp)$_2$ZrCl$_2$; this may be the reason for the low copolymerization activity of CAT20. To obtain more information of this observation, the chemical composition of the light and dark regions were analyzed by EDX measurement. The light spots showed the presence of sodium and chlorine; hence, these small particles (<1 μm) are ground seed bed particles what were not removed from the nascent polymer during the washings.

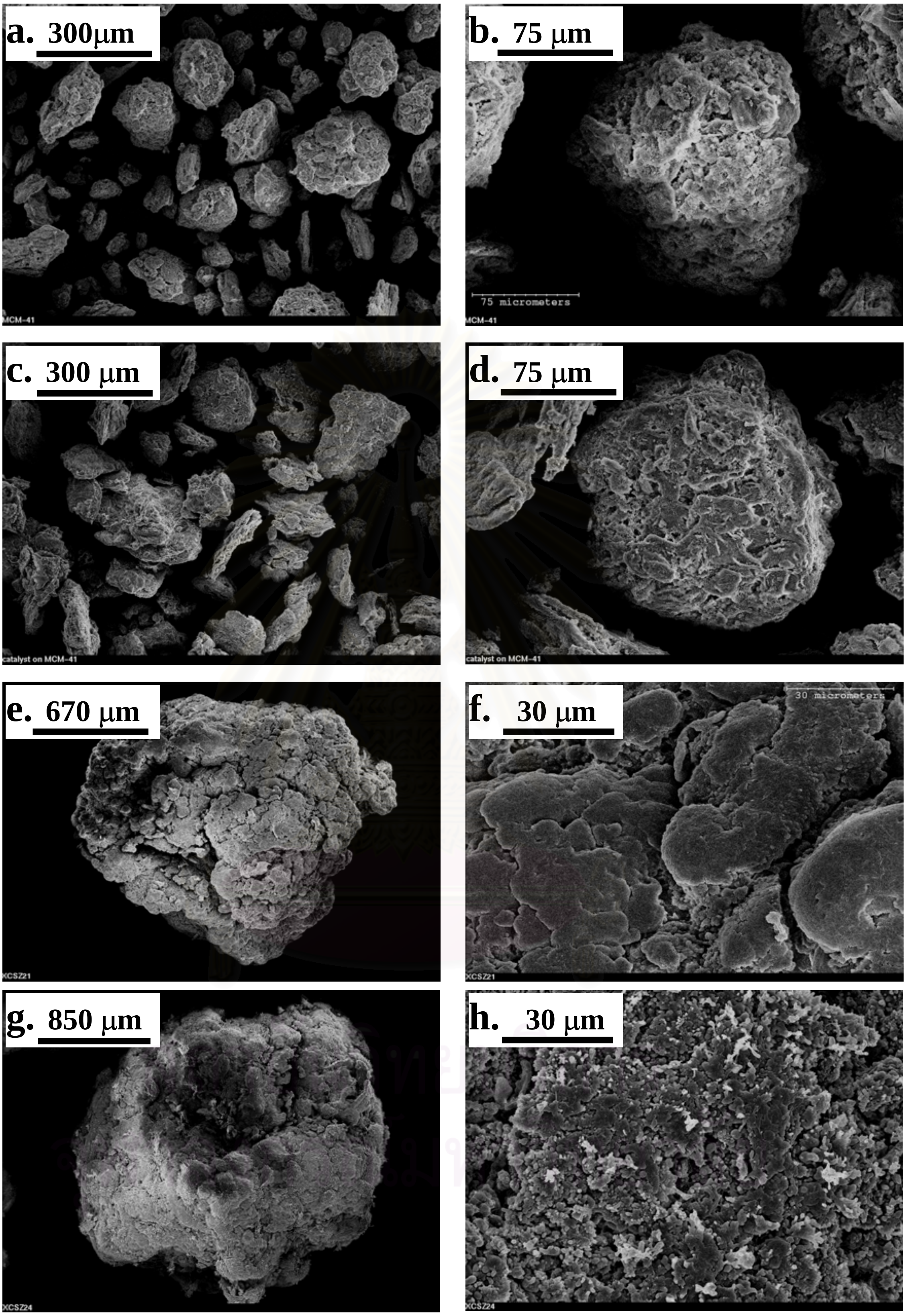

Figure 4.11. Scanning electron micrographs: (a,b) the MMS2.6 support, (c,d) CAT2.6-2, (e,f) the homopolymer produced with CAT2.6-2 at 70ºC, and (g,h) the copolymer produced at 70ºC (see Table 4.2 for polymerization conditions)

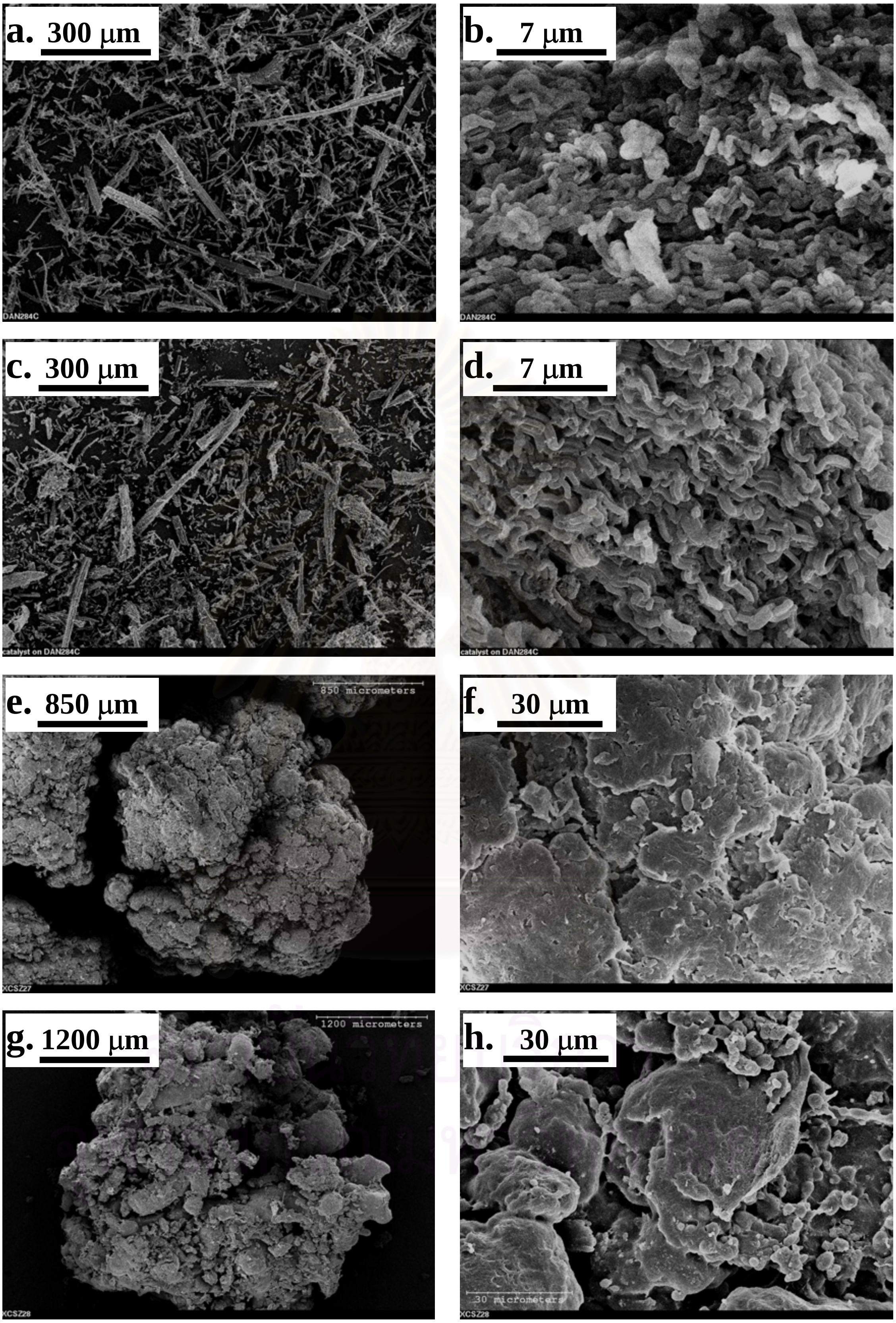

Figure 4.12. Scanning electron micrographs: (a,b) the MMS5.8 support, (c,d) CAT5.8, (e,f) the homopolymer produced with CAT5.8 at 70ºC, and (g,h) the copolymer produced at 70ºC (see Table 4.2 for polymerization conditions)

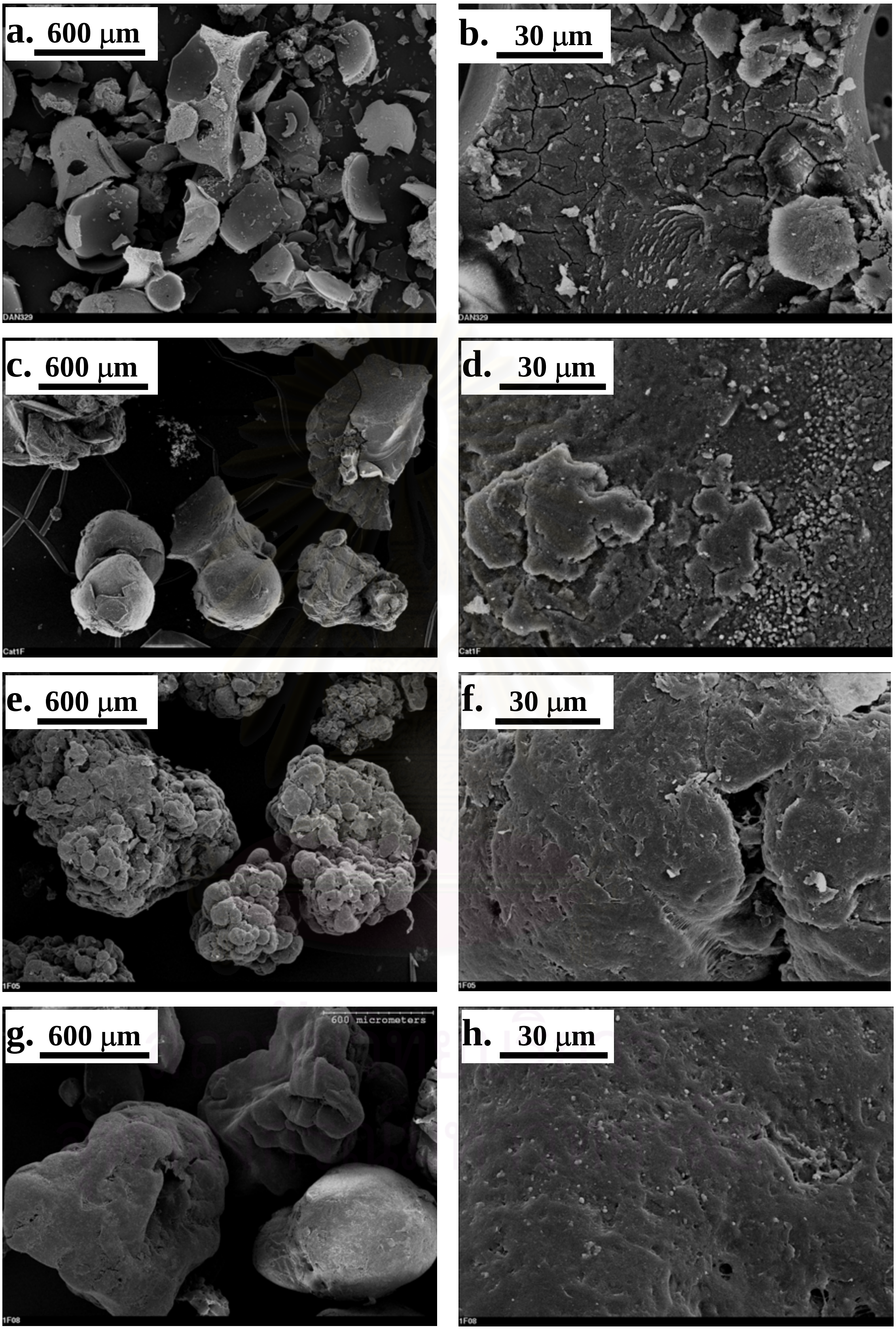

Figure 4.13. Scanning electron micrographs: (a,b) the MMS20 support, (c,d) CAT20, (e,f) the homopolymer produced with CAT20 at 70ºC, and (g,h) the copolymer produced at 70ºC (see Table 4.2 for polymerization conditions)

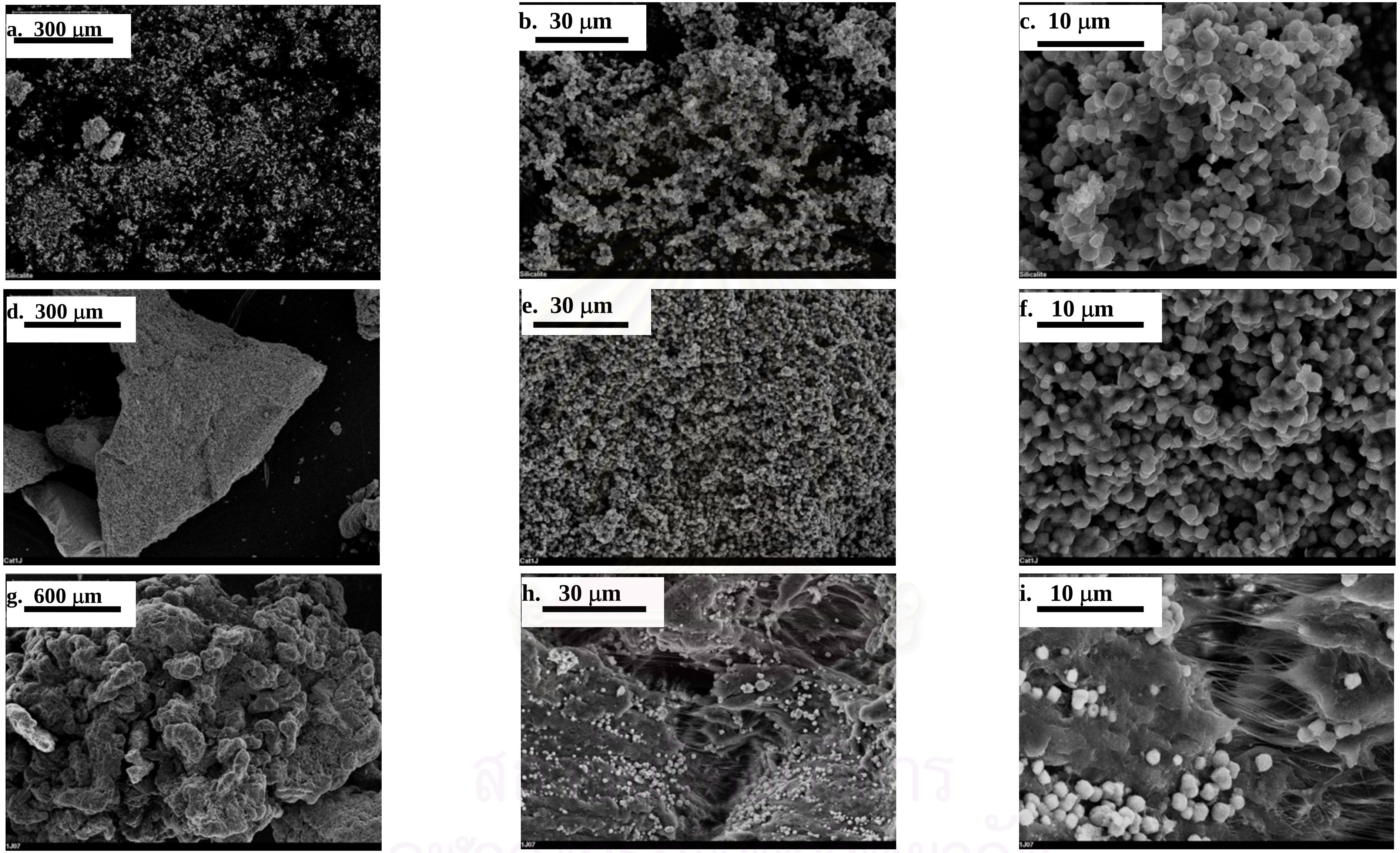

Figure 4.14. Scanning electron micrographs: (a-c) the S0.54 support, (d-f) CAT0.54, and (g-i) the homopolymer produced with CAT0.54 at 100ºC (see Table 4.2 for polymerization conditions)

Molar masses were measured for most of the products and the value of those are shown in Appendix A (see Table A3). It was found that the dependence of the molar masses on polymerization temperatures was reasonably well correlated by Equations 4.1 and 4.2.

$$ln(\mathrm{M_n}) = \mathbf{a_n} + \frac{\mathbf{b_n}}{\mathrm{T}} \qquad \textbf{--Eq (4.1)}$$

$$ln(\mathrm{M_w}) = \mathbf{a_w} + \frac{\mathbf{b_w}}{\mathrm{T}} \qquad \textbf{--Eq (4.2)}$$

Equation (4.1) would be the expected correlation for the number-average molecular weight (M_n) as a function of temperature if transfer to monomer was the main-chain termination reaction. The values of the constants $\mathbf{a_n}$, $\mathbf{b_n}$, $\mathbf{a_w}$ and $\mathbf{b_w}$, as well as the correlation coefficients $\mathbf{r^2}$, for the various catalysts for which products were obtained at four or more temperatures are listed in Table 4.4. Plots illustrating the best fit (CAT15) and the worst fit (CAT5.8) for polymers made with mesoporous molecular sieve-supported catalysts are shown in Figure 4.15. The lines for the polydispersities in Figure 4.15 are given by the ratios of Equations (4.2) and (4.1), and the data points are based on the ratios of the measured weight-average (M_w) and number average(M_n) molar mass values. The polydispersities for all the MMS-supported catalysts were essentially independent of temperature with values of 2.3-2.7 for all catalysts except CAT20, for which the polydispersities varied from 2.7-3.1.

Table 4.4. Parameter Values for Molar Mass Correlations (Equations 4.1 and 4.2)

Catalyst	**Parameters for M_n (Equation 4.1)**			**Parameters for M_w (Equation 4.2)**		
	$\mathbf{a_n}$	$\mathbf{b_n}$	$\mathbf{r^2}$	$\mathbf{a_w}$	$\mathbf{b_w}$	$\mathbf{r^2}$
CAT2.6-2	7.469	1330	0.95	7.773	1546	0.98
CAT5.8	8.523	987	0.55	9.035	1121	0.68
CAT7.2	7.958	1200	0.86	8.957	1154	0.95
CAT10	8.875	845	0.91	10.034	748	0.91
CAT15	7.901	1216	0.96	8.966	1160	0.99
CAT20	8.359	963	0.95	8.806	1179	0.95
CAT0.54	6.176	1609	0.65	10.080	630	0.52

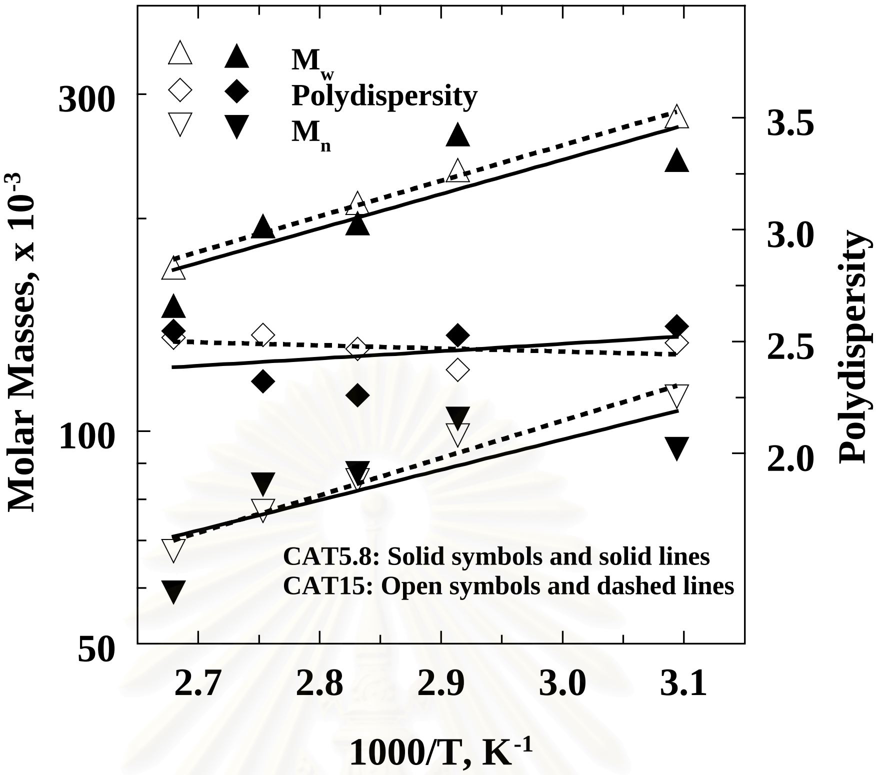

Figure 4.15. Sample plots of molar mass/temperature correlations

The molar masses for all catalysts decreased with increasing polymerization temperature, indicating that the overall activation energies for the propagation reactions were lower than those for the chain termination reactions. On the basis of the values of $\mathbf{b_n}$ in Table 4.4, the difference in the average values of the lumped termination and propagation activation energies, that is, ($E_{termination} - E_{propagation}$), is 9.1 kJ/mol; the ($E_{termination} - E_{propagation}$), on the basis of $\mathbf{b_w}$, is 9.6 kJ/mol. The average ratio of the lumped pre-exponential factors for propagation steps to termination steps, according to $\mathbf{a_n}$ values, is 3570. The molar masses for MMS-supported catalysts were relatively independent of the type of catalyst; this indicates that the nature of the active sites was relatively independent of the pore sizes of the mesoporousmolecular sieves. The molar masses of the polymers made with CAT0.54 were lower than those made with MMS-supported catalysts, and the polydispersity of polymers made with CAT0.54 increased with increasing temperature (see correlation values in Table 4.4). Therefore, the nature of the sites in the silicalite-supported catalyst (CAT054), in which neither MAO nor (n-BuCp)$_2$ZrCl$_2$ entered the pores, was different than those in the MMS-supported catalysts.

The molar masses for 1-hexene copolymers were lower than those of homopolymers made at similar temperatures and ethylene pressures; the copolymer and homopolymer molar masses are compared in Figure 4.16. The molar masses for the polymers made with CAT0.54 are not included in the trend lines shown in Figure 4.16 because the molar masses for both the homopolymer and copolymer made with CAT0.54 were much lower than those of polymers made with MMS-supported catalysts. The polydispersity of the copolymer made with CAT0.54 was 7.1, indicating the presence of multiple types of catalytic sites in this catalyst.

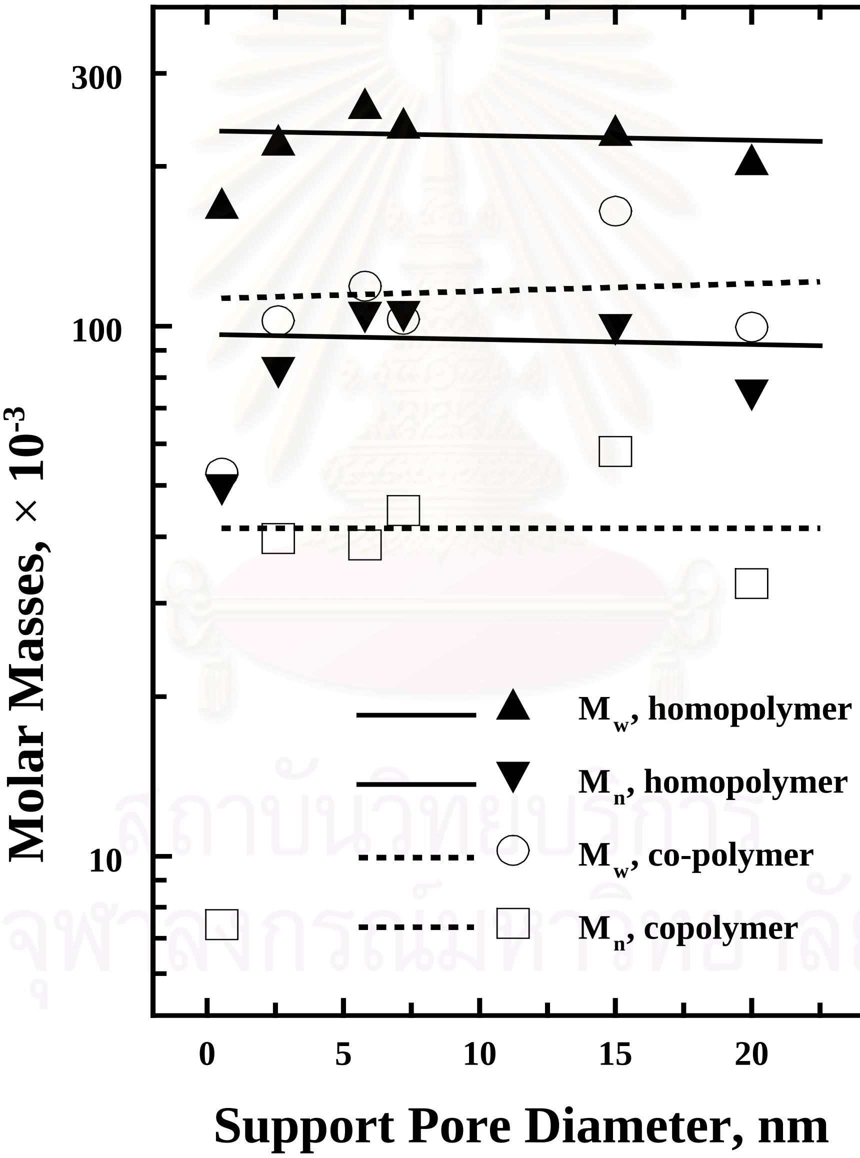

Figure 4.16. Molar masses for homopolymers and copolymers made at 70°C with catalysts of different pore sizes

The molar masses of homopolymers made at 100 psi of ethylene pressure (Runs 16 and 18; Table 4.1) were lower than the molar masses of homopolymers made with the same catalysts at 200 psi of ethylene pressure (Runs 17 and 19; Table 4.1). For CAT2.6-2, M_w decreased from 187×10^3 to 155×10^3, and for CAT5.8, M_w decreased from 187×10^3 to 153×10^3 with a decrease in the ethylene pressure from 200 to 100 psi. The polydispersities for polymers made at 100 psi of ethylene pressure were 2.7, whereas the polydispersities were 2.4 and 2.3 for polymers made at 200 psi with CAT2.6-1 and CAT5.8, respectively. The dependence of the molar masses on ethylene pressure indicates that chain termination by modes other than transfer to monomer occurred. Molar masses would essentially independent of ethylene pressure for the case in which chain transfer to monomer is the main mode of chain termination if the common assumption holds that both propagation and transfer-to-monomer rates are first-order in the monomer (Kissin, 1985).

CHAPTER V

Rate and Product Properties of Polyethylene Produced by Copolymerization of 1-Hexene and Ethylene in the Gas-Phase System

The previous observations have shown that the pore size of mesoporous molecular sieves used for the preparing $(n\text{-BuCp})_2\text{ZrCl}_2$-MAO/mesoporous molecular sieve catalyst had a significant affect on the activity of the catalysts. The most active catalyst had pore diameters of 2-6 nm. No results on the effect of temperature and 1-hexene concentration on copolymerization activity were included in the previous chapter. Control of copolymerization behavior is crucial for LLDPE production. Hence, additional copolymerization experiments with freshly prepared catalysts and characterization of the produced polymers, including determination of 1-hexene incorporation, were carried out to obtain more insight into the copolymerization processes over mesoporous molecular sieve-supported $(n\text{-BuCp})_2\text{ZrCl}_2$ catalysts. Additional polymerizations of these experiments were carried out with a new small-pore catalyst, CAT2.5, to investigate the effects of temperature and 1-hexene concentration on polymer properties and catalytic activities. Additional characterization of polymers produced in gas-phase with $(n\text{-BuCp})_2\text{ZrCl}_2$-MAO on the supports with different pore size was also carried out; these results are presented in the current chapter. Temperature rising elution fractionation (TREF), size exclusion chromatography (SEC), and differential scanning calorimetry (DSC) were used for characterization of the products. A version of this part has been submitted to the journal of Polymer for publication.

5.1. Effect of Temperature and 1-Hexene Concentration on Gas-Phase Copolymerization Activity

Additional polymerization experiments were carried out with the new small-pore catalyst, CAT2.5; conditions used for these runs are described in Table 5.1. The 1-hexene partial pressure was significantly less than the 1-hexene vapor pressure for all runs except run 9 for which the initial partial pressure of 1-hexene was only slightly less than its vapor pressure. The vapor pressure of 1-hexene was calculated using the Antoine equation and the constants in Poling et al. (2001). The effect of

1-hexene concentration on the activity and temperature profiles are shown in Figure 5.1. The amount of 1-hexene had a large effect on the rate profile and the total yield.

Table 5.1. Description of polymerization runs.

Run	**Catalyst**		**Initial Amount $1\text{-}C_6H_{12}$ (mL)**	**Initial $1\text{-}C_6H_{12}$ Concent. mol/m^3**	**Initial Temp (°C)**	**Total Pressure (MPa)**	**Total PE Yield (g)**	**Run Length (h)**
	Type	**Amount (mg)**						
1	CAT2.5	50.5	0.0	0.0	80	1.34	28.3	1.97
2	CAT2.5	51.2	0.50	4.2	80	1.34	35.7	2.01
3	CAT2.5	50.6	1.40	11.8	80	1.35	51.5	1.98
4	CAT2.5	50.8	2.23	18.8	80	1.34	24.5	1.90
5	CAT2.5	48.0	2.20	18.5	80	1.35	12.6	1.93
6	CAT2.5	49.9	3.06	25.8	80	1.34	22.6	1.98
7	CAT2.5	50.1	5.61	47.2	80	1.35	3.1	1.88
8	CAT2.5	51.0	5.03	42.3	80	1.41	2.4	1.93
9	CAT2.5	46.2	2.24	18.9	40	1.37	2.2	1.95
10	CAT2.5	48.1	2.22	18.6	60	1.41	3.1	1.96
11	CAT2.5	47.6	2.21	18.6	90	1.37	18.0	1.97
12	CAT2.5	45.5	2.20	18.5	100	1.37	5.6	1.90
13	CAT20	51.1	3.40	28.6	70	1.37	6.5	2.00
14	CAT20	49.6	3.46	29.1	70	1.37	3.3	1.02
15	CAT20	53.5	3.47	29.2	70	1.38	0.7	0.51
16	CAT0.54	50.2	3.30	27.8	70	1.38	5.7	2.01
17	CAT2.6	51.6	3.23	27.2	70	1.38	34.3	2.05
18	CAT5.8	50.8	3.30	27.8	70	1.37	14.4	2.09
19	CAT7.2	50.1	3.43	28.9	70	1.37	3.4	2.00
20	CAT15	49.1	3.38	28.4	70	1.38	0.6	2.00

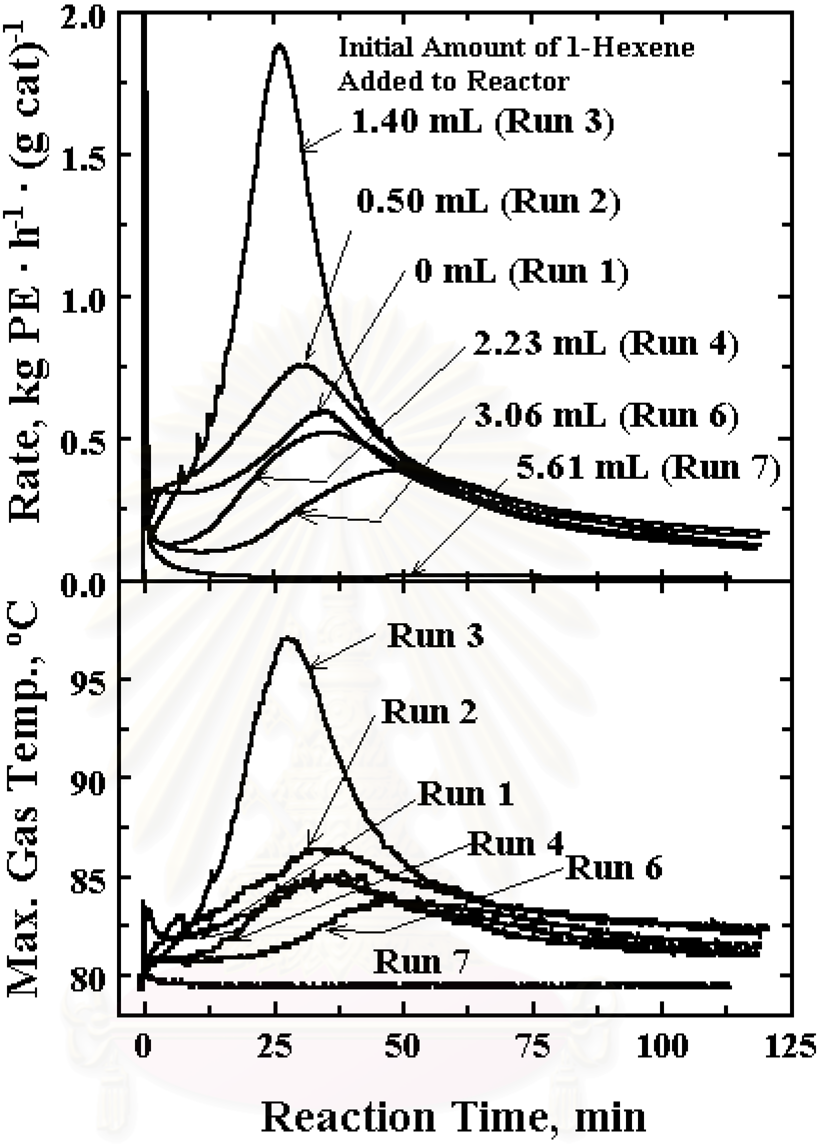

Figure 5.1. Effect of 1-hexene concentration on rate and temperature profiles (CAT2.5)

For initial 1-hexene concentrations of <12 mol/m^3 (Runs 2 and 3) the polymer yields were higher than the homopolymer yield (Run1); for initial 1-hexene concentrations >18 mol/m^3, the yields (Runs 4 to 8) were lower than the homopolymer yield. Various effects of comonomer concentration on polymerization rates in slurry reactors have been reported; Yoon et al. (2000) did not observe a comonomer effect except for ethylene/1-hexene at 40°C, while Galland et al. (1999) and Britto et al. (2001) reported that ethylene/1-hexene polymerization rates were much higher than ethylene homopolymerization rates at 60°C. Britto and coworkers suggested that the presence of the comonomer makes the polymer product more amorphous and soluble and these factors increase the accessibility to catalytically active sites. In gas-phase polymerization no dissolving of the polymer occurs; hence, this cannot be responsible for the comonomer effect we observed. We also observed that at high 1-hexene concentrations the polymerization rates are very low even though the degree of product crystallinity decreased with increasing 1-hexene concentration (see TREF results below).

The initial rates of polymerization provide a possible cause for the 1-hexene dependence of the polymerization rate (see rates of polymerization at times <10 min in Figure 5.1). The highest initial rate is observed for homopolymerization (Run 1) and the initial polymerization rate decreases monotonically with increasing 1-hexene concentrations. However, for low 1-hexene concentrations (Runs 2 and 3) the rate increased rapidly and exceeded the homopolymerization rate after a few minutes. The increase in polymerization rates at higher 1-hexene concentration was much lower, and at the highest 1-hexene concentration (Run 7) no increase in rate occurred. A repeat run at high 1-hexene concentrations was done (Run 8) which confirmed the low rates at high 1-hexene concentrations. These observations suggest that 1-hexene increases the accessibility of ethylene to the catalytic sites; this can be due to more amorphous polymer being formed in the presence of 1-hexene, as proposed by Britto et al. (2001), because this would result in higher ethylene solubility in the polymer. It is also possible that fracturing of catalyst particles is improved in the presence of 1-hexene. The decrease in rates at the higher 1-hexene concentrations may be due to the coordination of 1-hexene to the catalytic sites which greatly reduces ethylene insertion even though ethylene concentration in the amorphous polymer surrounding the catalytic sites is high. It is interesting to note that the rates of polymerization at reaction times greater than 1 h were approximately equal for initial 1-hexene contents of <26 mol/m^3; the reason for this is not known.

The rapid increase in the polymerization rate at the low 1-hexene concentration was accompanied by significant increases in the gas-phase temperatures (see bottom panel of Figure 5.1). The increases in the temperature resulted in additional increases in rate, but the conclusion that small amounts of 1-hexene resulted in large increases in rate is valid even if Runs 2 and 3 were not isothermal because the increase in the temperature is the result of the increased rate caused by the presence of 1-hexene. Note: Problems with temperature control during gas-phase polymerizations were recognized early in gas-phase polymerization studies with metallocene catalysts (Roos et al., 1997).

The effect of gas-phase temperature on copolymerization rates is shown in Figure 5.2. These runs were done with an initial 1-hexene concentration of 18.7 (±0.2) mol/m^3; the maximum rates at this 1-hexene content were such that the increases in gas-phase temperature were small. Only for Run 4 was there an appreciable temperature increase and this was ≤ 5°C; the temperature rise for all the other runs in this temperature series, was ≤ 2°C (see bottom panel of Figure 5.2). Total polymer yields were very low for polymerization temperatures of 40 and 60°C; repeat runs at these temperatures confirmed the low yields at 40 and 60°C. Yields were highest at 80°C and then decreased with increasing temperature. Results presented in Chapter IV, for a similar catalyst, CAT2.6, showed that the copolymerization activity was also high at 70°C. The results show that the activation and deactivation rates of CAT2.5 are very temperature sensitive. The polymerization rates after 2 h of polymerization at 80, 90 and 100°C were 0.12, 0.07 and 0.00 kg PE/(h· g cat), respectively. All the activity profiles shown in Figure 5.2 have a maximum, and the reaction time required to reach this maximum increased with decreasing temperature, for instance, at 100°C the rate maximum occurred after 11 min while 62 min were required at 40°C. Average product yields for 2 h polymerization times increased by a factor of 8 for a temperature increase from 60 to 80°C, and the maximum rates of polymerization for this temperature change increased by a factor of 14. The above results show that high gas-phase polymerization rates for the mesoporous molecular sieve supported $(n\text{-BuCp})_2ZrCl_2$ catalyst resulted for narrow ranges of temperature (80 to 90ºC) and 1-hexene concentration (about 5 to 20 mol/m^3); much lower rates were observed outside of theses ranges.

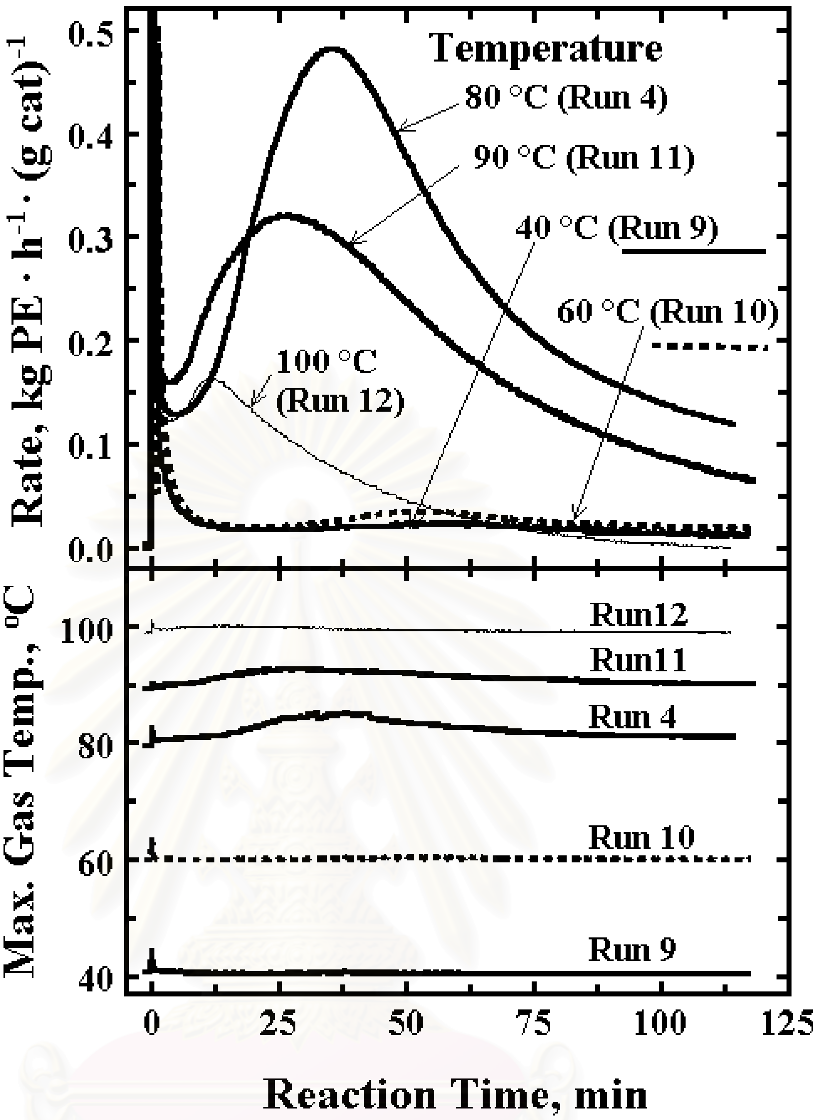

Figure 5.2. Effect of reaction temperature on rate profiles (CAT2.5)

Estrada and Hamielec (1994) and Soga et al. (1995) observed that properties of polyethylene produced in the slurry phase with homogenous metallocene catalysts were a function of reaction time. Three runs (runs 13 –15) were done to determine whether similar reaction-time dependent properties are obtained with a supported (*n*-BuCp)$_2$ZrCl$_2$ catalyst during gas-phase polymerization. CAT20 was used for these runs and the duration of these runs was 2.0, 1.0 and 0.5 h (other conditions are given in Table 5.1). The activity and temperature profiles are shown in Figure 5.3, and the properties of the products produced are discussed in the sections below.

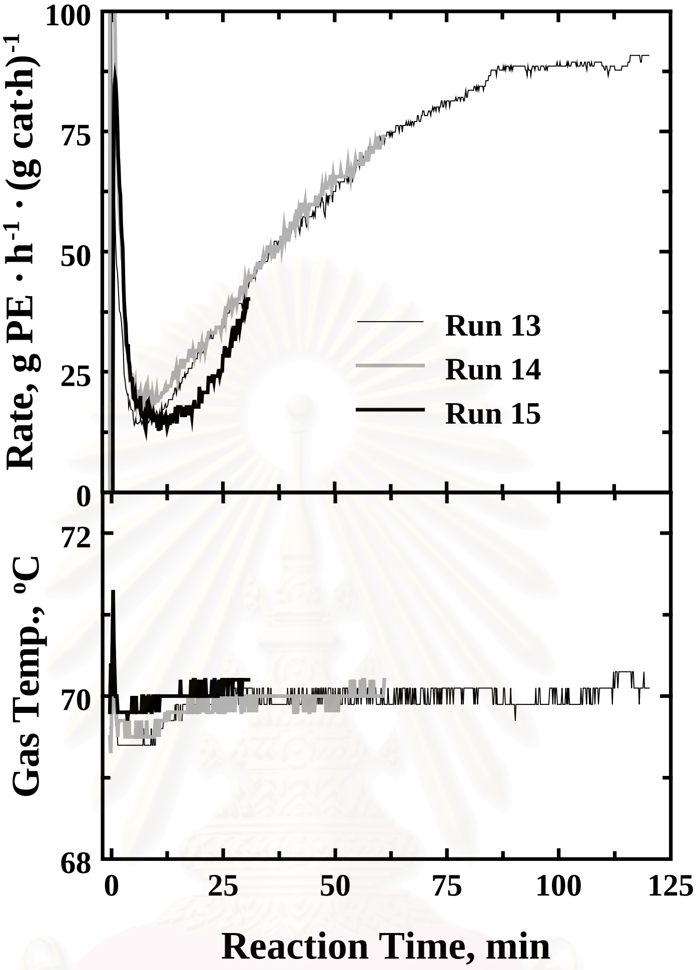

Figure 5.3. Rate and temperature profiles for runs of different duration (CAT20)

The reproducibility of activity profiles during the first 30 and 60 min for the three runs shown in Figure 5.3 was very good.

5.2. Characterization by Temperature Rising Elution Fractionation (TREF)

TREF provides information on the structure of the polyethylene molecules (short chain branching distribution or methylene sequence distribution); it does not provide information on the morphology of the nascent polymer because the nascent structure is destroyed during the dissolution of the polymer. Analytical TREF analyses, and DSC analyses discussed in the following section, were done on all the samples. The TREF results are summarized in Table 5.2.

Table 5.2. Summary of TREF Results.

Run	Average CH_3 Concentrations [CH_3 Groups/1000 C]		C_W/C_N	Fraction Homo-Polymer	Fraction 1-Hexene Reacted	1-Hexene Concentrations (mol/m^3)	
	C_N	C_W				Initial	Final
1	0.5	0.5	1.02	0.99	--	0	0
2	3.1	9.3	2.98	0.88	1.00	4.2	0
3	2.9	4.2	1.44	0.80	0.96	11.8	0.5
4	5.7	8.8	1.55	0.47	0.56	18.8	8.3
5	7.3	9.3	1.28	0.09	0.37	18.5	11.7
6	9.0	11.9	1.32	0.07	0.59	25.8	10.6
7	23.2	27.1	1.17	0.00	0.11	47.2	42.0
8	24.1	27.0	1.12	0.00	0.09	42.3	38.5
9	28.7	35.8	1.25	0.05	0.25	18.9	14.2
10	13.7	16.6	1.21	0.05	0.17	18.6	15.2
11	7.5	9.0	1.20	0.05	0.55	18.6	8.3
12	8.6	9.8	1.14	0.02	0.19	18.5	15.0
13	22.3	28.5	1.28	0.03	0.38	28.6	17.7
14	23.7	28.3	1.19	0.05	0.20	29.1	23.3
15	18.1	23.2	1.29	0.08	0.03	29.2	28.3
16	24.8	29.1	1.17	0	0.38	27.8	17.2
17	9.1	16.1	1.77	0.34	0.86	27.2	3.8
18	12.5	21.4	1.71	0.16	0.48	27.8	14.5
19	16.4	22.2	1.35	0.16	0.14	28.9	24.9
20	19.3	25.1	1.33	0.11	0.03	28.4	27.5

The average concentration of short chain branches, C_N expressed as CH_3 groups per 1000 carbon atoms, was obtained from the TREF profiles, like those shown in Figure 5.4, by Equation 5.1

$$C_N = \frac{\int_{t_o}^{t_f} (IR)_{signal} [CH_3]_t \, dt}{\int_{t_o}^{t_f} (IR)_{signal} \, dt} = \frac{\int_{T_o}^{T_f} (IR)_{signal} [CH_3]_T \, dT}{\int_{T_o}^{T_f} (IR)_{signal} \, dT} \quad \text{---- } \mathbf{(5.1)}$$

where $[CH_3]_t$ and $[CH_3]_T$ are the concentrations of CH_3 groups per 1000 carbon atoms in the eluted polyethylene as a function of elution time and elution temperature, respectively and $(IR)_{signal}$ is the time varying output of the IR cell during the TREF elution. Equation 3.1 was used to calculate $[CH_3]_T$. The elution time and elution temperature can be interchanged in Equation 5.1 because the temperature was a linear function of time. An estimate of the 'broadness' of the short chain branching contribution can be obtained from the C_W/C_N ratio (Zhang et al., 2000); C_W is defined by Equation 5.2.

$$C_W = \frac{\int_{t_o}^{t_f} (IR)_{signal} [CH_3]_t^2 \, dt}{\int_{t_o}^{t_f} (IR)_{signal} [CH_3]_t \, dt} = \frac{\int_{T_o}^{T_f} (IR)_{signal} [CH_3]_T^2 \, dT}{\int_{T_o}^{T_f} (IR)_{signal} [CH_3]_T \, dT} \quad \text{---- } \mathbf{(5.2)}$$

The fraction of homopolymer, F_{homo}, was taken as the fraction of polymer which eluted above 90.5ºC, as shown in Equation 5.3.

$$F_{homo} = \frac{\int_{90.5}^{T_f} (IR)_{signal} [CH_3]_T \, dT}{\int_{T_o}^{T_f} (IR)_{signal} \, dT} \quad \text{---- } \mathbf{(5.3)}$$

An elution temperature of 90.5ºC, according to Equation 3.1, corresponds to a concentration of 4 $[CH_3]$ groups per 1000 carbons.

The fraction of the initially added 1-hexene which was consumed by polymerization, $F_{C6,reacted}$, was estimated from the average short chain branch content, C_N, and the amount of polymer produced, m_{PE}, by using Equation 5.4.

$$F_{C6,reacted} = \frac{m_{C6,PE}}{m_{C6,0}} = \frac{0.006\, m_{PE}\, C_N}{\rho_{C6}\ V_{C6,0}} \qquad \textbf{---- (5.4)}$$

where $m_{C6,PE}$ is the amount of 1-hexene incorporated into the polymer; $m_{C6,0}$ is the mass of 1-hexene charged to the reactor; ρ_{C6} is the density of liquid 1-hexene (0.6731 g/cm^3) and $V_{C6,0}$ is the volume of 1-hexene fed to the reactor at the beginning of the run. The gas-phase 1-hexene concentration was measured by gas chromatography at the beginning and at the end of the run for Run 5. The measured 1-hexene concentration at the end of Run 5 was 6.4 mol/m^3, which corresponds to 0.50 g of 1-hexene in the gas phase (the final void volume of the reactor was about 935 cm^3 after subtracting the volumes of the product and the salt seedbed). The initial amount of 1-hexene charged to the reactor was 1.48 g (2.20 mL). Therefore, 66% of the 1-hexene was removed from the gas phase; some of the 1-hexene was reacted and some was dissolved in the 12.6 g of product. According to the TREF analysis, 37% of the 1-hexene was removed due to reaction; this requires that 0.43 g of 1-hexene was dissolved in the 12.6 g of product, i.e. 0.034 g 1-hexene per gram of product. The solubility of 1-hexene in the product from Run 5 was estimated to be 0.02 to 0.04 g 1-hexene per gram of polyethylene from the results obtained by (Moore, 2000; and Moore and Wanke 2001). The agreement between the 1-hexene consumption obtained by gas chromatography and that based on the TREF results is an indication that the short chain branching concentration measured is reliable.

Multiple peaks in TREF profiles are usually attributed to the presence of different types of catalytic sites (Soga et al., 1995 and Soares and Hamielec, 1995); the TREF profiles for Runs 13 –15 in Figure 5.4 all have two distinct peaks. This suggests that CAT20 has at least two different types of catalytic sites. The intensity of the high temperature peak at about 96°C decreases with increasing reaction time; this PE eluted at 96°C is essentially an ethylene homopolymer (C_N<2). Soga and coworkers also observed that the fraction of highly-crystalline PE decreased with increasing reaction time obtained for ethylene/1-hexene copolymerization in the slurry phase using a homogeneous Cp_2ZrCl_2 – MAO catalyst. The change in the fraction of crystalline PE with increasing reaction time implies that the concentration of catalytic sites responsible for the formation of the crystalline PE decreased with time. This decrease can be due to the rapid deactivation of these sites or to the transformation of these sites to sites which incorporated 1-hexene more readily; such a transformation has been suggested by Estrada and Hamielec (1994). It should be pointed out that the 1-hexene concentration at the end of the 2-h run, Run 13, was less than the 1-hexene concentration at the end of the shorter runs; nevertheless, the fraction of homopolymer formed decreased with increasing reaction time (see Table 5.2).

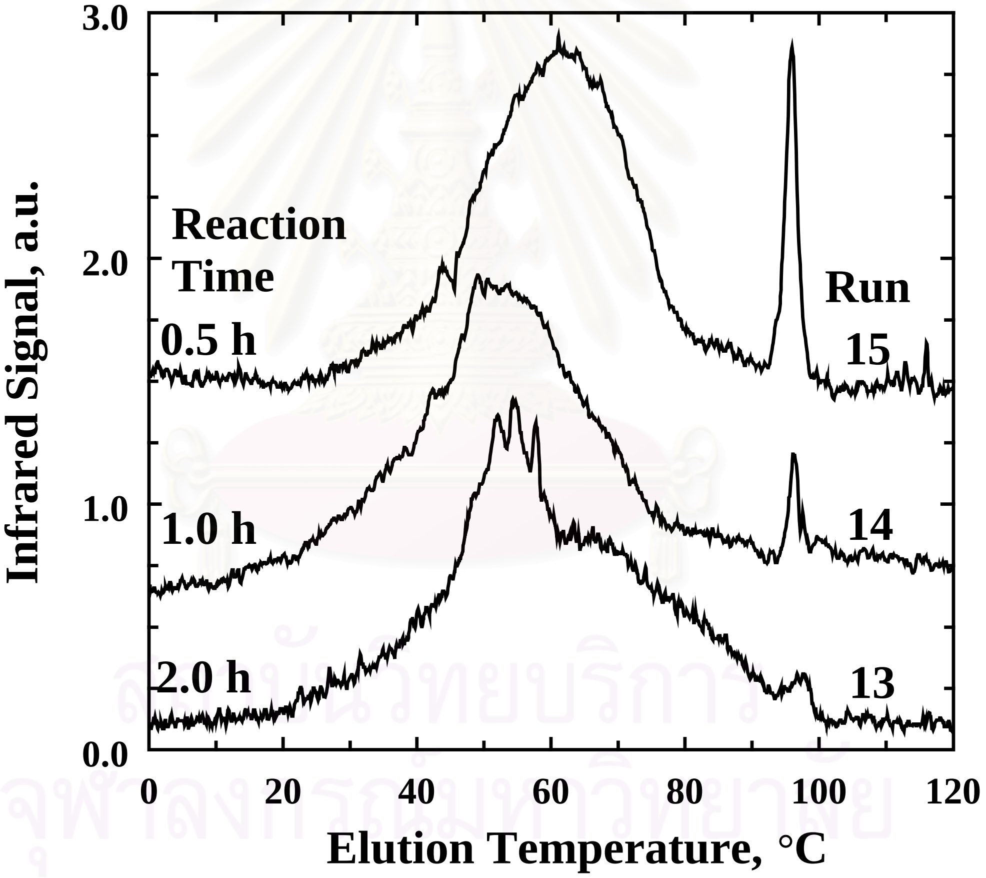

Figure 5.4. Effect of reaction time on TREF profiles (CAT 20; patterns offset for clarity)

The pore size of the supports had a significant effect on the short chain branching distribution of the products made with the different catalysts; the TREF profiles of LLDPE made at similar reaction conditions, with catalysts of different pore size, are shown in Figure 5.5. All the TREF profiles in Figure 5.5, except the one for CAT0.54, have two or more distinct maxima; again indicating multiple types of catalytic sites. An interesting feature of the TREF profiles in Figure 5.5 is the systematic variation in their shape for increases in the support pore diameter from 2.6 to 20 nm. The TREF profile for CAT0.54 (Run 16), does not seem to fit the trend; CAT0.54 appears to behave as if it had large pores. This is reasonable because no reaction occurred inside the pores of this catalyst. The results of this behavior have previously shown that all the catalytic active species were on the outer surface; hence, this catalyst can be considered to have pores of infinite size.

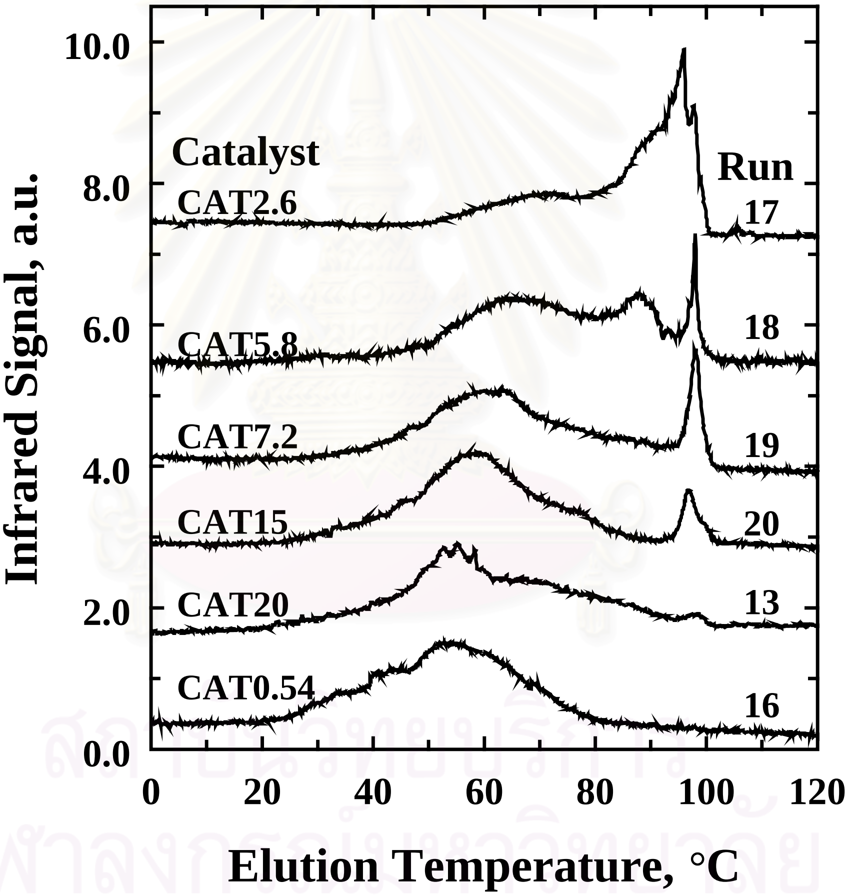

Figure 5.5. Effect of support pore size on TREF profiles (patterns offset for clarity)

Two distinct peaks, one in the temperature range of 55 to 70°C and the other at about 98°C, are present in the TREF profiles. The low temperature peak is dominant in the large pore catalysts while the high temperature peak is more pronounced for the small pore catalysts. A third peak at about 88°C is clearly visible in the profile for CAT5.8 (two repeat TREF analyses for this sample showed the same three peaks). This peak is also visible as a shoulder in the profile for CAT2.6. The presence of three distinct TREF peaks suggests that at least three different types of catalytic sites are present in these catalysts. The catalytic site corresponding to the peak at 98°C produced ethylene homopolymer while the other two sites had differing 1-hexene incorporation rates. The results, discussed above, for the runs of varying lengths (Runs 13-15) showed that the homopolymerization sites were also present in significant amounts at short polymerization times for the large-pored CAT20. However, the homopolymerization sites disappeared within the first two hours of polymerization for CAT20. The homopolymer content of products decreased with increasing pore size of the catalysts (see Table 5.2; Runs 13, 17 – 20). From these observations it is concluded that the nature of catalytic sites made during the impregnation of the supports with MAO and (n-BuCp)$_2$ZrCl$_2$ is affected by the support pore size. The structure of the MAO adsorbed on the pore walls is probably a function of the pore size (Sano et al., 1999a, 1999b, 2000, and 2001a), and this may be responsible for the observed effect of pore size on catalytic behavior.

A new catalyst with small pores, CAT2.5, was prepared to determine the effect of 1-hexene concentration and temperature on catalytic behavior and product properties. The TREF profiles of products made with CAT2.5 at 80°C and different 1-hexene concentration are shown in Figure 5.6 (note the logarithmic scale of the ordinate). These profiles again show two main peaks; the high temperature peak being the dominant peak at low 1-hexene concentration and the low temperature peak being dominant at high 1-hexene concentrations. The shoulder on the high temperature peak becomes more prominent with increasing 1-hexene concentrations (Runs 2 – 4). At intermediate 1-hexene concentrations (Runs 5 and 6), the peak at 90°C is dominant, and at high 1-hexene concentration only the low temperature peak is present.

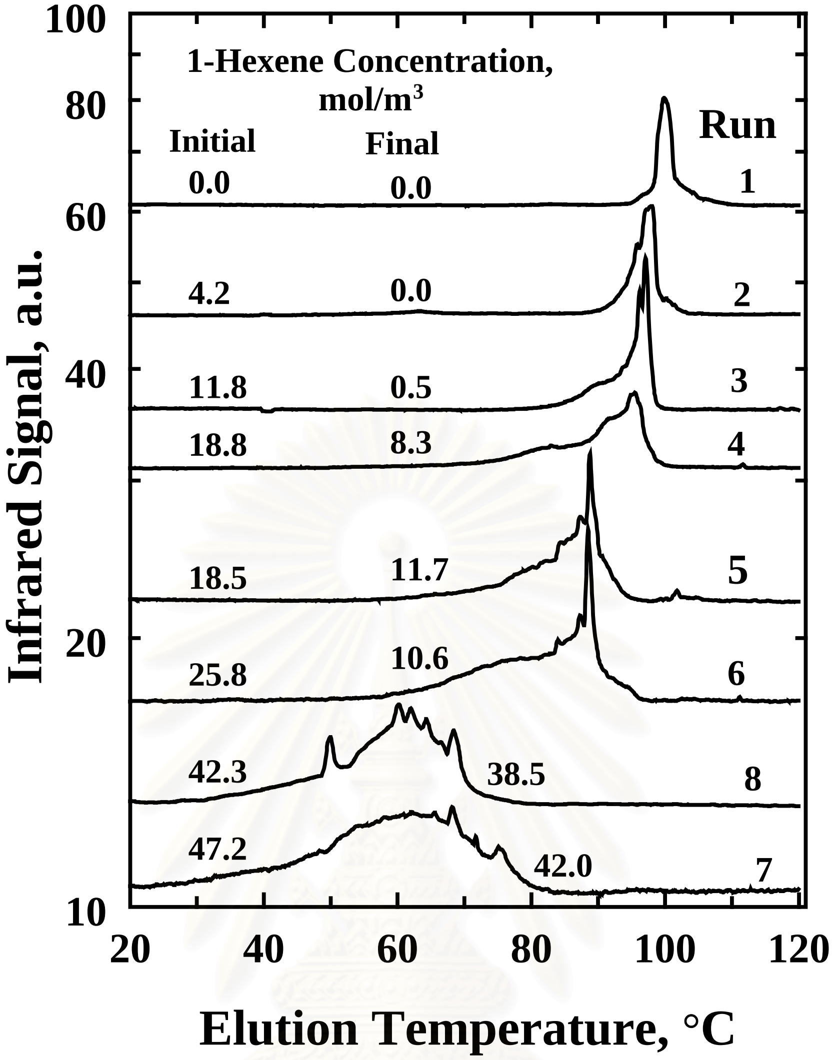

Figure 5.6. Effect of initial 1-hexene concentration on TREF profiles (CAT2.5; note logarithmic ordinate; patterns offset for clarity)

These results suggest that the activation of the catalytic sites is affected by the 1-hexene concentration; homopolymerization sites do not appear to be present at high 1-hexene concentrations. It is possible that 1-hexene participates in the conversion of homopolymerization sites to copolymerization sites.

Temperature also affects the short chain branching distribution; Figure 5.7 shows the TREF profiles of products made with CAT2.5 at different temperatures with similar initial 1-hexene concentrations. The TREF profiles for products made at reaction temperatures of 40 and 60°C (Runs 9 and 10) indicate that these materials were mainly copolymer; the shape of the profiles were similar to those obtained at high 1-hexene concentrations at 80°C (see Figure 5.6). This is reasonable since the solubility of 1-hexene increases significantly with decreasing temperature. Increasing reaction temperature from 80 to 90 and 100°C resulted in small increases in 1-hexene incorporation, but the yield of product at 100°C was less than the yield at 80 and 90°C.

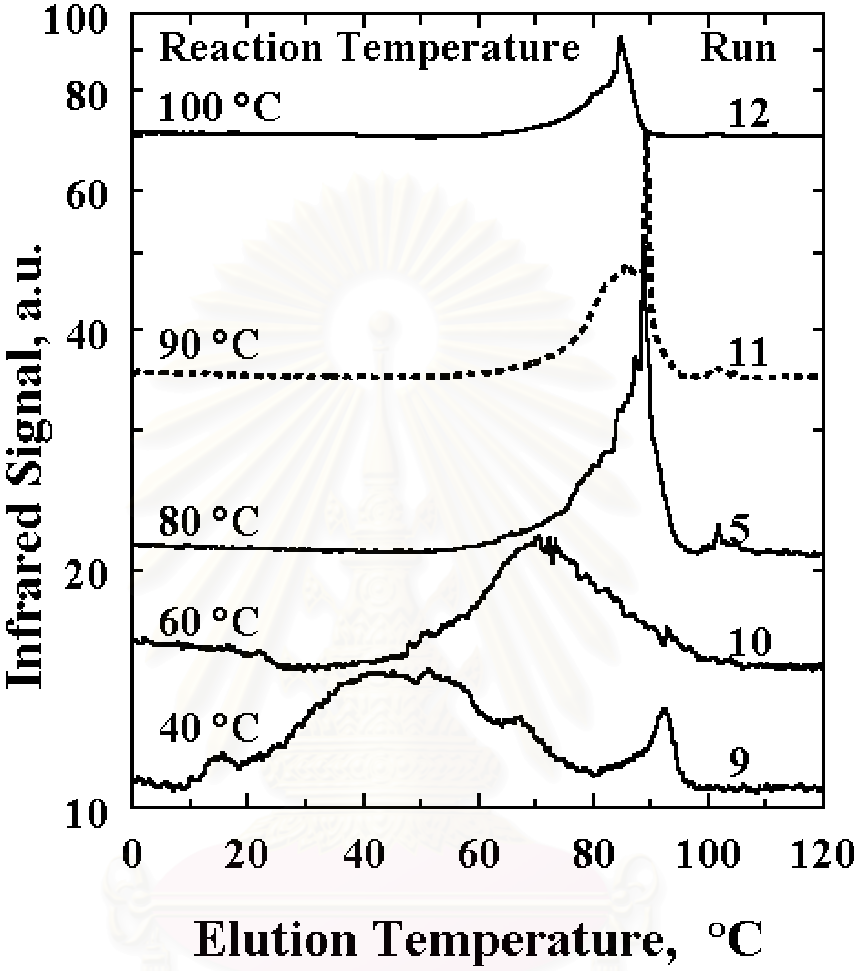

Figure 5.7. Effect of reaction temperature on TREF profiles (CAT2.5; note logarithmic ordinate; patterns offset for clarity)

The broadness of the short chain branching distribution is due to the presence of different types of catalytic sites as well as to variations in the 1-hexene concentration during the runs; the C_W/C_N values in Table 5.2 are an indication of the broadness of the short chain branching distribution. The TREF results showed that reaction time, support pore size, 1-hexene concentration and reaction temperature all significantly influenced the short chain branching distribution of the LLDPE made with (n-BuCp)$_2$ZrCl$_2$ supported on MAO-treated mesoporous silicas. The TREF results also indicate that different types of catalytic sites are present in these catalysts and that the pore size influences the type of sites present.

5.3. Characterization by Differential Scanning Calorimetry (DSC)

Information about the morphology can be obtained by DSC, that is, variations in melting indicate the presence of crystalline lamellae with different thicknesses (Zhou and Wiles, 1997). DSC analysis of nascent product, that is, polymer in the state in which it is removed from the reactor, can provide indirect information on the existence of multiple types of catalytic sites if DSC scans of polymers produced at similar conditions with different catalysts have reproducible differences. Two consecutive DSC scans were done on each sample to determine whether the DSC features of the nascent and recrystallized product were a function of the type of catalyst and the polymerization conditions. The first scan consisted of heating the nascent polymer in the calorimeter from 0ºC to 160ºC at a rate of 10ºC/min, followed immediately by cooling to 0ºC at the same rate. The second complete scan was done immediately after the first scan at the same heating rates. Figure 5.8 shows the endotherms and exotherms for the two scans for the product from Run 7. The scans in Figure 5.8 show that the endotherms for the nascent polymers have several maxima indicating that crystalline lamellae with different thicknesses were present in the nascent product. This could be an indication of different types of catalytic sites. The endotherm for the second scan shows that melting and solidification of the first scan removes the complex structure of the endotherm.

The DSC endotherms of the nascent polymer must have reproducible features if the endotherms are to be an indication of differences in the nature of the catalyst. DSC endotherms for the runs with different lengths of polymerization are shown in Figure 5.9 (Runs 13 –15; CAT20). The similarity of the three endotherms for the nascent polymers (see Figure 5.9a) is striking; this reproducibility of the complex structure of the endotherm for the nascent polymers shows that the maxima in the endotherms are not the result of random events but are related to the nature of the catalyst and polymerization conditions; much of this detail is lost in the endotherms for the second scans (see Figure 5.9b). A short polymerization time (0.5 h; Run 15) resulted in endotherms in which the main peak is at high temperature (i.e. large lamellae). The main peak for Run 15 is at 125ºC while the main peaks for products

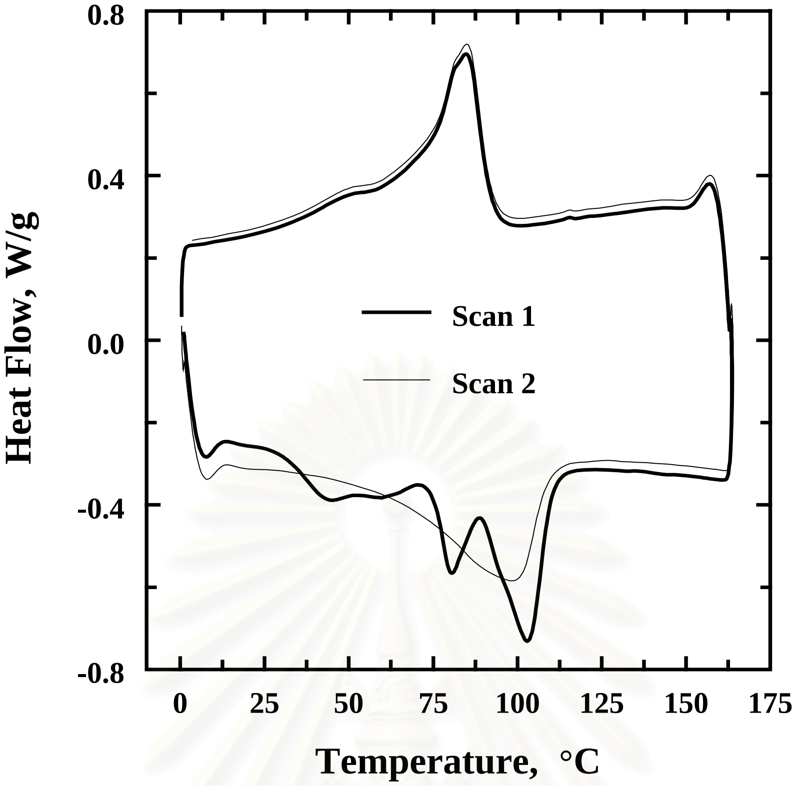

Figure 5.8. Illustration of DSC endotherms and exotherms for two complete scans (Run 7)

made with longer polymerization time are at 94 and 96ºC. This is surprising because the average 1-hexene concentration was higher during the short runs; i.e. less1-hexene was consumed during the short runs and about the same amount of 1-hexene was added at the beginning of the runs (see Table 5.2 for initial and final 1-hexene concentrations). The observation that the amount of low crystallinity polymer, that is, decrease in melting temperature, increases with increasing polymerization time is in agreement with the TREF profiles discussed above and the observations by Soga et al. (1995) for ethylene/1-hexene copolymerization in the slurry phase using a homogeneous Cp_2ZrCl_2 – MAO catalyst.

The DSC endotherms for nascent polymers made at similar polymerization conditions (Runs 13 and 16-20) with catalysts having different initial pore sizes are shown in Figure 5.10. It is clear that the initial pore size has a marked effect on the nascent product morphology. Products made with catalysts with support pore sizes >7 nm (Runs 13, 19 and 20) had DSC endotherms with 4 or 5 maxima indicating multiple types of catalytic sites. Nascent products made with CAT2.6 and CAT5.8

had simpler endotherms (Runs 17 and 18); the nascent product made with CAT2.6 only has one major peak in its endotherm. This indicates that catalytic sites in catalysts with initial pore size in the 2 to 6 nm range are not as varied as the catalytic sites in catalysts with larger initial pore sizes. Just as with the TREF results, the product made with the silicalite support (CAT0.54; Run 16) did not follow this above trend of greater product homogeneity with decreasing support pore size because the (n-BuCp)$_2$ZrCl$_2$ did not enter the 0.54 nm pores of the support particles, that is, the MAO and (n-BuCp)$_2$ZrCl$_2$ coated the external surface of the support particles. The main peak in the endotherms for the large pore catalysts (Runs 13, 19 and 20) and for CAT0.54 (run 16) is at 96ºC, while the main peaks for the small pore size catalysts (runs 17 and 18) are at about 120ºC (Temperatures of maxima in the endotherms are listed in Table 5.3). The very systematic variation in the shapes of endotherms for nascent product as a function of initial catalyst pore size shows that the DSC endotherms of nascent polymer provides useful information about the catalytic polymerization process.

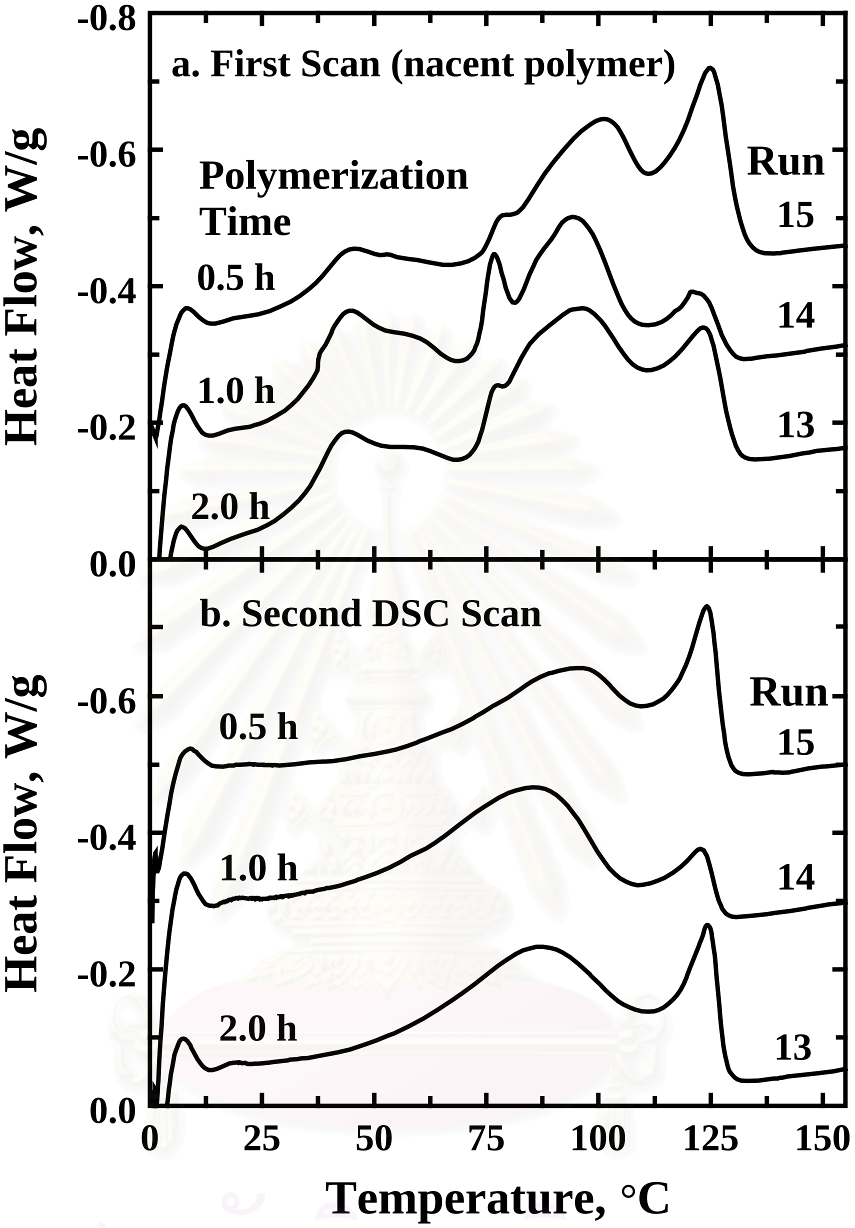

Figure 5.9. Effect of reaction time on DSC endotherms for Scans 1 and 2 (CAT20)

Table 5.3. Summary of DSC Results.

Run	Initial Temp. (°C)	Range of 1-C_6H_{12} Concentr. (mol/m^3)	Catalyst	Maxima in DSC Endotherms[a] (°C)					Crystallinity[b] %	
				T_1	T_2	T_3	T_4	T_5	Scan 1	Scan 2
1	80	0.0	CAT2.5	-	-	-	-	139*	56	58
2	80	4.2 – 0.0	CAT2.5	-	-	-	-	134*	55	54
3	80	11.8 – 0.5	CAT2.5	-	-	105	-	129*	46	46
4	80	18.8 – 8.3	CAT2.5	-	-	95	119*	-	42	40
5	80	18.5 – 11.7	CAT2.5	-	-	95	119*	-	41	38
6	80	25.8 – 10.6	CAT2.5	-	-	101	119*	-	35	35
7	80	47.2 – 42.0	CAT2.5	45	81	103*	-	-	26	20
8	80	42.3 – 38.5	CAT2.5	45	86	102*	-	-	27	19
9	40	18.9 – 14.2	CAT2.5	41	82*	100	118*	-	27	15
10	60	18.6 – 15.2	CAT2.5	42	89	-	112*	-	33	25
11	90	18.6 – 8.3	CAT2.5	-	80	-	120*	-	36	33
12	100	18.5 – 15.0	CAT2.5	-	77	-	117*	-	34	32
13	70	28.6 – 17.7	CAT20	44	78	96*	124	-	30	21
14	70	29.1 – 23.3	CAT20	45	77	94*	122	-	24	17
15	70	29.2 – 28.3	CAT20	45	78	101	125*	-	25	17
16	70	27.8 – 17.2	CAT0.54	46	78	96*	-	-	27	22
17	70	27.2 – 3.8	CAT2.6	-	-	88	123*	-	35	38
18	70	27.8 – 14.5	CAT5.8	43	-	88	118*	137	34	29
19	70	28.9 – 24.9	CAT7.2	44	-	96*	125	136	21	14
20	70	28.4 – 27.5	CAT15	44	73	97*	123	137	26	16

[a] The main DSC peak in the endotherm is indicated by an asterisk (*).

[b] DSC crystallinity based on ΔH_{fusion} = 290 J/g for crystalline polyethylene [Ottani and Porter, (1991)].

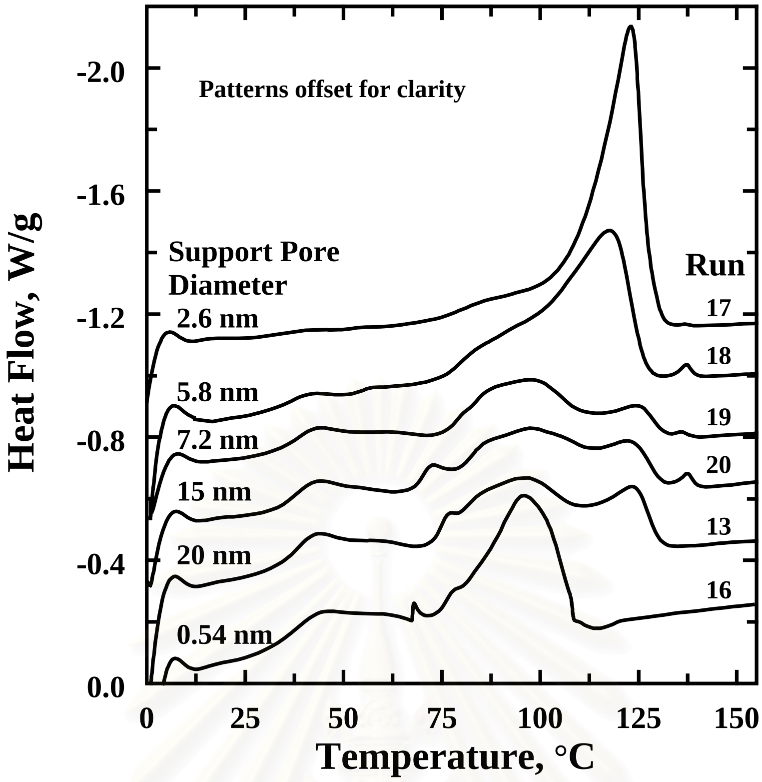

Figure 5.10. Effect of pore size on DSC endotherms

DSC endotherms of products made with CAT2.5 at various 1-hexene concentrations are shown in Figure 5.11. Increases in the initial concentration of 1-hexene resulted in systematic decreases in the temperature of the main peak in the endotherm as well as in the crystallinity based on the integrated heat of melting (see Table 5.3; Runs 1 - 8). For initial 1-hexene concentrations ≤25 mol/m^3 (Runs 1-6), the endotherm was dominated by a single peak with a peak temperature, which decreased from 139 to 119ºC with increasing 1-hexene concentration. A secondary peak, of increasing intensity with increasing 1-hexene concentration, started to appear for these runs at about 105 to 95ºC. For initial 1-hexene concentrations >40 mol/m^3 (Runs 7 and 8), the high temperature peak at ≥119 ºC disappeared and the peak at about 100 ºC became the dominant peak. The marked change in the shapes of the DSC endotherms for the change in initial 1-hexene concentration from 26 to 42 mol/m^3 suggests that different types of catalytic sites interact differently with 1-hexene.

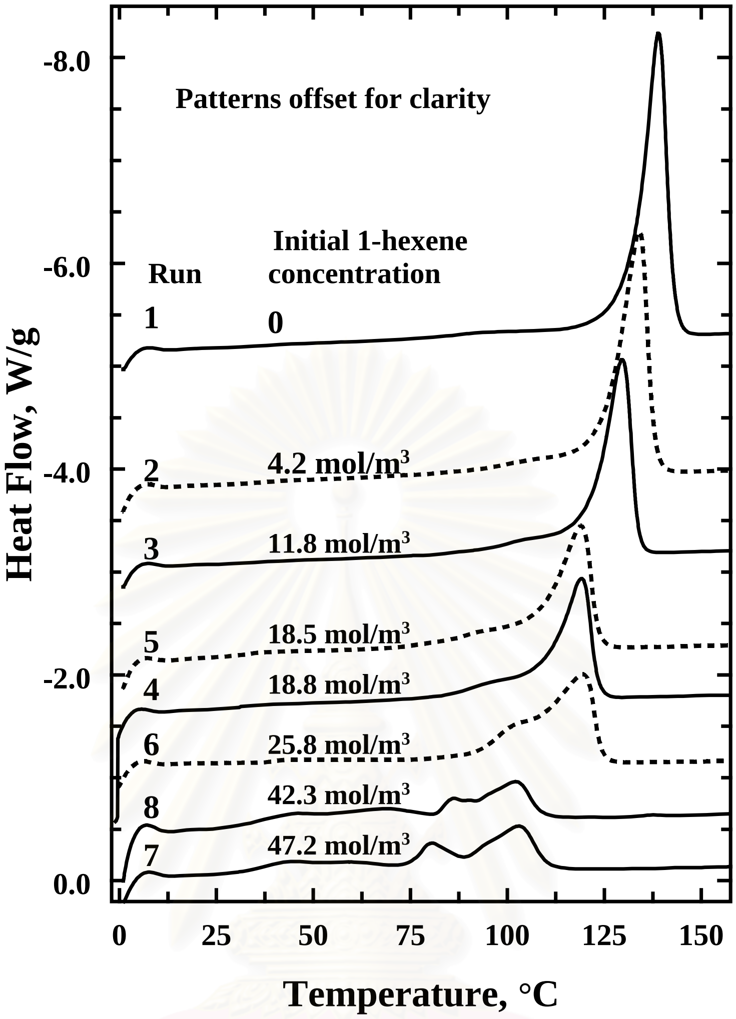

Figure 5.11. Effect of initial 1-hexene concentration on DSC endotherms

Changes in reaction temperature, at the same initial 1-hexene concentration, also results in products with different DSC endotherms. Results for products made with CAT2.5 are shown in Figure 5.12. The endotherms for the products made at 80 to 100ºC had their main peak centered at 117 to 120ºC with a shoulder towards the low temperature side. The endotherms for products made at 40 and 60ºC had multiple maxima somewhat similar to those obtained with products made at high 1-hexene concentrations (Figure 5.12; Runs 7 and 8). This is reasonable since the solubility of 1-hexene in polyethylene at constant 1-hexene conentration increases significantly as the temperature is decreased (Moore and Wanke, 2001).

The crystallinities calculated from the enthalpy melting show an interesting trend (last 2 columns of Table 5.3). The crystallinities from Scan 1 and Scan 2 were approximately equal for all the relatively narrow endotherms, which had one or two peaks, while the crystallinities based on DSC Scan 2 were considerably lower than the crystallinities based on Scan 1 for all the broad endotherms which had more than two peaks. The lower crystallinity for Scan 2 for the broad endotherms is due to the disappearance of the low temperature peak in Scan 2 (cf. endotherms for Scans 1 and 2 in Figure 5.9).

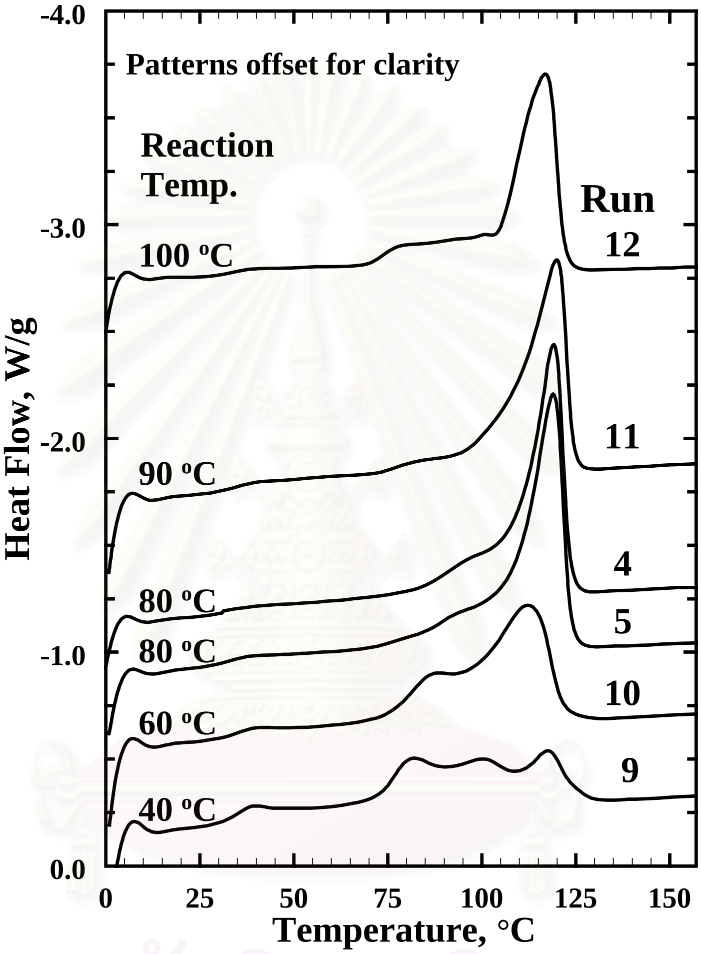

Figure 5.12. Effect of reaction temperature on DSC endotherms

TREF and DSC studies indicate the heterogeneous nature of the catalytic sites in the supported (*n*-BuCp)$_2$ZrCl$_2$ catalysts. DSC results generally indicated a greater degree of heterogeneity in catalytic sites as a function of pore size than the TREF results (cf. Figures 5.5 and 5.10), 1-hexene concentration (cf. Figures 5.6 and 5.11) and reaction temperature (cf. Figures 5.7 and 5.12). Only for the low 1-hexene concentration experiments with CAT2.5 were the DSC profiles less complex than the TREF profiles (see Figures 5.6 and 5.11). Additional DSC characterization using thermally fractionated samples as well as TREF–DSC cross-fractionation studies may reconcile these differences.

5.4. Molar Mass

In Chapter IV it is reported that support pore size does not have a significant effect on molar masses for ethylene/1-hexene copolymers made at 70 °C with mesoporous silica-supported (*n*-BuCp)$_2$ZrCl$_2$ catalysts. The effect of 1-hexene concentration on molar masses of PE made with CAT2.5 at 80 °C is shown in Figure 5.13. In Figure 5.13, the molar masses are plotted as a function of the 'average' 1-hexene concentration; the average 1-hexene concentration is taken as the arithmetic average of the initial and final 1-hexene concentration (see Table 5.2). A similar plot is obtained for molar masses as a function of initial 1-hexene concentration. As expected, the number average molar mass, M_N, decreases with increasing 1-hexene concentration. The mass average molar mass, M_W, is relatively unaffected by increases in 1-hexene concentration; this results in an increase in polydispersity from about 2.5 at low 1-hexene concentrations to a value of 4.0 at an average 1-hexene concentration of 45 mol/m^3.

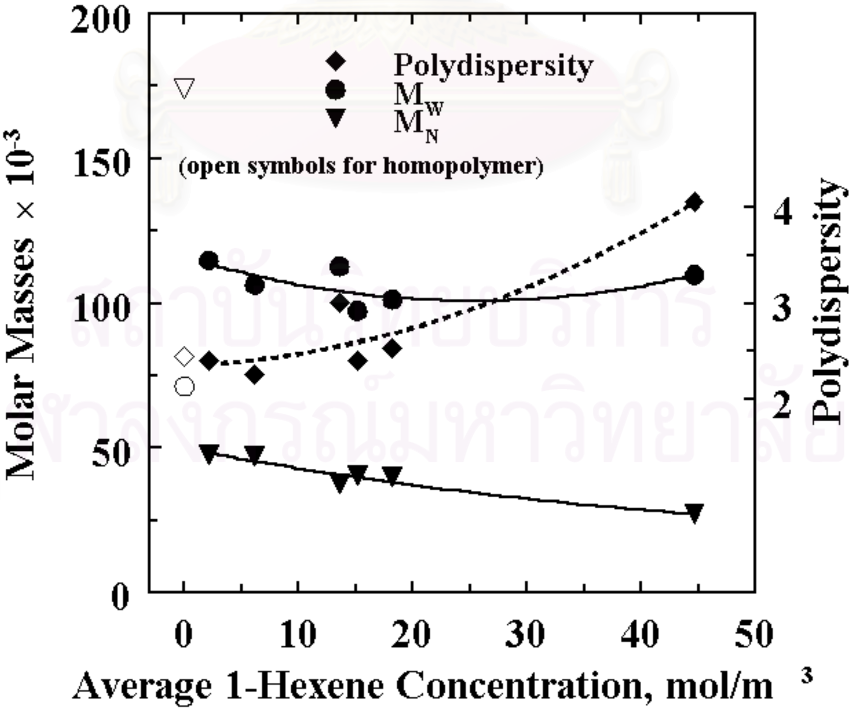

Figure 5.13. Effect of 1-hexene concentration on molar mass and polydispersity (CAT2.5; Runs 1 to 7)

The effect of temperature on molar masses of PE made with CAT2.5 at 80°C and an initial 1-hexene concentration of 18.7 (±0.2) mol/m^3 is shown in Figure 5.14. The molar masses are plotted as a function of reciprocal temperature and the equations describing the molar masses are shown in Equations 5.5 and 5.6:

$$ln[\mathrm{M_N}] = 7.946 + \frac{997}{\mathrm{T}} \qquad \text{with T in K} \qquad \text{---- (5.5)}$$

and

$$ln[\mathrm{M_W}] = 8.306 + \frac{1197}{\mathrm{T}} \qquad \text{with T in K} \qquad \text{---- (5.6)}$$

The decrease in molar masses with increasing temperature shows that the activation energies for chain termination are larger than those for propagation; based on Equation 5.5, the lumped activation energy for termination exceeds the lumped activation energy for propagation by about 8.3 kJ/mol. The relatively good correlation of M_N with 1/T, even though the properties of products as indicated by TREF and DSC varied significantly with temperature, suggests that the temperature dependencies of the propagation and termination reactions are not significantly affected by the changes in 1-hexene incorporation rates.

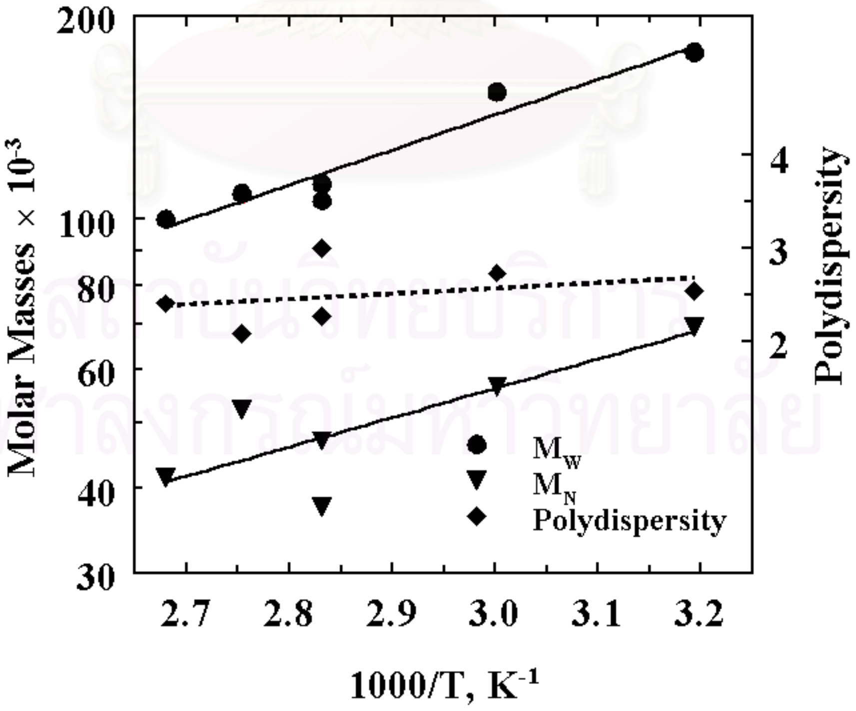

Figure 5.14. Effect of reaction temperature on molar mass and polydispersity (CAT2.5; Runs 4, 5, and 9-12)

CHAPTER VI

Slurry-Phase Polymerization of Ethylene and Ethylene/α-Olefins

The results in Chapter IV and V showed that the pore size of mesoporous molecular sieves used for the preparing (*n*-BuCp)$_2$ZrCl$_2$-MAO/mesoporous molecular sieve catalyst, the polymerization conditions and the 1-hexene concentration had significant effects on the gas-phase polymerization activity and polymer properties. There has been an increasing focus on the development of supported metallocene catalyst systems to make them suitable for use in commercial slurry and gas-phase polymerization processes. However, limited information is available in the open literature on the various factors, which affect the performance of supported metallocene catalysts in gas- and slurry-phase polymerization. In this chapter, the results of a systematic study are reported on the effects of operating conditions on the activities of (*n*-BuCp)$_2$ZrCl$_2$ supported on silicalite, mesoporous molecular sieves and silica gel. A 100 mL stainless steel reactor operated in the semibatch mode was used and total pressure was 115 psia (reported as 100 psig) for these studies. The influences of the pore size in ranges 2.5-16 nm of mesoporous molecular sieve supports and polymerization conditions on the slurry-phase polymerization were investigated. The molar masses of the products, characteristics of catalyst and polymer structure are discussed. The description of supports and catalysts were provided in Table 3.1 and 3.2B, respectively. The rate of polymerization of ethylene and ethylene/α-olefins, i.e. 1-hexene, 1-octene, 1-decene, in the slurry-phase system is presented.

6.1. Preliminary Results in Slurry-Phase Polymerization

A number of preliminary experiments were done to determine suitable reactor conditions for slurry-phase operation. The effect of solvents, polymerization temperatures, amounts of external MAO, amounts of TIBA, and 1-hexene concentrations were investigated using the CATBA-S1 prepared by impregnation of MAO-treated silica gel with (*n*-BuCp)$_2$ZrCl$_2$. The preliminary results are divided into 3 sets of the experiments, i.e. Sets A, B, and C.

The first set of experiments (Set A.) was performed to determine the influence of polymerization medium and polymerization temperature on the catalytic activity with 0.6 mmol of TIBA (Runs 1 to 9) and 1.14 mmol of Al as external MAO (Runs 10 to 18) added to the polymerization media. Toluene, heptane, and decane, previously distillated to remove the trace of impurities, were used as the polymerization media. The results of average polymerization activities and molar masses for these experiments are listed in Table 6.1. From the results shown in Table 6.1, (Runs 1 to 18), it is evident that the polymerization medium can have a significant effect on the polymerization activity of the supported metallocene catalyst system, possibly explained by Tait (2000) that the more polar the medium the higher the polymerization activity; the average polymerization activity was higher in toluene and heptane than in decane at all of the polymerization temperatures, except for Runs 10. The average activities in the toluene and heptane, with TIBA in the polymerization medium, were about the same (cf. Runs 1 and 4, Runs 2 and 5), even though the toluene has higher polarity than heptane. This observation can possibly be explained by larger amounts of impurities in the toluene than heptane because toluene absorbs more readily than heptane. It is worth noting that the choice of hexane or heptane as the polymerization medium is dictated by the impossibility of using toluene as the solvent for large-scale polyolefin manufacture (Scheirs and Kaminsky, 1999). The polymerization activity increased with increasing polymerization temperature up to 70°C and then decreased at 80°C for all of the diluents (cf. Runs 2 and 3, and Runs 5 and 6). This is attributed to the deactivation of catalyst at higher temperatures. TIBA and MAO had different effects on the polymerization activities. Activities were generally higher with the addition of external MAO than with the addition of TIBA, but here were no general trends in the difference in activity with TIBA and MAO for the different diluents and temperature. TIBA did affect the changes of the catalytic activities for all of the solvents as seen in an increase of the activities from 50°C to 70°C and from 50°C to 80°C by the factors of about 3 and 2, respectively. While the use of MAO, the average activities increased by the factors of about 4 and 4.5 from 50°C to 70°C and from 50°C to 80°C for toluene. For heptane and decane, increases in the polymerization temperature from 50°C to 70°C and from 50°C to 80°C resulted in activity increases by factors of 2 and 1.7 and 1.6 and 1.4, respectively. It can be concluded that external MAO acts as a co-catalysts as well as a scavenger because rates with MAO were higher than rates with TIBA in all by one of the runs (i.e. Run 10).

Table 6.1. Results of Preliminary Experiments for Set A.

Slurry-Phase Ethylene Polymerization Using TIBA

Types of Solvents	Run	Catalyst (mg)	Temp. (ºC)	Average Activity (g PE/g cat·h)	Molar Masses		
					Mn	Mw	PD
Toluene	1	53.5	50	63	66879	175785	2.63
	2	52.3	70	161	26826	70307	2.62
	3	54.2	80	127	22864	60789	2.66
Heptane	4	50.9	50	69	52453	163252	3.11
	5	53.2	70	167	27166	75489	2.78
	6	51.1	80	150	29486	78720	2.67
Decane	7	51.5	50	41	58961	179675	*3.05
	8	50.4	70	130	41111	144829	*3.52
	9	51.9	80	85	26937	78519	2.91

Slurry-Phase Ethylene Polymerization Using MAO

Types of Solvents	Run	Catalyst (mg)	Temp. (ºC)	Average Activity (g PE/g cat·h)	Molar Masses		
					Mn	Mw	PD
Toluene	10	50.2	50	42	100785	319589	3.17
	11	51.0	70	175	18227	80599	*4.42
	12	49.5	80	190	11589	49070	4.23
Heptane	13	49.4	50	104	78624	253580	*3.23
	14	50.9	70	200	24040	68878	2.87
	15	49.7	80	177	14157	44152	3.12
Decane	16	49.6	50	82	75740	261184	3.45
	17	50.9	70	133	37685	148385	3.94
	18	50.7	80	117	18922	63832	3.37

(Reaction conditions: Ethylene Pressure = 100 psi, Amount of Catalyst = 52 (±3) mg, Polymerization Length = 15 min, Solvent Volume = 30 mL, Amount of TIBA=0.6 mmol, and 1.14 mmol of Al as external MAO was added to the reactor) * Bimodal Molar Mass Distribution

The molar masses results shown in Table 6.1 indicated that the polymerization medium, temperature and type of external alkyl had significant effects on the molar masses. Increases in temperature for all runs, except one (Run 6) resulted in decreases in Mn and Mw. The polydispersities were relatively independent of the polymerization temperature and polymerization media, but higher values of polydispersities were obtained with external MAO (2.8-4.5) compared with TIBA (2.6-3.5). The decreases in molar masses with increasing polymerization temperature were observed in gas-phase polymerization as well, the decrease in molar masses with increasing temperature can be explained by overall activation energies for the propagation reactions being lower than those for the chain termination reactions. To provide more information on these results, the molar masses were plotted with the correlation previously shown in the Equations (4.1) and (4.2). It was found that the dependence of the molar masses on the polymerization temperatures was reasonably well correlated by those equations. The difference in the values of the lumped termination and propagation activation energies, that is, $E_{termination}$-$E_{propagation}$ are shown in the Table 6.2.

Table 6.2. The difference in the values of the lumped termination and propagation activation energies based on b_n and b_w values

Types of Polymerization mediums	$E_{termination}$-$E_{propagation}$ using TIBA (kJ/mol)		$E_{termination}$-$E_{propagation}$ using MAO (kJ/mol)	
	Based on b_n	Based on b_w	Based on b_n	Based on b_w
Toluene	35	35	70	60
Heptane	20	25	54	56
Decane	23	24	42	42

Equation 4.1 describes variation of the number-average molecular weight (Mn) as a function of temperature if transfer to monomer is the main-chain termination reaction. The results in Table 6.2 show that the overall activation energies for the propagation reactions were lower than those for the chain termination reactions for all of the polymerization mediums; the main chain termination by transfer to monomer is prevalently observed for toluene as the medium. The activation energies

for chain termination reactions using MAO were higher than those of TIBA. It is clearly indicated that the increases in the amount of MAO by about a factor of 2 resulted in significant changes in the differences of the average values of the lumped termination and propagation activation energies. The reason for the larger temperature effect of external MAO compared to TIBA is not known, but transfer to aluminum alkyl in addition to the transfer to monomer may be responsible for the observed behavior.

Large amounts of MAO cannot be used in commercial operations due to economic reasons. The next set of experiments (Set B) was done to determine the influence at 70°C of the amount of TIBA on the average activities, rate profiles and molar mass properties for polymerization media with different polar properties. It was expected the amount of TIBA would affect the catalytic behavior because the activities and activity profiles for gas-phase operation were found to be affected by the amount of TIBA (see Chapter IV).

From the results presented in Table 6.3 and Figures 6.1-6.3, it can be seen that the average activities increase with increases the amount of TIBA added into toluene. However, this behavior was not observed for heptane and decane. For heptane and decane the highest average activities were observed when 0.6 mmol of TIBA were added; larger amounts of TIBA resulted in decreases in activity. The activities profiles are shown in Figures 6.1-6.3 indicate that the polymerization medium affects the shape of the activity profiles; the activity profiles for toluene and decane were broad (see Figures 6.1 to 6.3); however, the profiles for toluene was not as broad as for decane. The activity profiles had an initial period of increasing activity followed by decay in activity. The delay of initial period of increasing activation rate was the longest for decane. The influence of amount of TIBA on the shape of the activity profiles was as marked as for gas-phase operation (see Figure 4.2). The reason for the two maxima in the rate profiles observed for Runs 2, 21, and 22, all with toluene, is not known. The increase of the amount of TIBA from 2.4 to 4.8 and to 7.2 mmol in the toluene (Runs 22, 23, and 24) slowed down the deactivation rate. This is in agreement with the increase in the activity with larger amounts of TIBA. A possible explanation of this observation is that catalyst leaching occurred in the polar medium supporting the idea that the lower deactivation rate is more homogeneous-like with the narrow molar mass distribution as shown below.

Table 6.3. Results of Preliminary Experiments for Set B. (Reaction conditions: Ethylene Pressure = 100 psi, Amount of Catalyst = 52 (±3) mg, Polymerization Length = 15 min, Solvent Volume = 30 mL, and Polymerization Temperature = 70°C)

Types of Solvents	**Run**	**Catalyst (mg)**	**Amount of TIBA (mmol)**	**Average Activity (g PE/g cat·h)**	**Molar Masses**		
					Mn	**Mw**	**PD**
Toluene	19	53.5	0	35	73066	199109	2.72
	2	52.3	0.6	161	26826	70307	2.62
	20	51.9	1.2	245	27785	63385	2.28
	21	50.2	1.8	266	28404	67249	2.37
	22	49.7	2.4	256	23029	56079	2.44
	23	49.9	4.8	302	22009	46860	2.13
	24	49.5	7.2	319	18294	43452	2.38
Heptane	25	49.4	0	2.6	n.d.	n.d.	n.d.
	5	53.2	0.6	167	27166	75489	2.78
	26	54.0	1.2	53	20989	68262	3.25
	27	52.2	1.8	54	24989	91990	3.68
	28	52.3	2.4	57	20420	80805	3.96
Decane	29	51.3	0	2.8	49845	123116	2.47
	8	50.4	0.6	129	41111	144829	3.52
	30	51.2	1.2	122	23937	87382	3.65
	31	49.4	1.8	55	21087	61030	*2.89
	32	50.2	2.4	52	17222	54849	*3.18

* Bimodal Molar Mass Distribution

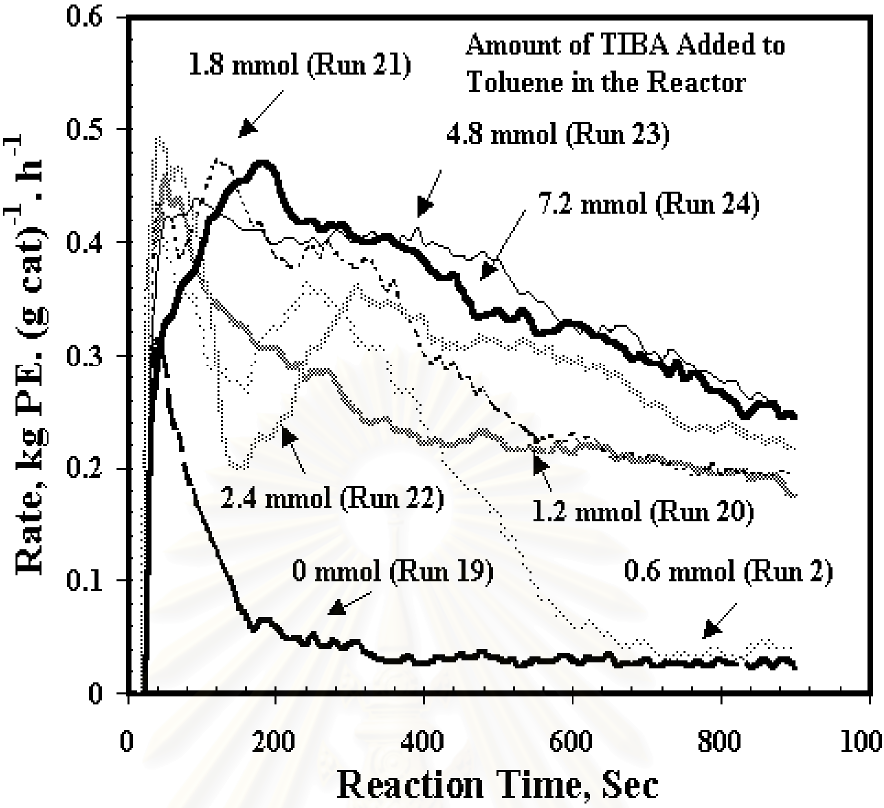

Figure 6.1. Effect of the amount of TIBA on the activity profile using toluene

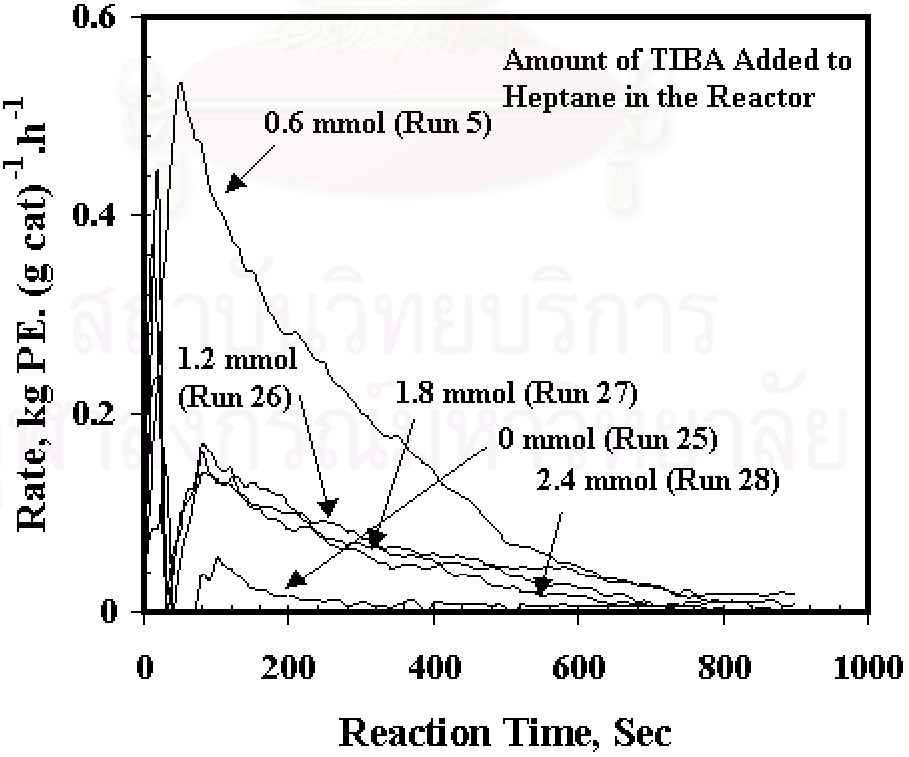

Figure 6.2. Effect of the amount of TIBA on the activity profile using heptane

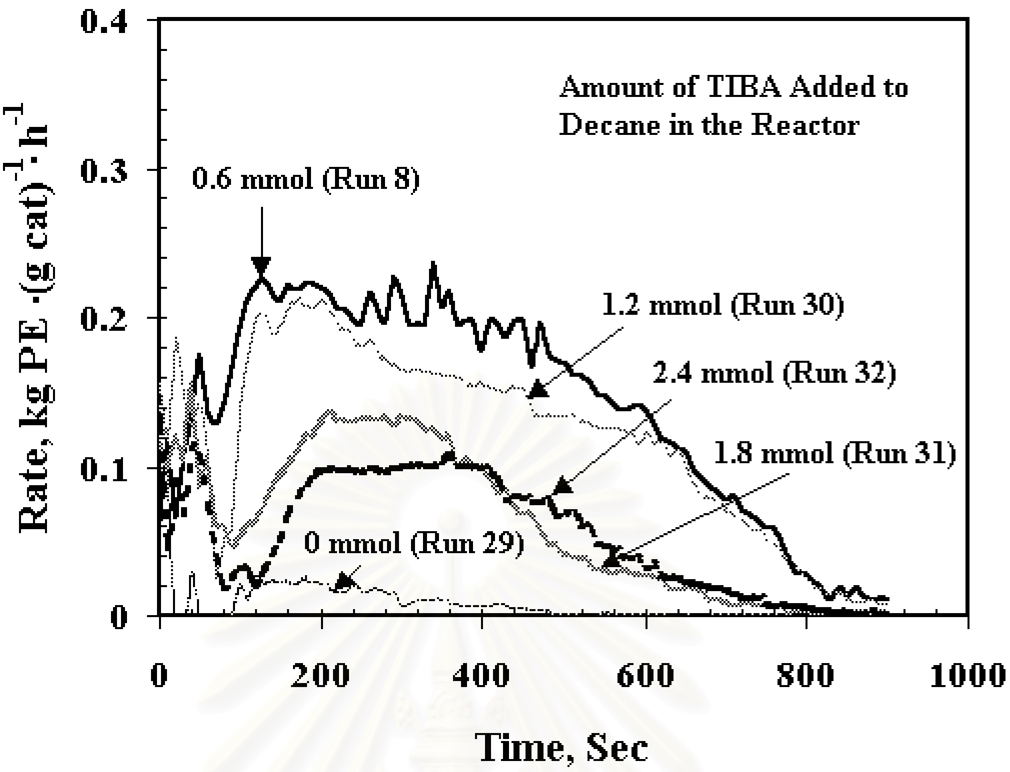

Figure 6.3. Effect of the amount of TIBA on the activity profile using decane

From the molar masses results shown in Table 6.3, it can be concluded that the amount of TIBA had a significant effect on the molecular weight in the toluene and decane media, that is the increase of amount of TIBA resulted in decreases in molecular weight indicated that chain transfer to alkyls occurred. No significant changes were observed with the heptane. The polydispersities were independent of the amount of TIBA. However, the polydispersities for toluene were narrower than for other diluents, probably due to the homogeneous behavior resulting from the catalyst leaching process. The diffusion rates of monomer as well as the solubilities of monomer in the different media also affected the overall rate.

Finally, the last set of the preliminary experiments (Set C) was performed to determine the effect of amount of 1-hexene on the polymerization rates; results are summarized in Table 6.4. Heptane was used as the suspension medium for these polymerization experiments at 70°C. From the results shown in Table 6.4, it can be concluded that the comonomer effect was not observed except for 3 mL of 1-hexene (Run 34) for which the average activity was slightly higher than for homopolymerization (c.f. Runs 5 and 34). A similar trend is shown in the Figure 6.4, that is, the highest maximum rate of polymerization was observed for 3 mL of 1-

hexene (Run 34) and the maximum polymerization rates decrease monotonically with increasing 1-hexene amounts. However, for 1 mL of 1-hexene (Run 33), the initial rate was slightly lower than the homopolymerization (Run 5). The initial activation at higher amounts of 1-hexene (6-10 mL; see Runs 36 to 38) was much less than for smaller amounts of 1-hexene. Larger amounts of 1-hexene resulted in broad activity profiles with low maximum activities. The reason of decreases in rates at higher 1-hexene amount may be due to the coordination of 1-hexene to the catalytic sites, which reduces the ethylene insertion and/or propagation. Molar masses were not significantly changed with increasing the amounts of 1-hexene as shown in Table 6.4. The polydispersities are in the ranges of 2.3 to 2.8. TREF and DSC analysis for the variation of amount of 1-hexene are described later in Section 6.4 and 6.5.

Table 6.4. Results of Preliminary Experiments for Set C. (Reaction conditions: Ethylene Pressure = 100 psi, Amount of Catalyst = 51 (±3) mg, Polymerization Length = 15 min, Heptane Volume = 30 mL, and Polymerization Temperature = 70°C)

Run	Catalyst (mg)	Amount of TIBA (mmol)	Amount of 1-hexene (mL)	Average Activity (g PE/g cat·h)	Molar Masses		
					Mn	**Mw**	**PD**
5	53.2	0.6	0	167	27166	75489	2.78
33	50.2	0.6	1.0	131	28142	79811	2.84
34	50.4	0.6	3.0	173	37495	86960	2.32
35	49.4	0.6	4.5	137	31788	75372	2.37
36	49.8	0.6	6.0	72	27422	74997	2.73
37	49.9	0.6	8.0	43	29288	79793	2.72
38	50.5	0.6	10.0	23	26887	65739	2.45

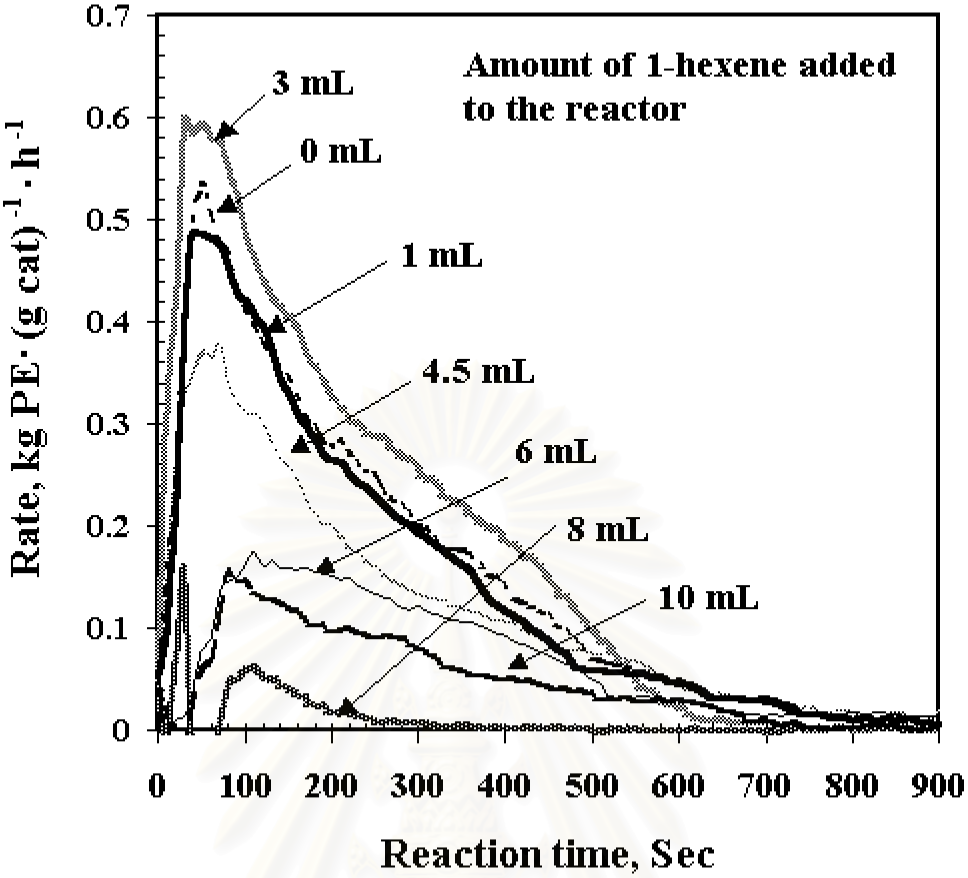

Figure 6.4. Effect of the amount of 1-hexene for copolymerization at 70°C on the activity profile

6.2. Influence of Support Pore Size and Polymerization Temperature on the Homopolymerization and Copolymerization Activities in Slurry-Phase System

6.2.1. Homopolymerization Results

The previous investigation (Chapter 4) showed that average polymerization activities were strong functions of support pore diameters and polymerization temperature for gas-phase homopolymerization and copolymerization. These results showed that catalysts made with supports MMS2.6 and MMS5.8 had the maximum average rates; supports with larger pores yielded catalysts with lower activities, and the catalyst made with the small-pore silicalite had the lowest homopolymerization activities at all temperatures. Also, the observation of the dependence of the activity on the pore diameters of the MMS supports appeared to decrease as the polymerization temperature increased, that is, at 100ºC, the variation in the average activities was a factor of three, whereas the activities at 90, 80, 70 and 50ºC varied by factors of about 4, 5, 6 and 7, respectively. Experiments were done to determine whether this interesting dependence of activity on pore size of supports also occurs during slurry polymerization. In this investigation homopolymerization and copolymerization of ethylene/α-olefins, i.e. 1-hexene, 1-octene, and 1-decene was studied. The homopolymerization activities for catalysts made with the various MMS supports, with pore diameters in the range of 2.5-16 nm, and a silicalite-supported catalysts were measured at an ethylene pressure of 100 psi and temperatures of 50-80ºC using heptane as the medium. For all experiments, 0.6 mmol of TIBA was used. The average activities are summarized in Table 6.5 and shown in Figure 6.5; these results showed very similar trends as observed in gas-phase system, i.e. that the average polymerization activities were also a function of temperature and support pore diameter. These results showed that catalysts made with supports MMS2.5 and MMS2.6 had the maximum average activities; supports with larger pores yielded catalysts with lower activities. The reason of this dependence of activity on support size has been discussed in Chapter IV; the effect of pore size was attributed to the fractionation of MAO by the different sized pores. The catalyst made with the small-pore silicalite had high homopolymerization activities at all temperatures, but not as high as MMS2.5 and 2.6. Increases of polymerization temperature resulted in increased activity for the 50 to 80ºC range studied. These observations can be explained by the leaching of MAO and (n-BuCp)$_2$ZrCl$_2$ from the external surface of the silicalite into the heptane because the MAO and (n-BuCp)$_2$ZrCl$_2$ in CABA0.54 were all located on the external surface of the silicalite partilces. This leaching resulted in homogeneous-like behavior. This is the probable reason for the high actvity of CATBA0.54. Sano and coworkers used silynated silicalite support in the preparation techniques. They found that the fractionated MAO in the toluene solution (MAO left in solution) yielded high activity. The dependence of the activity on the pore diameter of the MMS supports seem to decrease as the polymerization temperature increased, that is, at 80ºC, the variation in the average activities was a factor of ten, whereas the activities at 70, and 50ºC varied by factors of about 20. However, this trend is not as clear as obtained in gas-phase polymerization because in slurry activities were only measured at the temperatures up to 80ºC while temperatures up to 100ºC were used in the gas-phase studies.

The dependence of activity on the pore size of supports was also observed with addition of external MAO to the reactor; that is, catalyst made with CATBA2.5 had the maximum average activity and supports with larger pores yielded catalysts with lower activities. However, the effect of external MAO addition had a moe pronounced effect on catalysts with the larger pores, i.e. for the small pore sizes activities increased by a factor of 1.1-1.6, whereas for the larger pored supports of 12.5 and 16 nm the activity increased by the factor of 2 and 6.5, respectively. It is possible that the external MAO added to the reactor promoted or increased the activation of sites after the fracturing of the particles with large pore. However, the leaching and activation of Zr species from the large-pored catalysts by external MAO could be the main factor for the large increases in activities for CATBA12.5 and CATBA16 resulting from the addition of external MAO as proposed by Tait (2000).

The activity profiles for homopolymerization with different pore diameters of MMS supports were recorded at all temperatures and shown in Figure 6.6-6.10. The gas-phase activity profiles were affected by the support pore diameters. For the slurry-phase and gas-phase polymerization, the activity profiles became broader with increasing pore size, but the effect was less pronounced for slurry polymerizations. All activity profiles showed a period of activation followed by deactivation, but the rates of activation and deactivation were functions not only of the temperature but also of the support pore diameter. Deactivation rates were more sensitive to temperature than activation rates; that is, there was a higher activation energy for the deactivation process(es) than for the activation process(es) of the catalytic sites. The polymerization temperature also affected the rates of activation and deactivation. For the runs at 80ºC, there was an initial rapid increase in actvity followed by a rapid decrease in activity for all catalysts except CATBA0.54 (see dotted lines in Figures 6.6 to 6.10). The deactivation rate at 80ºC was higher than the deactivation rate at lower temperatures for all catalysts, except for CATBA0.54. The activities for CATBA0.54 at all temperatures, except for cases with externally added MAO, were essentially constant after an initial activation period (see Figure 6.10). This again supports the homogenous-like nature of CATBA0.54 during slurry polymerization. The reason for the deactivation for the runs with externally added MAO is not known. Addition of external MAO, rather than TIBA, to the reactor resulted in higher maximum as well as higher average activities for all catalysts.

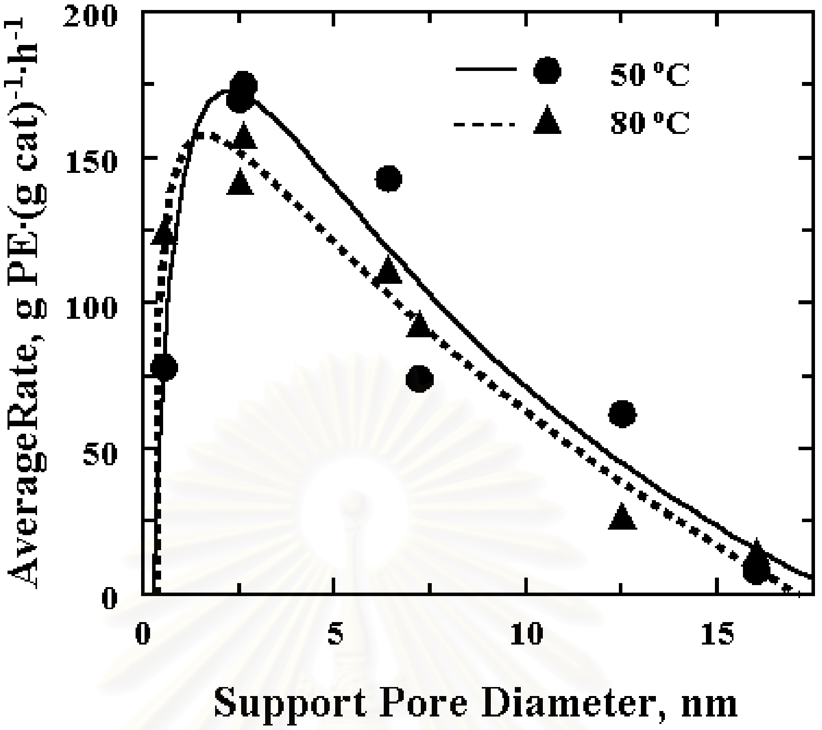

Figure 6.5. Average rate for homopolymerization as a function of support pore diameter

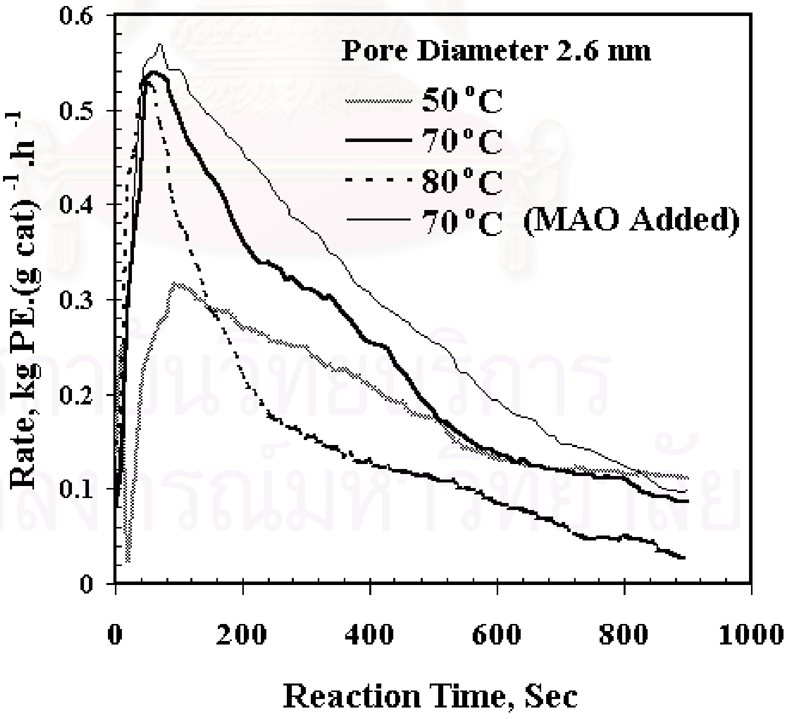

Figure 6.6. Activity and temperature profiles as a function of the reaction temperature for CATBA2.6

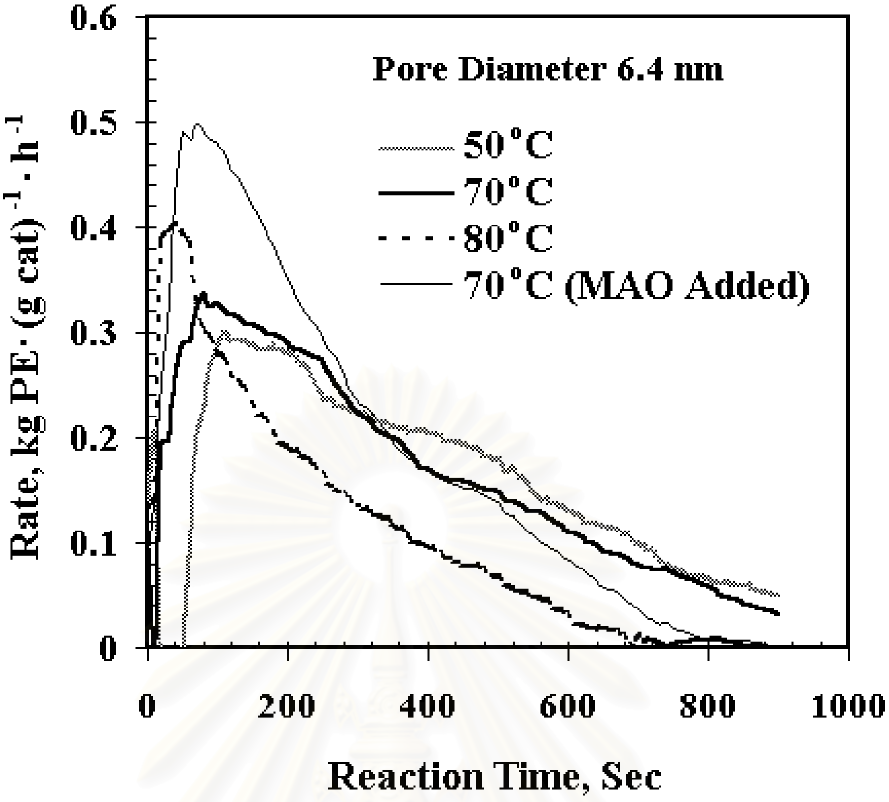

Figure 6.7. Activity and temperature profiles as a function of the reaction temperature for CATBA6.4

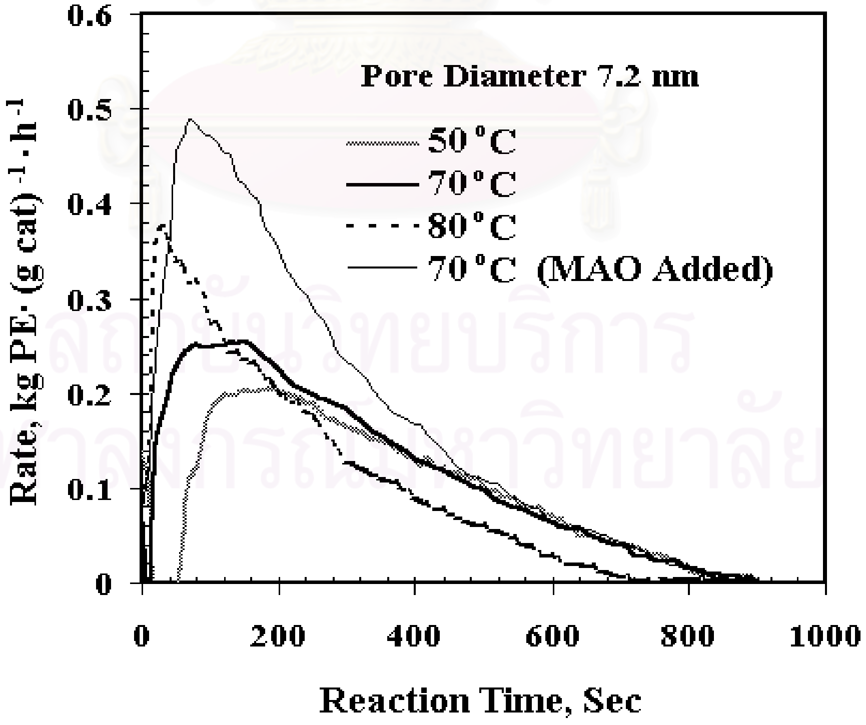

Figure 6.8. Activity and temperature profiles as a function of the reaction temperature for CATBA7.2

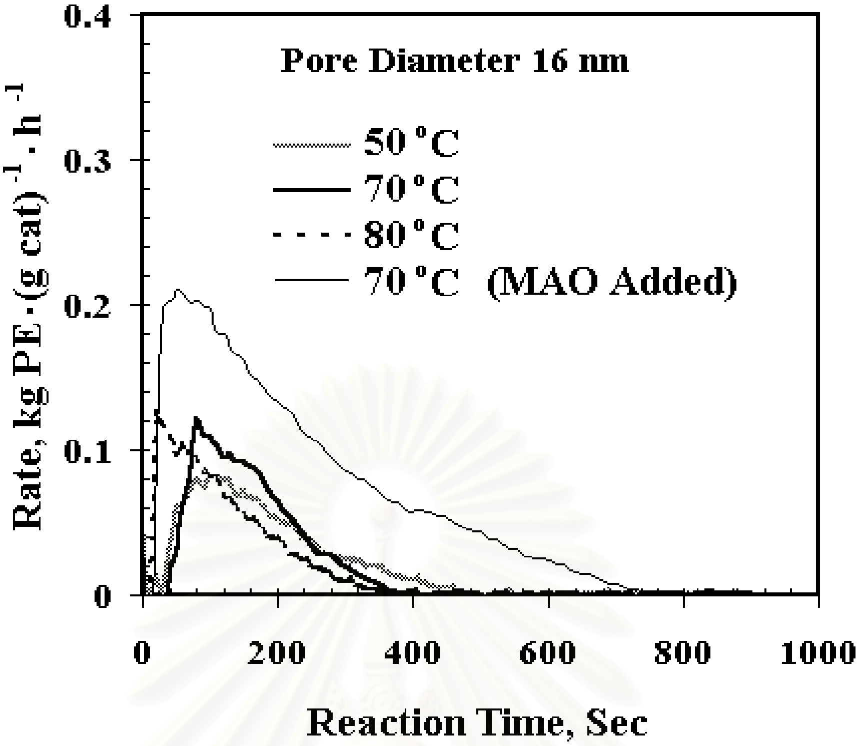

Figure 6.9. Activity and temperature profiles as a function of the reaction temperature for CATBA16

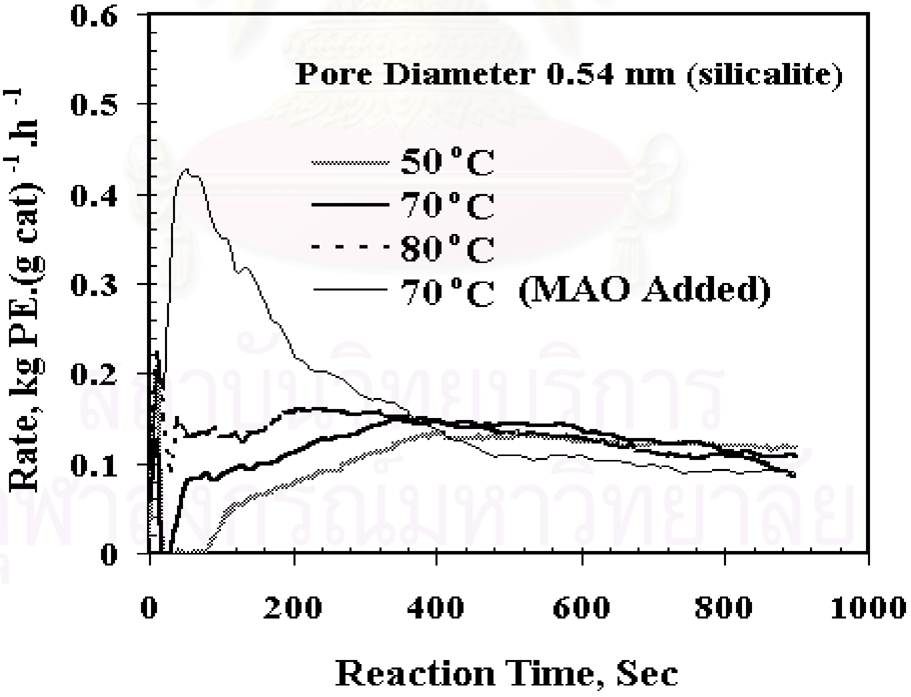

Figure 6.10. Activity and temperature profiles as a function of the reaction temperature for CATBA0.54

Table 6.5. Average Ethylene Polymerization Activities as Function of Temperature and Support (Reaction Conditions: Ethylene Pressure = 100 psi; Amount of Catalyst = 51 (±2) mg; Amount of TIBA = 0.6 mmol; heptane = 30 mL; and Polymerization Length = 15 min)

Slurry-Phase Average Polymerization Activities, g PE/(g cat·h)										
Catalyst	Support Pore Diameter (nm)	Al/Zr Ratio	Homopolymerization					Copolymerization of Ethylene/α-olefins**		
			50ºC	70ºC	80ºC	External MAO added*		1-hexene	1-octene	1-decene
						Al_{MAO}/Zr	70ºC			
CATBA0.54	0.54	170	78	111	125	630	181	220	190	155
CATBA2.5	2.5	170	170	210	142	600	292	226	230	171
CATBA2.6	2.6	170	175	230	158	610	276	246	239	175
CATBA6.4	6.4	170	143	155	112	610	167	220	170	152
CATBA7.2	7.2	170	74	102	93	610	163	182	166	146
CATBA12.5	12.5	170	62	35	27	620	73	50	43	30
CATBA16	16	170	8	12	15	620	78	40	25	10

[*] 0.44 mL of MAO was added to the reactor in addition to the TIBA

[**] Copolymerization carried out at 70 °C using heptane as the solvent, and 3 mL of amount of comonomer added to the reactor

6.2.2. Copolymerization Results

Copolymerization activities for ethylene/1-hexene, 1-octene, and 1-decene were measured at 70ºC. The amount of liquid comonomer injected into the reactor at the beginning of each copolymerization run was 3 mL. The average copolymerization activities, listed in Table 6.4 and shown in Figure 6.11 (for 1-hexene), were also dependent on the support pore diameter. The copolymerization activity profiles at 70ºC are illustrated in Figures 6.12-6.14 for ethylene/1-hexene, 1-octene, and 1-decene, respectively.

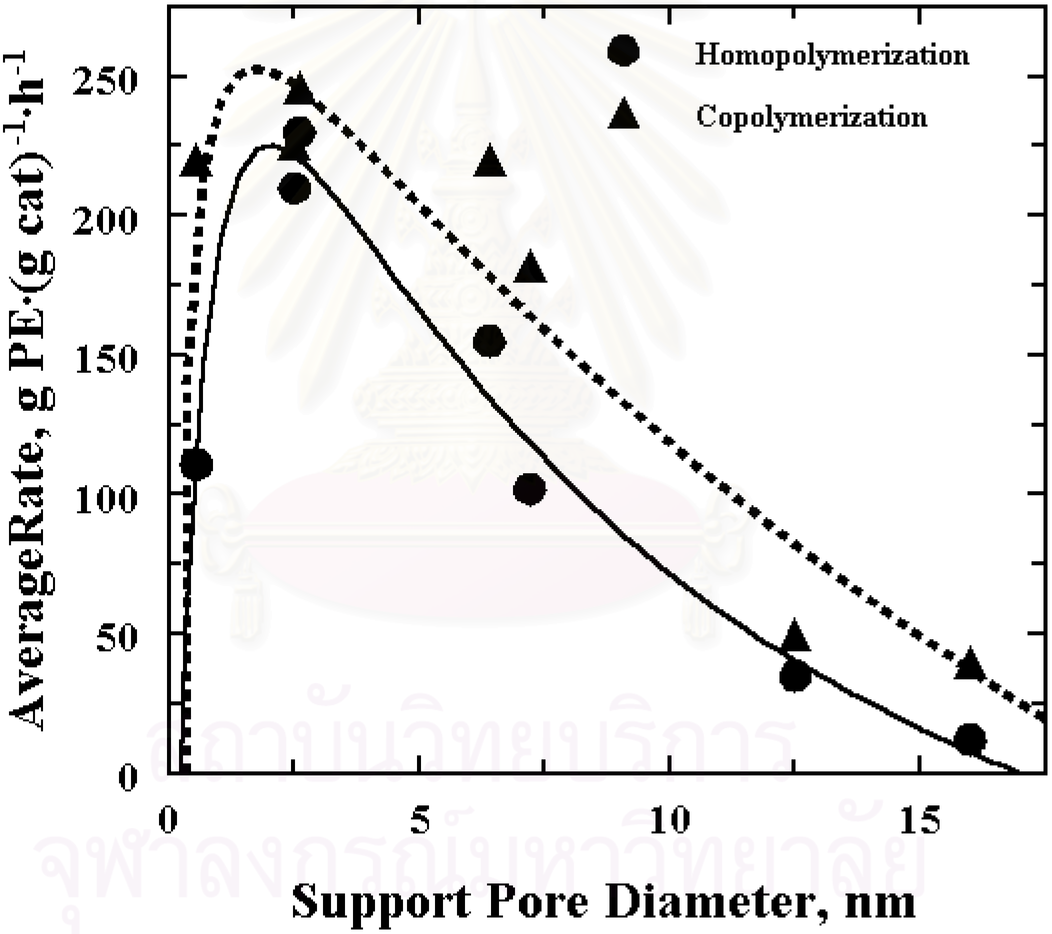

Figure 6.11. Comparison of average homo- and co-polymerization for ethylene/1-hexene activities at 70°C.

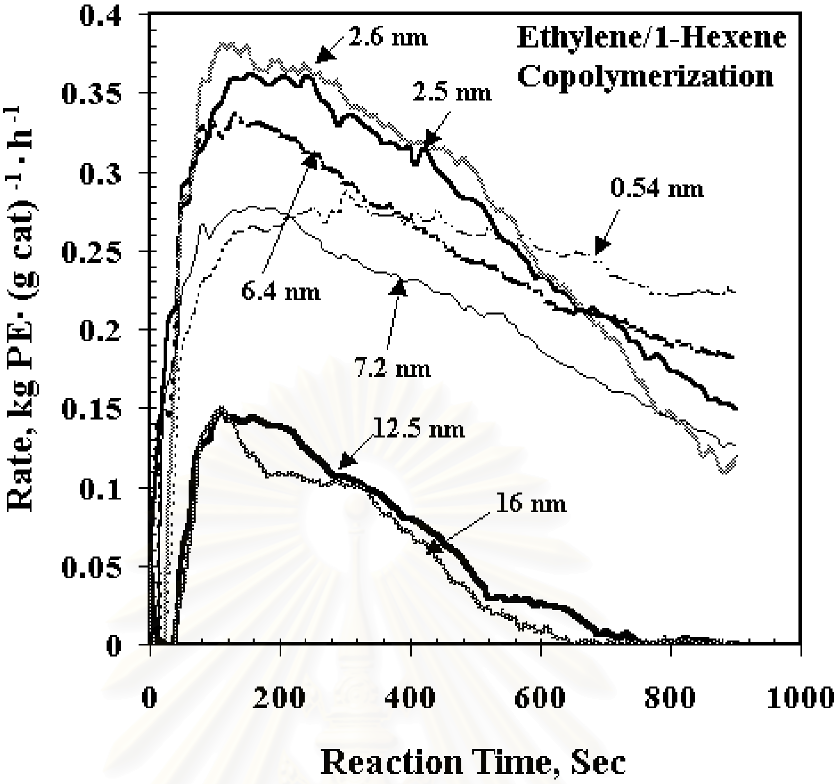

Figure 6.12. Activity profiles for 1-hexene/ethylene copolymerization made with various pore diameters of supported catalysts

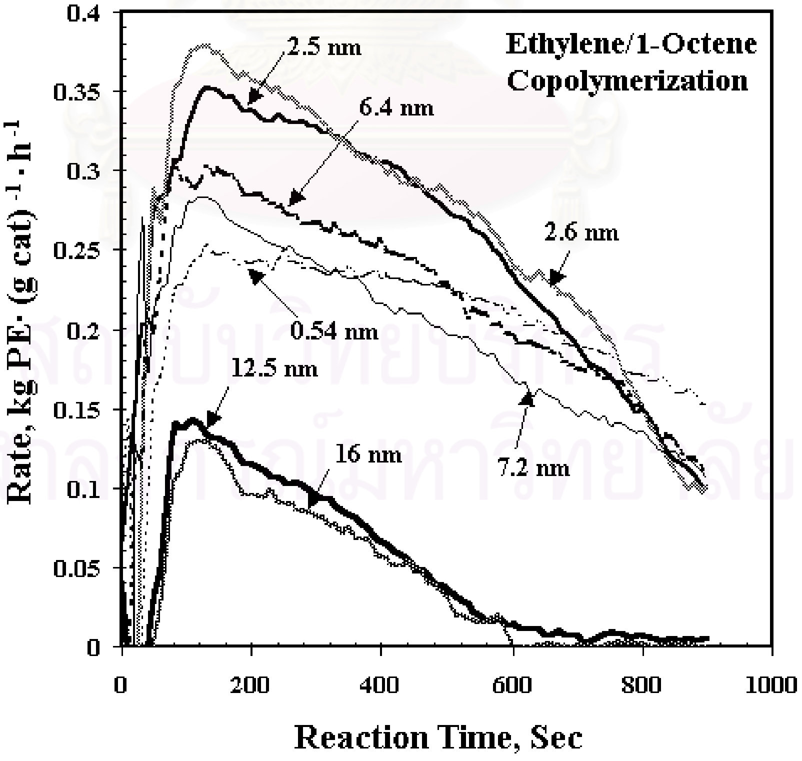

Figure 6.13. Activity profiles for 1-octene/ethylene copolymerization with various pore diameters of supported catalysts

For slurry-phase copolymerization of all the ethylene/α-olefins studied, the average copolymerization activities were also dependent on the pore diameter. The comonomer effects on the activity were clearly found for the slurry-phase systems, but it was not observed for all the gas-phase polymerizations. The comonomer effect in the slurry-phase polymerization has been discussed by several investigators; Yoon et al did not observe the comonomer effect except for ethylene/1-hexene at 40°C whereas Galland et al. and Britto et al. observed the comonomer effect for ethylene/1-hexene copolymerization. Britto et al. suggested that the presence of the comonomer makes the polymer product more amorphous and soluble and these factors increase the accessibility to catalytically active sites. The investigations with the higher olefins in slurry-phase systems, i.e. 1-hexene, 1-octene, and 1-decene, with catalyst made with supports having various pore diameters showed that the 1-hexene and 1-octene showed similar average activities for the MMS with small pore. For larger pore diameters, the average activities for ethylene/1-octene were less than those for 1-hexene. It seems that the higher olefins resulted in the lower activity than the lower olefins; this is evident from the results with 1-decene for all of the catalysts. The relative reactivity, diffusivity and solubility of comonomers are the likely reasons of this behavior. More information on comonomer incoporation and chemical compositions of the products is required to understand the observations for the different monomers.

The presence of comonomers resulted in the broadening of the activity profiles for all the MMS-supported catalysts (cf. Figures 6.6 to 6.9 with Figures 6.12 to 6.14). The commonomers also had a significant effect on the moloar masses; this will be discussed in the next section.

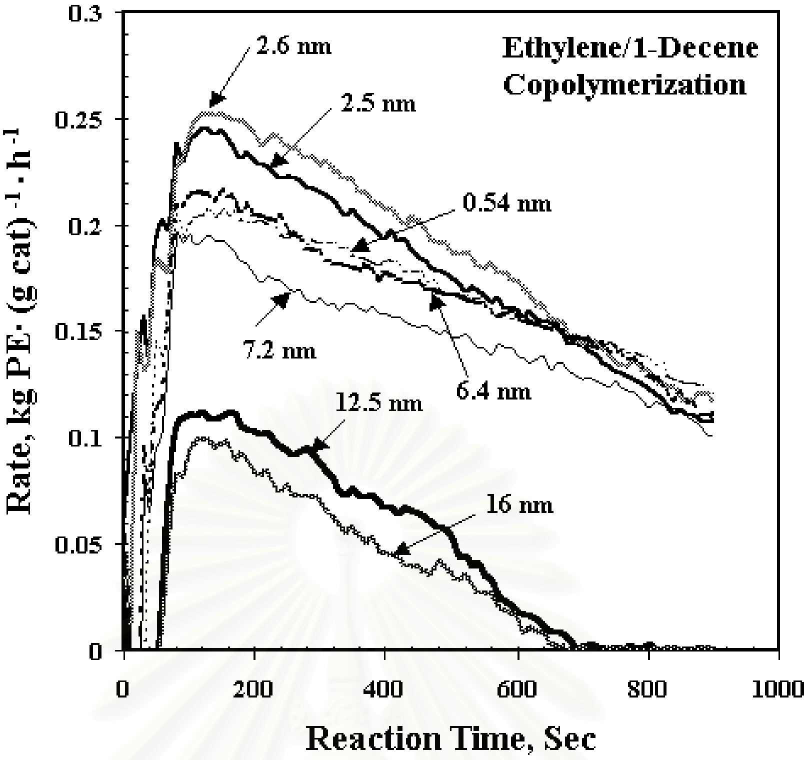

Figure 6.14. Activity profiles for 1-decene/ethylene copolymerization with various pore diameters of supported catalysts

6.3. Molar Mass Properties and Characteristics of Catalyst and Polymer Made with Various Catalysts

Scanning electron microscopy was used to examine the structure of supports, catalysts, and obtained polymer products. Representative characertistic are shown in the micrographs shown in Figures 6.15 to 6.18; additional micrographs are shown in Appendices A and B. Some of the morphological characteristics of supports and catalysts have already been shown in Chapter IV (Figures 4.11 to 4.14).

Supports MMS2.5 and MMS2.6 had the similar particle morphology (see Figure B1 and B2 in Appendix B). Supports MMS6.4-16 had the fiber morphology (Figure B.3) somewhat similar to support MMS5.8 (see Figure 4.12). The structures of catalysts made with supports used in the slurry-phase system were very similar to the starting supports, but the fiber morphologies of CATBA6.4, CATBA7.2, CATBA12.5, and CAT16 were not replicated into the produced polymer products as shown in Figure 6.15 for the MMS12.5 and CAT12.5. The morphology of the homopolymers was relatively open for all of catalysts, but not as open as copolymers.

However, the morphologies of homopolymers and copolymers obtained from slurry polymerization were more open than the polymers from gas-phase polymerizations as shown in Figure 6.16. Polymers made in the slurry phase have a more open structure than polymers made in the gas-phase because the liquid organic diluent present during slurry polymerization swells the product particles and subsequent drying results in a more open structure.

The top panel (see Figure 6.16 a,b) illustrates the homogeneous nature of CATBA0.54 in the slurry phase. The scanning electron micrographs of homopolymer produced in gas-phase polymerization (Figure 6.16a) clearly show the silicalite particles in the polymer matrix (the white solid particles). No such silicalite particles were observed in the product made in the slurry with CATBA0.54 indicating that the polymerization in the slurry phase occurred away from the silicalite partilces. This is strong evidence for that the MAO and $(n\text{-BuCp})_2ZrCl_2$ were removed from the silicalite particles during slurry polymerization.

No significant changes in the polymer structure were observed with the variation of the type of comonomer and polymerization temperature for homopolymer with MMS supported catalysts, but the increase in the polymerization temperature of catalyst made with silicalite support resulted in an increase of amount of fibers in homopolymer product. The products made in the preliminary slurry-phase experiments with CATBA-S1 had similar structures even though the solvent, temperature, and amount of TIBA were changed. However, the amount of TIBA and the use of MAO in each solvent seem to have had a significant affect on the particle size of polymer. These results are illustrated in Figures 6.17 and 6.18; all micrographs in these figures have the same magnification. It can be seen that an increase in the amount of TIBA from 0.6 mmol to 2.4 mmol resulted in decrease of the polymer particle size for polymerization in toluene (Figure 6.17 a and b). A polymer particle sizes were smaller when TIBA was increased to 4.8 and 7.2 mmol (Figures 6.17 c and d). No such effect of TIBA concentration on polymer particle size was observed for polymerization in heptane and decane (see Figure 6.18). Addition of external MAO affected polymer particle size for polymerizations in toluene and heptane, but not in decane (see Figures 6.17 and 6.18).

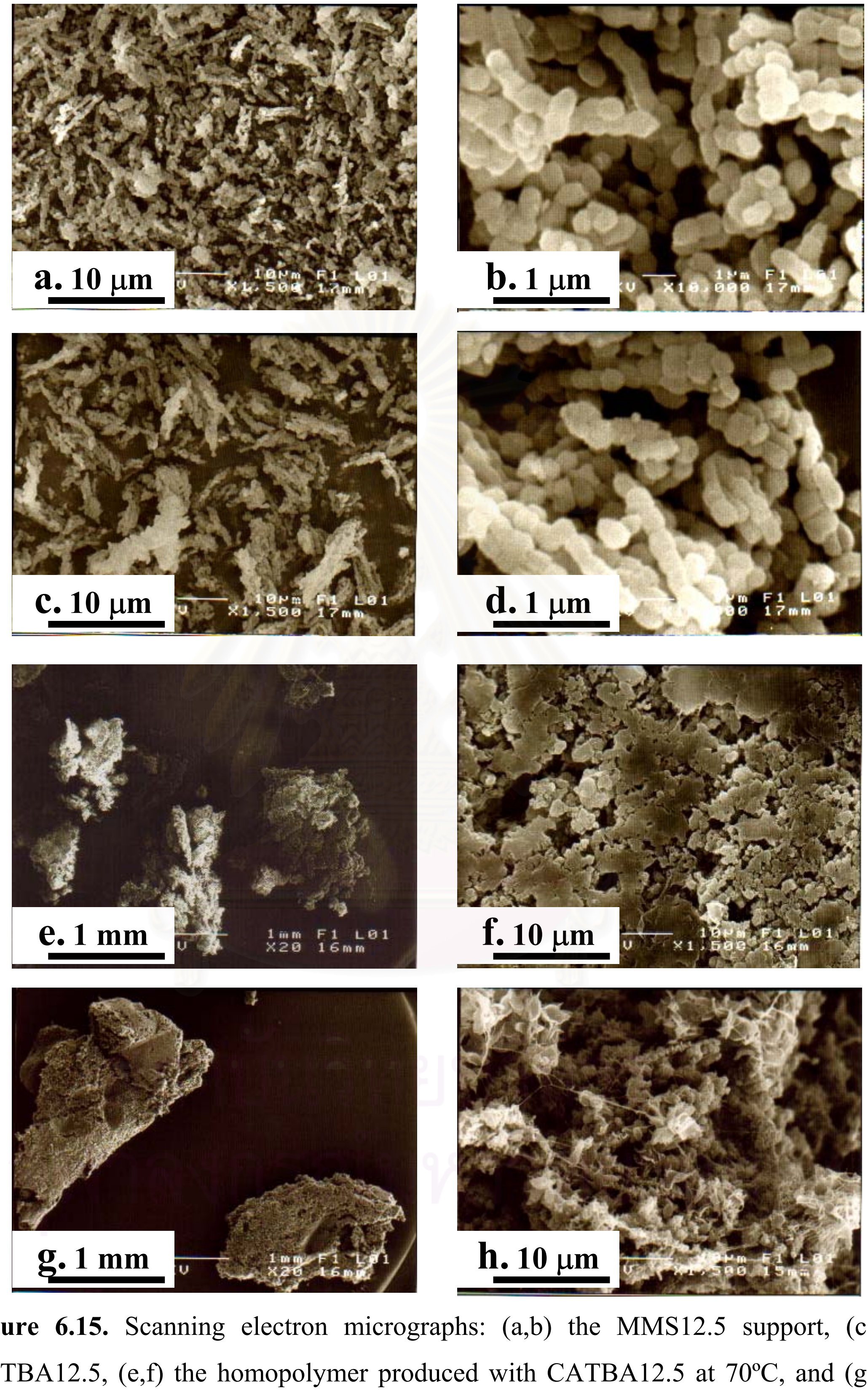

Figure 6.15. Scanning electron micrographs: (a,b) the MMS12.5 support, (c,d) CATBA12.5, (e,f) the homopolymer produced with CATBA12.5 at 70ºC, and (g,h) the copolymer of ethylene/1-hexene produced at 70ºC

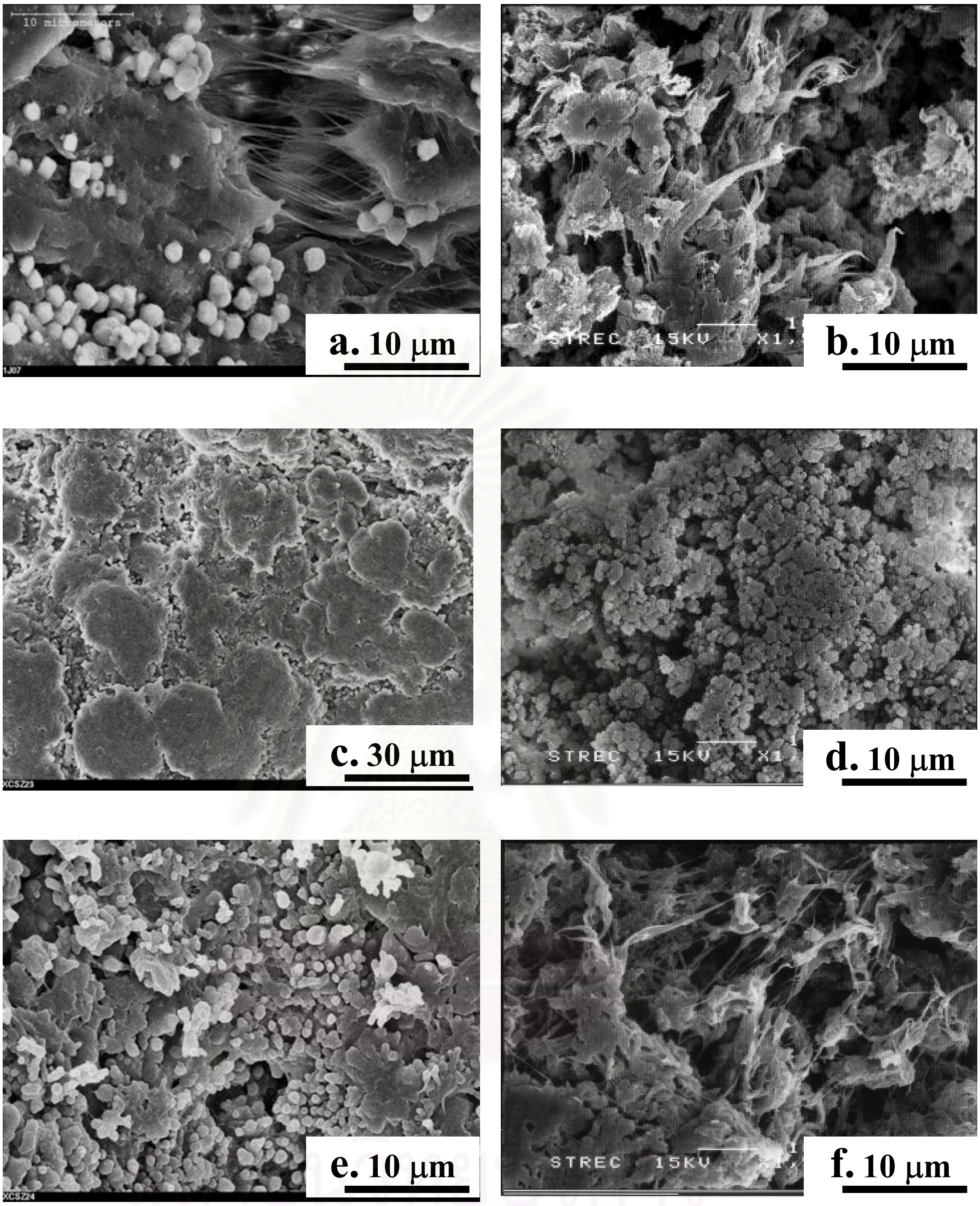

Figure 6.16. Comparison of homopolymer and copolymer produced in gas-phase (left) and slurry-phase system (right); (a,b) homopolymer made with support silicalite, (c,d) homopolymer made with MMS2.6, and (e,f) copolymer produced with support MMS2.6

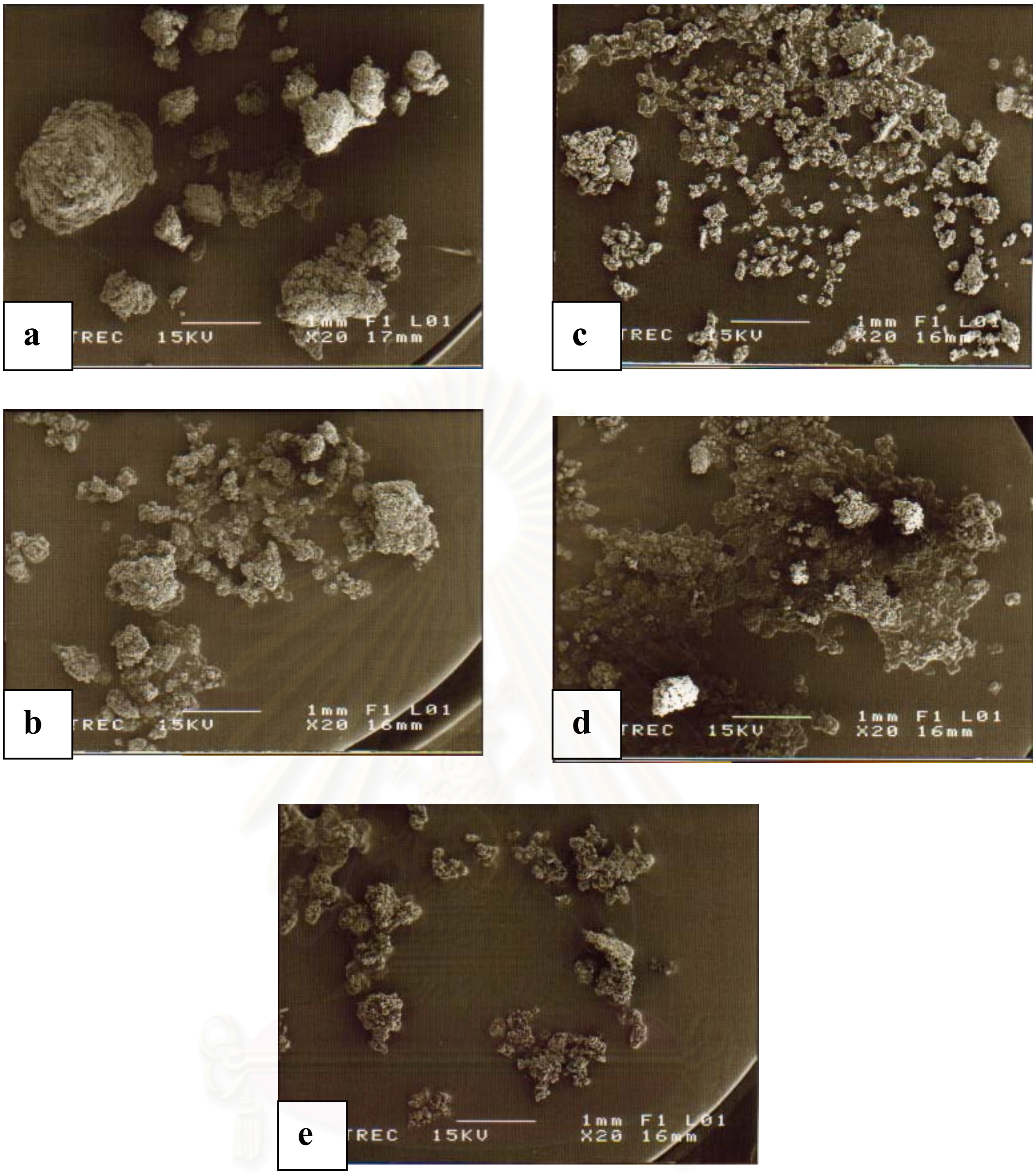

Figure 6.17. Scanning electron micrographs of the particles made in toluene medium (preliminary runs – see Tables 6.1 and 6.3): (a) 0.6 mmol of TIBA, (b) 2.4 mmol of TIBA, (c) 4.8 mmol of TIBA, (d) 7.2 mmol of TIBA , and (e) 0.44 mL of MAO

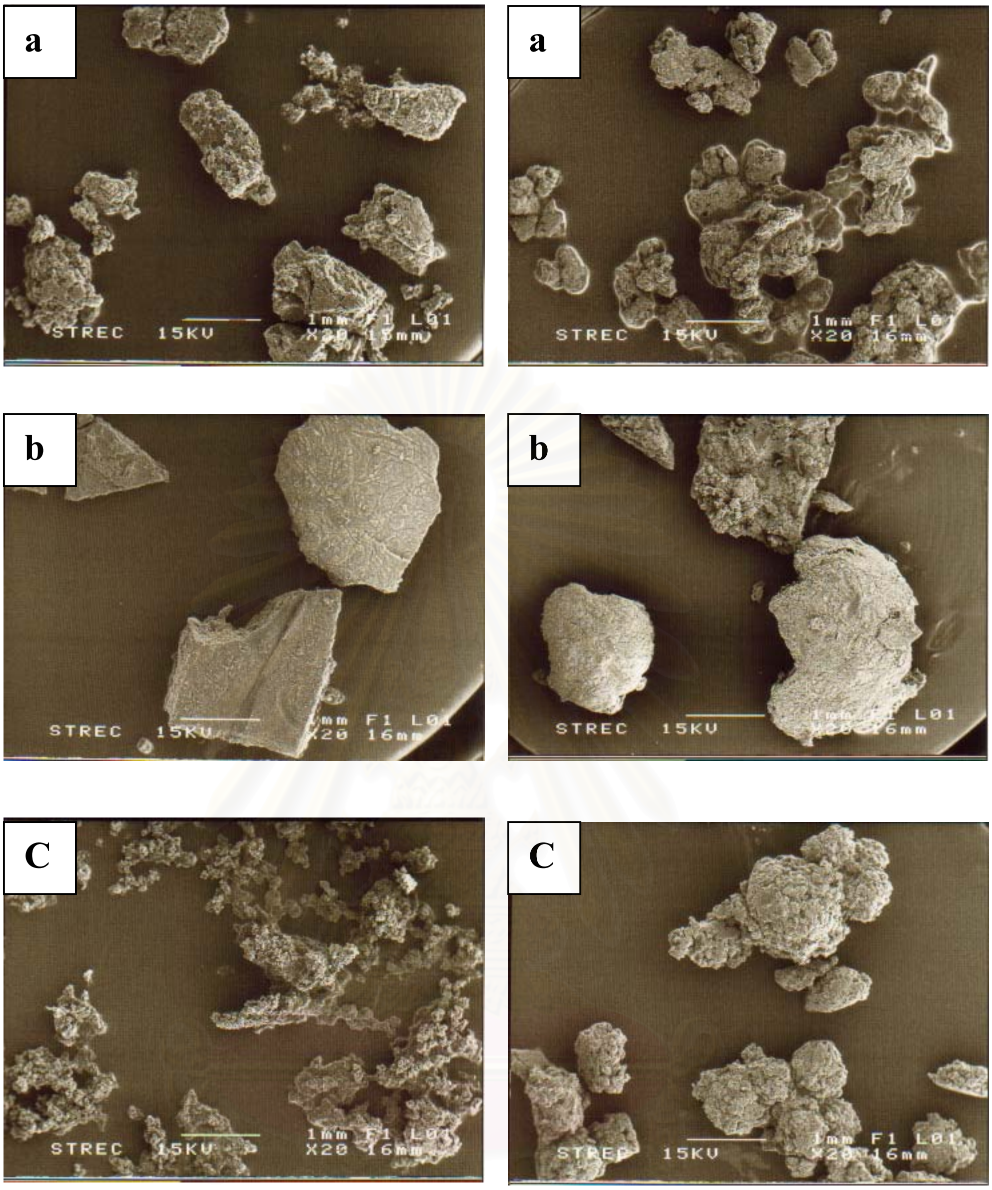

Figure 6.18. Scanning electron micrographs of product particles made in heptane (left) and decane (right) (preliminary runs- see Table 6.1 and 6.3): (a) 0.6 mmol of TIBA, (b) 2.4 mmol of TIBA, and (c) 0.44 mL of MAO

Molar masses were measured for most of the products obtained from slurry-phase runs so that the influence of pore size diameters and polymerization conditions on molar masses could be determined. It was found that the dependence of the molar masses on the polymerization temperatures was reasonably well correlated by Equations 4.1 and 4.2 used for correlating the molar mass for products made in the gas phase. The values of the molar masses, along with reaction conditions, are listed in Appendix B (Table B3). The parameter values for molar mass correlations (Equations 4.1 and 4.2) are listed in Table 6.6, and the fit for CATBA7.2 is shown in Figure 6.19. The line for the polydispersities in Figure 6.19 is given by the ratio of Equation 4.2 to 4.1, and the data points are based on the ratio of the measured M_w and M_n values. The polydispersities showed similar trend as observed in gas-phase system, that is for all the MMS-supported catalysts the polydispersities were essentially independent of temperature with values 2 to 3, except for CATBA2.5 where they varied from 2.3 to 3.4. For the silicalite supported catalysts, CATBA0.54, the polydispersities varied from 2.2 to 4.0.

For all catalysts, the molar masses of the products decreased with increasing polymerization temperature, indicating that the overall activation energies for the propagation reactions were lower than those for the chain termination reactions. On the basis of the values of b_n in Table 6.5, the difference in the average values of the lumped termination and propagation activation energies, that is, $E_{termination}$-$E_{propagation}$, is 17.9 kJ/mol; the average $E_{termination}$-$E_{propagation}$, based on b_w, is 19.7 kJ/mol. The average ratio of the lumped pre-exponential factors for propagation steps to termination steps, according to a_n values, is 119.5. For gas-phase ethylene polymerization, the correlations for the same ranges of pore sizes and temperatures as used in the slurry studies, i.e. 2.6-15 nm and 50-80°C, yield the $E_{termination}$-$E_{propagation}$, of 6.9 kJ/mol and 8.1 kJ/mol based on b_n and b_w, respectively. The molar masses for slurry-phase ethylene polymerization were slightly lower than the gas-phase ethylene polymerization. The difference in the ethylene concentration for the gas-phase and slurry-phase experiments are a possible reason for the differences in the molar masses; results for gas-phase polymerizations showed that moloar masses were a function of ethylene concentration (see Chapter IV).

Table 6.6. Parameter Values for Molar Mass Correlations (Equations 4.1 and 4.2)

Catalyst	Parameters for Mn			Parameters for Mw		
	a_n	b_n	r^2	a_w	b_w	r^2
CATBA0.54	-1.108	3986	0.8619	3.240	2873	0.9878
CATBA2.5	1.753	3052	0.9954	-0.332	4129	0.9003
CATBA2.6	9.280	666	0.8076	8.773	1087	0.9997
CATBA6.4	6.976	1445	0.9951	8.042	1319	0.9696
CATBA7.2	1.243	3181	0.9897	1.509	3448	0.9950
CATBA12.5	4.614	2300	0.9440	6.970	1776	0.9569
CATBA16	4.834	2261	0.9682	5.236	2449	0.9637

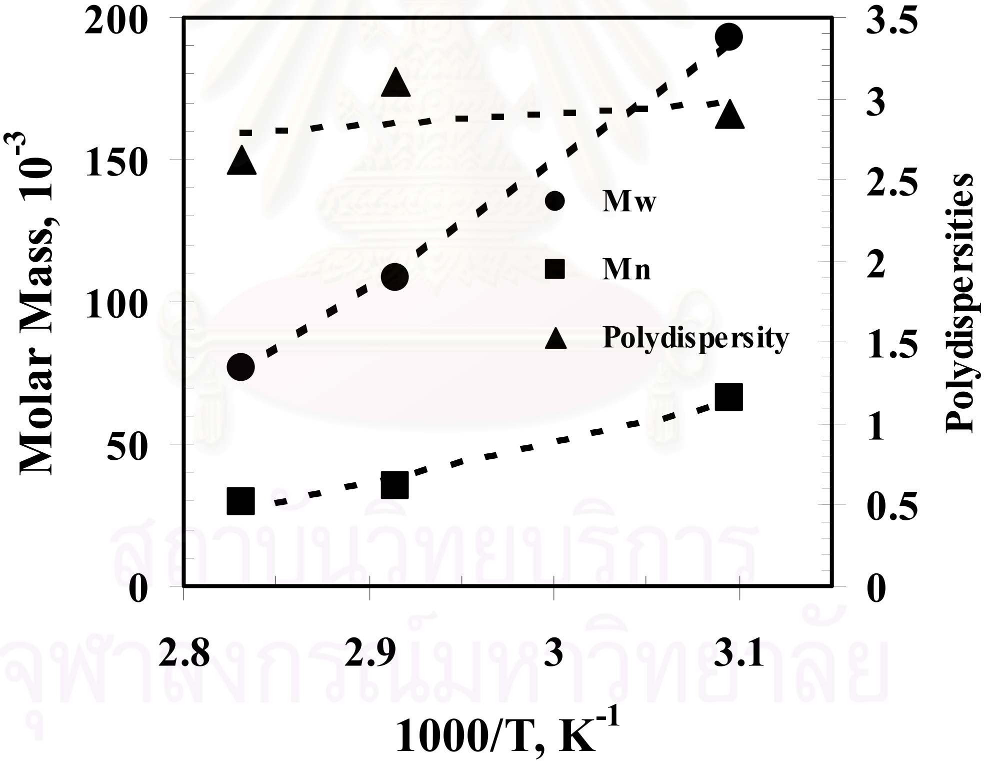

Figure 6.19. Sample plots of molar mass/temperature correlations for the best fit of CATBA7.2

Surprisingly, the molar masses of homopolymers for all of polymerization temperatures increased slightly with increasing the support pore sizes, especially for the larger pore sizes (12.5 and 16 nm). In case of gas-phase polymerization, no significant changes of molar masses with pore size were observed. For the large pore, the increase in molar masses was also observed for copolymerization.

The molar masses for 1-hexene copolymers were lower than those of the homopolymers made at the similar temperature as shown in Figure 6.20. These trends were also observed for 1-octene and 1-decene. Molecular weight (Mw) increased with increasing support pore diameter. The relations of molecular weight and support pore size for the different types of α-olefins and for the homopolymer made with external MAO are plotted in Figure 6.21. The molecular weights of copolymer increased as the support pore diameter increased, especially for ethylene/1-decene. When MAO was added to the reactor at 70°C, the molar masses of those polymers were lower than homopolymers produced with TIBA added. The molar masses of the homopolymer made with the addition of external MAO were similar in magnitude to the copolymers (see Figure 6.21). The polysispersity obtained with slurry-phase systems were independent of the different pore size diameters of supports for homopolymer and copolymer of 1-octene and 1-decene whereas the polydispersities slightly increased with increasing pore size for 1-hexene and external MAO; the average values of polydispersities are about 2.5, and 3.5 for homopolymer produced with the use of TIBA and MAO respectively, while the polydispersities were 2.7, 2.8, and 2.6 for copolymer made with 1-hexene, 1-octene, and 1-decene. The catalyst made with the silicalite support were not included in these comparisons since this is a different type of catalyst because the MAO and (*n*-BuCp)$_2$ZrCl$_2$ did not enter the pores of the silicalite.

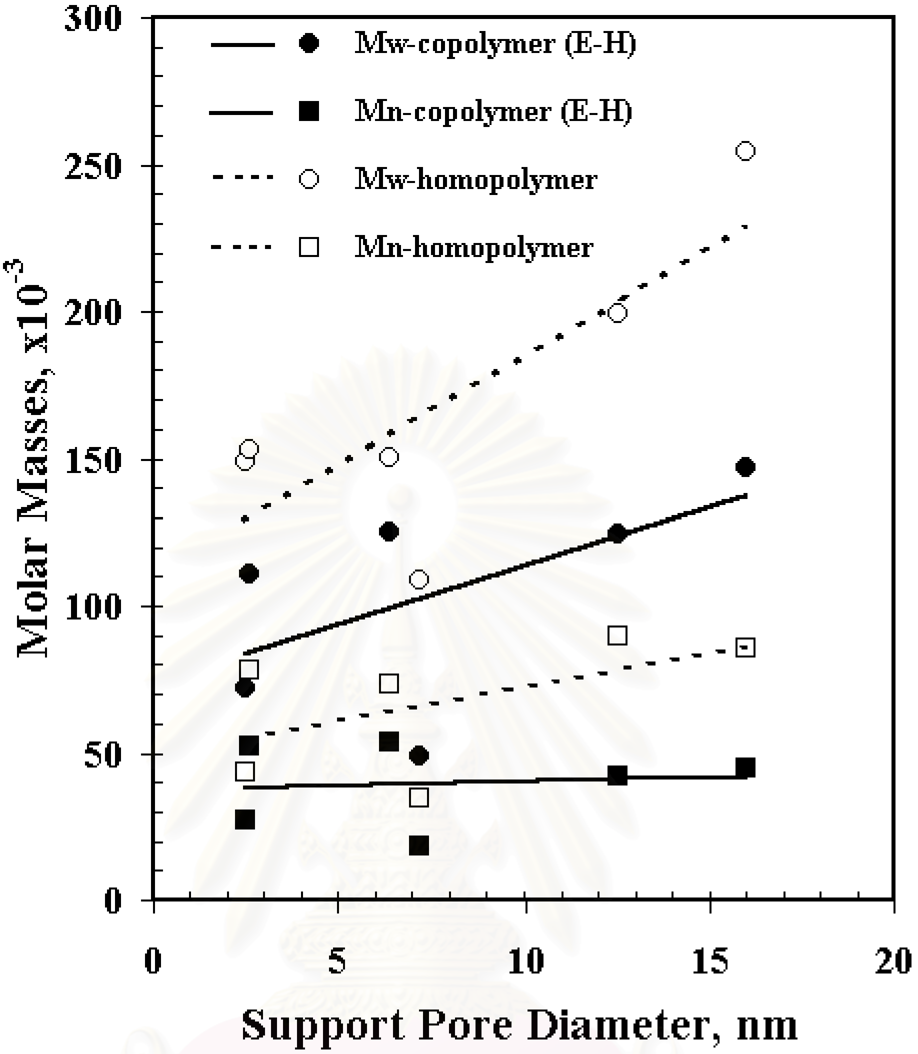

Figure 6.20. Molar masses for homopolymers and copolymers of 1-hexene made at 70°C in slurry phase with catalysts of different pore sizes (2.5-16 nm)

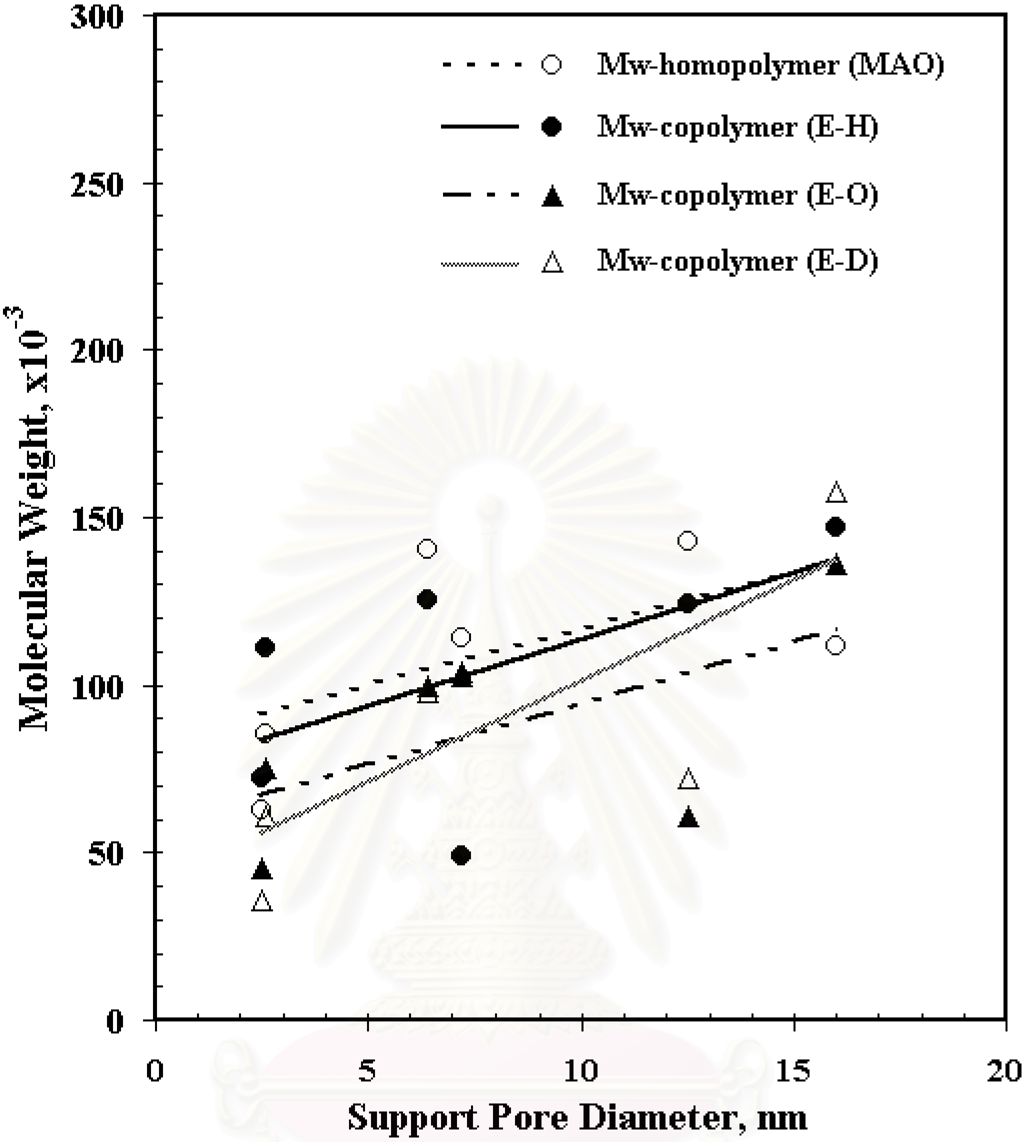

Figure 6.21. Molecular weight for homopolymers with the use of MAO and copolymers of 1-hexene made at 70°C in slurry phase with catalysts of different pore sizes (2.5-16 nm)

6.4. Characterization by Temperature Rising Elution Fractionation (TREF)

The previous observation from TREF analysis of products made in gas-phase experiments showed that the TREF profile depended on many factors, i.e. support pore size, polymerization conditions and 1-hexene concentration. However, TREF analysis does not provide information on the morphology of the nascent polymer because the nascent structure is destroyed during the solution of polymer. Therefore, the TREF and DSC analysis of LLDPE products made in slurry-phase polymerization were carried out and are reported in Sections 6.4 and 6.5, respectively. The summary of TREF results and TREF profiles of products made with CATBA-S1 at 70°C and the variation of the amount of 1-hexene are listed in Table 6.7 and shown in Figure 6.22. It was found that the increase in 1-hexene amounts resulted in decrease of 1-hexene consumed by polymerization (see Table 6.7) and in a systematic slightly decrease in the temperature of peak. The TREF profiles for all of products made at the different of 1-hexene amounts indicate that these materials were mainly copolymer, i.e. all the products eluted at temperatures <90°C.

Table 6.7. Summary of TREF results for ethylene/1-hexene copolymer with the variation of the amount of 1-hexene made with CATBA-S1

Run	Amount of 1-Hexene Added (mL)	Average CH_3 Concentrations [CH_3 Groups/1000 C]		C_W/C_N	Fraction Homo-Polymer	Fraction 1-Hexene Reacted
		C_N	C_W			
33	1.0	8.0	12.6	1.57	0.01	0.12
34	3.0	11.6	17.2	1.22	0.01	0.08
35	4.5	11.8	12.1	1.03	0.02	0.04
36	6.0	16.1	22.8	1.41	0.01	0.02
37	8.0	15.3	16.7	1.09	0.01	0.01
38	10.0	15.6	18.3	1.17	0.00	0.00

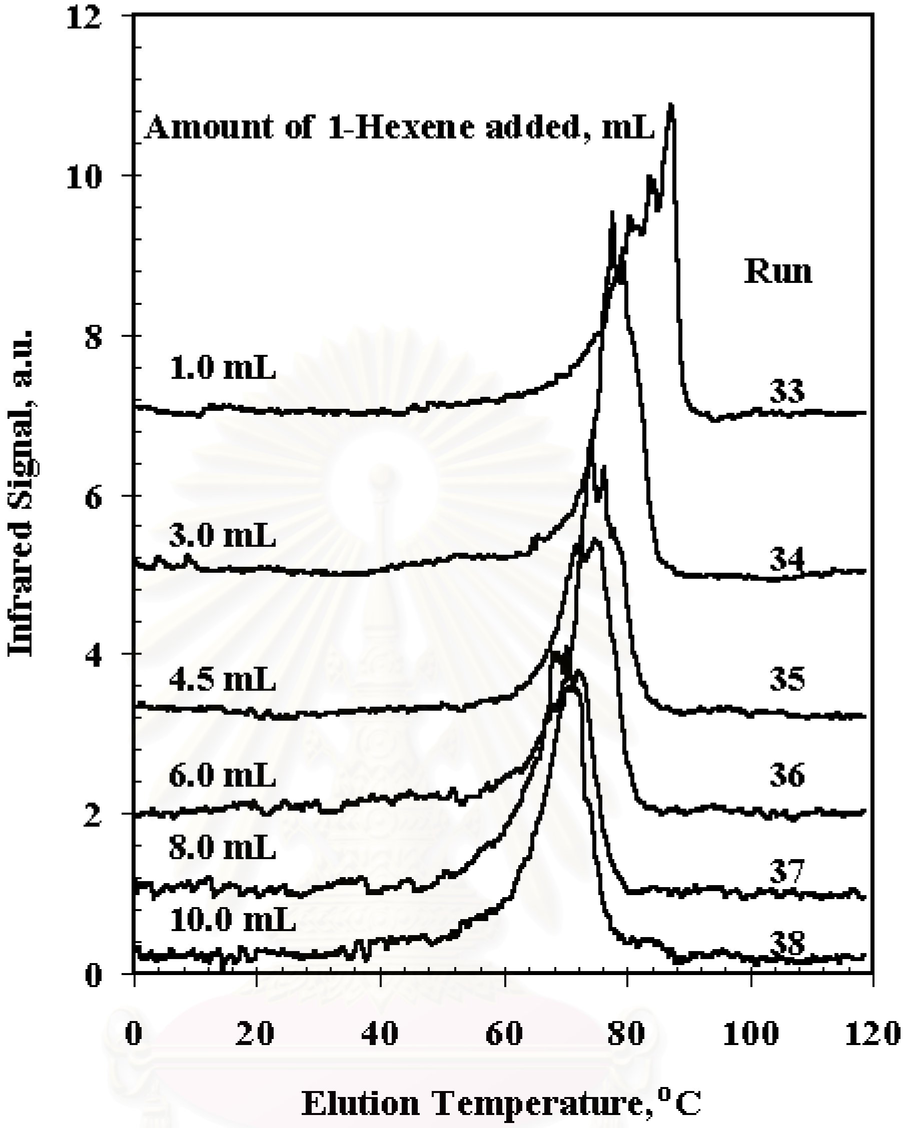

Figure 6.22. Effect of amount of 1-hexene on TREF profiles for ethylene/1-hexene copolymer (pattern offset for clarity)

Previous TREF results for gas-phase experiments showed that the pore size of supports had a significant effect on the short chain branching distribution of the products made with the different catalysts indicating that the types of catalytic sites were influenced by the support pore size. TREF analyses were done on the ethylene/α-olefins copolymers made in slurry operation with the catalysts having different of pore sizes. These results were summarized in Table 6.8 and the TREF profiles for ethylene/1-hexene, ethylene/1-octene, and ethylene/1-decene copolymers made at similar reaction conditions are shown in Figures 6.23 to 6.25.

Table 6.8. Summary of TREF results for different of support pore size

Type Of Olefin	Catalyst	Average CH_3 Concentrations [CH_3 Groups/1000 C]		C_W/C_N	Fraction Homo-Polymer	Fraction comonomer Reacted
		C_N	C_W			
1-Hexene	CATBA0.54	26.6	30.3	1.14	0.00	0.21
	CATBA2.5	11.0	13.9	1.26	0.02	0.09
	CATBA2.6	14.1	15.5	1.10	0.03	0.12
	CATBA2.6*	12.7	14.3	1.12	0.02	0.12
	CATBA6.4	15.9	16.8	1.05	0.00	0.13
	CATBA7.2	20.2	23.5	1.16	0.00	0.14
	CATBA12.5	10.3	11.8	1.14	0.04	0.02
	CATBA16	9.3	13.6	1.47	0.08	0.01
1-Octene	CATBA0.54	20.2	23.0	1.14	0.00	0.19
	CATBA2.5	8.0	10.0	1.26	0.03	0.09
	CATBA2.6	11.9	13.7	1.15	0.02	0.14
	CATBA6.4	7.2	8.9	1.23	0.12	0.06
	CATBA7.2	9.5	10.7	1.13	0.00	0.07
	CATBA12.5	6.2	8.1	1.31	0.09	0.01
	CATBA16	6.4	9.6	1.51	0.22	0.01
1-Decene**	CATBA0.54	18.5	23.2	1.26	0.01	0.17
	CATBA2.5	9.3	11.1	1.19	0.03	0.09
	CATBA2.6	5.1	8.2	1.61	0.54	0.05
	CATBA6.4	3.2	4.0	1.25	0.78	0.03
	CATBA7.2	7.3	8.2	1.12	0.02	0.06
	CATBA16	6.5	10.3	1.54	0.42	0.00

* The repeated product obtained with CATBA2.6 was measured for TREF analysis.

** The polymer product of ethylene/1-decene with CATBA12.5 was not reliable due to the increasing of pressure in the TREF column during measurement.

Some of the TREF profiles for ethylene/1-hexene copolymers shown in Figure 6.23 have multiple maxima, i.e products made with CATBA12.5 and CATBA16. This indicates that these catalysts have multiple types of catalytic sites. The small peak at 98°C for the product made with CATBA16 is due to ethylene homopolymer showing that this catalyst has homopolymerization sites as well as copolymerization sites, which produced product which eluted at lower temerpatures. In case of small pore catalysts, only one dominant peak in range of 50 to 90°C was observed, i.e. only copolymer was produced with the catalyst made from supports having pore sizes ≤7.2 nm. These observations are different than those for gas-phase operation. The systematic variations in the TREF profiles showing decreasing elution temperatures with increases in the support pore diameter from 2.6 to 20 nm observed for gas-phase polymerization (Figure 5.5) was not observed for slurry polymerization (Figure 6.23). The TREF profiles for slurry operation showed that the low temperature peak was dominant for the small pore sizes and the high temperature peak appeared for the large pore catalyst. The reason of these results is probably associated with the difference of transformation behavior of the catalytic sites between gas-phase and slurry-phase polymerization. It is important to note that the polymerization lengths for gas-phase and slurry-phase are different, i.e. the gas-phase runs were 120 min in length while the slurry-phase runs were only of 15 min duration. As shown in the Chapter 5, the homopolymerization sites for CATBA20 were only present of initially and disappeared for long polymerization times. The intensity of the high temperature TREF peak at 96°C, indicating homopolymerization, was dominantly observed for the short polymerization time (0.5 h) for CAT20. TREF profiles for CATBA0.54 in which all the catalytic active species were on the outer surface showed a broad peak at low temperature similar to that obtained for the gas-phase product.

Owing to the vapor pressure limitation in gas-phase polymerization, significant incorporation of higher olefins, such as 1-octene and 1-decene, is not possible. Therefore, slurry-phase polymerization with higher α-olefins was used to determined whether the type of olefin affects the activity of these catalysts. The TREF profiles of ethylene/1-octene, shown in Figure 6.24, indicate that the crystallinities of the products made with 1-octene were significantly different than the ethylene/1-hexene polymer, especially for products made with the large pore catalysts. For example, the shoulder peak found in range of 70-80°C for ethylene/1-hexene copolymer made with CATBA16 disappeared for the 1-octene product. The TREF profile for the 1-octene product made with CATBA12.5 only had a single beak, while the 1-hexene copoloymer had two distinct peaks. In general, the products made with 1-octene had a higher elution temperature (Figure 6.24) than the products made with 1-hexene (Figure 6.23). This means that the 1-octene copolymer less short chain branching and higher fractions of homopolymer (see in Table 6.8).

The 1-decene copolymers had even higher average elution temperatures than the 1-octene (see Figure 6.25) for all of catalysts. The broadness of the short chain branching distribution is due to the presence of different types of catalytic sites as well as to variations in the 1-hexene concentration during the runs; the C_W/C_N values in Table 6.8 are an indication of the broadness of the short chain branching distribution.

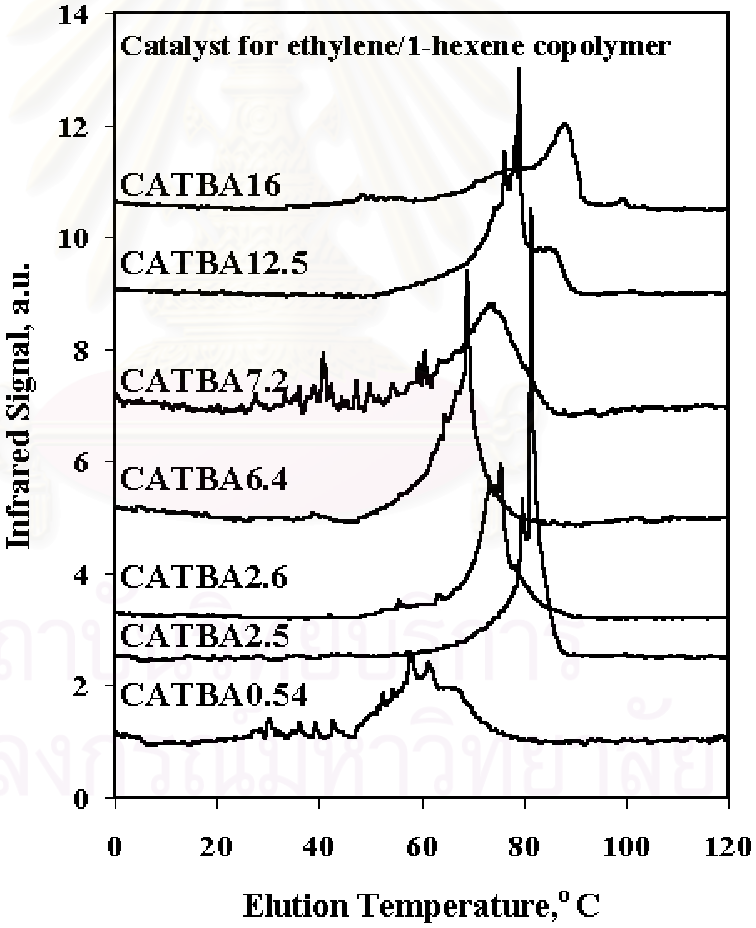

Figure 6.23. Effect of support pore size on TREF profiles for ethylene/1-hexene copolymer (pattern offset for clarity)

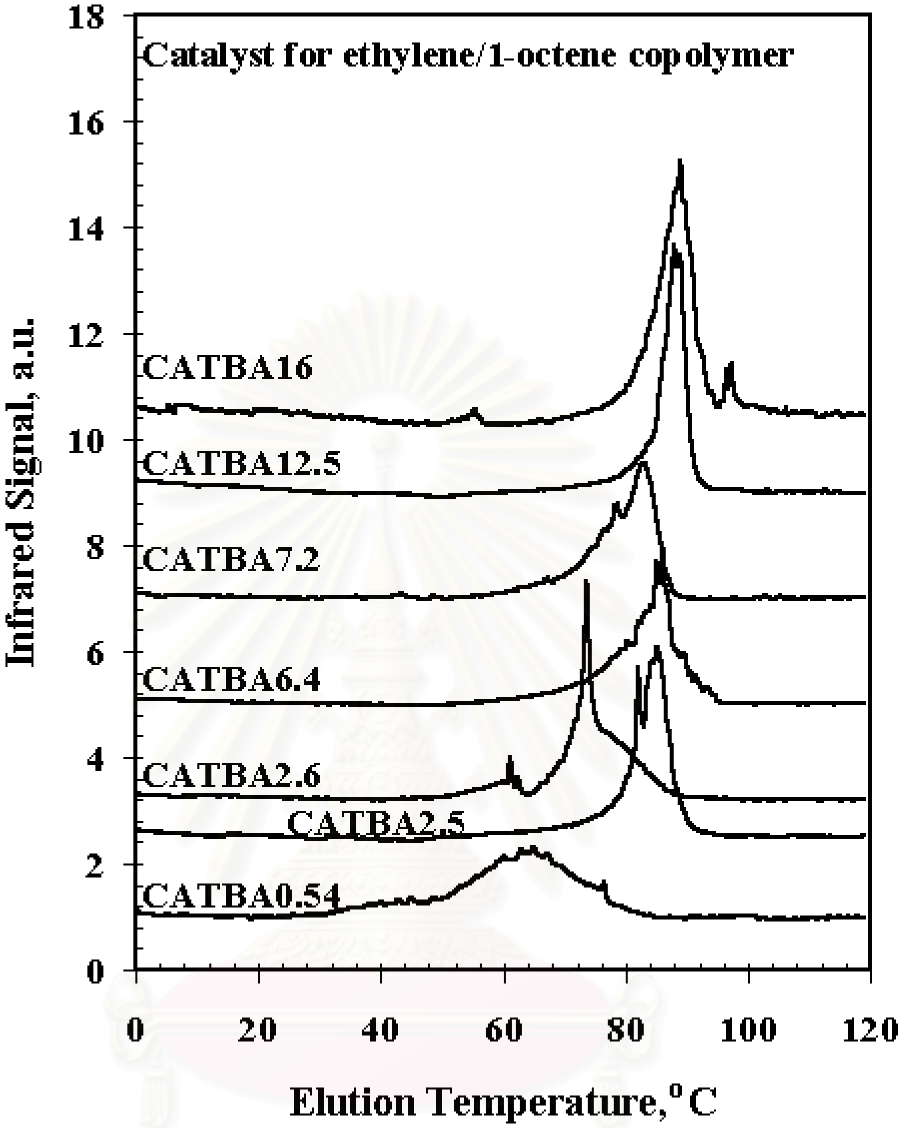

Figure 6.24. Effect of support pore size on TREF profiles for ethylene/1-octene copolymer (pattern offset for clarity)

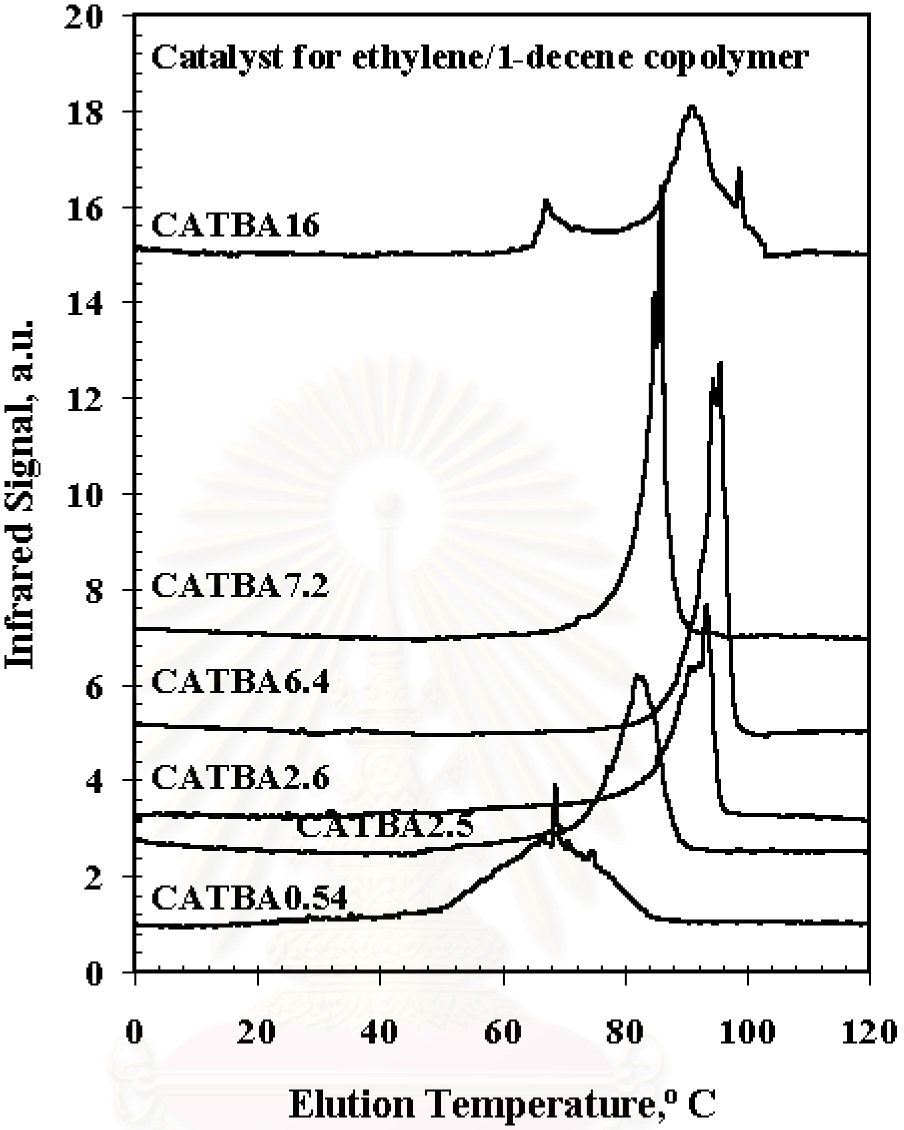

Figure 6.25. Effect of support pore size on TREF profiles for ethylene/1-decene copolymer (pattern offset for clarity)

The higher crystallinities of the polymers made with 1-octene and 1-decene compared to those made with 1-hexene may be due to the lower incorporation rates of the large olefins as well as the lower diffusion rates of the larges olefins. Experiments at different concentration and temperatures are required to determine the cause for the different behavior of the different comonomers. Nevertheless, it can be concluded that the pore size affect the types of catalytic sites present since the TREF profiles for all three comonomers were a function of support pore size.

6.5. Characterization by Differential Scanning Calorimetry (DSC)

The DSC analysis of nascent polymer for two consecutive DSC scans was done on each sample to determine the features of the nascent and recrystallized product since it was found that for gas-phase polymerization the DSC profiles were a function of the catalyst and the polymerization conditions. Figure 6.26 shows the DSC endotherms for first and second scan with the variation of amount of 1-hexene for the products from the preliminary experiments of Set C. Increases in the amount of 1-hexene from 1 to 10 mL resulted in the systematic decrease in the temperature of the peak in the endotherm from 120 to 103°C for the first and second DSC scans. Only one peak was present in the endotherms for the first and second scans. Increasing of amount of 1-hexene, in general, resulted in broadening of the DSC profile for both the first and second scans, as well as a reduction in the area under the endotherms, i.e. a decrease in the crystallinities. The temperature of the peak as well as the percent of crystallinities computed from the heat of fusion for the first and second scan are summarized in Table 6.9.

Table 6.9. DSC runs with enthalpy and temperature of the peak obtained from preliminary experiments in Set C

Run	**Amount of 1-Hexene Added (mL)**	**First DSC Scan**		**Second DSC Scan**	
		T (°C)	**χ (%)**	**T (°C)**	**χ (%)**
33	1.0	121	58.9	120	39.1
34	3.0	116	50.6	114	32.4
35	4.5	113	41.2	110	29.1
36	6.0	109	46.0	108	28.4
37	8.0	108	40.3	107	25.6
38	10.0	102	28.1	103	17.1

No significant difference of the temperature of the peak of the endotherms for the first scan and second scan was observed, although the second scan for all except Run 38, had slightly lower peak temperatures. It is interesting to note that the crystallinities of the nascent polymer (scan 1) were significantly higher than the crystallinities of the recrystallized polymer (scan 2).

The DSC endotherms for nascent polymers for ethylene/1-hexene, ethylene/1-octene, and ethylene/1-decene made with catalysts having different initial pore sizes at similar polymerization conditions are shown in Figures 6.27 to 6.29 and maxima in endotherms and crystallinities are summarized in Table 6.10. The DSC results suggest a greater degree of heterogeneity in catalytic sites as a function of pore size than indicated by the TREF results (cf. Figures 6.23 and 6.27). The plots in Figure 6.27 clearly show that the pore size of the catalyst supports had a marked effect on the nascent product morphology. Ethylene/1-hexene copolymer made with catalysts having initial support pore diameters > 7 nm had DSC endotherms with 2 maxima indicating that at least two different types of catalytic sites are present in these catalysts. Nascent product made with CATBA2.6 and CATBA6.4 had similar endotherms with the main peak at 114°C and the shoulder towards the low temperature side (103-106°C); the nascent product made with CATBA2.5 only has one major peak in its endotherm. It seems that the larger initial pore sizes had variation of catalytic sites in catalysts more pronounced than the small pore sizes. Also, CATBA0.54 did not follow this trend of greater product homogeneity with decreasing support pore size because, as stated earlier, the pores in CATBA054 did not contain the MAO nor the (n-BuCp)$_2$ZrCl$_2$. Some of the second DSC scans, surprisingly, retained some of the complex structure of the first scan, i.e. shoulders on the peaks in the second scan. The crystallinities calculated from the enthalpy of melting based on the second scan were considerably lower than the crystallinities from the first scan, similar to the observation for the products made with CATBA-S1.

The DSC for first scan of nascent product of ethylene/1-octene shown in Figure 6.28 showed only one major peak, except for CATBA0.54. As found by TREF, the 1-octene product had higher melting temperatures (larger lamellae size) than the 1-hexene products. Hence it can be concluded that the homopolymerization was much more dominant for ethylene/1-octene than for ethylene/1-hexene.

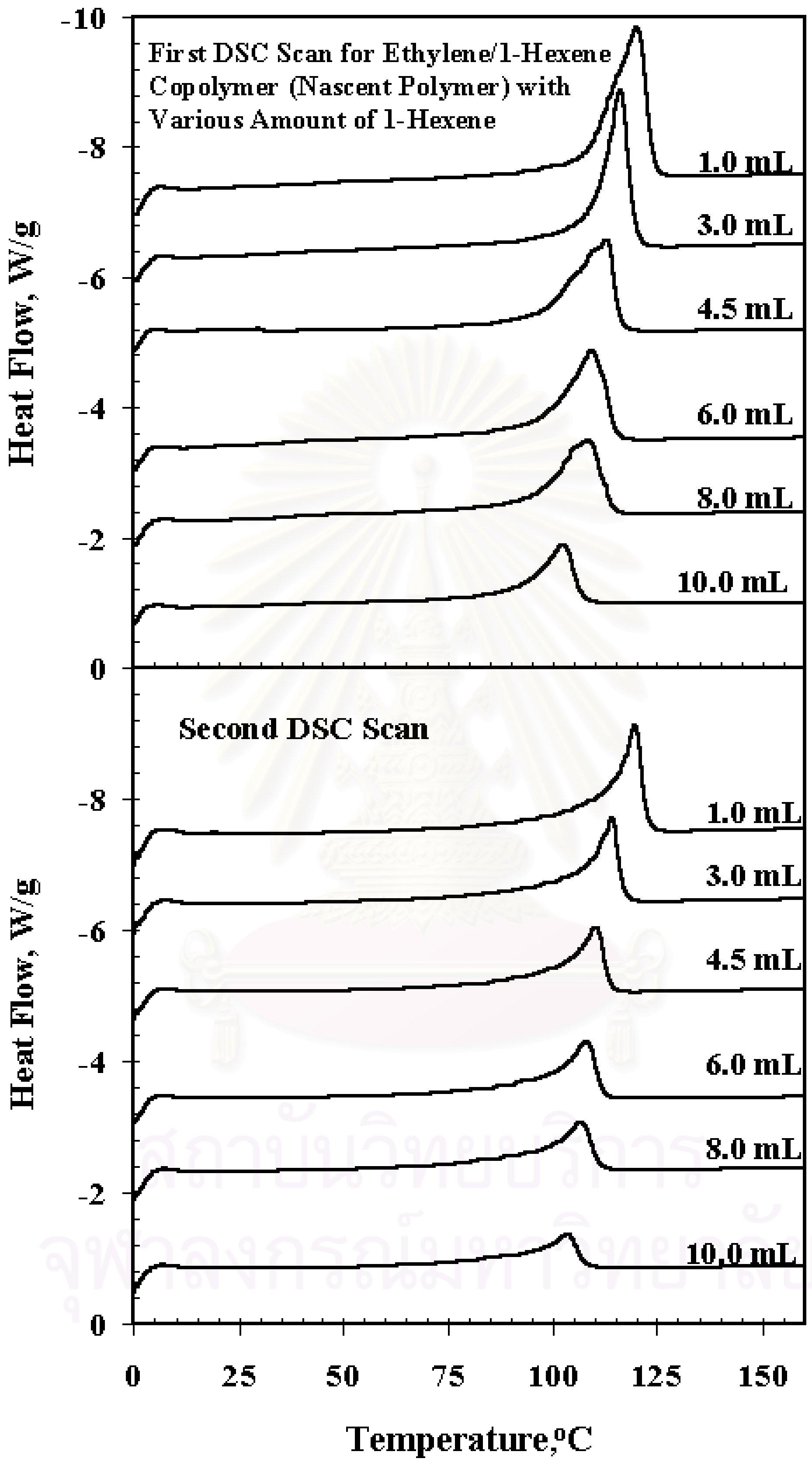

Figure 6.26. Effect of amount of 1-hexene on DSC endotherms in preliminary results of set C (Patterns off set for clarity)

Table 6.10. Summary of DSC results.

Type of comonomer	Catalyst	Pore Dia. (nm)	Maxima in DSC Endotherms^{a} (°C)						Crystallinity^{b} %	
			First Scan			Second Scan			Scan 1	Scan 2
			T_1	T_2	T_3	T_1	T_2	T_3		
1-Hexene	CATBA0.54	0.54	102*	111	-	98	108*		30	20
	CATBA2.5	2.5	-	116*	-	-	115*	-	51	33
	CATBA2.6	2.6	106	114*	-	101	112		40	26
	CATBA6.4	6.4	103	114*	-	101	112*		32	21
	CATBA7.2	7.2	109	114*	-	-	112*	-	46	33
	CATBA12.5	12.5	-	115*	137	-	116*	134	53	31
	CATBA16	16	109	115*	-	-	113	-	27	14
1-Octene	CATBA0.54	0.54	104*	113	-	101	109*	-	39	27
	CATBA2.5	2.5	-	117*	-	-	118*	-	50	33
	CATBA2.6	2.6	-	115*	-	-	115*	-	38	28
	CATBA6.4	6.4	-	119*	-	-	120*	-	41	31
	CATBA7.2	7.2	-	116*	-	-	115*	-	53	37
	CATBA12.5	12.5	-	120*	-	-	121*	-	51	30
	CATBA16	16	-	117*	-	-	119*	-	39	18
1-Decene	CATBA0.54	0.54	106*	114	-		110*	-	40	29
	CATBA2.5	2.5	-	116*	-	-	116*	-	38	30
	CATBA2.6	2.6	-	-	125*	-	-	123*	39	31
	CATBA6.4	6.4	-	-	127*	-	-	126*	36	30
	CATBA7.2	7.2	-	117*	-	-	118*	-	56	38
	CATBA12.5	12.5	-	120*	131	-	-	126*	45	31
	CATBA16	16	-	120*	130	-	-	121*	42	21

[a] The main DSC peak in the endotherm is indicated by an asterisk (*), [b] DSC crystallinity based on ΔH_{fusion} = 290 J/g for crystalline polyethylene [Ottani and Porter, (1991)].

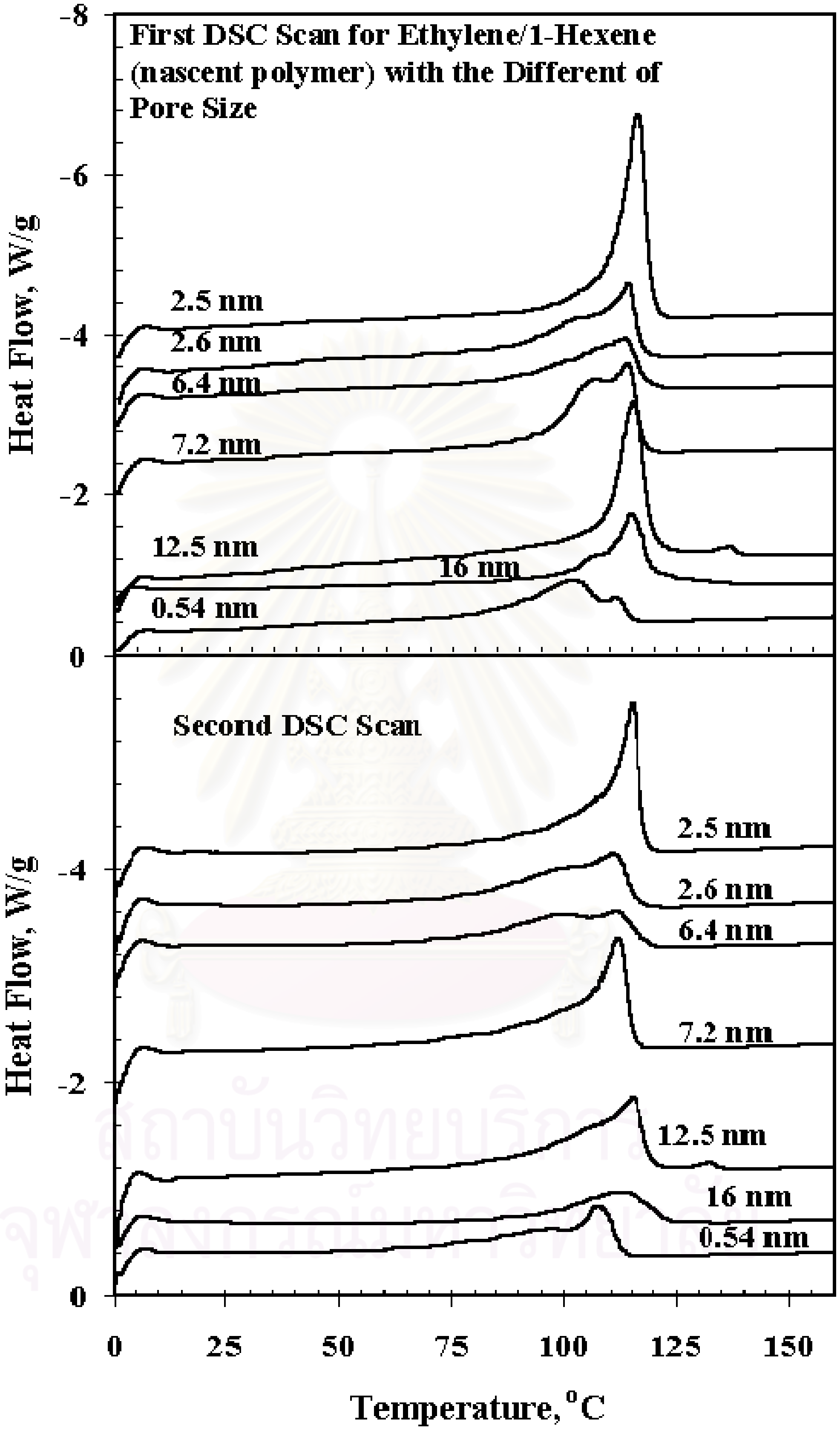

Figure 6.27. Effect of pore size on DSC endotherms for ethylene/1-hexene copolymer (Patterns off set for clarity)

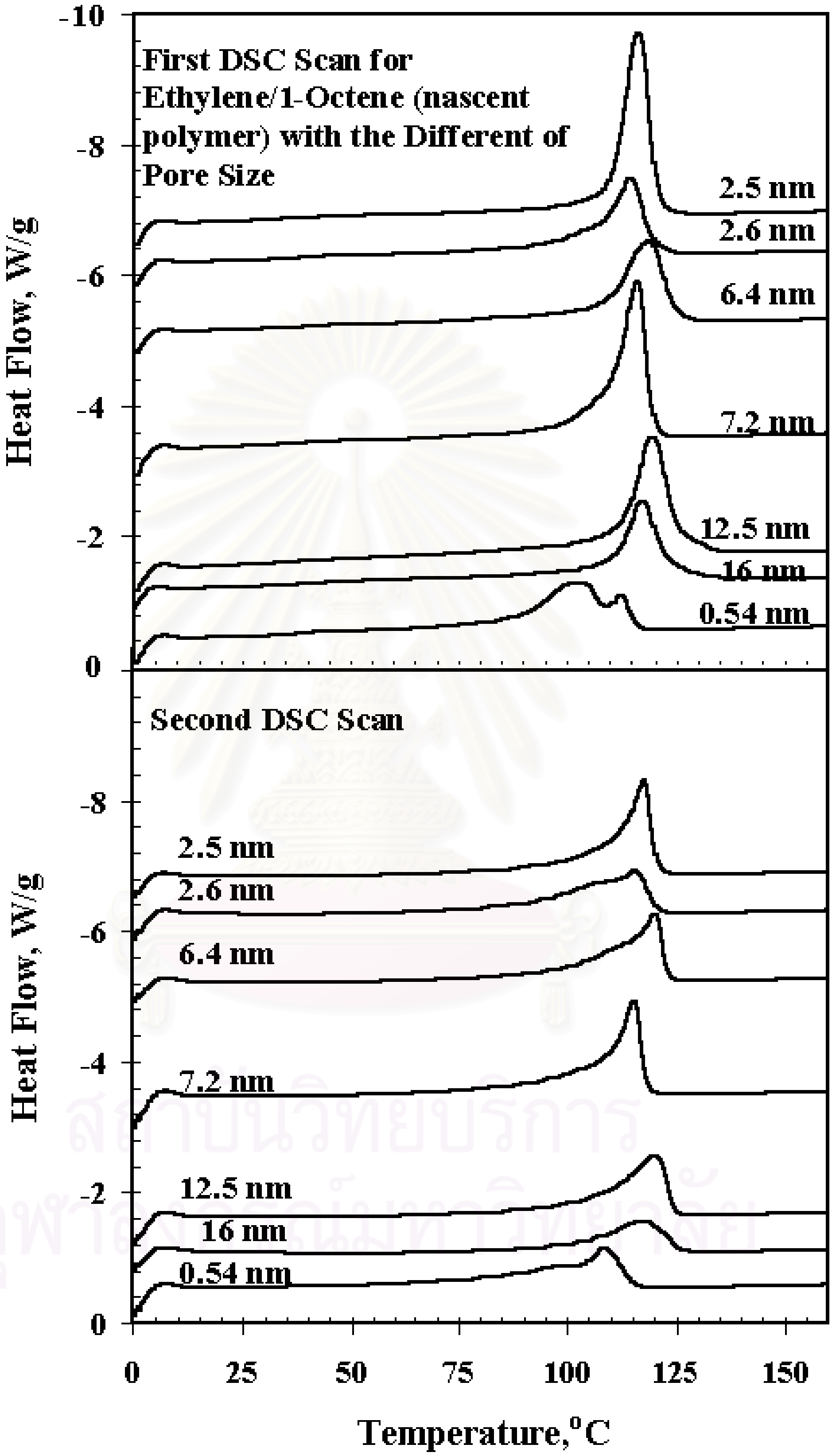

Figure 6.28. Effect of pore size on DSC endotherms for ethylene/1-octene copolymer (Patterns off set for clarity)

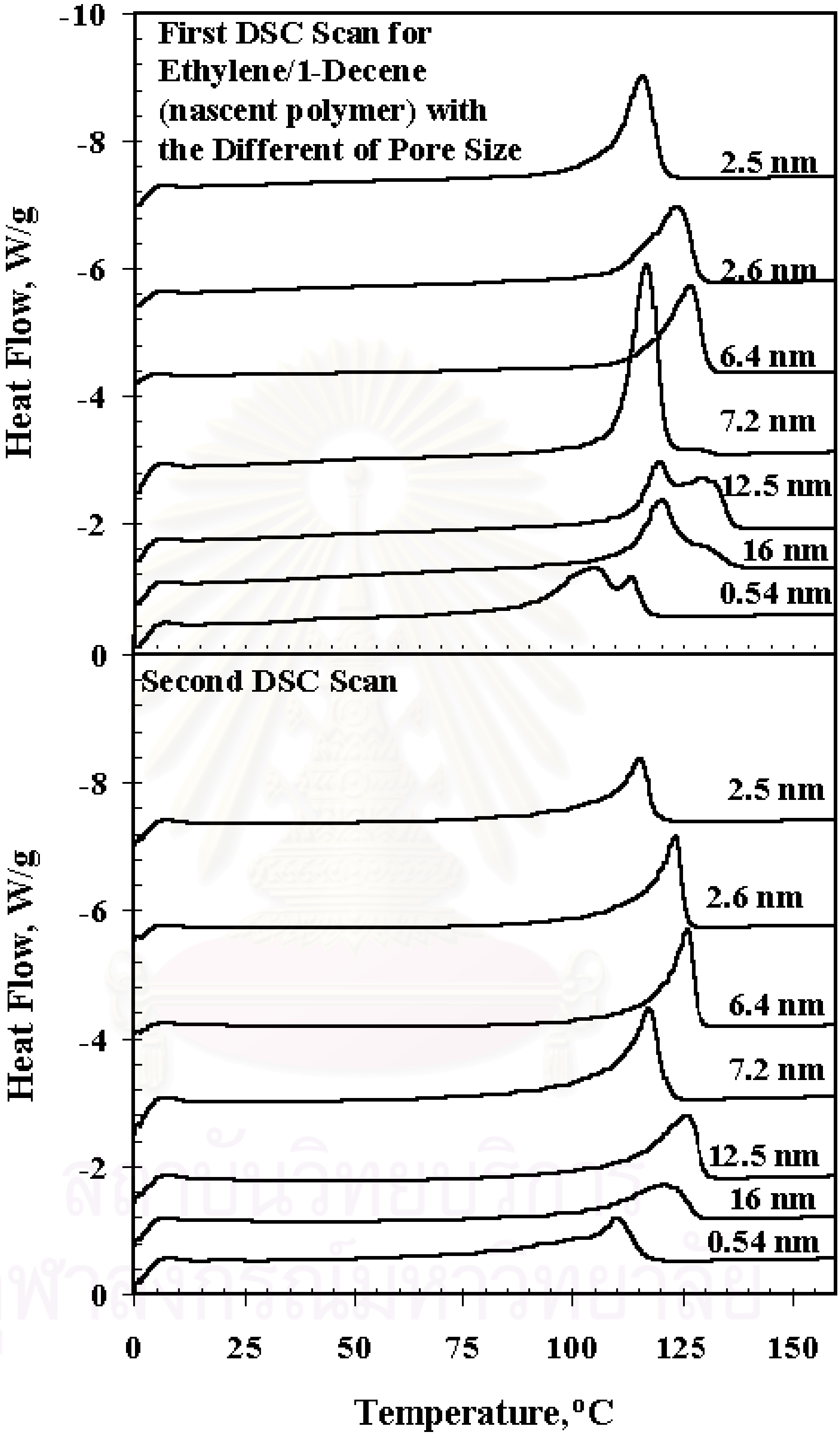

Figure 6.29. Effect of pore size on DSC endotherms for ethylene/1-decene copolymer (Patterns off set for clarity)

Again, the trend of higher melting temperatures for ethylene/1-decene compared to ethylene/1-hexene was observed (see Figure 6.29). The endotherms for the first scan with the large pore catalyst support (CATBA12.5 and CATBA16) had two peaks while only one peak were observed with the products made with smaller pore sized catalysts.

TREF and DSC analysis indicated the heterogeneous nature of the catalytic sites in the supported catalysts. DSC results with nascent product were found to be more sensitive than TREF for indicating variations in product properties with support pore size. The higher α-olefins resulted in an increase in the temperature in the endotherms (1-decene>1-octene>1-hexene) indicated less incorporation of comonomer with higher α-olefins.

CHAPTER VII

Comparison of Gas- and Slurry-Phase Results

In this chapter, the gas-phase and slurry-phase results for homopolymerization and copolymerization are compared with an emphasis of the effects of support pore size on catalyst performance and product properties. Many factors influence catalytic behavior and product properties as was observed in gas-phase and slurry-phase results (see in Chapter IV-VI), as well as reports in the open literature (Chapter II). When comparing the effect of pore size for gas and slurry operation, it should be kept in mind that several other factors besides the reaction medium were different in the current studies. These other differences for gas-phase and slurry-phase polymerizations are listed below.

(A) Materials: TIBA and MAO used for gas-phase and slurry-phase experiments were obtained with the different sources; it is possible. The oligomers in the MAO mixtures were different and this could have had a significant effect on the catalytic properties. The range of support pore size used for gas phase (2.6-25 nm) and slurry phase (2.5-16 nm) were also different only supports MMS2.6 and 7.2 were the same supports.

(B) Catalyst preparation: Similar impregnation methods were used for catalyst preparation, but there were some variation such as the support pretreatment procedure. For the gas phase catalysts the thermal pretreatment of the support was done under flowing ultra-pure nitrogen while a vacuum pretreatment was used for the slurry catalysts.

(C) Polymerization procedures: The operating procedures, in addition to the slurry and gas phase difference, were different in other aspects. The sequence of exposure of catalyst to TIBA, ethylene and 1-hexene was different for the gas and slurry operations. For the slurry operation the catalysts were frozen at liquid nitrogen temperatures in the suspending liquid; no such freezing of the catalysts was done for the gas-phase experiments. The ethylene and 1-hexene concentrations and the polymerization lengths were also different.

However, a comparison of the support pore size is still meaningful if the pore size effect is more dominant than the differences in catalyst preparation and operating conditions. The comparisons of activity profiles, polymer yields, molar masses, short chain branches, and crystallinities for gas-phase and slurry-phase polymerization are presented below.

7.1. Comparison of Activity Profiles, Average Polymerization Activities, and Polymer Yields

It was observed that the yield of polymer per gram of catalyst for gas-phase polymerization (2 h) was typically several-fold higher than for slurry-phase polymerization (15 min), except for the silicalite-supported catalysts made with CAT0.54 and CATBA0.54, that is, the PE yield for slurry-phase operation with the silicalite supported catalyst was higher than for gas-phase operation.

All activity profiles, for both gas and slurry operation, showed a period of activation followed by deactivation, except for CATBA0.54 in heptane slurries. The activity profiles for gas phase and slurry phase had significantly different activation and deactivation rates, that is, the rates for slurry polymerization increased much more rapidly than those for gas-phase polymerizations, and the deactivation rates for the slurry were also much more rapid than those for the gas phase. These effects are illustrated in Figures 7.1 and 7.2 for homopolymerization and copolymerization, respectively. For most of the slurry runs, the activity was very low after 15 min of reaction time, whereas for gas phase runs, many catalysts still had considerable activity after 1 h of polymerization. All activity profiles for copolymerization were broader than homopolymerization for gas-phase and slurry-phase polymerizations.

As shown in Figure 7.3, the average rates in gram of PE per gram of catalyst and per hour for gas-phase and slurry-phase homopolymerization were frequently of similar magnitude at the various polymerization temperatures. It can be seen from the results in Figure 7.3 that the average polymerization rates were a strong function of support pore diameter and polymerization temperature for both gas- and slurry-phase polymerizations.

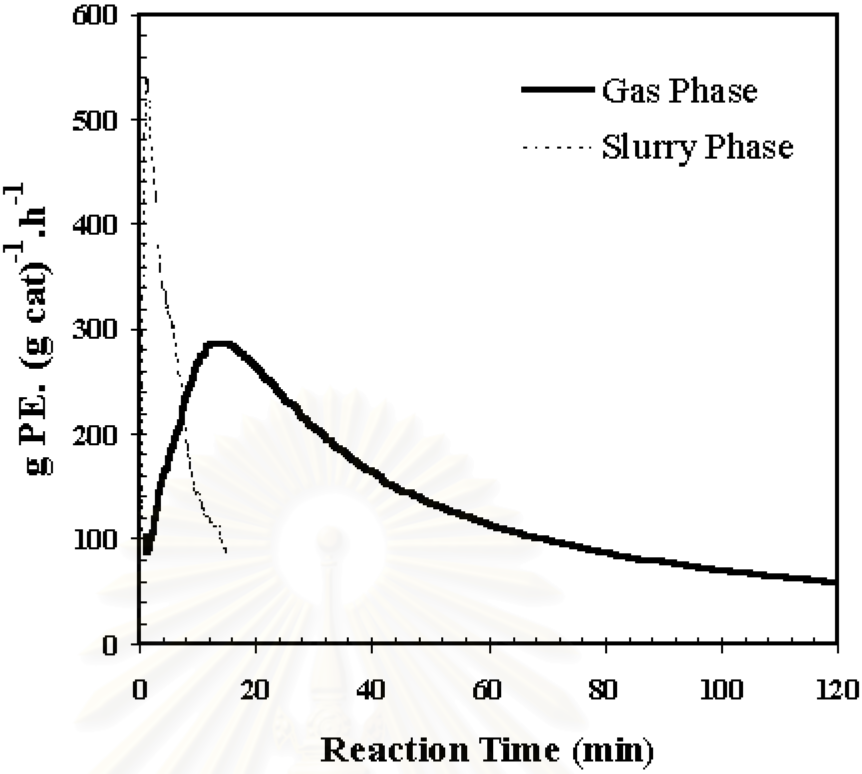

Figure 7.1. Comparison of the activity profiles for gas-phase and slurry-phase ethylene polymerization made with CAT2.6 and CATBA2.6 at 70°C

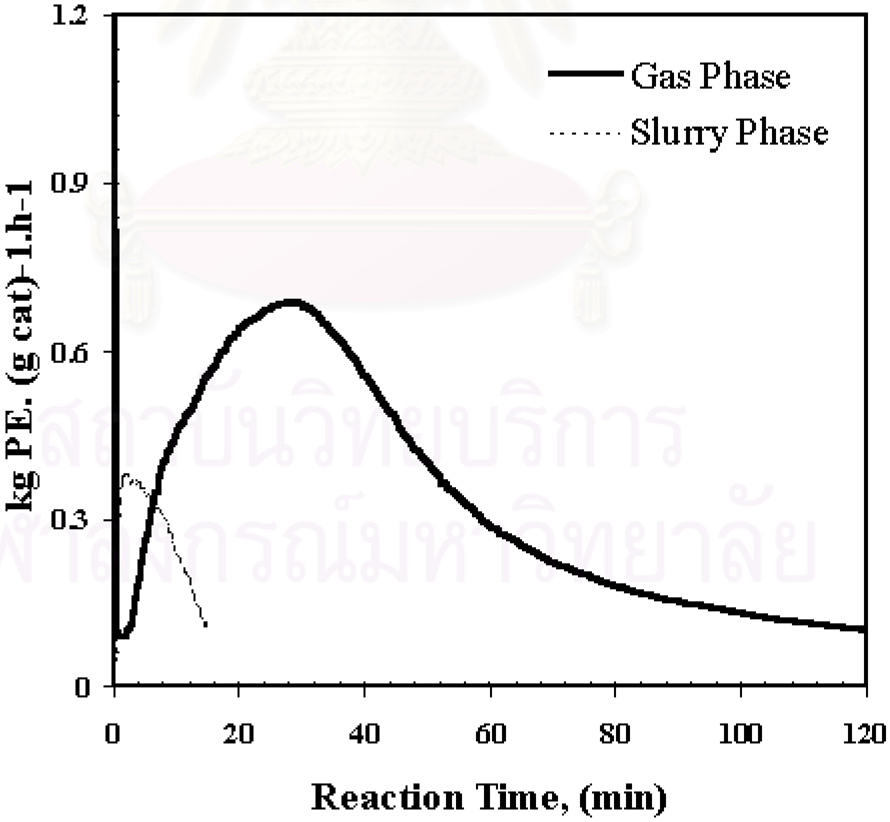

Figure 7.2. Comparison of the activity profiles for gas-phase and slurry-phase ethylene/1-hexene copolymerization made with CAT2.6 and CATBA2.6 at 70°C

For gas-phase polymerization the maximum activity was observed with catalyst made by MMS supports having pore diameter in range of 2 to 6 nm whereas slurry phase the maximum activity observed with catalyst made with MMS support 2.5 and 2.6 nm. Average activities declined monotonically for larger support pore diameters, i.e. gas-phase activities for support pore size 20 and 25 nm were low at all polymerization temperatures. The catalysts were most active at 70°C indicating that catalyst deactivation was more temperature sensitive than activation. Average activities in heptane slurries for CATBA0.54 and CATBA2.6 showed high activities. The high activity for CATBA0.54 is attributed to catalyst leaching because MAO and (n-BuCp)$_2$ZrCl$_2$ did not enter the small silicalite pores. The effect of support pores size on average activity was also very marked for both gas-phase and slurry-phase copolymerization (see Figure 7.4). Average rates in slurry-phase copolymerizations for all of support pore sizes, except for CAT2.6, were higher than for gas-phase copolymerizations. The effect of pore size was more marked at pores sizes ≥7.2 nm for gas-phase operation and at support pores ≥10 nm for slurry-phase operation. Moreover, this effect was also observed for slurry operation with the higher olefins resulted in decreasing the average rates.

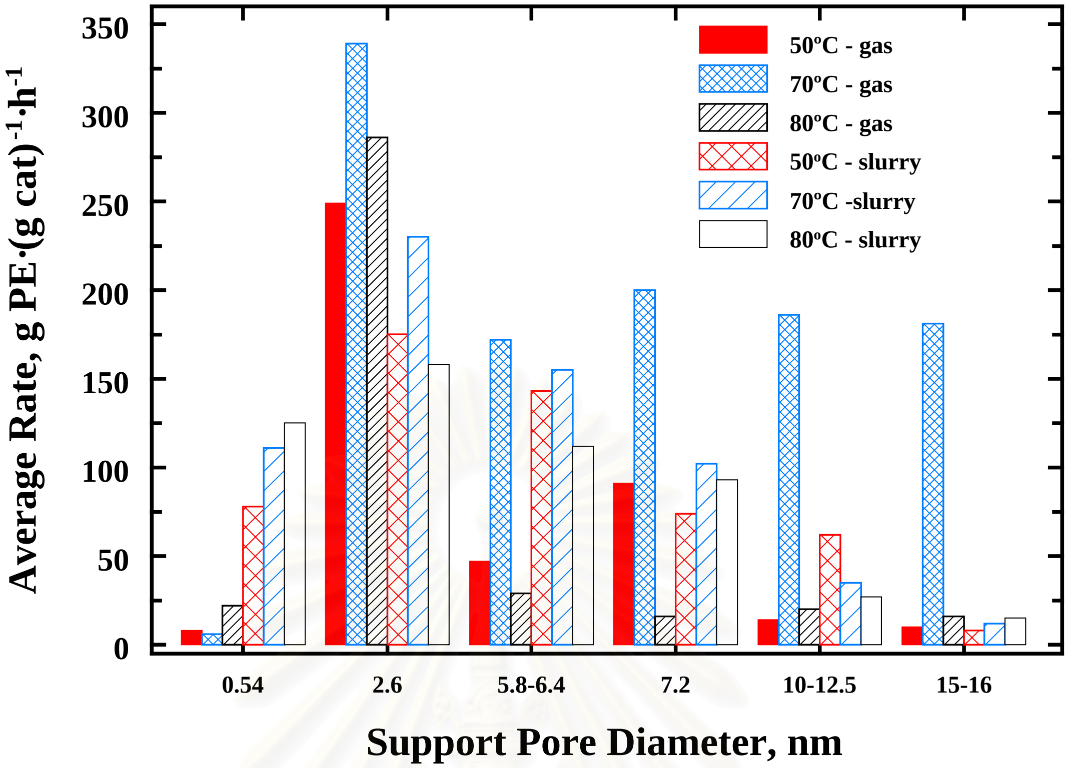

Figure 7.3. Comparison of average rates as a function of support pore diameter for gas and slurry homopolymerizations at various polymerization temperatures

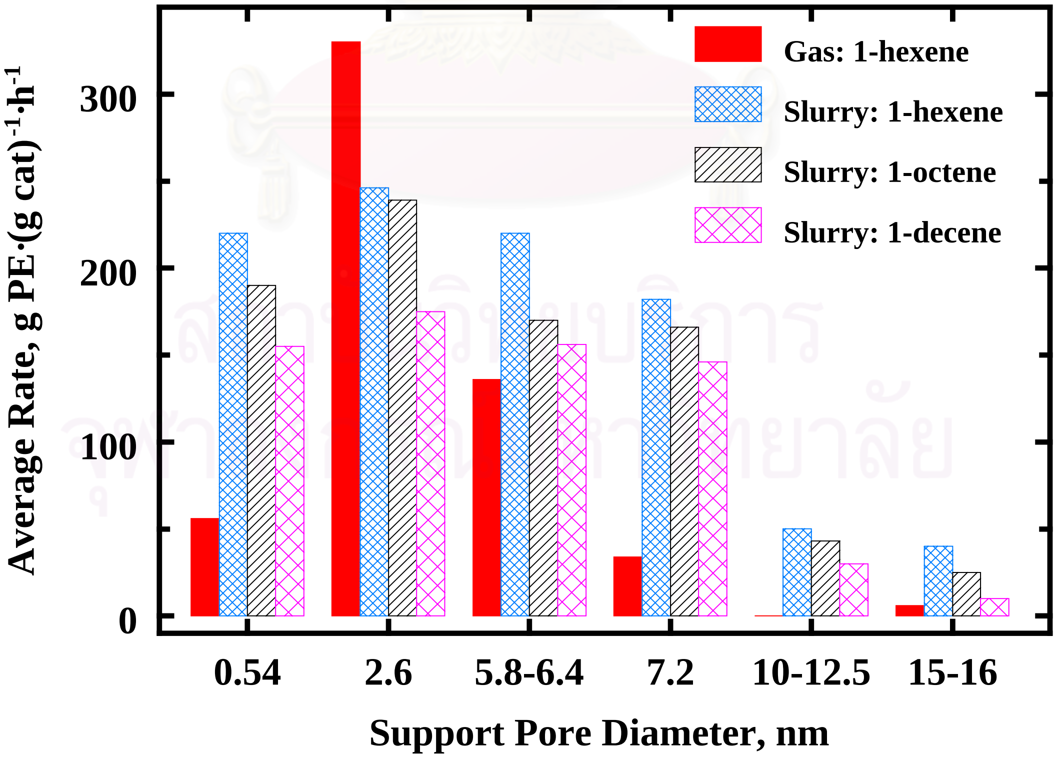

Figure 7.4. Comparison of average rates as a function of support pore diameter for gas and slurry copolymerizations at 70°C

7.2. Comparison of Molar Masses

The effects of support pore size on M_W, M_N, and polydispersities, for ethylene homopolymerization and ethylene/1-hexene copolymerization in the gas phase and slurry phase are shown in Figure 7.5-7.7, respectively. It was observed that the M_W and M_N (see in Figure 7.5 and 7.6) were essentially independent of support pore diameter for gas-phase polymerization, but increased with increasing support pore size for slurry-phase polymerizations. This observation was also found for copolymerizations. The M_W for product made in slurries had lower values than the gas-phase products. The polydispersities were essentially independent of support pore size for gas- and slurry-phase homopolymerization, whereas they increased with increasing the pore size for copolymerization for both gas-phase and slurry modes of operation (see in Figure 7.7)

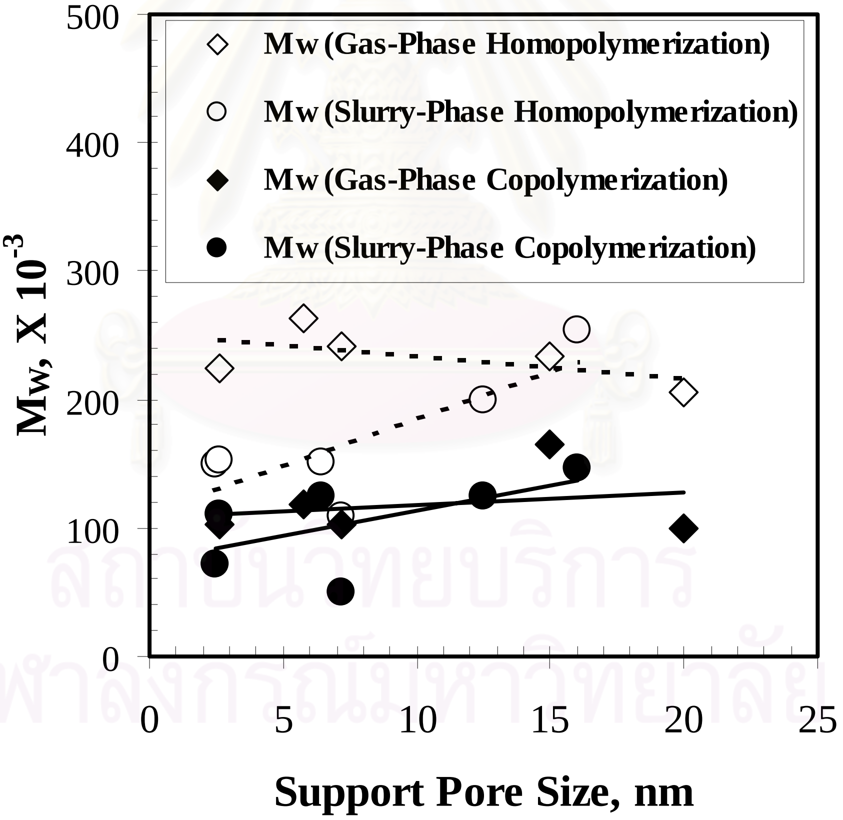

Figure 7.5. Comparison of M_W for gas-phase and slurry-phase polymerization with variations of support pore diameters

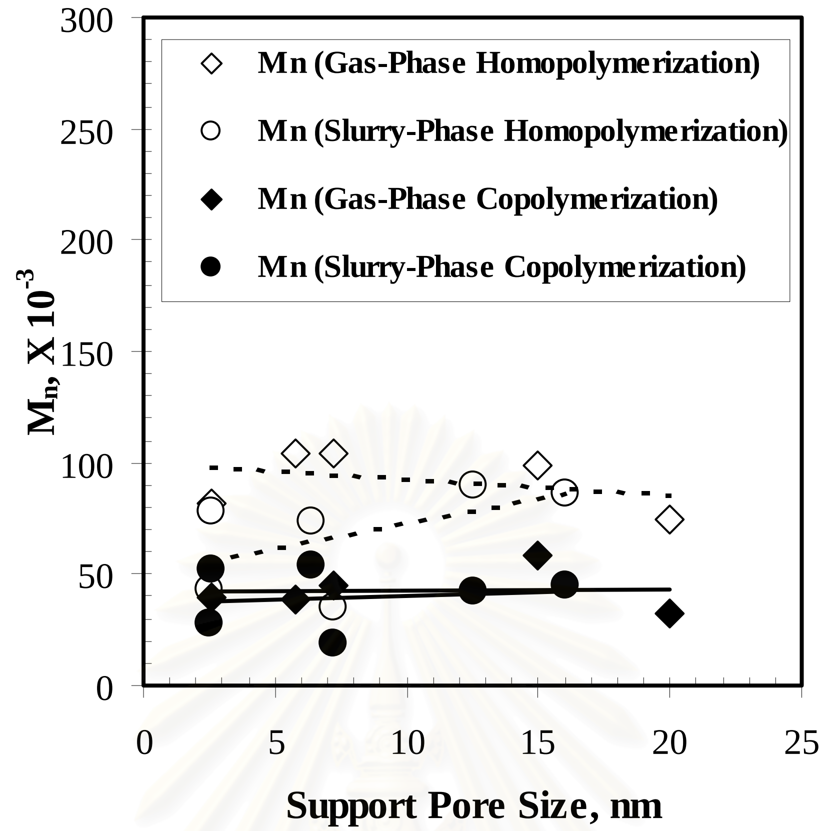

Figure 7.6. Comparison of M_N for gas-phase and slurry-phase polymerization with variations of support pore diameters

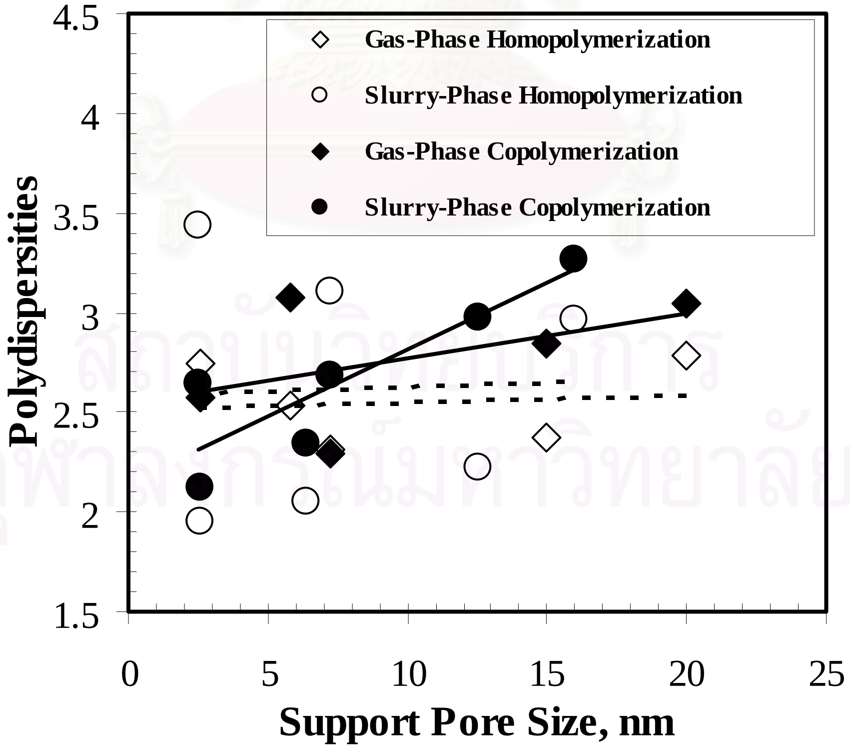

Figure 7.7. Comparison of polydispersities for gas-phase and slurry-phase polymerization with variations of support pore diameters

It seems that the polydispersities for slurry phase were higher than the gas phase; this was probably associated with the leaching of catalyst into the heptane during slurry operation.

7.3. Comparison of Short Chain Branch Concentration

Short chain branching concentrations for gas-phase copolymerization with 1-hexene for MMS-supported catalysts, i.e. not including CAT0.54, increased with increasing support pore size; however, no such trend was observed for slurry copolymerization with 1-hexene (see Figure 7.8). This difference in behavior is not surprising because the concentrations of 1-hexene were much different in the gas and slurry phases; the initial concentration of 1-hexene in the slurry phase was about 30 times as high as the initial concentration in the gas phase.

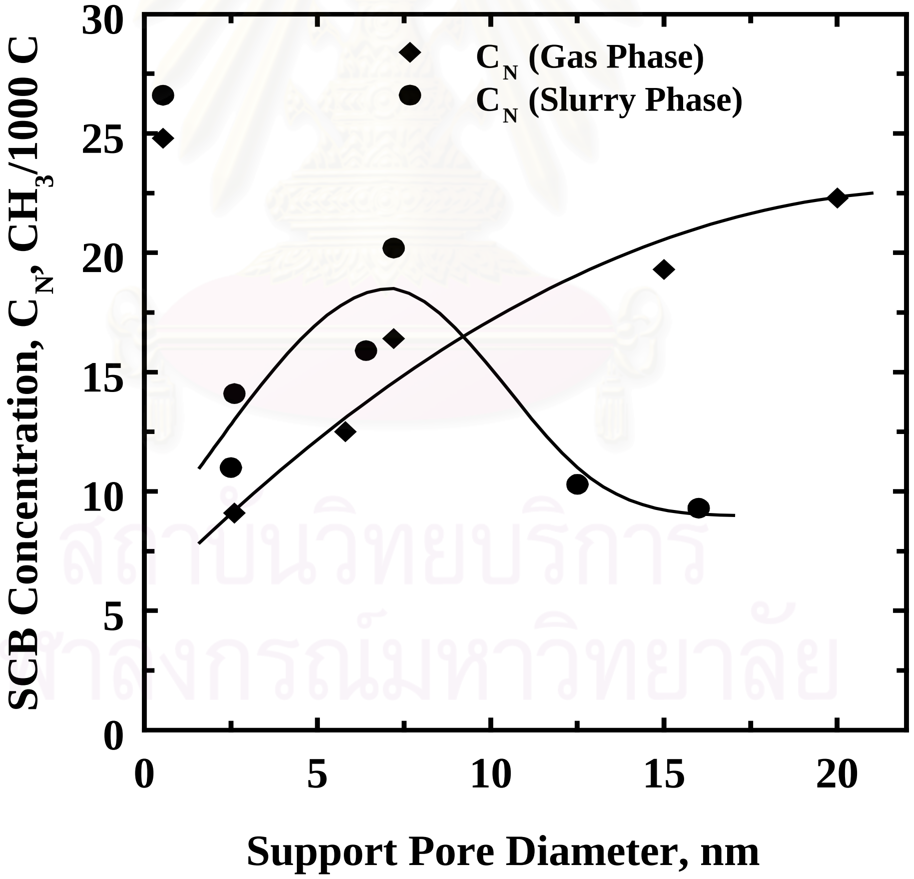

Figure 7.8. Comparison of short chain branches for gas-phase and slurry-phase polymerization of ethylene/1-hexene with variations of support pore diameters

The TREF profiles for many of the products made by both gas-phase and slurry-phase polymerization showed two or more maxima. This indicates great heterogeneity in short chain branching and can only be attributed to the presence of different types of catalytic sites in the supported catalysts.

7.4. Comparison of Differential Scanning Calorimetry

The only comparable DSC results are for 1-hexene copolymers made at 70°C with about 3 mL of 1-hexene added at the beginning of each run. The DSC-based crystallinities for the nascent polymers (Scan 1) and the melt-recrystallized polymers (Scan 2) from gas-phase and slurry-phase polymerizations are plotted as a function of support pore size in Figures 7.9 and 7.10. These results show that there is not a simple relationship between DSC crystallinities and support pore size. However, further analysis revealed certain relationships between crystallinities of gas-phase and slurry-phase products.

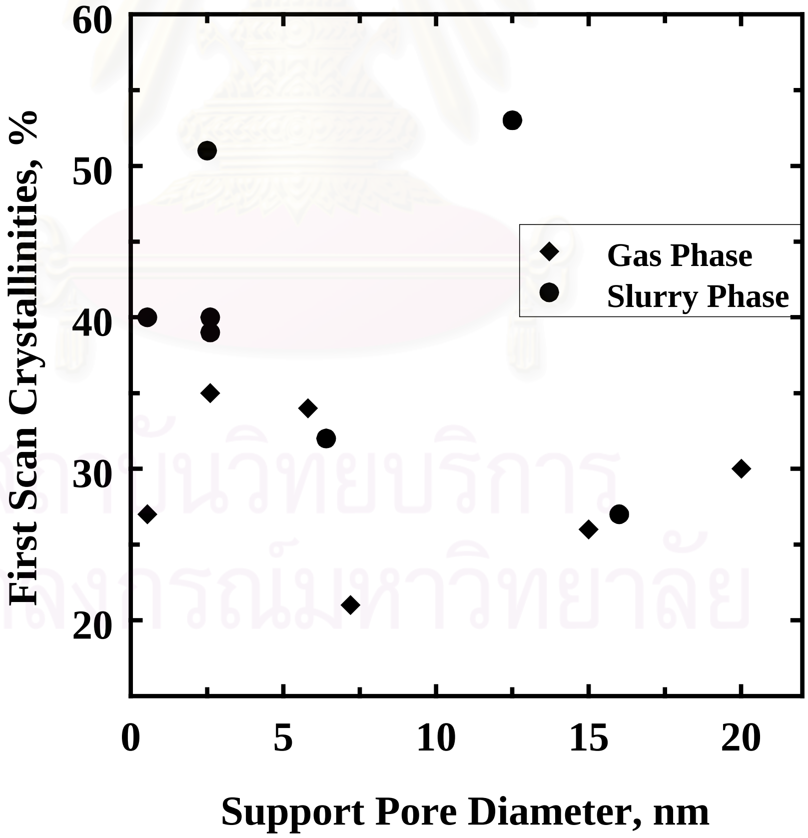

Figure 7.9. Relationship between support pore size and crystallinity of nascent products (Scan 1)

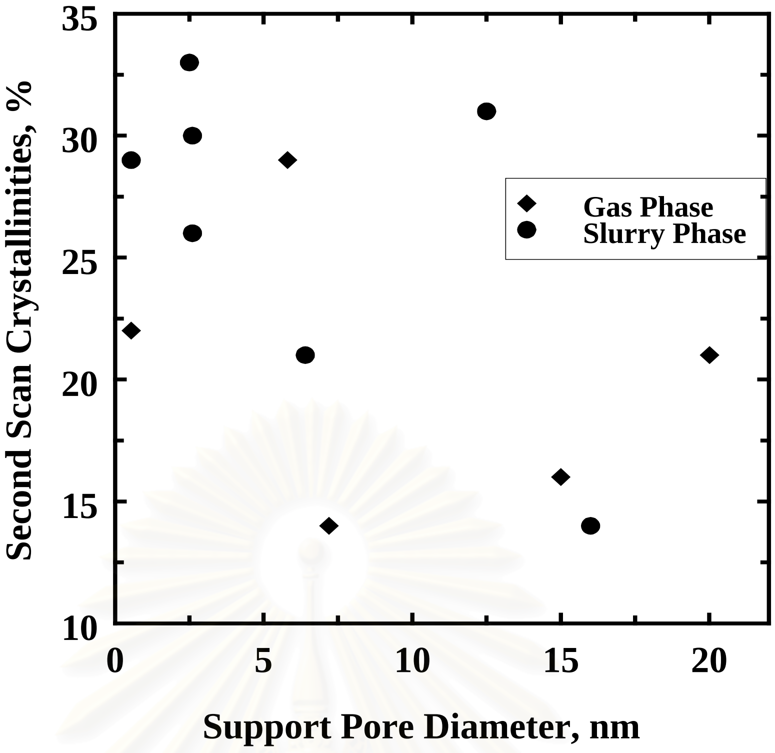

Figure 7.10. Relationship between support pore size and crystallinity of melt-recrystallized products (Scan 2)

The crystallinities for the nascent products (Scan 1) were higher that the second scan crystallinities for all runs but one, and the nascent crystallinities for products from slurry runs were higher that the nascent crystallinities from gas-phase runs; this is shown in Figure 7.11.

It is also useful to compare the normalized changes in crystallinity between first and second scans; the normalized change in crystallinity is defined by Equation 7.1 and are shown in Figure 7.12.

$$\textbf{Normalized Change in Crystallinity} = \frac{[\text{Scan 1} - \text{Scan 2 Crystallinities}]}{\text{Scan 2 Crystallinity}} = \frac{[X_1 - X_2]}{X_2} \qquad \textbf{----(7.1)}$$

Again the changes in crystallinities are more pronounced for the slurry products compared with the gas-phase products; they changes in crystallinities between the first and second scan appear to increase with increasing pore size except for CAT20 (see in Figure 7.12).

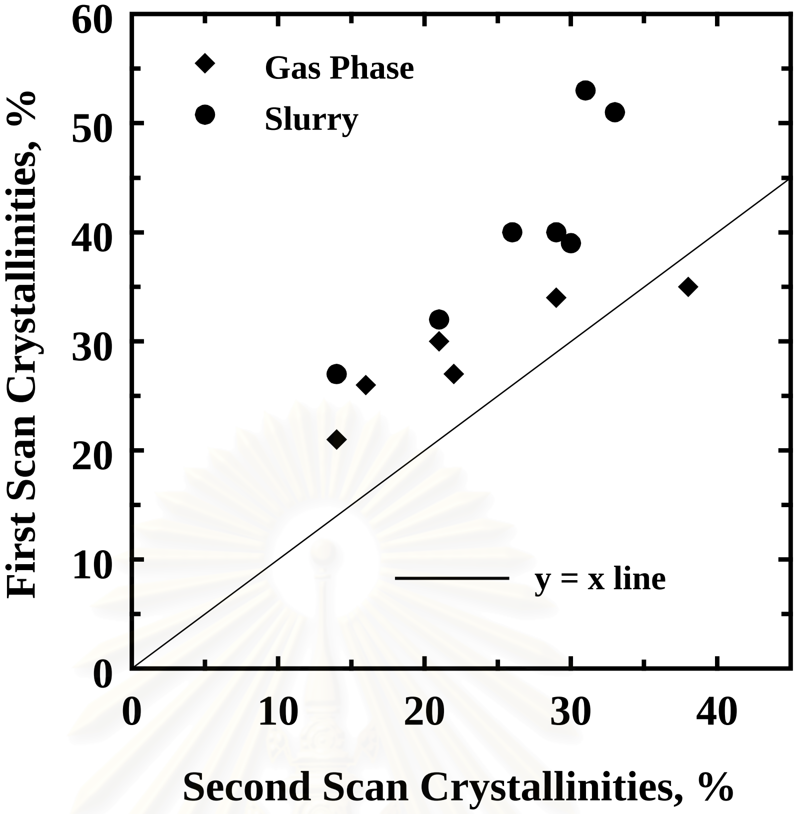

Figure 7.11. Comparison of 1st and 2nd DSC scan crystallinities for ethylene/ 1-hexene copolymers

The shapes of the DSC scans for nascent polymers as well as for some of the melt-recrystallized products has multiple maxima for both gas-phase and slurry polymerizations. This is a strong indication for the presence of multiple of catalytic sites in these catalysts.

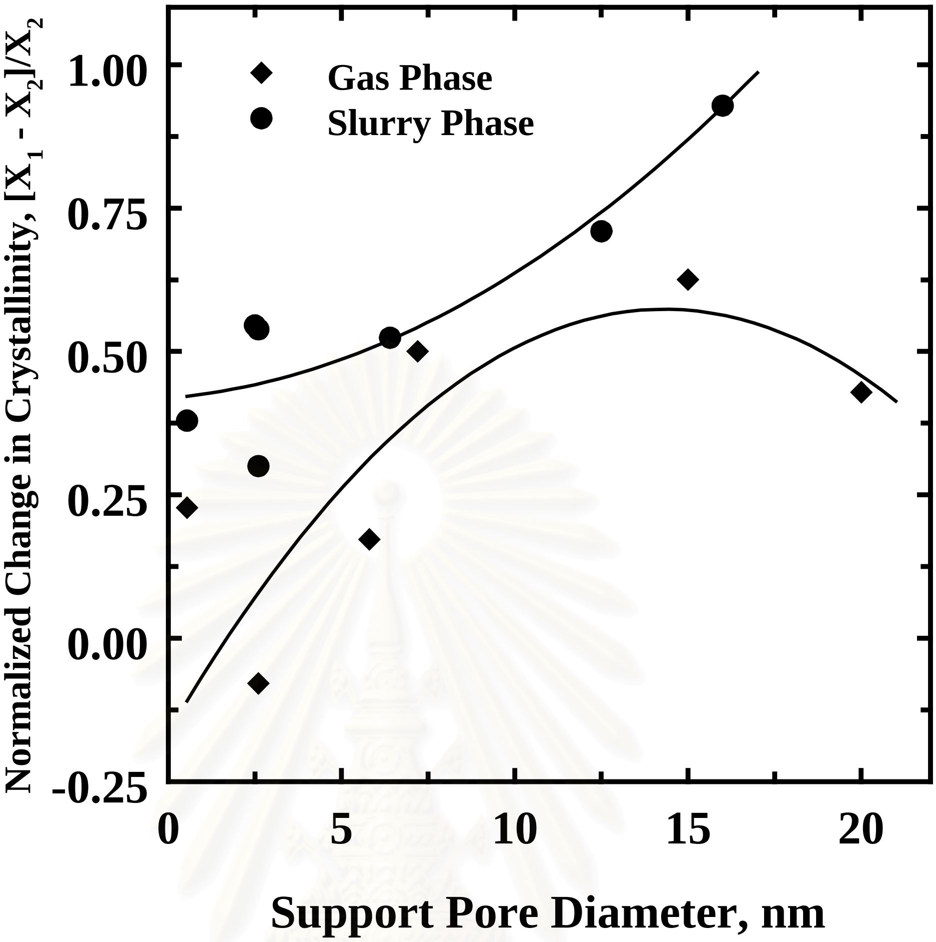

Figure 7.12. Changes in crystallinity between first and second DSC scan.

7.5. Summary

The results for both slurry and gas-phase operation show, without doubt, that the support pore size has a profound influence on the catalytic behavior and polymer product properties for catalysts made by supporting (n-BuCp)$_2$ZrCl$_2$ on MAO-treated mesoporous molecular sieves. For both slurry and gas-phase polymerizations, the maximum activities occurred for catalysts made with mesoporous molecular sieves having pore diameters less than 6 nm. TREF and DSC results clearly showed that the (n-BuCp)$_2$ZrCl$_2$/MAO-MMS catalyst were not single-site catalysts and that the types of sites were a function of the support pore size.

CHAPTER VIII

CONCLUSIONS AND RECOMMENDATIONS

The conclusions of the current work and suggestions for the future studies in the area of the gas-phase and slurry-phase polymerization of ethylene and ethylene/α-olefins and characterization of the resulting polymer are presented in this chapter.

8.1. CONCLUSIONS

8.1.1 Gas Phase Ethylene Polymerization and Copolymerization

The aforementioned results have shown that gas-phase ethylene polymerization activities as well as activity profiles of $(n\text{-BuCp})_2ZrCl_2$ supported on mesoporous molecular sieves were functions of pore size of the mesoporous molecular sieves. The highest activity catalysts were those prepared with supports having pore diameters of 2 to 6 nm. All the gas-phase activity profiles had an initial activation period followed by deactivation, and the deactivation was more temperature sensitive than the activation. Overheating of the catalyst/polymer particles during the initial stages of polymerization could be the cause of the rapid catalyst deactivation. The MMS-supported catalysts were also active for 1-hexene/ethylene copolymerization. Molar masses decreased with increasing polymerization temperature, but the polydispersities were essentially independent of the polymerization temperature; the average value of the polydispersity was 2.5. The molar masses and polydispersities were not functions of the pore size of the MMS support pore size. The activity and activity profiles were very strong functions of the amount of TIBA added; increases in the amounts of TIBA resulted in slower activation and broader activity profiles. The marked effect of TIBA concentration on activity profiles is useful for the optimization of reactor conditions for improved productivity and operating stability.

Gas-phase ethylene polymerization rates as well as 1-hexene incorporation rates over $(n\text{-BuCp})_2ZrCl_2$ supported on MAO-treated mesoporous molecular sieves are a strong function of the pore size of the support. Catalysts with support pore size in the 2 to 6 nm range had the highest ethylene polymerization rates, and catalysts with larger pore size had higher 1-hexene incorporation rates. Ethylene polymerization rates were a strong function of 1-hexene concentration and temperature. For a small-pored catalyst (CAT2.5), the polymerization rate was highest at 80 °C. Low concentration of 1-hexene (4 to 12 mol/m^3) caused significant increases in ethylene polymerization rates compared to ethylene homopolymerization rate. The copolymerization rates were lower than the homopolymerization rate at 1-hexene concentrations above 20 mol/m^3. The variations in rate behavior with support pore size suggest that the pore size of the support affects the type and concentration of active sites.

TREF characterization of the products made with different pore size catalysts and different polymerization conditions confirmed that the mesoporous molecular sieve-supported $(n\text{-BuCp})_2ZrCl_2$ catalysts contained multiple types of catalytic sites and that the type and/or concentration of the various catalytic sites was dependent on the pore size of the support. TREF analysis of products obtained from experiments for different lengths of polymerization showed that the distribution of sites was time dependent; sites with no or low 1-hexene incorporation rates were more prevalent at short polymerization times. DSC results with nascent products confirmed the TREF results. The DSC experiments with the nascent products showed that multi-peaked DSC endotherms were reproducible and were very dependent on catalyst and the polymerization conditions. This suggests that DSC of nascent polymer is a useful method for providing information on heterogeneity of catalytic sites in supported polymerization catalysts. The molar masses were not a strong function of support pore size and the variation of molar masses with 1-hexene concentration and temperature followed the expected trends, i.e. decreases in molar masses with increasing 1-hexene concentration and increasing temperature.

8.1.2. Slurry-Phase Ethylene Polymerization and Copolymerization

The results of a systematic study for slurry-phase ethylene polymerization and copolymerization reported on the effects of operating conditions on the activities of $(n\text{-BuCp})_2ZrCl_2$ supported on silicalite, mesoporous molecular sieves and silica gel. It was found that the polymerization medium, polymerization temperature, and external TIBA and MAO had different effects on the polymerization activities and molar masses. The product particle sizes were strongly dependent on the polymerization medium and amount of external alkyl. The influence of pore diameter of mesoporous molecular sieve supports on average activities were similar to that observed for the gas-phase system. The average polymerization activities were also a strong function of the temperature. These results showed that catalysts made with supports MMS2.5 and MMS2.6 had the maximum average activities; supports with larger pores yielded catalysts with lower activities. Also, for slurry-phase polymerizations the activity profiles were found to broaden with increasing pores size, but the effect was less pronounced than for gas-phase polymerizations. All activity profiles showed a period of activation followed by deactivation, but the rates of activation and deactivation were functions not only of the temperature but also of the support pore diameter. Deactivation rates were more sensitive to temperature than activation rates. The average copolymerization activities for slurry-phase copolymerization of all ethylene/α-olefins, were also dependent on the pore diameter and higher olefins comonomers resulted in the lower activitiy. Molar masses decreased with increasing polymerization temperature, but the molar masses for all of polymerization temperatures were slightly increased with increasing support pore size. The molecular weights of copolymers increased as the support pore diameter increased. The molar masses of homopolymers produced with external MAO were lower than with TIBA; addition of external MAO resulted in copolymer molar masses similar to those of homopolymers. The polydispersities were essentially independent of the polymerization temperature and support pore diameter; the average value of the polydispersity was about 2.5 and 3.5 for homopolymer produced with the use of TIBA and external MAO respectively, while the polydispersities were of 2.7, 2.8, and 2.6 for copolymers of 1-hexene, 1-octene, and 1-decene.

TREF characterization of the products made with different pore sized catalysts for slurry-phase system confirmed that the mesoporous molecular sieve-supported $(n\text{-BuCp})_2\text{ZrCl}_2$ catalysts contained multiple types of catalytic sites. Catalysts with small pore size of support had the high comonomer incorporation rates, this is different than the trend for gas-phase operation. However, rates of ethylene polymerization decreased with increasing support pore size for slurry polymerization as it did for gas-phase polymerization. DSC of polymers provided information on heterogeneity of catalytic sites in supported polymerization catalysts more clearly than TREF results. The types of comonomer strongly affected on the incorporation rate; the higher α-olefins (1-decene>1-octene>1-hexene) resulted in the less incorporation of comonomer.

8.2. RECOMMENDATIONS

- The morphology or shape of support pore size should be investigated to provide more guidance for the development of more active supported metallocene catalysts for homopolymerization and copolymerization because the difference of temperature gradients inside the growing catalyst/polymer particles (initial catalyst particle size) might be associated with the activation rates and deactivation rates.
- Multiple types of catalytic sites were observed for gas-phase and slurry-phase polymerization with metallocene supported mesoporous molecular sieves with different pore sizes; thus, investigations of reaction kinetics of this catalytic system are of great interest with the objective of obtaining information on the catalyst activation and deactivation steps.
- More detailed characterization of molecular structure of LLDPE, by cross-fractionation in terms of molar mass and short chain branching (TREF-SEC cross fractionation) is recommended since this would provide more detailed insight into the propagation and chain transfer reactions for the various catalytic sites.
- TREF and DSC studies indicate the heterogeneous nature of the catalytic sites in the supported $(n\text{-BuCp})_2ZrCl_2$ catalysts. DSC results generally indicated a greater degree of heterogeneity in catalytic sites as a function of pore size than the TREF results. Therefore, additional DSC characterization using thermally fractionated samples as well as TREF-DSC cross-fractionation studies may be useful for obtaining greater detail on the inter- and intramolecular heterogeneities of the LLDPEs.

- A study of the direct synthesis of MAO in different size of pore by controlled hydrolysis of trimethylaluminum as the initial step in the catalyst synthesis may be a means of obtaining new high-activity supported metallocene catalysts for gas-phase and slurry-phase polymerization.

REFERENCES

Abiru, T., Mizuno, A., and Weigand, F. Microstructural Characterization of Polypropylene-Butene-1 Copolymer Using Temperature Rising Elution Fractionation. **Journal of Applied Polymer science** 68 (1998): 1493-1501.

Adisson, E., Ribeiro, M., Deffieux, A., and Fontanille, M. Evaluation of the Heterogeneity in Linear Low-Density Polyethylene Comonomer Unit Distribution by Differential Scanning Calorimetry Characterization of Thermally Treated Sample. **Polymer** 33 (1992): 4337-4342.

Agnillo, L. D., Soares, J. B. P., and Penlidis, A. Round-Robin Experiment in High-Temperature Gel Permeation Chromatography. **Journal of Polymer Science: Part B: Polymer Physics** 40 (2002): 905-921.

Alt, H. G., and Koppl, A. Effect of the Nature of Metallocene Complexes of Group IV Metals on Their Performance in Catalytic Ethylene and Propylene Polymerization. **Chemical Reviews** 100 (2000): 1205-1221.

Alt, H. The Heterogenization of Homogeneous Metallocene Catalysts for Olefin Polymerization. **Journal of The Chemical Society; Dalton Transactions** (1999): 1703-1709.

Arai, T., Ban, H. T., Uozumi, T., and Soga, K. Synthesis of Polysiloxane-Supported Zirconocene Catalysts and Application to Ethene Polymerization. **Macromolecular Chemistry and Physics** 198 (1997): 229-237.

Babushkin, D. E., Semikolenova, N. V., Panchenko, V. N., Sobolev, A. P., Zakharov, V. A., and Talsi, E. P. Multinuclear NMR Investigation of Methylaluminoxane. **Macromolecular Chemistry and Physics** 198 (1997): 3845-3854.

Bajgur, C. S., and Sivaram, S. The Evolution of New Generation “Single-Site” Ziegler-Natta Polymerization Catalysts. **Current Science** 78 (11) (2000): 1325-1335.

Barron, A. R., Mason, M. R., Smith, J. M., and Bott, S.G. Hydrolysis of Tri-tert-butylaluminum: The First Structural Characterization of Alkylalumoxanes $[(R_2Al)_2O]_n$ and $(RAlO)_n$. **Journal of the American Chemical Society** 115 (1993): 4971-4984.

Bett, K. E., Crossland, R., Ford, H., and Gardner, A. K. Polyethylene 1933-83. **Proceedings of the Golden Jubilee Conference, The Plastics and Rubber Institute, London** (1983): B1.1 – B1.31.

Bianchini, D., Bichinho, K. M., and Santos, J. H. Z. D. Polyethylenes Produced with Zirconocene Immobilized on MAO-Modified Silicas. **Polymer** 43 (2002): 2937-2943.

Bonner, J. G., Frye, C. J., and Capaccio, G. A Novel Calibration for the Characterization of Polyethylene Copolymers by Temperature Rising Elution Fractionation. **Polymer** 34 (1993): 3532-3534.

Borrajo, J., Cordon, C., Carella, J. M., Toso, S., and Goizueta, G. Modelling the Fractionation Process in TREF System: Thermodynamic Simple Approach. **Journal of Polymer Science: Part B: Polymer Physics** 33 (1995): 1627-1632.

Brandao, S. T., Correa, M. L., Boaventura, J. S., and Vianna, S. C. Supported Cp_2ZrCl_2 as Catalyst for Ethylene Polymerization. **Studies in Surface Science and Catalysis** 130 (2000): 3849-3854.

Brintzinger, H. H., Fischer, D., Mulhaupt, R., Rieger, B., and Waymouth, R. M. Stereospecific Olefin Polymerization with Chiral Metallocene Catalysts. **Angewandte Chemie International Edition in English** 34 (1995): 1143-1170.

Britovsek, G. J. P., Gibson, V. C., and Wass, D. F. The Search for New-Generation Olefin Polymerization Catalysts: Life Beyond Metallocenes. **Angewandte Chemie International Edition in English** 38 (1999): 429-447.

Britto, M. L., Galland, G. B., Santos, J. H. Z. D., and Forte, M. C. Copolymerization of Ethylene and 1-Hexene with $Et(Ind)_2ZrCl_2$ in Hexane. **Polymer** 42 (2001): 6355-6361.

Bryant, P. L., Harwell, C. R., Mrse, A. A., Emery, E. F., Gan, Z., Caldwell, T., Reyes, A. P., Kuhns, P., Hoyt, D. W., Simeral, L. S., Hall, R. W., and Butler, L. G. Structural Characterization of MAO and Related Aluminum Complexes. 1. Solid-State 27Al NMR with Comparison to EFG Tensors from ab Initio Molecular Orbital Calculations. **Journal of the American Chemical Society** 123 (2001): 12009-12017.

Buckalew, L., Schumacher, J.W. Chemical Economics Handbook-SRI International.

Plastics and Resins August (2000): 580.1321.

Cam, D., and Giannini, U. Concerning the Reaction of Zirconocene Dichloride and Methylaluminoxane-Homogeneous Ziegler-Natta Catalytic-System for Olefin Polymerization. **Makromolekulare Chemie-Macromolecular Chemistry and Physics** 193 (5) (1992): 1049-1055.

Cam, D., Sartori, F., and Maldotti, A. Reduction of Bis(eta-5-cyclopentadienyl) Zirconium Dichloride in the Presence of Methylalumoxane. **Macromolecular Chemistry and Physics** 195 (8) (1994):2817-2826.

Cerrada, M. L., Benavente, R., and Perez, E. Influence of Thermal History on Morphology and Viscoelastic Behavior of Ethylene-1-Octene Copolymers Synthesized with Metallocene Catalysts. **Journal of Materials Research** 16 (2001): 1103-1111.

Chakravarti, S., and Ray, H. Kinetic Study of Olefin Polymerization with a Supported Metallocene Catalyst. II. Ethylene/1-Hexene Copolymerization in Gas Phase. **Journal of Applied Polymer Science** 80 (2001a): 1096-1119.

Chakravarti, S., Ray, H., and Zhang, S. X. Kinetic Study of Olefin Polymerization with a Supported Metallocene Catalyst. IV. Comparison of Bridged and Unbridged in Gas Phase. **Journal of Applied Polymer Science** 81 (2001b): 1451-1459.

Chemcial Industries Newsletter SRI Consulting Issue 3 (2000): 1-4.

Chen, E. Y. X., and Marks, T. J. Cocatalysts for Metal-Catalyzed Olefin Polymerization: Activators, Activation Processes, and Structure-Activity Relationships. **Chemical Reviews** 100 (2000): 1391-1434.

Chien, J. C. W. Supported Metallocene Polymerization Catalysis. **Topics in Catalysis** 7 (1999): 23-36.

Chien, J. C. W., and Hsieh, J. T. T. Supported Catalysts for Sterospecific Polymerization of Propylene. **Journal of Polymer Science: Part A: Polymer Chemistry** 14 (8) (1976): 1915-1932.

Choi, K. Y., and Ray, W. H. Polymerization of Olefins Through Heterogeneous Catalysts II. Kinetics of Gas Phase Propylene Polymerization with Ziegler-Natta Catalysts. **Journal of Applied Polymer Science** 30 (3) (1985b): 1065-1081.

Choi, K. Y., and Ray, W. H. Recent Developments in Transition Metal Catalyzed Olefin Polymerization-A Survey I. Ethylene Polymerization. **Journal of Molecular Science–Reviews in Macromolecular Chemistry and Physics** C25 (1) (1985a): 1-55.

Chu, K. J., Shan, C. L. P., Soares, J. B. P., and Penlidis, A. Copolymerization of Ethylene and 1-Hexene with In-Situ Supported Et[Ind]$_2$ZrCl$_2$. **Macromolecular Chemistry and Physics** 200 (1999): 2372-2376.

Chu, K. J., Soares, J. B. P., and Penlidis, A. Polymerization Mechanism for In Situ Supported Metallocene Catalysts. **Journal of Polymer Science: Part A: Polymer Chemistry** 38 (2000): 462-468.

Chung, J. S., Tairova, G., Zhang, Y., Hsu, J. C., McAuley, K. B., and Bacon, D. W. Polymer-Supported Metallocene Catalysts for Gas-Phase Ethylene Polymerization. **Korean Journal of Chemical Engineering** 19 (4) (2002): 597-600.

Ciardelli, F., Altomare, A., and Michelotti, M. From Homogeneous to Supported Metallocene Catalysts. **Catalysis Today** 41 (1998): 149-157.

Coates, G. W. Precise Control of Polyolefin Stereochemistry Using Single-Site Metal Catalysts. **Chemical Reviews** 100 (2000): 1223-1252.

Custonguay, L. A., and Rappe, A. K. Ziegler-Natta Catalysis-A Theoretical-Study of the Isotactic Polymerization of Propylene. **Journal of the American Chemical Society** 114 (14) (1992): 5832-5842.

Dusseault, J. J. A., and Hsu, C. C. MgCl$_2$ Supported Ziegler-Natta Catalysts for Olefin Polymerization: Basic Structure, Mechanism, and Kinetic Behavior. **Journal of Molecular Science–Reviews in Macromolecular Chemistry and Physics** C33 (2) (1993): 103-145.

Eberhardt, A. M., Ferreira, M. L., and Damiani, D. E. Heterogeneization of Polymerization Catalysts. **Polymer Engineering and Science** 41 (6) (2001): 946-954.

Echevskaya, L. G., Zakharov, V. A., Semikolenova, N. V., Mikenas, T. B., and Sobolev, A. P. Polymerization of Ethylene Using Supported Zirconocene Catalysts. **Polymer Science Series A** 43 (3) (2001): 220-227.

Elicabe, G., Cordon, C., Carella, J. Modeling the Fractionation Process in TREF System. III. Model Validation with Low Molar Mass and Homopolymers. **Journal of Polymer Science: Part B: Polymer Physics** 34 (1996): 1147-1154.

Estrada J. M. V., and Hamielec A. E. Modeling of Ethylene Polymerization with Cp_2ZrCl_2/MAO Catalyst. **Polymer** 35 (1994): 808-818.

Feng, Y., and Jin, X. Effect of Self-Nucleation on Crystallization and Melting Behavior of Polypropylene and Its Copolymers. **Journal of Applied Polymer science** 72 (1999): 1559-1564.

Ferreira, M. L., and Damiani, D. E. Catalysts Based on Supported Metallocenes for α-Olefin Polymerization. **Macromolecular Chemistry and Physics** 202 (2001): 694-700.

Ferreira, M. L., Belelli, P. G., Juan, A., and Damiani, D. E. Theoretical and Experimental Study of the Interaction of Methylaluminoxane (MAO)-Low Temperature Treated Silica: Role of Trimethylaluminium (TMA). **Macromolecular Chemistry and Physics** 201 (2000): 1334-1344.

Fillon, B., Wittmann, J. C., Lotz, B., and Thierry, A. Self-Nucleation and Recrystallization of Isotactic Polypropylene (α Phase) Investigated by Differential Scanning Calorimetry. **Journal of Polymer Science: Part B: Polymer Physics** 31 (1993): 1383-1393.

Fink, G., Steinmetz, B., Zechlin, J., Przybyla, C., and Tesche, B. Propene Polymerization with Silica-Supported Metallocene/MAO Catalysts. **Chemical Reviews** 100 (2000): 1377-1390.

Fischer, D., Jungling, S., and Mulhaupt, R. Donor-Modified and Acceptor-Modified Metallocene-Base Homogeneous Ziegler-Natta Catalysts. **Makromolekulare Chemie-Macromolecular Symposia** 66 (1993): 191-202.

Fischer, E.O. **Angewandte Chemie** 22 (1952): 620.

Flanigen, E. M., Bennet, J. M., Grose, R. W., Cohen, J. P., Patton, R.L., and Smith, J. V. Silicalite, A New Hydrophobic Crystalline Silica Molecular Sieve. **Nature** 271 (1978): 512-516.

Foxley, D. Inovation in the Gas Phase. **Chemistry & Industry** 8 (1998): 305-308.

Francuskiewicz, F. <u>Temperature Rising Elution Fractionation</u> Springer-Verlag, Berlin

Heidelberg (1994).

Frauenrath, H., Keul, H., and Hocker, H. Deviation from Single-Site Behavior in Zirconocene/MAO Catalyst Systems, I Influence of Monomer, Catalyst, and Cocatalyst Concentration. **Macromolecular Chemistry and Physics** 202 (2001): 3543-3550.

Galland, G. B., Seferin, M., Mauler, R. S., and Dos Santos, J. H. Z. Linear Low-Density Polyethylene Synthesis Promoted by Homogeneous and Supported Catalysts. **Polymer International** 48 (1999): 660-664.

Galli, P. The Reactor Granule Technology: A Revolutionary Approach to Polymer Blends and Alloys. **Macromolecular Symposia** 78 (1994): 269-284.

Giannetti, E., Nicolett, G. M., and Mazzocchi, R. Homogeneous Ziegler-Natta Catalysis. II. Ethylene Polymerization by IVB Transition Metal Complexes/Methyl-aluminoxane Catalyst Systems. **Journal of Polymer Science: Polymer Chemistry Edition** 23 (1985): 2117-2133.

Glockner, G. Temperature Rising Elution Fractionation: A Review. **Journal of Applied Polymer Science, Applied Polymer Symposium** 45 (1990): 1-24.

Goretzki, R., Fink, G., Tesche, B., Steinmetz, B., Rieger, R., and Uzick, W. Unusual Ethylene Polymerization Results with Metallocene Catalysts Supported on Silica. **Journal of Polymer Science: Part A: Polymer Chemistry** 37 (1999): 677-682.

Graefe, J., Gurtzgen, S., Muller, K. H., Schneider, J., and Schrader, R. (Witco GmbH) **U.S. Patent** 5,427,992 (1995).

Gupta, V. K., Satish, S., and Bhardwaj, I. S. Metallocene Complexes of Group 4 Elements in the Polymerization of Monoolefins. **Journal of Molecular Science–Reviews in Macromolecular Chemistry and Physics** C34 (3) (1994): 439-514.

Ha, K. S., Yoo, K. Y., and Rhee, H. K. Modeling and Analysis of a Slurry Reactor System for Heterogeneous Olefin Polymerization: The Effects of Hydrogen Concentration and Initial Catalyst Size. **Journal of Applied Polymer Science** 79 (2001): 2480-2493.

Haag, M. C., Krug, C., Dupont, J., Galland, G. B., Dos Santos, J. H. Z., Uozumi, T., Sano, T., and Soga, K. Effects of Al/Zr Ratio on Ethylene-Propylene Copolymerization with Supported-Zirconocene Catalysts. **Journal of Molecular**

Catalysis A: Chemical 169 (2001): 275-287.

Hamielec, A. E., and Shouli, T. Metallocene Catalysts-Applications in the Manufacture of Polyethylenes and High-Impact Polypropylenes in Gas-Phase Polymerization Processes. **Macromolecular Symposium** 152 (2000): 9-14.

Hamielec, A.E., and Soares, J.B.P. Polymerization Reaction Engineering Metallocene Catalysts. **Progress in Polymer Science** 21 (1996): 651-706.

Harlan, C. J., Mason, M. R. and Barron, A. R. Tert-Butylaluminum Hydroxides and Oxides-Structural Relationship Between Alkylaluminoxanes and Alumina Gels. **Organometallics** 13 (8) (1994): 2957-2969.

Harrison, D., Coulter, I. M., Wang, S., Nistala, S., Kuntz, B. A., Pigeon, M., Tian, J., and Collins, S. Olefin Polymerization Using Supported Metallocene Catalysts: Development of High Activity Catalysts for Use in Slurry and Gas Phase Ethylene Polymerizations. **Journal of Molecular Catalysis A: Chemical** 128 (1998): 65-77.

Hlatky, G. G. Heterogeneous Single-Site Catalysts for Olefin Polymerization. **Chemical Reviews** 100 (2000): 1347-1376.

Hlatky, G. G. Metallocene Catalysts for Olefin Polymerization Annual Review For 1996. **Coordination Chemistry Reviews** 181 (1999): 243-296.

Hong, S. C., Ban, H. T., Kishi, N., Jin, J., Uozumi, T., and Soga, K. Ethene Polymerization with a Poly(styrene-co-divinylbenzene) Beads Supported rac-$Ph_2Si(Ind)_2ZrCl_2$ Catalyst. **Macromolecular Chemistry and Physics** 199 (1998): 1393-1397.

Huang, J. C. K., Lacombe, Y., Lynch, D. T., and Wanke, S. E. Effect of Hydrogen and 1-Butene Concentrations on the Molecular Properties of Polyethylene Produced by Catalytic Gas-Phase Polymerization. **Industrial & Engineering Chemistry Research** 36 (4) (1997): 1136-1143.

Huang, Y. H., Yu, Q., Zhu, S., Remple, G. L., and Li, L. ESR Studies on Oxidation State of Titanocene and Zirconocene Catalysts. **Journal of Polymer Science: Part A: Polymer Chemistry** 37 (1999): 1465-1472.

Imanishi, Y., and Naga, N. Recent Delvelopments in Olefin Polymerizations with Transition Metal Catalysts. **Progress in Polymer Science** 26 (2001): 1147-1198.

Imhoff, D. W., Simeral, L. S., Sangokoya, S. S., and Peel, J. H. Characterization of Methylaluminoxanes and Determination of Trimethylaluminum Using Proton NMR. **Organometallics** 17 (1998): 1941-1945.

Ioku, A., Hasan, T., Shiono, T., and Ikeda, T. Effect of Cocatalysts on Propene Polymerization with [t-BuNSiMe$_2$(C$_5$Me$_4$)]TiMe$_2$. **Macromolecular Chemistry and Physics** 203 (2002): 748-755.

Jaber, I. A., and Ray, H. Polymerization of Olefins through Heterogeneous Catalysis. XIV. The Influence of Temperature in the Solution Copolymerization of Ethylene. **Journal of Applied Polymer Science** 50 (1993a): 201-215.

Jaber, I. A., and Ray, H. Polymerization of Olefins Through Heterogeneous Catalysis. XV. The Influence of Pressure in the Solution Copolymerization of Ethylene. **Journal of Applied Polymer Science** 50 (1993b): 217-231.

Jaber, I. A., and Ray, H. Polymerization of Olefins Through Heterogeneous Catalysis. XII. The Influence of Hydrogen in the Solution Copolymerization of Ethylene. **Journal of Applied Polymer Science** 49 (1993c): 1695-1707.

Jaber, I. A., and Ray, H. Polymerization of Olefins through Heterogeneous Catalysis. XIII. The Influence of Comonomer in the Solution Copolymerization of Ethylene. **Journal of Applied Polymer Science** 49 (1993d): 1709-1724.

Janiak, C., and Rieger, B. Silica Gel Supported Zirconocene Dichloride/ Methylaluminoxane Catalysts for Ethylene Polymerization: Effect of Heterogenation on Activity, Polymer Microstructure and Product Morphology. **Angewandte Makromolekulare Chemie** 215 (1994): 47-57.

Jejelowo, M.O., Lynch, D.T., and Wanke, S.E. Comparison of Ethylene Polymerization in Gas-Phase and Slurry Reactors. **Macromolecules** 24 (1991): 1755-1761.

Jenny, C., and Maddox, P. Supported Polyolefin Catalysts **Current Opinion in Solid State & Materials Science** 3 (1998): 94-103.

Johnson, L.K., Killian, C.M., and Brookhart, M. New Pd (II)-Based and Ni (II)-Based Catalysts for Polymerization of Ethylene and Alpha-Olefins. **Journal of the American Chemical Society** 117 (1995): 6414-6415.

Johnson, L.K., Mecking, S., and Brookhart, M. Copolymerization of Ethylene and Propylene with Functionalized Vinyl Monomers by Pd (II) Catalysts. **Journal of**

the American Chemical Society 118 (1996): 267-268.

Junior, P. A. D. C., Nele, M., and Coutinho, F. M. B. Study on Ethylene Polymerization by Homogeneous Cp_2ZrCl_2/Methylaluminoxane Catalyst System. **European Polymer Journal** 38 (2002): 1471-1476.

Kageyama, K., Tamazawa, J., and Aida, T. Extrusion Polymerization: Catalyzed Synthesis of Crystalline Linear Polyethylene Nanofibers within A Mesoporous Silica. **Science** 285 (24 September) (1999): 2113-2115.

Kakugo, M., Miyatake, T., Mizunuma, K., and Kawai, Y. Characteristics of Ethylene-Propylene and Propylene-1-Butene Copolymerization Over $TiCl_3.{}^1/_3AlCl_3$-$Al(C_2H_5)_2Cl$. **Macromolecules** 21 (1988): 2309-2313.

Kallio, K., Wartmann, A., and Reichert, K. H. Effect of Light on the Activity of Metallocene Catalysts in the Gas-Phase Polymerization of Ethylene. **Macromolecular Rapid Communication** 22 (2001): 1330-1334.

Kamfjord, T., Wester, T. S., and Rytter, E. Supported Metallocene Catalysts Prepared by Impregnation of MAO Modified Silica by a Metallocene/Monomer Solution. **Macromolecular Rapid Communication** 19 (1998): 505-509.

Kaminsky, W. Metalorganic Catalysts for Synthesis and Polymerization. Springer (1999).

Kaminsky, W. New Polymers by Metallocene Catalysis. **Macromolecular Chemistry and Physics** 197 (1996): 3907-3945.

Kaminsky, W., and Laban, A. Metallocene Catalysts. **Applied Catalysis A: General** 222 (2001): 47-61.

Kaminsky, W., and Renner, F. High Melting Polypropenes by Silica-Supported Zirconocene Catalysts. **Macromolecular Rapid Communication** 14 (1993): 239-243.

Kaminsky, W., and Strubel, C. Gas-Phase Polymerization of 1,3-Butadiene with Supported Half-Sandwich-Titanium-Complexes. **Macromolecular Chemistry and Physics** 201 (2000): 2519-2531.

Kaminsky, W., Strubel, C., Lechert, H., Genske, D., and Woo, S. I. Syndiotactic Polypropene with MCM-41 Supported Metallocene $[Me_2C(Cp)(Flu)]ZrCl_2$. **Macromolecular Rapid Communication** 21 (2000): 909-912.

Karbashewski, E., Kale, L., Rudin, A., Tchir, W. J., Cook, D. G., and Pronovost, J. O.

Characterization of Linear Low Density Polyethylene by Temperature Rising Elution Fractionation and by Differential Scanning Calorimetry. **Journal of Applied Polymer Science** 44 (3) (1992): 425-434.

Karbashewski, E., Rudin, A., Kale, L., Tchir, W. J., and Cook, D. G. A Note on the Effect of Comonomer Sequence Distribution on TREF Branching Distribution. **Polymer Engineering and Science** 33 (20) (1993): 1370-1371.

Karol, F. J. The Polyethylene Revolution. **Chemtech** 13 (4) (1983): 222-228.

Keating, M. Y., and McCord, E. F. Evaluation of the Comonomer Distribution in Ethylene Copolymers Using DSC Fractionation. **Thermochimica Acta** 243 (2) (1994): 129-145.

Keating, M., Lee, I. H., and Wong, C. S. Thermal Fractionation of Ethylene Polymers in Packaging Application. **Thermochimica Acta** 284 (1996): 47-56.

Kelusky, E. C., Elston, C. T., and Murray, R. E. Characterizing Polyethylene-Based Blends with Temperature Rising Fractionation (TREF) Techniques. **Polymer Engineering and Science** 27 (20) (1987): 1562-1571.

Kim, J. D., and Soares, J. B. P. Copolymerization of Ethylene and 1-Hexene with Supported Metallocene Catalysts: Effect of Support Treatment. **Macromolecular Rapid Communication** 20 (1999): 447-350.

Kim, J. D., and Soares, J. B. P. Copolymerization of Ethylene and 1-Hexene with Supported Metallocene Catalysts: Effect of Support Treatment. **Macromolecular Rapid Communication** 20 (1999): 347-350.

Kissin, Y. V. <u>Isospecific Polymerization of Olefins.</u> Springer-Verge, New York (1985).

Ko, Y. S., and Woo, S. I. Copolymerization of Ethylene and α-Olefin Using $Et(Ind)_2ZrCl_2$ Entrapped inside the Regular and Small Pores of MCM-41. **Macromolecular Chemistry and Physics** 202 (2001): 739-744.

Ko, Y. S., Han, T. K., Park, J. W., and Woo, S. I. Propene Polymerization Catalyzed over MCM-41 and VPI-5-Supported $Et(Ind)_2ZrCl_2$ Catalysts. **Macromolecular Rapid Communication** 17 (1996): 749-758.

Kong, Y., and Hay, J. N. The Measurement of the Crystallinity of Polymers by DSC **Polymer** 43 (2002): 3873-3878.

Koppl, A., Alt, H. G., and Schmidt, R. Poly(organosiloxane) Microgels as Supports for

Heterogeneous Methylalumoxane Cocatalysts. **Journal of Organometallic Chemistry** 577 (2) (1999): 351-357.

Kristen M. O. Supported Metallocene Catalysts with MAO and Boron Activators. **Topics in Catalysis** 7 (1999): 89-95.

Lacombe, Y. TREF and SEC Characterization of Ethylene/1-Butene Copolymers Produced at Various 1-Butene and Hydrogen Pressures, **M.Sc. Thesis**, University of Alberta, Edmonton, Canada, (1997).

Lee, D. H., and Shin, S. Y. Ethylene Polymerization with Metallocene and Trimethylaluminum-Treated Silica. **Macromolecular Symposia** 97 (1995): 195-203.

Lee, D. H., and Yoon, K. B. Ethylene Polymerization Initiated with the Cp_2ZrCl_2-methylaluminoxane Catalyst System Supported on α-Cyclodextrin. **Macromolecular Rapid Communication** 15 (1994): 841-843.

Lee, D. H., and Yoon, K. B. Polymerization of Ethylene by Using Zirconocene Catalyst Anchored on Silica with Trisiloxane and Pentamethylene Spacers. **Macromolecular Rapid Communication** 18 (1997): 427-431.

Lehmus, P., Härkki, O., Leino, R., Luttikhedde, H. J.G., Näsman, J. H., and Seppälä, J. V. Copolmerization of Ethylene with 1-Hexene or 1-Hexadecene Over Ethylene, Dimethylsilylene and 1,4-Butanediylsilylene Bridged Bis(indenyl) and Bis(tetrahydroindenyl) Zirconium Dichlorides. **Macromolecular Chemistry Physics** 199 (1998):1965-1972.

Lehtinen, C., Starck, P., and Lofgren, B. Co- and Terpolymerizations of Ethene and α-Olefins with Metallocenes. **Journal of Polymer Science, Part A: Polymer Chemistry** 35 (1997): 307-318.

Licht, E. H., and Alt, H. G. Metallacyclic Zirconocene Complexes as Catalysts for Homogeneous and Heterogeneous Ethylene Polymerization. **Journal of Molecular Catalysis A: Chemical** 154 (1-2) (2000): 65-72.

Lin, C. H. Control of Polymer Particle Size by Supported Metallocene Catalysts. **Catalysis Letters** 68 (2000): 63-65.

Liu, J., and Rytter, E. Bimodal Polyethylenes Obtained with a Dual-Site Metallocene Catalyst System. Effect of Trimethylaluminium Addition. **Macromolecular**

Rapid Communication 22 (2001): 952-956.

Liu, S., Meng, F., Yu, G., and Huang, B. Preparation of Polymer-Supported Zirconocene Catalysts and Olefin Polymerization. **Journal of Applied Polymer Science** 71 (1999): 2253-2258.

Long, N. J. Metallocenes: An introduction to sandwich complexes. London, Blackwell Science Ltd., (1998)

Loos, J., Arndt-Roseau, M., Weingarten, U., Kaminsky, W., and Lemstra, P. J. Melting Behavior of Nascent Polyolefins Synthesized at Various Polymerization Conditions. **Polymer Bulletin** 48 (2002): 191-198.

Luan, Z., Maes, E. M., van der Heide, P. A. W., Zhao, D., Czernuszewicz, R. S., and Kevan, L. Incorporation of Titanium into Mesoporous Silica Molecular Sieve SBA-15. **Chemistry of materials** 11 (1999): 3680-3686.

Lynch, D. T., and Wanke, S. E., Reactor Design and Operation for Gas-Phase Ethylene Polymerization Using Ziegler-Natta Catalysts, **The Canadian Journal of Chemical Engineering** 69 (1991): 332-339.

Mabison, G., and Spitz, R. Ethylene and Propylene Copolymerization Using Chromium Oxide Catalyst. **European Polymer Journal** 21 (3) (1985): 245-249.

Marques, M. D. F. V., and Conte, A. The Influence of the Preparating Conditions of SiO_2 Supported Cp_2ZrCl_2 Catalyst on Ethylene Polymerization. **Journal of Applied Polymer Science** 86 (2002): 2054-2061.

Marques, M. D. F. V., Henriques, C. A., Monteiro, J. L. F., Menezes, S. M. C., and Coutinho, F. M. B. Bis(cyclopentadienyl)Zirconium Dichloride Supported on Zeolite for Ethylene Polymerization. **Macromolecular Chemistry and Physics** 198 (1997): 3709-3717.

Maschico, G., Bruni, C., Tullio, L. D., and Ciardelli, F. Analysis of the Molecular Weight Distribution (MWD) in Polymerization Processes: Contribution of Different Families of Active Sites to the MWD of Polyethylene Prepared Using Supported Transition Metal Catalysts. **Macromolecular Chemistry and Physics** 199 (1998): 415-421.

Mathot, V. B. F. The Crystallization and Melting Region in Calorimetry and Thermal Analysis of Polymers. Edited by Vincent B. F. Mathot, Hanser Publishers, New

York (1994).

Mckenna, T. F., and Soares, J. B. P. Single Particle Modeling for Olefin Polymerization on Supported Catalysts: A Review and Proposals for Future Developments. **Chemical Engineering Science** 56 (2001): 3931-3949.

Meng, F., Yu, G., and Huang, B. Polymer-Supported Zirconocene Catalyst for Ethylene Polymerization. **Journal of Polymer Science: Part A: Polymer Chemistry** 37 (1999): 37-46.

Meshkova, I. N., Ushakova, T. M., Ladygina, T. A., Kovaleva, N. Y., and Novokshonova, L. A. Ethylene Polymerization with Catalysts on the Base of Zr-cenes and Methylaluminoxanes Synthesized on Zeolite Support. **Polymer Bulletin** 44 (2000): 461-468.

Monrabal, B. Crystallization Analysis Fractionation: A New Approach for the Composition Analysis of Semicrystalline Polymers. **Macromolecular Symposia** 110 (1996): 81-86.

Monrabal, B. Crystallization Analysis Fractionation: A New Technique for the Analysis of Branching Distribution in Polyolefins. **Journal of Applied Polymer Science** 52 (1994): 491-499.

Monrabal, B., Blanco, J., Nieto, J., and Soares, J. B. P. Characterization of Homogeneous Ethylene/1-Octene Copolymers Made with a Single-Site Catalyst. CRYSTAF Analysis and Calibration. **Journal of Polymer Science: Part A: Polymer Chemistry** 37 (1999): 89-93.

Moore, S. J. <u>Solubility of α-Olefins in Polyethylenes</u> **M.Sc. Thesis**, Department of Chemical and Materials Engineering, University of Alberta, Canada (2000).

Moore, S. J., and Wanke, S. E. Solubility of Ethylene, 1-Butene and 1-Hexene in Polyethylenes **Chemical Engineering Science** 56 (2001): 4121-4129.

Moroz, B. L., Semikolenova, N. V., Nosov, A. V., Zakharov, V. A., Nagy, S., and Reilly, N. J. O. Silica –Supported Zirconocene Catalysts: Preparation, Characterization and Activity in Ethylene Polymerization. **Journal of Molecular Catalysis A: Chemical** 130 (1998): 121-129.

Morse, P. M. New Catalysts Renew Polyolefins. **Chemical & Engineering News** 76 (27) (1998): 11-16.

Muller, A. J., Hernandez, Z. H., Arnal, M. L., and Sanchez, J. J. Successive Self-Nucleation/Annealing (SSA): A Novel Technique to Study Molecular Segregation During Crystallization. **Polymer Bulletin** 39 (1997): 465-472.

Naga, N., Shiono, T., and Ikeda, T. Cyclopolymerization of 1,7-Octadiene with Metallocene/Methylaluminoxane. **Macromolecular Chemistry and Physics** 200 (1999): 1466-1472.

Naik, S. D., and Ray, W. H. Particle Morphology for Polyolefins Synthesized with Supported Metallocene Catalysts. **Journal of Applied Polymer Science** 79 (2001): 2565-2579.

Nishida, H., Uozumi, T., Arai, T., and Sofa, K. Polystyrene-Supported Metallocene Catalysts for Olefin Polymerization. **Macromolecular Rapid Communication** 16 (1995): 821-830.

Ottani, S., and Porter, R. S. A Calorimetric Investigation on High Molecular Weight Polyethylene Reactor Powders. **Journal of Polymer Science: Part B: Polymer Physics** 29 (1991): 1179-1188.

Panchenko, V. N., Semikolenova, N. V., Danilova, I. G., Paukshtis, E. A., and Zakharov, V.A. IRS Study of Ethylene Polymerization Catalyst SiO_2/Methylaluminoxane/Zirconocene. **Journal of Molecular Catalysis A: Chemical** 142 (1999): 27-37.

Pasynkiewicz, S. Alumoxanes-Synthesis, Structures, Complexes, and Reactions. **Polyhedron** 9 (2-3) (1990): 429-453.

Paulino, I. S., Filho, A. P. D. O., Souza, J. L. D., and Schuchardt, U. Ethylene Polymerization with Zirconocene-MAO Supported on Molecular Sieves. **Studies in Surface Science and Catalysis** 130 (2000): 929-934.

Phillip Townsend Associates Newsletter for Plastics and Chemical Industries Vol. 56. June (2001).

Pigeon, M. G., and Rudin, A. Branching Measurement by Analytical TREF: A Fully Quantitative Technique. **Journal of Applied Polymer Science** 51 (1994): 303-311.

Pigeon, M. G., and Rudin, A. Comparison of Analytical and Preparative TREF Analysis: A Mathematical Approach to Correcting Analytical TREF Data. **Journal of Applied Polymer Science** 47 (1993): 685-696.

Poling, B. E., Prausnitz, J. M., and O' Connell, J. P. The Properties of Gases and Liquids. 5 th Edition, New York, McGraw Hill (2001): 7.4 and A.53.

Quijada, R., Rojas, R., Alzamora, L., Retuert, J., and Rabagliati, F. M. Study of Metallocene Supported on Porous and Nonporous Silica for the Polymerization of Ethylene. **Catalysis Letters** 46 (1997): 107-112.

Quijada, R., Rojas, R., Narvaez, A., Alzamora, L., Retuert, J., and Rabagliati, F. M. The Effect of Reaction Parameters on Catalytic Activity in the Polymerization of Ethylene Using Supported and Unsupported Metallocene Catalysts. **Applied Catalysis A: General** 166 (1998): 207-213.

Rahiala, H., Beurroies, I., Eklund, T., Hakala, K., Gougeon, R., Trens, P., and Rosenholm, J. B. Preparation and Charaterization of MCM-41 Supported Metallocene Catalysts for Olefin Polymerization. **Journal of Catalysis** 188 (1999): 14-23.

Rangwala, H. A., Szymura, J. A., Wanke, S. E., and Otto, F. D. Preparation and Characterization of Pt/Silicalite Catalysts with High Pt Loadings. **The Canadian Journal of Chemical Engineering** 66 (1988): 843-848.

Rappe, A. K., Skiff, W. M., and Casewit, C. J. Modeling Metal-Catalyzed Olefin Polymerization. **Chemical Reviews** 100 (2000): 1435-1456.

Reddy, S. S., and Sivaram, S. Homogeneous Metallocene-Methylaluminoxane Catalyst Systems for Ethylene Polymerization. **Progress in Polymer Science** 20 (1995): 309-367.

Resconi, L., Bossi, S., and Abis, L. Study on the Role of Methylalumoxane in Homogeneous Olefin Polymerization. **Macromolecules** 23 (1990): 4489-4491.

Resconi, L., Piemontesi, F., Franciscono, G., Abis, L., and Fiorani, T. Olefin Polymerization at Bis(pentamethylcyclopentadienyl) Zirconium and Hafnium Centers-Chain-Transfer Mechanisms. **Journal of the American Chemical Society** 114 (3) (1992): 1025-1032.

Ribeiro, M., Deffieux, A., and Portela, M. F. Supported Metallocene Complexes for Ethylene and Propylene Polymerizations: Preparation and Activity. **Industrial & Engineering Chemistry Research** 36 (1997): 1224-1237.

Riccardo, P., and Nicoletta, C. Synthesis of Syndiotactic Polystyrene: Reaction

Mechanism and Catalysis. **Progress in Polymer Science** 21 (1996): 47-88.

Richard, C. T. Overview of Recent Advances in Polyethylene Process and Product Technologies. **Plastics Rubber Composites Processing and Applications** 27 (1) (1998): 3-7.

Robinson, S. Breaking the Mold. **Chemistry & Industry** 12 (2001): 377-378.

Roos, P., Meier, G. B., Samson, J. J. C., Weickert, G., and Westerterp, K. R. Gas Phase Polymerization of Ethylene with a Silica-Supported Metallocene Catalyst: Influence of Temperature on Deactivation. **Macromolecular Rapid Communication** 18 (1997): 319-324.

Sacchi, M. C., Zucchi, D., Tritto, I., and Locatelli, P. Silica-Supported Metallocenes: Stereochemical Comparison Between Homogeneous and Heterogeneous Catalysis. **Macromolecular Rapid Communication** 16 (1995): 581-590.

Sailors, H. R., and Hogan, J. P. History of Polyolefins. **Journal of Macromolecular Science Chemistry** A15 (7) (1981): 1377-1402.

Sangokoya, S. (Ethyl Co.) **U.S. Patent** 5,248,801 (1993).

Sano, T., Doi, K., Hagimoto, H., Wang, Z. B., Uozumi, T., and Soga, K. Potential Use of MCM-41 for Adsorptive Separation of Methylalumoxane. **Studies in Surface Science and Catalysis** 125 (1999a): 777-784.

Sano, T., Doi, K., Hagimoto, H., Wang, Z. B., Uozumi, T., and Soga, K. Adsorptive Separation of Methylaluminoxane by Mesoporous Molecular Sieve MCM-41. **Chemical Communications** 8 (1999b): 733-734.

Sano, T., Hagimoto, H., Jin, J., Oumi, Y., Uozumi, T., and Soga, K. Influences of Methylaluminoxane Separated by Porous Inorganic Materials on the Isospecific Polymerization of Propylene. **Macromolecular Rapid Communication** 21 (2000): 1191-1195.

Sano, T., Hagimoto, H., Sumiya, S., Naito, Y., Oumi, Y., Uozumi, T., and Soga, K. Application of Porous Inorganic Materials to Adsorptive Separation of Methylaluminoxane Used as Co-catalyst in Olefin Polymerization. **Microporous and Mesoporous Materials** 44-45 (2001a): 557-564.

Sano, T., Niimi, T., Miyazaki, T., Tsubaki, S., Oumi, Y., and Uozumi, T. Effective Activation of Metallocene Catalyst with AlMCM-41 in Propylene

Polymerization. **Catalysis Letters** 71 (1-2) (2001b): 105-110.

Santos, J. H. Z. D., Krug, C., Rosa, M. B. D., Stedile, F. C., Dupont, J., and Fonte, M. D. C. The Effect of Silica Dehydroxylation Temperature on the Activity of SiO_2-Supported Zirconocene Catalysts. **Journal of Molecular Catalysis A: Chemical** 139 (1999b): 199-207.

Santos, J. H. Z. D., Larentis, A., Rosa, M. B. D., Krug, C., and Baumvol, I. J. R. Optimization of a Silica Supported Bis(butylcyclopentadienyl)Zirconium Dichloride Catalyst for Ethylene Polymerization. **Macromolecular Chemistry and Physics** 200 (1999a): 751-757.

Santos, J. H. Z. D., Rosa, M. B. D., Krug, C., Stedile, F. C., Haag, M. C., Dupont, J., and Porte, M. D. C. Effects of Ethylene Polymerization Conditions on the Activity of SiO_2-Supported Zirconocene and on Polymer Properties. **Journal of Polymer Science: Part A: Polymer Chemistry** 37 (1999): 1987-1996.

Scheirs, J., and Kaminsky, W. Metallocene-Based Polyolefins: Preparation, Properties and Technology. Volume 1, John Wiley & Sons Ltd., (1999).

Schneider, H., Puchta, G. T., Kaul, F. A. R., Raudaschi, S. G., Lefebvre, F., Saggio, G., Mihalios, D., Herrmann, W. A., and Basset, J. M. Immobilization of Eta(5)-cyclopentadienyltris(dimethylamido) Zirconium Polymerization Catalysts on a Chlorosilane- and HMDS-Modified Mesoporous Silica Surface: A New Concept for Supporting Metallocene Amide Towards Heterogeneous Single-Site-Catalysts. **Journal of Molecular Catalysis A: Chemical** 170 (1-2) (2001): 127-141.

Schwecke, C., and Kaminsky, W. Syndiospecific Polymerization of Styrene with BzCpTiCl3 and Methylaluminoxane as Cocatalysts. **Journal of Polymer Science: Part A: Polymer Chemistry** 39 (2001): 2805-2812.

Semikolenova, N. V., and Zakharov, V. A. On the Interaction of Supported Zirconocene Catalysts with Alkylaluminum Co-Catalysts. **Macromolecular Chemistry and Physics** 198 (1997): 2889-2897.

Sensarma, S., and Sivaram, S. A Magnesium Chloride Supported Bis(cyclopentadienyl)-Zirconium (IV) Dichloride Catalyst for the Polymerization of Ethylene. **Macromolecular Chemistry and Physics** 200 (1999): 323-329.

Shan, C. L. P., Chu, K. J., Soares, J., and Penlidis, A. Using Alkylaluminium Activators to Tailor Short Chain Branching Distributions of Ethylene and 1-Hexene Copolymers Produced with In-Situ Supported Metallocene Catalysts. **Macromolecular Chemistry and Physics** 201 (16) (2000): 2195-2202.

Shan, C. L. P., Soares, J. B. P., and Penlidis, A. Ethylene/1-Octene Copolymerization Studies with In Situ Supported Metallocene Catalysts: Effect of Polymerization Parameters on the Catalyst Activity and Polymer Microstructure. **Journal of Polymer Science: Part A: Polymer Chemistry** 40 (2002): 4426-4451.

Siedle, A. R., Lamanna, W. M., Newmark, R. A., Stevens, J., Richardson, D. E., and Ryan, M. The Role of Noncoordinating Anions in Homogeneous Olefin Polymerization. **Makromolekulare Chemie-Macromolecular Symposia** 66 (1993): 215-224.

Siedle, A. R., Newmark, R. A., and Lamanna, W. M. Exchange-Reactions Between Dialkylzirconocene and Alkylaluminium Compounds. **Polyhedron** 9 (2-3) (1990): 301-308.

Simone, C. M., and Marques, M. F. V. Polyethylene Synthsis Using Zeolit as Support for Metallocene Catalyst. **European Polymer Journal** 37 (2001): 2123-2130.

Sinn, H. Proposals for Structure and Effect of Methylaluminoxane Based on Mass Balances and Phase Separation Experiments. **Macromolecular Symposia** 97 (1995): 27-52.

Sinn, H., Kaminsky, W., Vollmer, H.J., and Woldt, R. Livings Polymers on Polymerization with Extremely Productive Ziegler Catalyst. **Angewandte Chemie-International Edition in English** 19 (5) (1980): 390-392.

Soares, J. B. P., and Hamielec, A. E. Analyzing TREF Data by Stockmayer 's Bivariate Distribution. **Macromolecule Theory Simulation** 4 (2) (1995b): 305-324.

Soares, J. B. P., and Hamielec, A. E. Temperature Rising Elution Fractionation of Linear Polyolefins. **Polymer** 36 (8) (1995a): 1639-1654.

Soga, K., and Kaminaka, M. Copolymerization of Olefins with SiO_2-, Al_2O_3-, and $MgCl_2$-Supported Metallocene Catalysts Activated by Trialkylaluminiums. **Macromolecular Chemistry and Physics** 195 (1994): 1369-1379.

Soga, K., and Kaminaka, M. Polymerization of Propene with the Heterogeneous Catalyst System $Et[IndH_4]_2ZrCl_2/MAO/SiO_2$ Combined with Trialkylaluminium.

Macromolecular Rapid Communication 13 (1992): 221-224.

Soga, K., Kim, H. J., and Shiono, T. Highly Isospecific SiO_2-Supported Zirconocene Catalyst Activities by Ordinary Alkylaluminiums **Macromolecular Rapid Communication** 15 (1994): 139-143.

Soga, K., Shiono, T., and Kim, H. J. Activation of SiO_2-Supported Zirconocene Catalysts by Common Trialkylaluminiums. **Makromolekular Chemistry** 194 (1993): 3499-3504.

Soga, K., Uozumi, T., Arai, T., and Nakamura, S. Heterogeneity of Active Species in Metallocene Catalysts. **Macromolecular Rapid Communication** 16 (1995): 379-385.

Starck, P. Studies of the Comonomer Distribution in Low Density Polyethylenes Using Temperature Rising Elution Fractionation and Stepwise Crystallization by DSC. **Polymer International** 40 (2) (1996): 111-122.

Staub, R. B. Polyethylene 1933-83. **Proceedings of the Golden Jubilee Conference, The Plastics and Rubber Institute, London** (1983): B5.4.1 – B5.4.14.

Steinmetz, B., Tesche, B., Przybyla, C., Zechlin, J., and Fink, G. Polypropylene Growth on Silica-Supported Metallocene Catalysts: A Microscopic Study to Explain Kinetic Behavior Especially in Early Polymerization Stages **Acta Polymerica** 48 (9) (1997): 392-399.

Sugano, T., Matsubara, K., Fujita, T., and Takahashi, T. Characterization of Aluminoxanes by Al-27-NMR Spectra. **Journal of Molecular Catalysis** 82 (1) (1993): 93-101.

Tait, P. J. T., Monteiro, M. G. K., Yang, M., Richardson, J., and Ediati, R. Advances in Supported Metallocene Catalysis. **Polimery** 45 (2000): 314-322.

Tajima, K., Ogawa, G., and Aida, T. Novel Molecularly Hybridized Polyethylene/Silica Composite Materials: Polymerization of Ethylene with Supported Titanocenes by Mesoporous Silicalites. **Journal of Polymer Science: Part A: Polymer Chemistry** 38 (2000): 4821-4825.

Tannous, K., and Soares, J. B. P. Gas-Phase Polymerization of Ethylene Using Supported Metallocene Catalysts: Study of Polymerization Conditions. **Macromolecular Chemistry and Physics** 203 (2002): 1895-1905.

Thomann, Y., Sernetz, F. G., Thomann, R., Kressler, J., and Mulhaupt, R. Temperature Rising Elution Fractionation of a Random Ethylene/Styrene Copolymer. **Macromolecular Chemistry and Physics** 198 (3) (1997): 739-748.

Tritto, I., Mealares, C., Sacchi, M. C., and Locatelli, P. Methylaluminoxane: NMR Analysis, Cryoscopic Measurements and Cocatalytic Ability in Ethylene Polymerization. **Macromolecular Chemistry and Physics** 198 (1997): 3963-3977.

Trong, O. D., Giscard, D. D., Danumah, C., and Kaliaguine, S. Perspectives in Catalytic Applications of Mesostructured Materials. **Applied Catalysis A: General** 222 (2001): 299-357.

Tsutsui, T., and Kashiwa, N. Gas-Phase Polymerization of Propylene with a Solid Complex Catalyst Obtained from Et(Ind)$_2$ZrCl$_2$ and Methylaluminoxane. **Polymer** 32 (1991): 91-93.

Tudor, J., and Hare, D. O. Stereospecific Propene Polymerization Catalysis Using an Organometallic Modified Mesoporous Silicate. **Chemical Communication** (1997): 603-604.

Usami, T., Gotoh, Y., and Takayama, S. Generation Mechanism of Short-Chain Branching Distribution in Linear Low Density Polyethylenes. **Macromolecules** 19 (1986): 2722-2726.

Van Looveren, L. K., Dirk, E. D. V., Vercruysse, K. A., Geysen, D. F., Janssen, B., and Jacobs, P. A. Oligomerization of Propene on an Alumoxane-Grafted MCM-41 Host with Bis(cyclopentadienyl)Zirconium Dimethyl ($Cp_2Zr(CH_3)_2$). **Catalysis Letters** 56 (1998b): 53-56.

Van Looveren, L. K., Geysen, D. F., Vercruysse, K. A., Wouters, B. H., Grobet, P. J., and Jacobs, P. A. Methylaluminoxane MCM-41 as Support in the Co-Oligomerization of Ethene and Propene with [$\{C_2H_4$(1-indenyl)$_2\}Zr(CH_3)_2$]. **Angewandte Chemie International Edition** 37 (4)(1998a): 517-520.

Wang, L., Zhang, P. Y., Jiang, S., and Feng, L. X. Study of Ethylene Polymerization Catalyzed by nBu-Cp$_2$ZrCl$_2$/MAO Catalytic System and Their Polymerization Kinetics. **Journal of Applied Polymer Science** 81 (2001): 3186-3189.

Wang, Q., Weng, J., Xu, L., Fan, Z., and Feng, L. Multiple Active Sites Model of

Ethylene Polymerization with the Cp_2ZrCl_2-Aluminoxanes Catalytic System. **Polymer** 40 (1991): 1863-1870.

Weckhuysen, B. M., Rao, R. R., Pelgrims, J., Schoonheydt, R. A., Bodart, P., Debras, G., Collart, O., Van Der Voort, P., and Vansant, E. F. Synthesis, Spectroscopy and Catalysis of [Cr(acac)(3)] Complexes Grafted onto MCM-41 Materials: Formation of Polyethylene Nanofibers within Mesoporous Crystalline Aluminosilicates. **Chemistry-A European Journal** 6 (16) (2000): 2960-2970.

Wilkinson, G., and Birmingham, I. M. Bis-Cyclopentadienyl Compounds of Ti, Zr, V, Nb, and Ta. **Journal of the American Chemical Society** 76 (1954): 4281-4284.

Wilmes, G. M., Polse J. L., and Waymouth R. M. Influence of Cocatalyst on the Stereoselectivity of Unbridged 2-Phenylindenyl Metallocene Catalysts. **Macromolecules** 35 (18) (2002): 6766-6772.

Woo, S. I., Ko, Y. S., and Han, T. K. Polymerization of Ethylene Over Metallocenes Confined Inside the Supercage of a NaY Zeolite. **Macromolecular Rapid Communication** 16 (1995): 489-494.

Wu, L., Lynch, D. T., and Wanke, S. E. Kinetics of Gas-Phase Ethylene Polymerization with Morphology Controlled $MgCl_2$-Supported $TiCl_4$ Catalyst. **Macromolecules** 32 (24) (2000): 7990-7998.

Xie, T., Mcauley, K.B., Hsu, J.C.C., Bacon, D.W. Gas Phase Ethylene Polymerization: Production Processes, Polymer Properties, and Reactor Modeling. **Industrial & Engineering Chemistry Research** 33 (1994): 449-479.

Xu, J., and Feng, L. Application of Temperature Rising Elution Fractionation in Polyolefins. **European Polymer Journal** 36 (2000): 867-878.

Xu, J., Ji, P., Wu, J., Ye, M., Shi, L., and Wan, C. Study on the Determination of the Molecular Weight of Polyethylene with Ultrahigh Temperature GPC. **Macromolecular Rapid Communication** 19 (1998): 115-118.

Xu, J., Xu, X., and Feng, L. Short Chain Branching Distributions of Metallocene-Based Ethylene Copolymers. **European Polymer Journal** 36 (1999): 685-693.

Xu, J., Xu, X., Feng, L., Chen, L., and Chen, W. Characterization of Intramolecular Composition Heterogeneity of Metallocene-Based and Conventional Ethylene-Butene Copolymers Using TREF/DSC. **Macromolecular Chemistry and**

Physics 202 (2001): 1524-1530.

Xu, Z. G., Chakravarti, S., and Ray, H. Kinetic Study of Olefin Polymerization with a Supported Metallocene Catalyst. I. Ethylene/Propylene Copolymerization in Gas Phase. **Journal of Applied Polymer Science** 80 (2001): 81-114.

Yasuga, H. Organo Transition Metal Initiated Living Polymerizations. **Progress in Polymer Science** 25 (5) (2000): 573-626.

Ye, Z., Alsyouri, H., Zhu, S., and Lin, Y. S. Catalyst Impregnation and Ethylene Polymerization with Mesoporous Particle Supported Nickel-Diimine Catalyst. **Polymer** 44 (2003): 969-980.

Yiagopoulos, A., Yiannoulakis, H., and Kiparissides, C. Heat and Mass Transfer Phenomena During the Early Growth of a Catalyst Particle in Gas-Phase Olefin Polymerization: The Effect of Prepolymerization Temperature and Time. **Chemical Engineering Science** 56 (2001): 3979-3995.

Yoon, J. S., Lee, D. H., Park, E. S., Lee, I. M., Park, D. K., and Jung S. O. Copolymerization of Ethylene/α-Olefins Over (2-MeInd)$_2$ZrCl$_2$/MAO and (2-BzInd)$_2$ZrCl$_2$/MAO Systems. **Journal of Applied Polymer Science** 75 (2000): 928-937.

Ystenes, M. Predictions from the Trigger Mechanism for Ziegler-Natta Polymerization of Alpha-Olefins. **Macromolecular Symposia** 66 (1993): 71-81.

Ystenes, M., Eilertsen, J. L., Liu, J., Ott, M., Rytter, E., and Stovneng, J. A. Experimental and Theoretical Investigation of the Structure of Methylaluminoxane (MAO) Cocatalysts for Olefin Polymerization. **Journal of Polymer Science: Part A: Polymer Chemistry** 86 (2000): 3106-3127.

Yu, P., Muller, P., Said, M. A., Roesky, H. W., Uson, I., Bai, G., and Noltemeyer, M. Difference in Reactivity of Cyclopentadienyl Fluorides Using AlR$_3$ (R=Me, Et): Syntheses and Structures of Ti(III)-F(Cl)-Al Compounds (eta(5)-C$_5$Me$_5$)(2)Ti-2(mu-Cl)(6)Al$_2$Me$_4$, and (eta(5)-C$_5$Me$_5$)(2) Ti-2(mu-F)(8)Al$_4$Me$_8$, and [(eta(5)-C$_5$H$_4$Me)(2)Ti(mu-F)(2)AlEt$_2$](2). **Organometallics** 18 (9) (1999): 1669-1674.

Zakharov, I. I., Zakharov, V. A., and Zhidomiriv, G. M. A DFT quantum-Chemical Study on the Structures and Active Sites of Polymethylaluminoxane. **Macromolecular Theory and Simulations** 8 (3) (1999): 272-278.

Zhang, M. Characterization of Commercial Linear Low Density Polyethylenes by TREF, SEC, DSC, and Cross-Fractionation. **M.Sc. Thesis**, Department of Chemical and Materials Engineering, University of Alberta, Canada (2000).

Zhang, M., Lynch, D. T., and Wanke, S. E. Characterization of Commercial Linear Low-Density Polyethylene by TREF-DSC and TREF-SEC Cross-Fractionation. **Journal of Applied Polymer Science** 75 (2000): 960-967.

Zhou, J. M., Li, N. H., Bu, N. Y., Lynch, D. T., and Wanke, S. E. Gas-Phase Ethylene Polymerization over Polymer-Supported Catalysts. **Journal of Applied Polymer Science** (in press).

APPENDICES

Appendix A

Gas-Phase Polymerization

In the Appendix A, the descriptions of supports and catalysts, polymerization reaction conditions, average polymerization activities, scanning electron micrographs, and the results of size exclusion microscopy for gas-phase polymerization system are provided. The experimental details of all gas-phase polymerizations with the different pore diameters of mesoporous molecular sieve supports conducted in this research summarized in Appendix A are listed below.

- The BET surface analysis for all the supports used in this system was shown in Table A1.
- The catalysts compositions calculated are described in Table A2.
- The structure of supports and catalysts as well as resulting polymer obtained from homopolymerization and copolymerization produced with the different pore diameter are shown in Figure A1-8. Scanning electron micrograph results were carried out most of the samples. The parts of the morphology of polymers and copolymer produced at 70°C were chosen.
- All of the polymerization conditions, average polymerization activities, and the molar masses consisted of the number of average molecular weight (Mn), average molecular weight (Mw), and polydispersities (PD or Mw/Mn) with the different pore diameters of supports are summarized in Table A3. The average polymerization activities calculated by the obtained yield of polymer were reasonably correlated to the yielded calculated by integration of the ethylene feed rates with 95% confidence. For the molar masses are based on relative calibration; the molar masses were measured all of samples. The molar mass values were the average values of at least two measurements.

Table A1. Description of supports for gas-phase experiments

Catalyst Designation	**Pore Diameter (nm)**	**Surface Area (m^2/g)**	**Pore Volume, cm^3/g**	**Calculated Pore Dia, nm†**
MMS2.5	(2.5)	(890)	(0.61)	(2.7)
MMS2.6*	2.6 (3.0)	1130 (1175)‡	1.3 (0.76)	4.6 (2.6)
MMS5.8	5.8 (5.8)	980 (936)	0.8 (0.95)	3.3 (4.1)
MMS7.2	7.2	870	1.1	5.1
MMS10	10	412	1.3	12.6
MMS15.2	15.2	330	1.3	15.8
MMS20	20	310	1.6	20.6
MMS25	25	300	1.7	22.7
S0.54** (Silicalite)	0.56	435	--	--
S1*** (silica)	16	270	1.4	20.7

* MMS = mesoporous molecular sieves

** Silicalite

*** silica gel

‡ Values in brackets measured at University of Alberta; other values from Laval University.

† Calculated Pore Diameter (nm) originated from equation below

$$[\text{Pore Diameter in nm}]_{\text{calculated}} = 4{,}000 \times [\text{Pore Volume in cm}^3/\text{g}]/[\text{Surface Area in m}^2/\text{g}]$$

Table A2. Description of catalysts used for gas-phase experiments

Catalyst	**Support Pore Diameter (nm)**	**Support**	**Amount of Support Used (g)**	**Amount of MAO Added (mL)**	**Zr Content**		**Al/Zr ratio**
					mass %	**mmol/g**	
CAT0.54	0.54	S0.54	0.66	4.4	0.33	0.037	170
CAT2.6-1	2.6	MMS2.6	1.00	6.6	0.34	0.037	170
CAT2.6-2	2.6	MMS2.6	1.00	6.6	0.38	0.042	150
CAT2.6-3	2.6	MMS2.6	1.00	3.3	0.36	0.039	100
CAT5.8	5.8	MMS5.8	0.60	4.0	0.34	0.037	170
CAT7.2	7.2	MMS7.2	0.52	3.4	0.33	0.037	170
CAT10	10	MMS10	0.33	4.2	0.25	0.027	330
CAT15	15	MMS15	0.29	1.9	0.34	0.037	170
CAT20	20	MMS20	0.75	5.0	0.34	0.037	170
CAT25	25	MMS25	0.25	1.6	0.34	0.037	170
CATS1-1	16	S1	2.00	6.6	0.33	0.036	110
CATS1-2	16	S1	2.00	13.3	0.29	0.032	200
CAT-SD	a donated, uncharacterized (n-BuCp)$_2$ZrCl$_2$ /MAO/SiO$_2$ catalyst used in preliminary experiments.						

The catalyst compositions obtained from the MAO solution contained 10 mass% MAO with a density of 0.875 g/mL by assuming that the MAO contained 46.8 mass% Al, and the molecular weight of catalyst (n-BuCp)$_2$ZrCl$_2$ was 404.53.

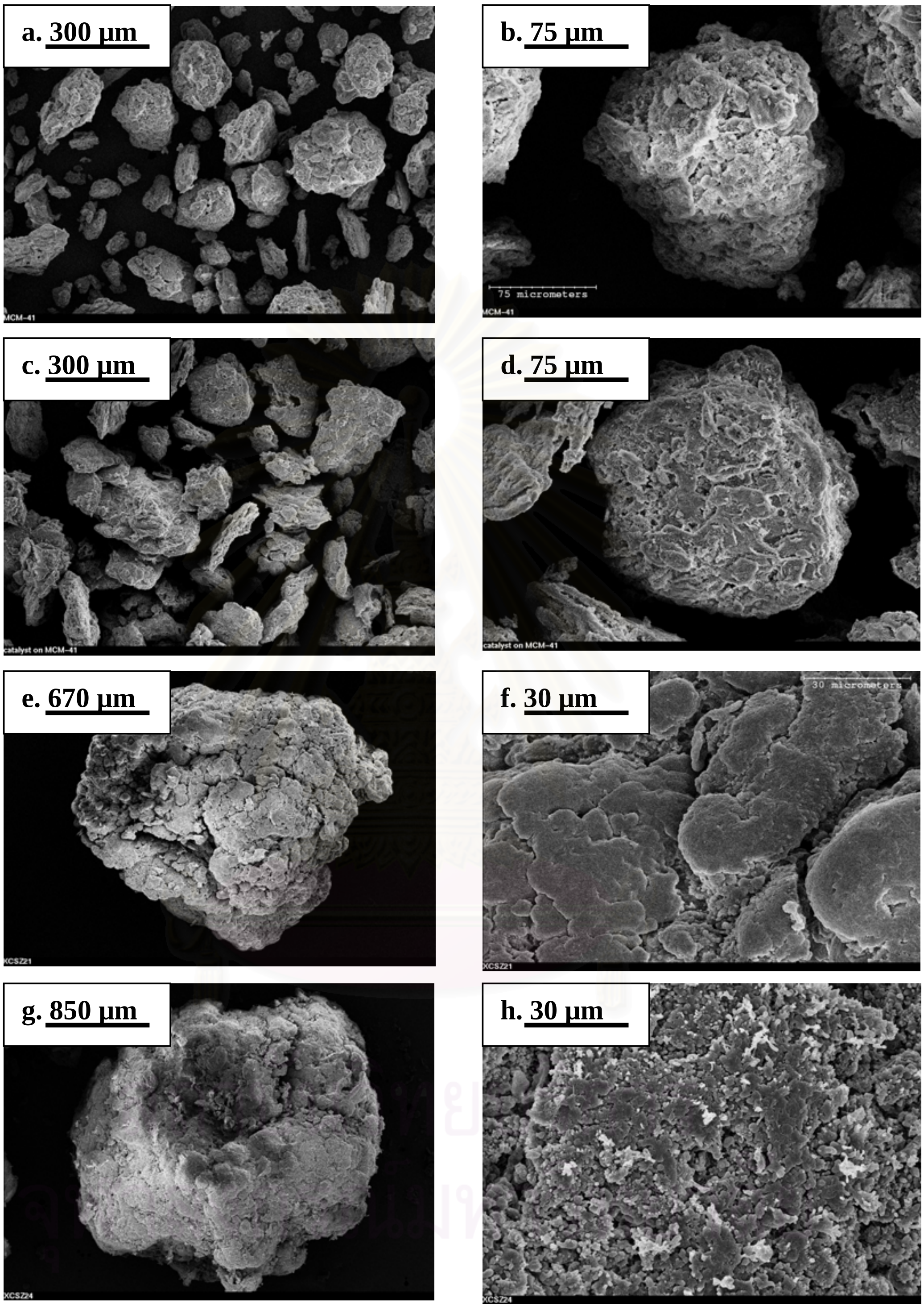

Figure A1. Scanning electron micrographs: (a,b) the MMS2.6 support, (c,d) CAT2.6-2, (e,f) the homopolymer produced with CAT2.6-2 at 70°C, and (g,h) the copolymer produced at 70°C

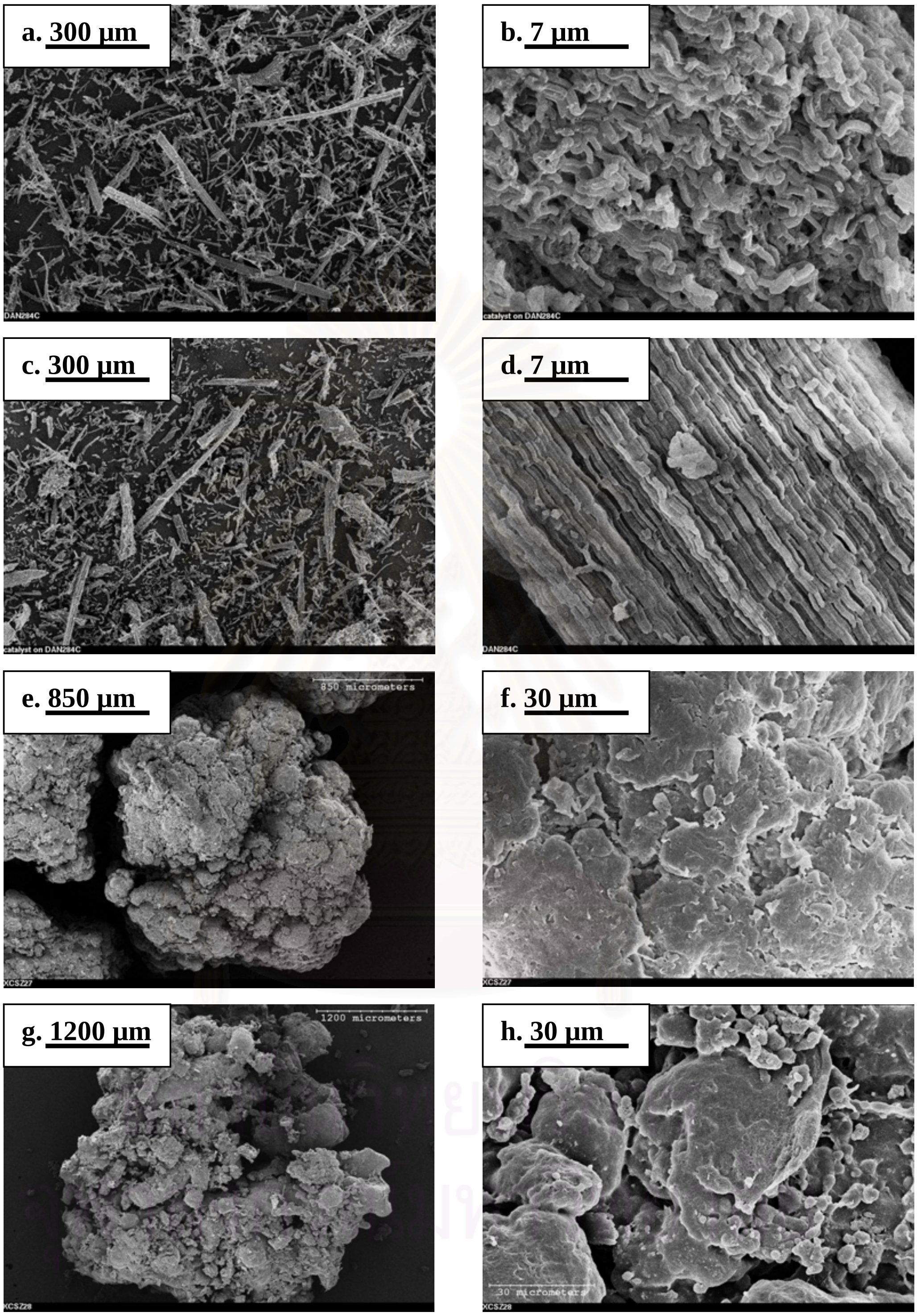

Figure A2. Scanning electron micrographs: (a,b) the MMS5.8 support, (c,d) CAT5.8-2, (e,f) the homopolymer produced with CAT5.8 at 70°C, and (g,h) the copolymer produced at 70°C

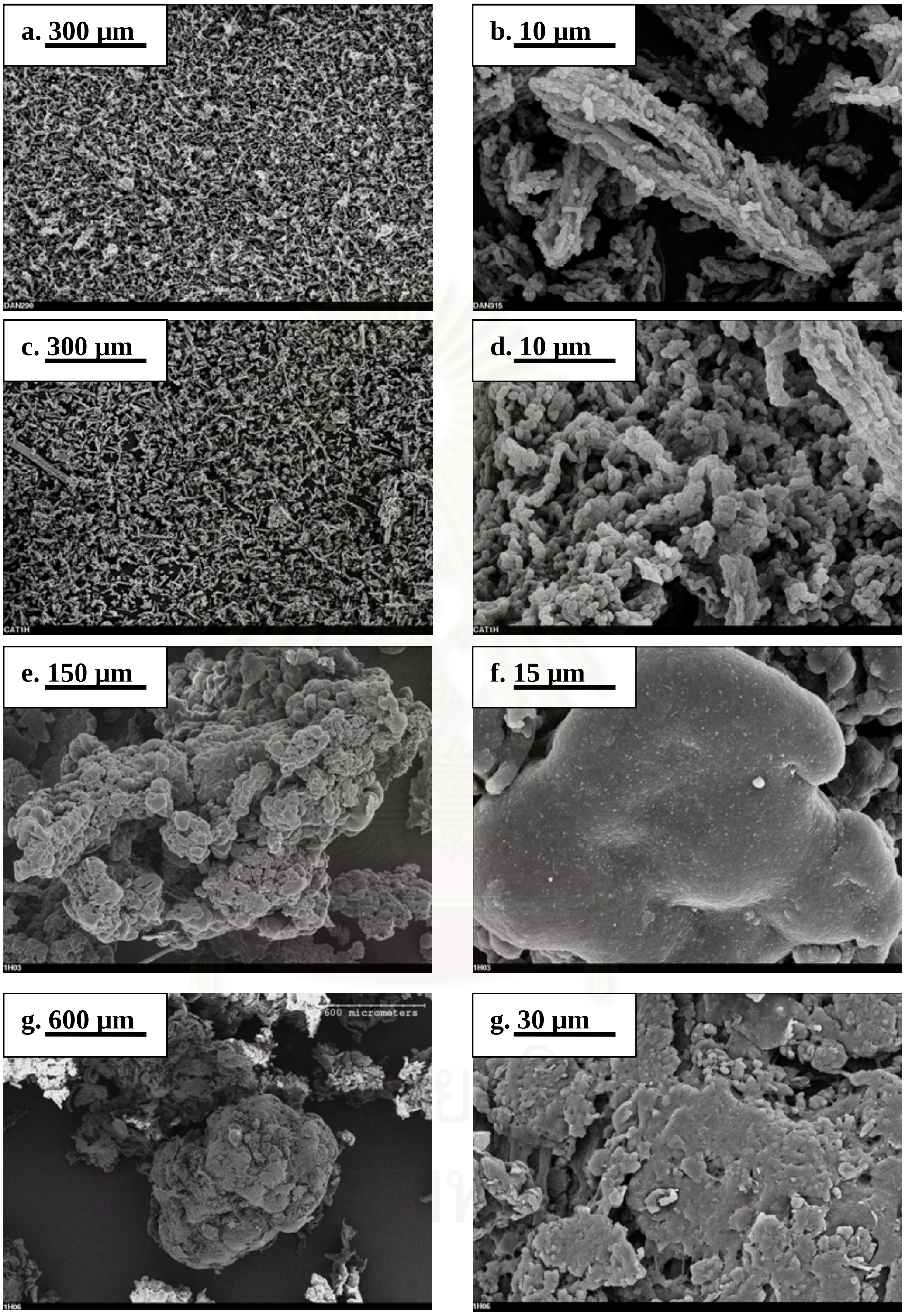

Figure A3. Scanning electron micrographs: (a,b) the MMS7.2 support, (c,d) CAT7.2, (e,f) the homopolymer produced with CAT7.2 at 70°C, and (g,h) the copolymer produced at 70°C

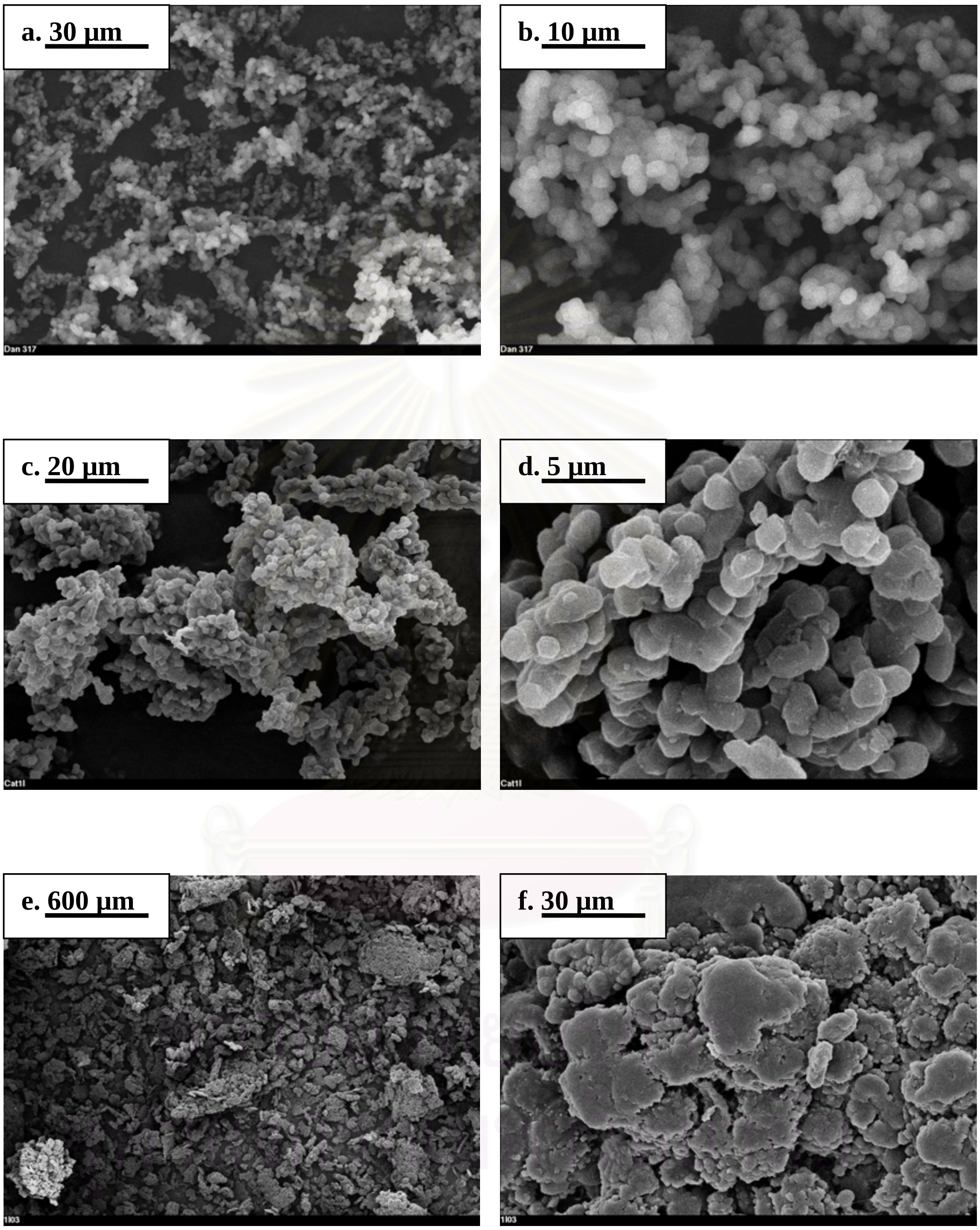

Figure A4. Scanning electron micrographs: (a,b) the MMS10 support, (c,d) CAT10, (e,f) the homopolymer produced with CAT10 at 70°C

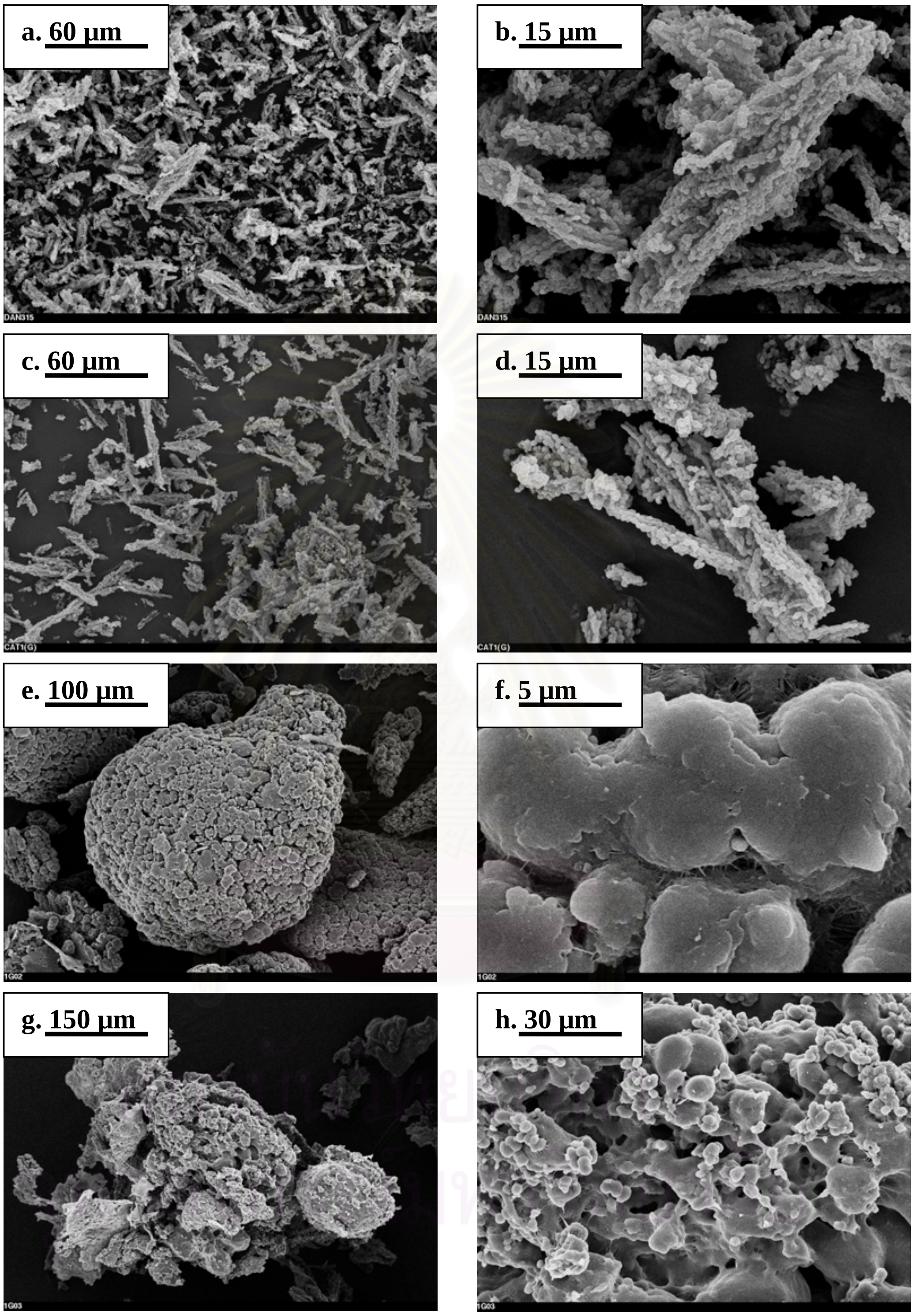

Figure A5. Scanning electron micrographs: (a,b) the MMS15 support, (c,d) CAT15, (e,f) the homopolymer produced with CAT15 at 70°C, and (g,h) the copolymer produced at 70°C

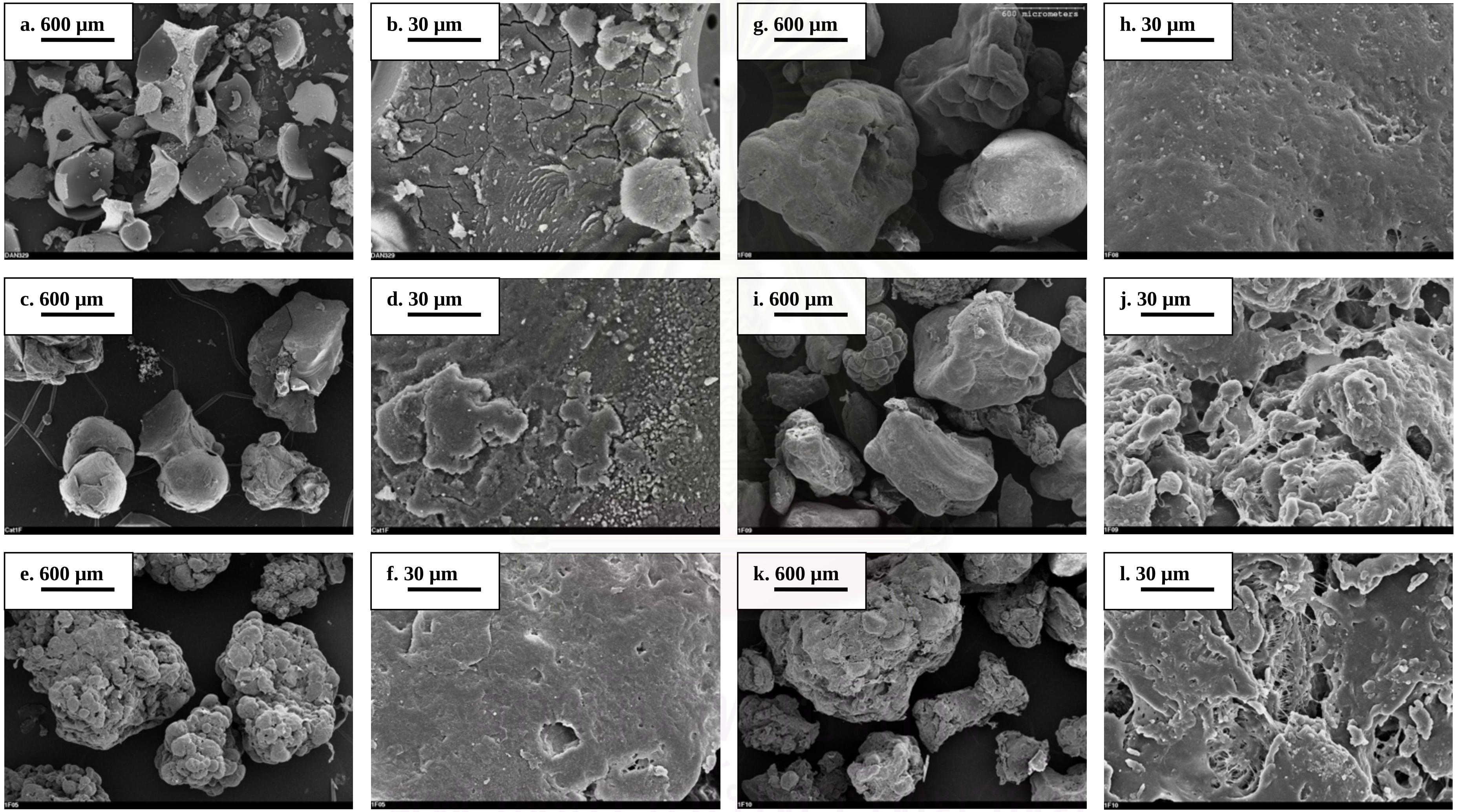

Figure A6. Scanning electron micrographs: (a,b) the MMS20 support, (c,d) CAT20, (e,f) the homopolymer produced with CAT20 at 70°C, (g,h) the copolymer produced at 70°C for 2 h, (i,j) for 1 h, and (k,l) for 0.5 h

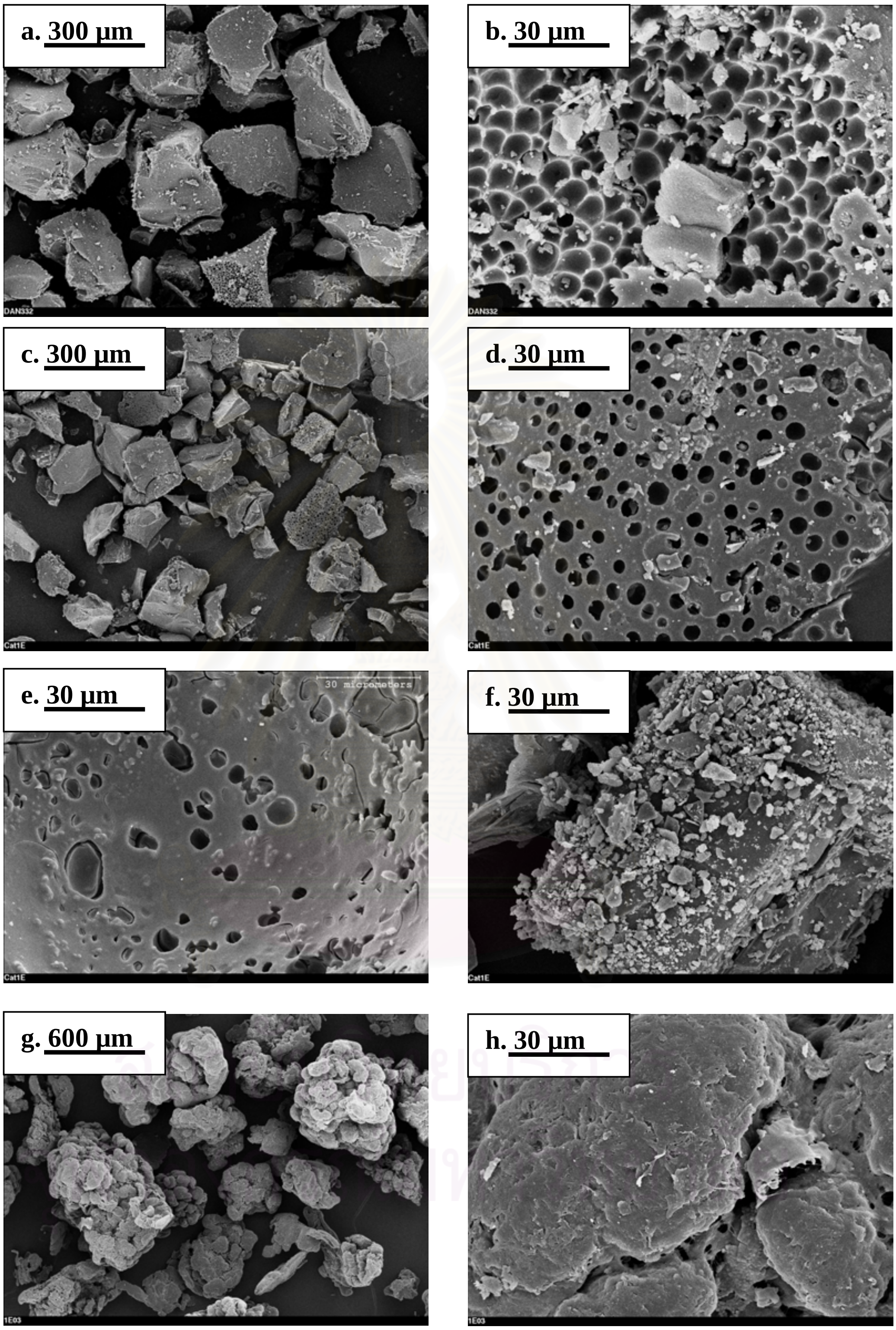

Figure A7. Scanning electron micrographs: (a,b) the MMS25 support, (c-f) CAT25, (g,h) the homopolymer produced with CAT25 at 70°C

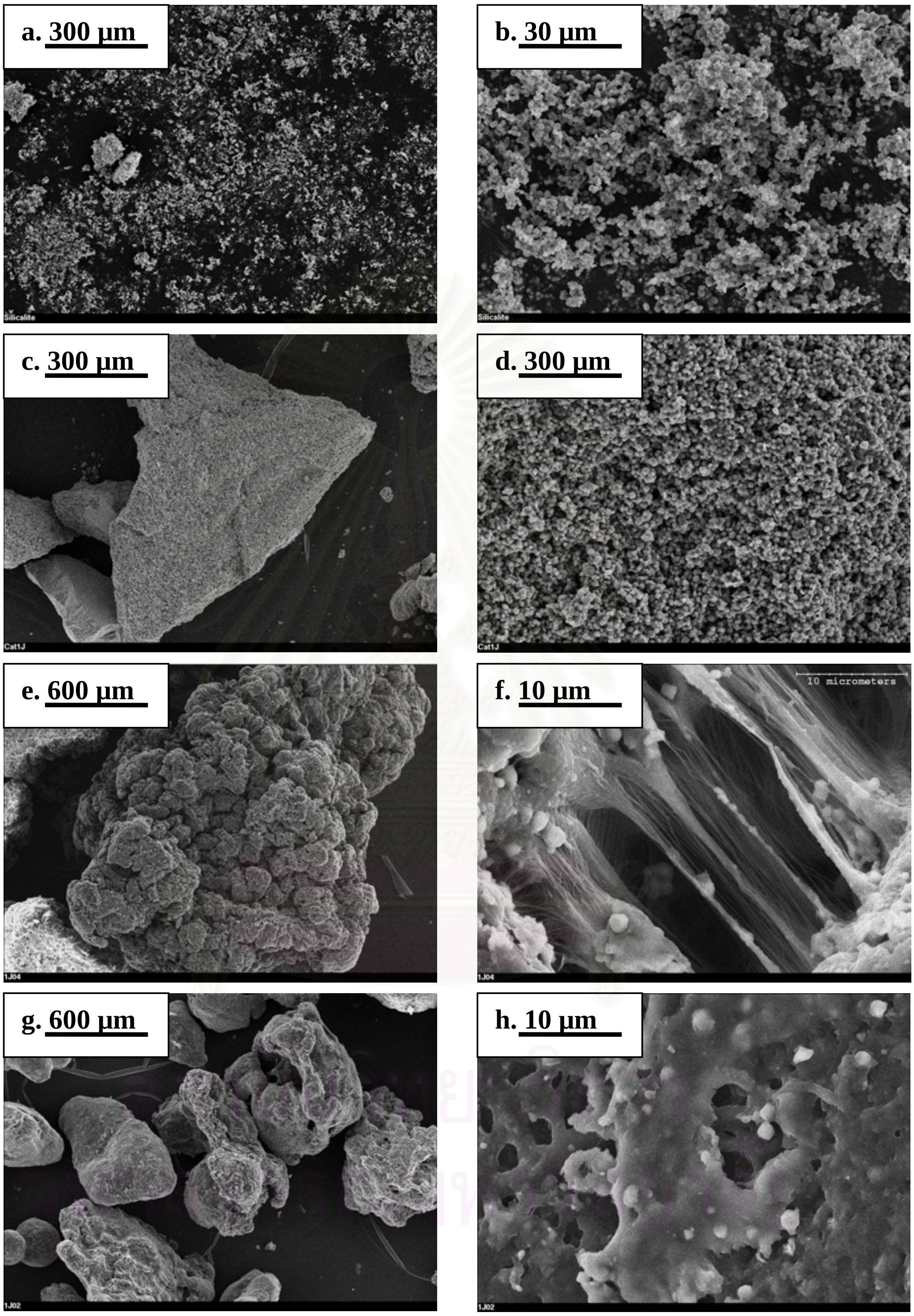

Figure A8. Scanning electron micrographs: (a,b) the S0.54 support, (c,d) CAT0.54, (e,f) the homopolymer produced with CAT0.54 at 70°C, and (g,h) the copolymer produced at 70°C

Table A3. Description of the polymerization runs and molar mass results with different pore diameters of mesoporous molecular sieve supports obtained from gas-phase polymerization results (Reaction conditions: ethylene pressure = 200 psi; amount of catalyst = 52 (±2) mg; amount of TIBA = 0.6mmol; polymerization time = 2h; and 3.2-3.4 mL of 1-hexene added at the beginning of each copolymerization run)

Catalyst	**Support Pore Diameter (nm)**	**Polymerization Temperature (°C)**		**Average Polymerization Activities [g PE/(g cat·h)]**	**Molar Mass**		
					Mw	**Mn**	**PD**
CAT0.54 (silicalite)	0.54	50		8	158522	69809	2.27
		70	Homopolymerization	6	170414	49104	3.47
			Copolymerization	56	52837	7423	7.12
		80		22	137602	59078	2.32
		90		5	129074	35526	3.63
		100		3	nd	nd	nd
CAT2.6-2	2.6	50		107	280481	108707	2.58
		70	Homopolymerization	210	224287	81849	2.74
			Copolymerization	324	102398	39750	2.6
		80		241	180177	74630	2.41
		90		206	172802	73882	2.34
		100		125	147618	59556	2.48

Table A.3. Continued

Catalyst	Support Pore Diameter (nm)	Polymerization Temperature (°C)		Average Polymerization Activities [g PE/(g cat·h)]	Molar Mass		
					Mw	Mn	PD
CAT5.8	5.8	50		47	242194	94287	2.57
		70	Homopolymerization	172	263119	104057	2.53
			Copolymerization	136	118960	38624	3.10
		80		294	196977	87161	2.26
		90		137	195118	84005	2.32
		100		152	150549	59105	2.55
CAT7.2	7.2	50		91	272091	110315	2.47
		70	Homopolymerization	200	241824	104348	2.32
			Copolymerization	34	102970	44881	2.29
		80		165	204976	83870	2.44
		90		92	195928	82861	2.36
		100		111	167000	65622	2.54

Table A.3. Continued

Catalyst	Support Pore Diameter (nm)	Polymerization Temperature (ºC)		Average Polymerization Activities [g PE/(g cat·h)]	Molar Mass		
					Mw	Mn	PD
CAT10	10	50		141	225037	94606	2.38
		70	Homopolymerization	186	205176	86740	2.37
			Copolymerization	0	nd	nd	nd
		80		208	192348	79033	2.43
		90		156	186597	76369	2.44
		100		98	160196	64946	2.47
CAT15	15	50		103	279110	111874	2.49
		70	Homopolymerization	181	234059	98598	2.37
			Copolymerization	6	164820	57987	2.80
		80		168	210238	85226	2.47
		90		111	195074	77107	2.53
		100		66	170341	67655	2.52

Table A.3. Continued

Catalyst	Support Pore Diameter (nm)	Polymerization Temperature (ºC)		Average Polymerization Activities [g PE/(g cat·h)]	Molar Mass		
					Mw	Mn	PD
CAT20	20	50		19	246222	82177	3.00
		70	Homopolymerization	37	206321	74203	2.78
			Copolymerization (0.5h)	63	101200	20190	5.00
			Copolymerization (1.0h)	64	99612	32682	3.05
			Copolymerization (2.0h)	22	103889	34279	3.03
		80		61	199329	63349	3.15
		90		55	169660	62230	2.73
		100		52	148677	54923	2.71
CAT25	25	50		nd	nd	nd	nd
		70	Homopolymerization	53	212478	82966	2.56
			Copolymerization	nd	nd	nd	nd
		80		60	169640	70242	2.41
		90		56	180174	67364	2.67
		100		nd	nd	nd	nd

Appendix B

Slurry-Phase Polymerization

In the Appendix B, the descriptions of supports and catalysts, polymerization reaction conditions, average polymerization activities, scanning electron micrographs, and the results of size exclusion microscopy for slurry-phase polymerization system were provided. The experimental details of all slurry-phase polymerizations with the different pore diameters of mesoporous molecular sieve supports conducted in this research summarized in Appendix B are listed below.

- The BET surface analysis for all the supports used in this system was shown in Table B1.
- The catalysts compositions calculated are described in Table B2.
- The structure of supports and catalysts as well as resulting polymer obtained from homopolymerization and copolymerization produced with the different pore diameter are shown in Figure B1-B7. Scanning electron micrograph results were carried out most of the samples. The parts of the morphology of polymers and copolymer produced at 70°C were chosen.
- All of the polymerization conditions, average polymerization activities, and the molar masses consisted of the number of average molecular weight (Mn), average molecular weight (Mw), and polydispersities (PD or Mw/Mn) with the different pore diameters of supports are summarized in Table B3. For the molar masses are based on relative calibration; the molar masses were measured all of samples. The molar mass values were the average values of at least two measurements.

Table B1. Description of supports used for slurry-phase experiments

Catalyst Designation	**Pore Diameter (nm)**	**Surface Area (m^2/g)**	**Pore Volume, cm^3/g**	**Calculated Pore Dia, nm†**
MMS2.5	(2.5)	(890)	(0.61)	(2.7)
MMS2.6*	2.6 (3.0)	1130 (1175)‡	1.3 (0.76)	4.6 (2.6)
MMS6.4	6.4	1240	1.5	4.8
MMS7.2	7.2	870	1.1	5.1
MMS12.5	12.5	296	1.2	12.6
MMS16	16	371	1.5	15.8
S0.54** (Silicalite)	0.54	435	--	--
S1*** (silica)	16	270	1.4	20.7

* MMS = mesoporous molecular sieves

** Silicalite

*** silica gel

‡ Values in brackets measured at UofA; other values from Laval.

Table B2. Description of catalysts used for slurry-phase experiments

Catalyst	Support pore diameter (nm)	Support	Amount of support used (g)	Amount of MAO Added (mL)	Zr Content		Al/Zr ratio
					mass %	mmol/g	
CATBA0.54	0.54	S0.54	2.00	7.7	0.33	0.037	170
CATBA2.5	2.5	MMS2.5	0.90	3.5	0.33	0.037	170
CATBA2.6	2.6	MMS2.6	0.71	2.7	0.33	0.037	170
CATBA6.4	6.4	MMS6.4	0.75	2.9	0.33	0.037	170
CATBA7.2	7.2	MMS7.2	0.82	3.2	0.33	0.027	170
CATBA12.5	12.5	MMS12.5	0.48	1.8	0.33	0.037	170
CATBA16	16	MMS16	0.37	1.4	0.33	0.037	170
CATBA-S1	16	S1	2.00	7.7	0.33	0.037	170

The catalyst compositions obtained from the MAO solution in toluene contained 2.598 mmol of Al per mL by assuming that 1 mmol of Al contained 0.058 g of MAO, and the molecular weight of catalyst (*n*-BuCp)$_2$ZrCl$_2$ was 404.53.

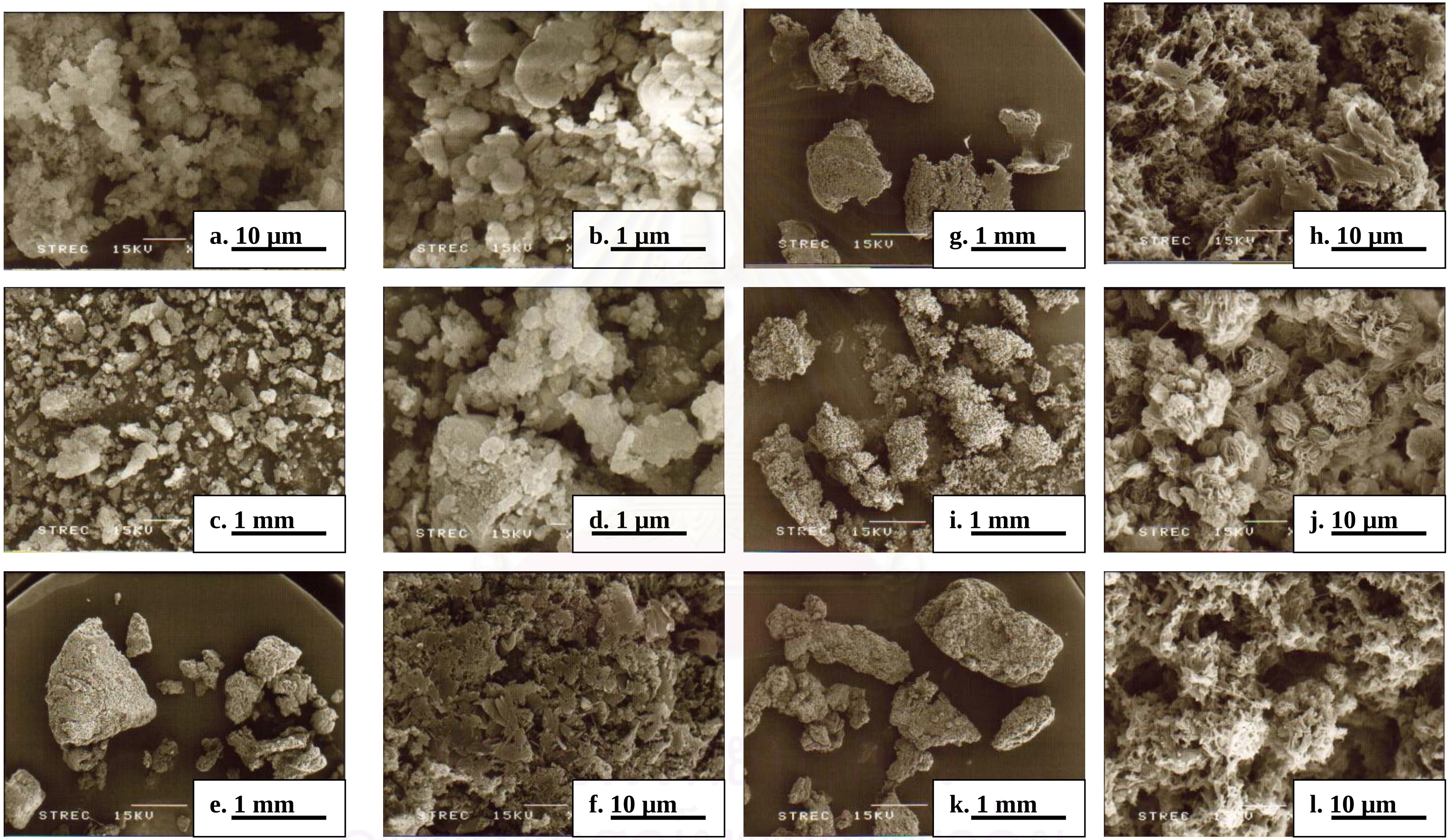

Figure B1. Scanning electron micrographs: (a,b) the MMS2.5 support, (c,d) CATBA2.5, (e,f) the homopolymer produced with CATBA2.5 at 70°C, and the copolymer produced at 70°C: (g,h) ethylene/1-hexene, (i,j) ethylene/1-octene, (k,l) ethylene/1-decene

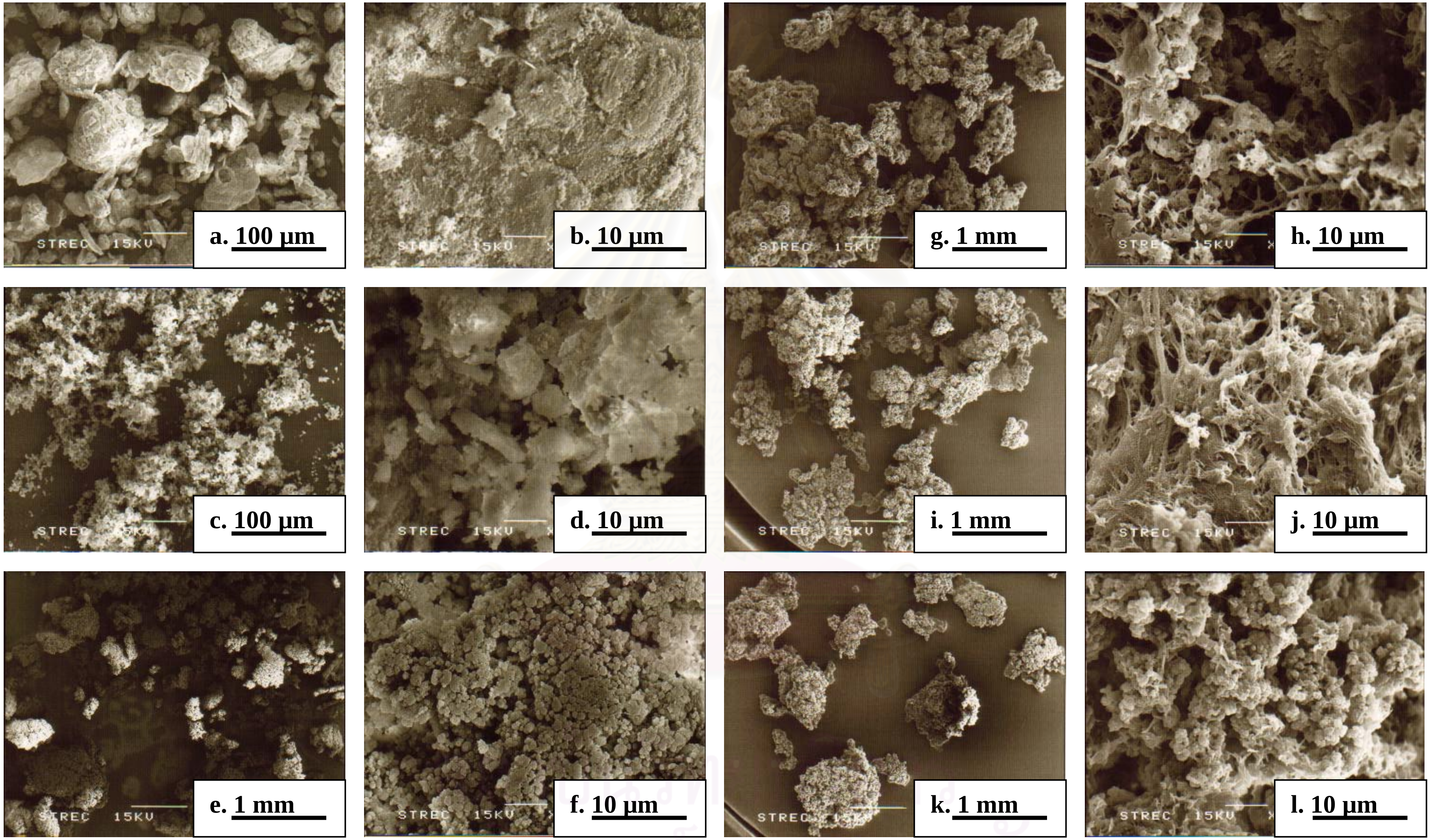

Figure B2. Scanning electron micrographs: (a,b) the MMS2.6 support, (c,d) CATBA2.6, (e,f) the homopolymer produced with CATBA2.6 at 70°C, and the copolymer produced at 70°C: (g,h) ethylene/1-hexene, (i,j) ethylene/1-octene, (k,l) ethylene/1-decene

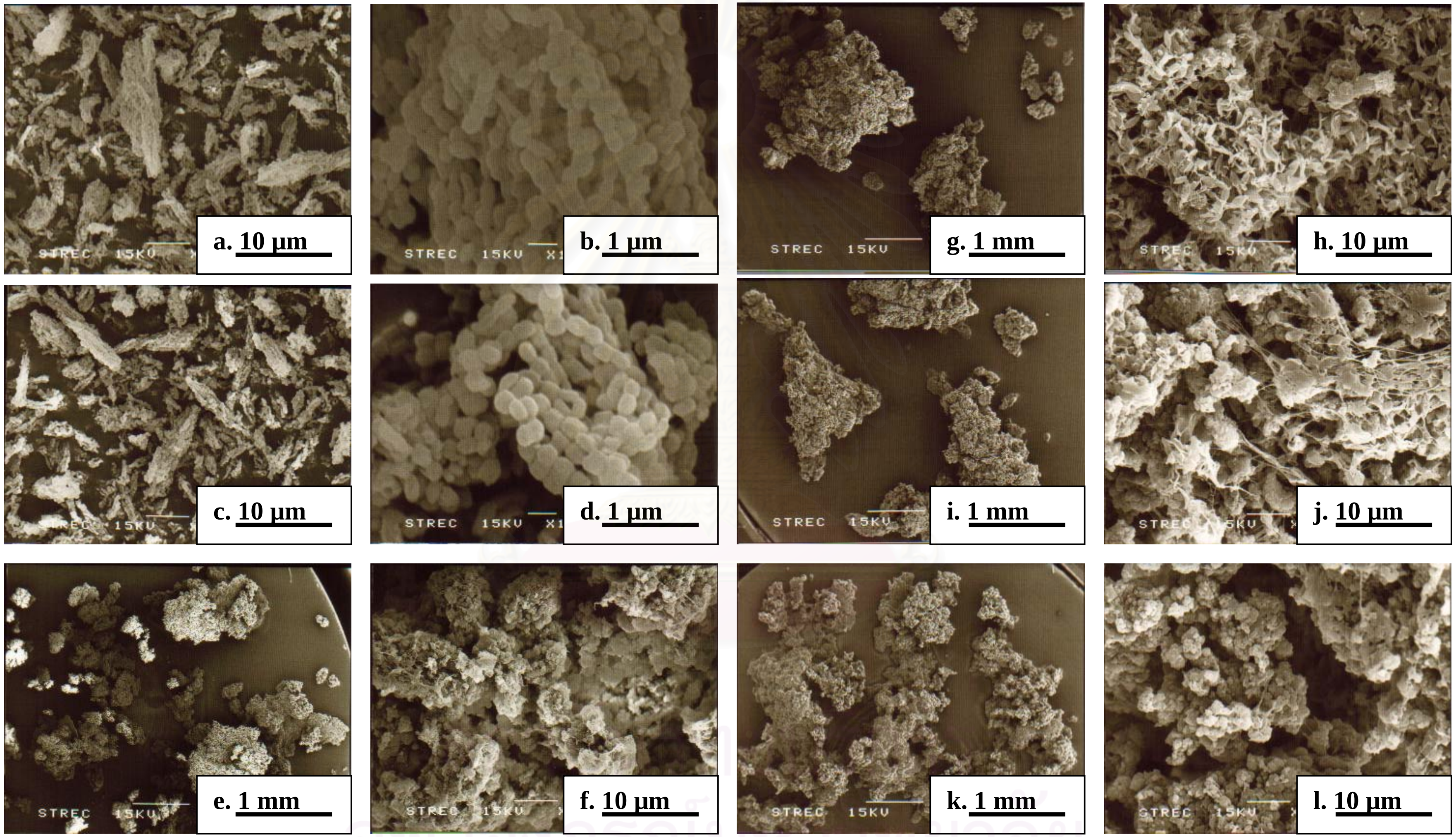

Figure B3. Scanning electron micrographs: (a,b) the MMS6.4 support, (c,d) CATBA6.4, (e,f) the homopolymer produced with CATBA6.4 at 70°C, and the copolymer produced at 70°C: (g,h) ethylene/1-hexene, (i,j) ethylene/1-octene, (k,l) ethylene/1-decene

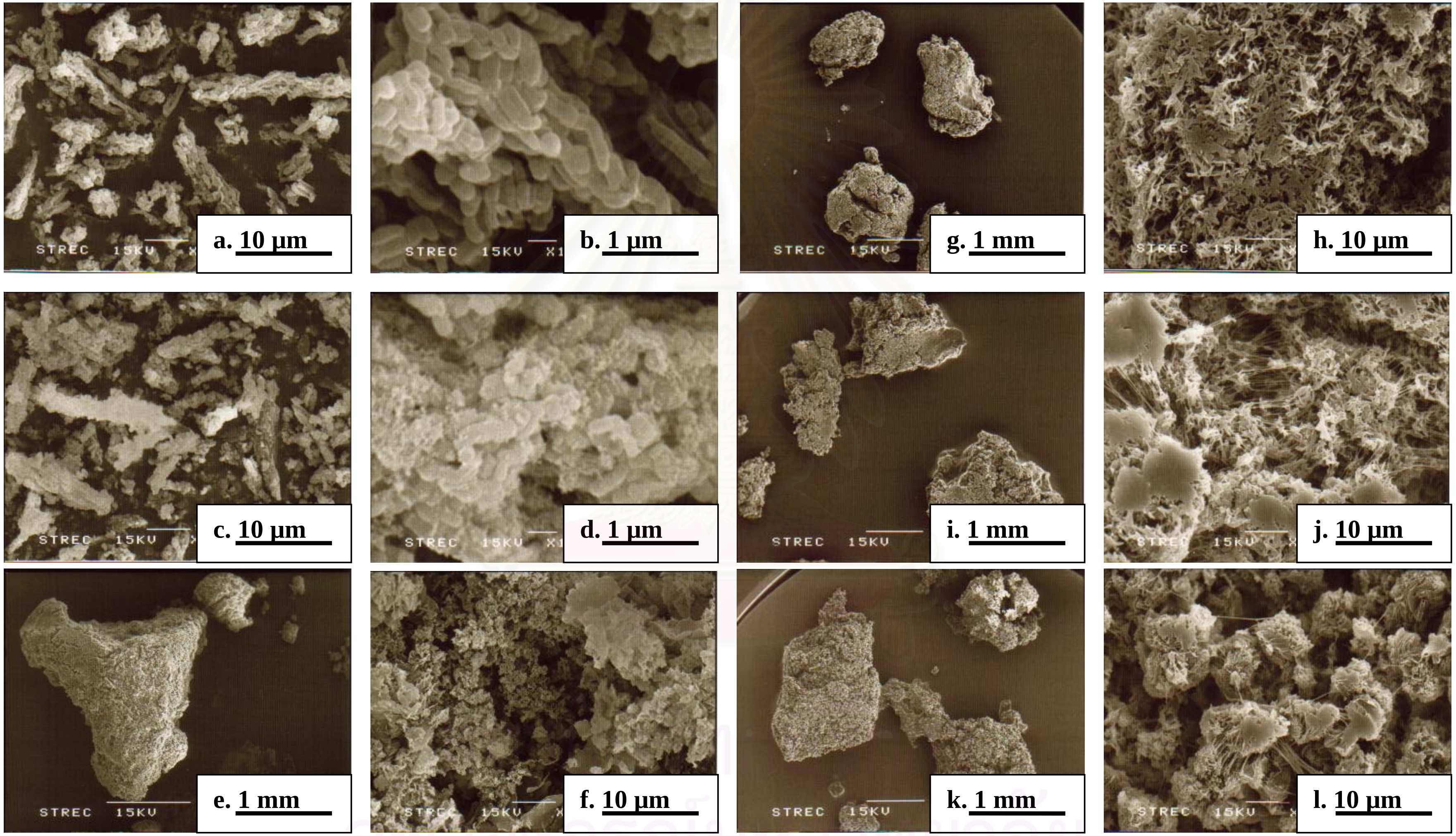

Figure B4. Scanning electron micrographs: (a,b) the MMS7.2 support, (c,d) CATBA7.2, (e,f) the homopolymer produced with CATBA7.2 at 70°C, and the copolymer produced at 70°C: (g,h) ethylene/1-hexene, (i,j) ethylene/1-octene, (k,l) ethylene/1-decene

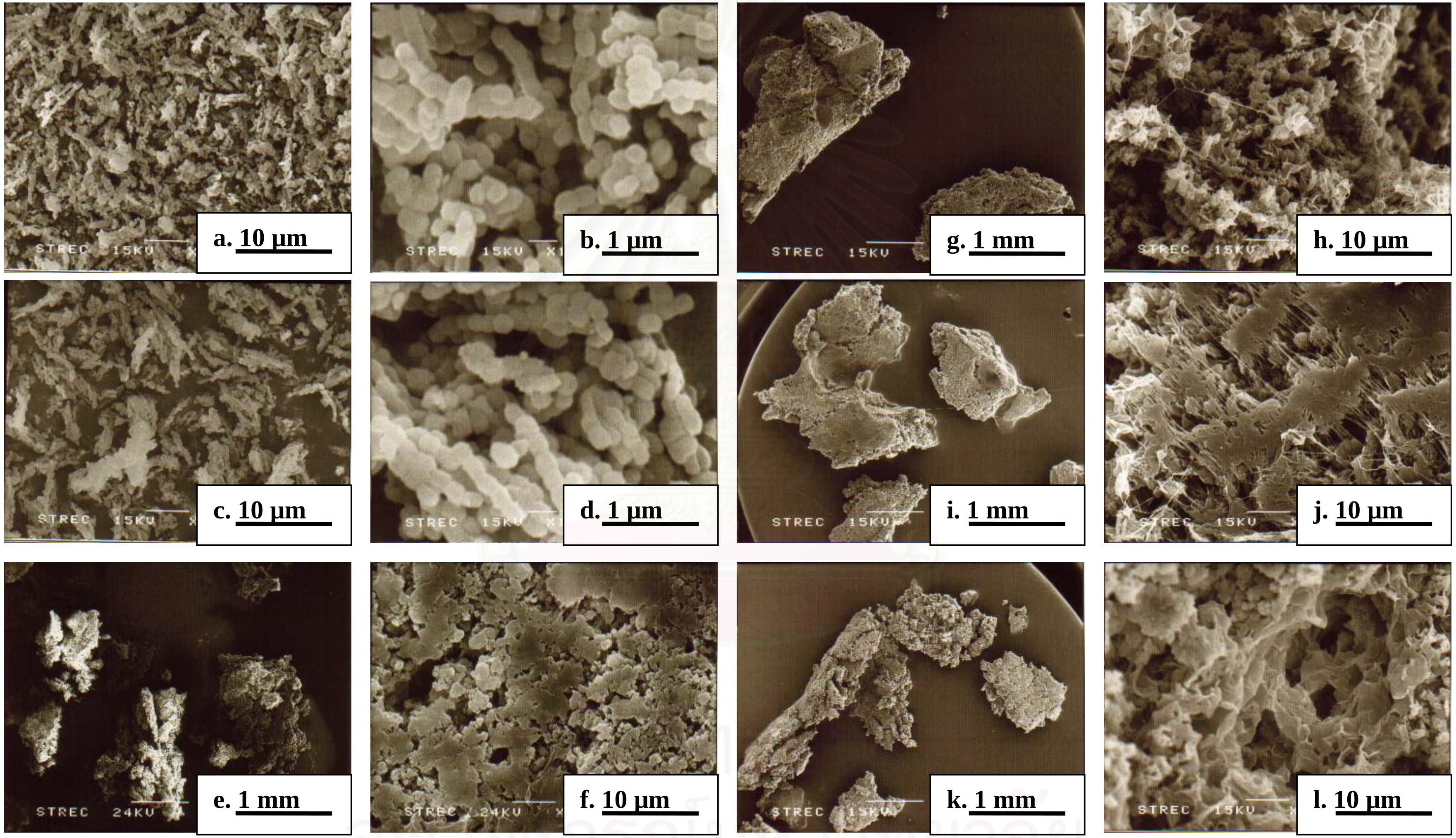

Figure B5. Scanning electron micrographs: (a,b) the MMS12.5 support, (c,d) CATBA12.5, (e,f) the homopolymer produced with CATBA12.5 at 70°C, and the copolymer produced at 70°C: (g,h) ethylene/1-hexene, (i,j) ethylene/1-octene, (k,l) ethylene/1-decene

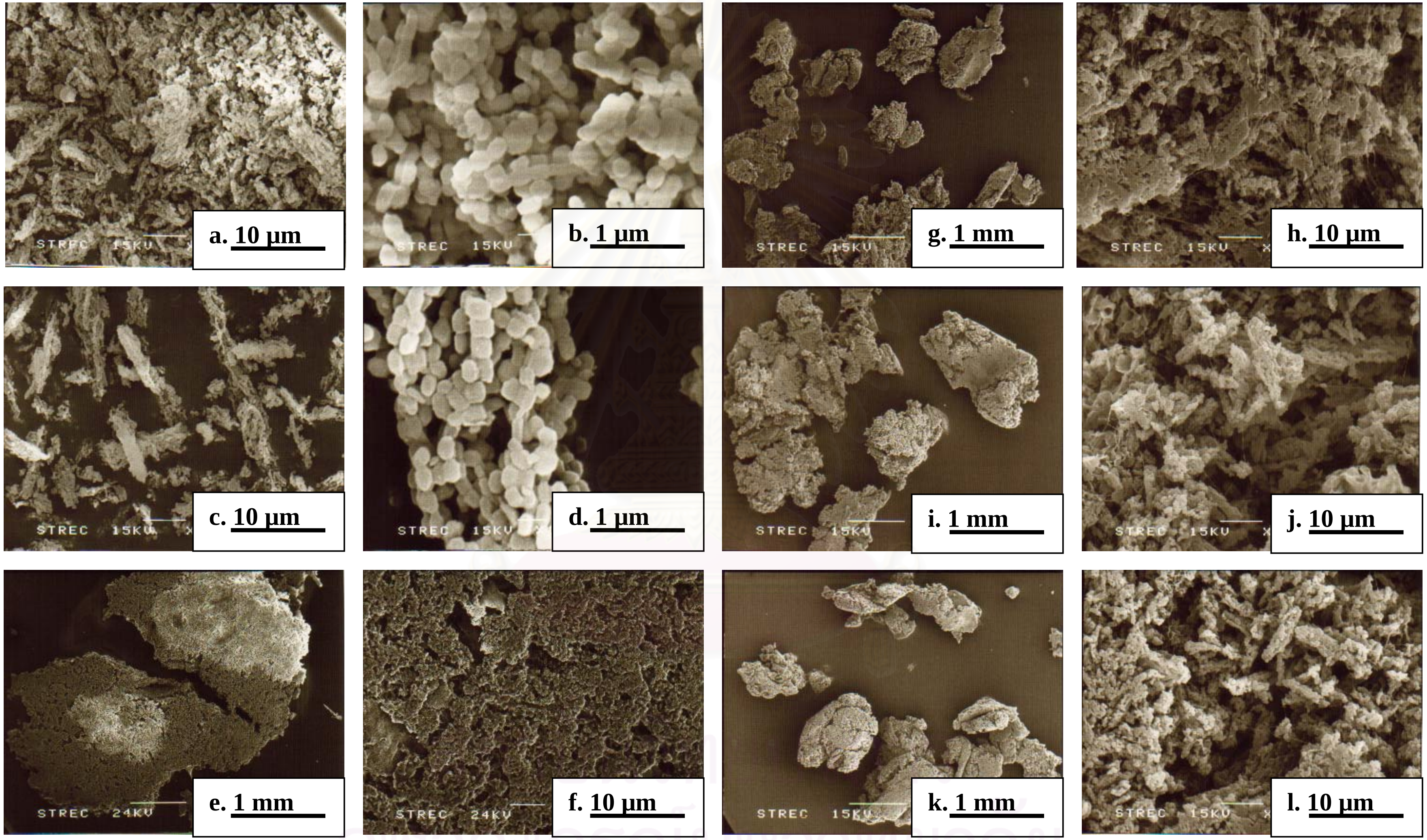

Figure B6. Scanning electron micrographs: (a,b) the MMS16 support, (c-f) CATBA16, (g,h) the homopolymer produced with CATBA16 at 70°C, and the copolymer produced at 70°C: (g,h) ethylene/1-hexene, (i,j) ethylene/1-octene, (k,l) ethylene/1-decene

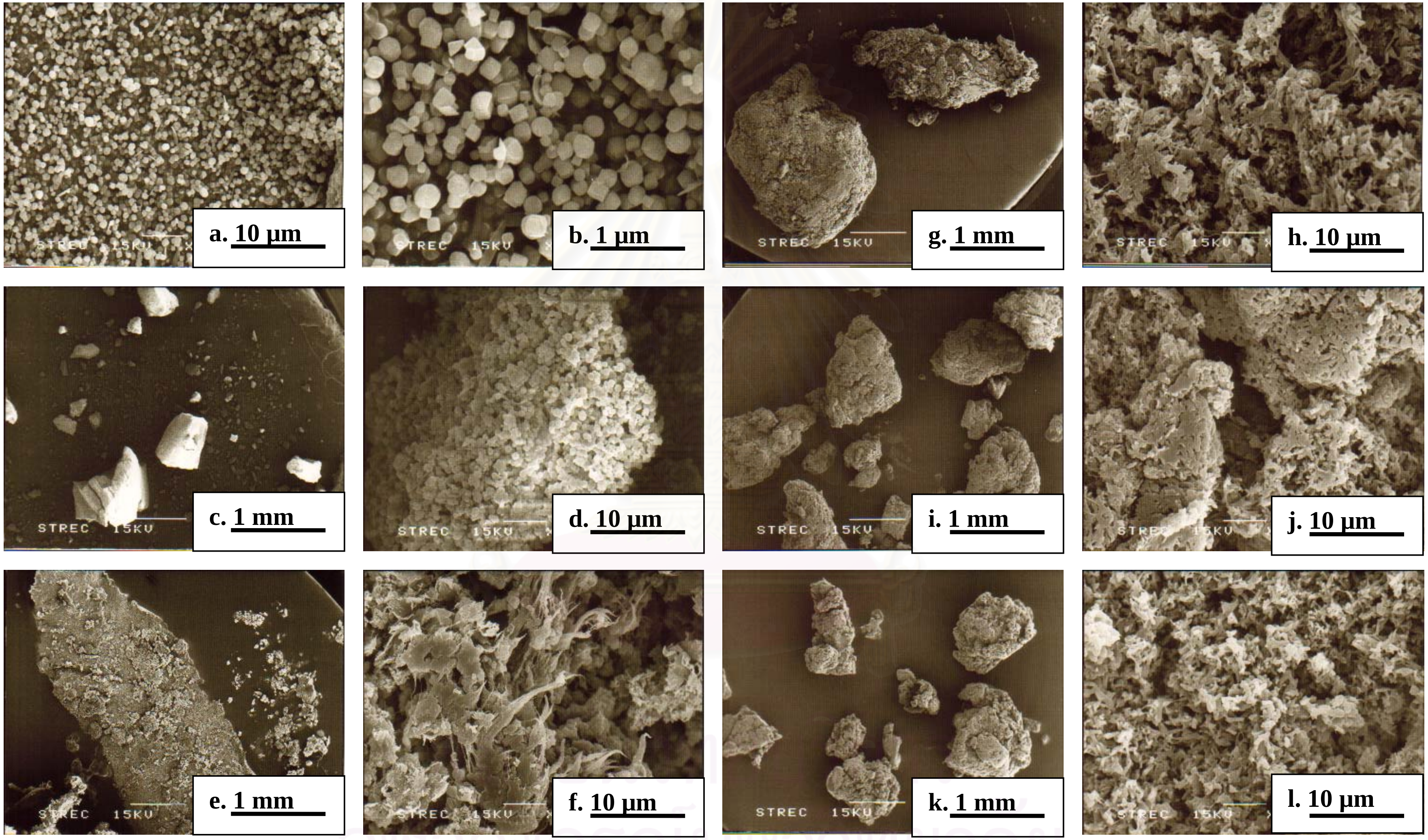

Figure B7. Scanning electron micrographs: (a,b) the S0.54 support, (c,d) CATBA0.54, (e,f) the homopolymer produced with CATBA0.54 at 70°C, and the copolymer produced at 70°C: (g,h) ethylene/1-hexene, (i,j) ethylene/1-octene, (k,l) ethylene/1-decene

Table B3. Description of the polymerization runs and molar mass results with different pore diameters of mesoporous molecular sieve supports obtained from slurry-phase polymerization results (Reaction conditions: ethylene pressure = 100 psi; amount of catalyst = 52 (±2) mg; amount of TIBA = 0.6mmol; polymerization time = 15 min; and 3 mL of comonomer added at the beginning of each copolymerization run)

Catalyst	**Support Pore Diameter (nm)**	**Polymerization Temperature (ºC)**		**Average Polymerization Activities [g PE/(g cat·h)]**	**Molar Mass**		
					Mw	**Mn**	**PD**
CATBA0.54 (silicalite)	0.54	50		78	182408	80943	2.25
		70	Homopolymerization	112	28694	115790	4.04
			Ethylene/1-Hexene	220	38477	15512	2.48
			Ethylene/1-Octene	190	45401	14177	3.20
			Ethylene/1-Decene	155	35840	14249	2.52
		80		125	84191	31066	2.71
CATBA2.5	2.5	50		170	238306	72150	3.30
		70	Homopolymerization	210	148841	43371	3.43
			Ethylene/1-Hexene	227	72261	27413	2.64
			Ethylene/1-Octene	230	75152	25931	2.90
			Ethylene/1-Decene	171	60711	24491	2.49
		80		142	74469	31969	2.33

Table B.3. Continued

Catalyst	Support Pore Diameter (nm)	Polymerization Temperature (ºC)		Average Polymerization Activities [g PE/(g cat·h)]	Molar Mass		
					Mw	Mn	PD
CATBA2.6	2.6	50		175	186769	82819	2.25
		70	Homopolymerization	230	152984	78366	1.95
			Ethylene/1-Hexene	246	111092	52390	2.12
			Ethylene/1-Octene	239	100096	43875	2.28
			Ethylene/1-Decene	175	97791	43998	2.22
		80		158	140494	68258	2.06
CATBA6.4	6.4	50		143	182060	93289	1.95
		70	Homopolymerization	155	150361	73351	2.05
			Ethylene/1-Hexene	221	125266	53598	2.34
			Ethylene/1-Octene	170	102767	45945	2.24
			Ethylene/1-Decene	152	103919	47860	2.17
		80		112	127026	63440	2.00

Table B.3. Continued

Catalyst	Support Pore Diameter (nm)	Polymerization Temperature (ºC)		Average Polymerization Activities [g PE/(g cat·h)]	Molar Mass		
					Mw	Mn	PD
CATBA7.2	7.2	50		74	192634	66283	2.90
		70	Homopolymerization	102	108605	35010	3.10
			Ethylene/1-Hexene	183	49292	18421	2.68
			Ethylene/1-Octene	166	60919	22273	2.74
			Ethylene/1-Decene	146	72537	28275	2.57
		80		93	76740	29255	2.62
CATBA12.5	12.5	50		62	254562	121210	2.10
		70	Homopolymerization	35	199225	89513	2.23
			Ethylene/1-Hexene	50	124506	41876	2.97
			Ethylene/1-Octene	43	136184	49489	2.77
			Ethylene/1-Decene	30	157557	61899	2.55
		80		27	156246	64151	2.44

Table B.3. Continued

Catalyst	Support Pore Diameter (nm)	Polymerization Temperature (ºC)		Average Polymerization Activities [g PE/(g cat·h)]	Molar Mass		
					Mw	Mn	PD
CATBA16	16	50		8	359500	140057	2.57
		70	Homopolymerization	12	254102	85839	2.96
			Ethylene/1-Hexene	40	147072	44913	3.27
			Ethylene/1-Octene	25	181443	43945	4.13
			Ethylene/1-Decene	10	176190	49709	3.54
		80		15	183835	79110	2.32

Appendix C

Procedure for Calculating SCB Distribution from TREF Analysis

The results of ATREF analysis are commonly presented as an elution curve of IR signal versus elution temperature. The TREF profile qualitatively represents the characteristics of crystallinity distribution of a LLDPE under investigation. It is of interest to translate the TREF profile into SCB distribution and to estimate average SCB content of the LLDPE. This is normally accomplished by using a calibration curve, which relates TREF elution temperature to short chain branch content.

Analytical TREF data consist essentially of a series of polymer masses (IR signal intensities) eluted at corresponding ascending elution temperatures. The TREF profile can be obtained simply by plotting IR signal against elution temperature, while SCB distribution can be obtained by transforming the elution temperatures using the TREF calibration curve in Figure C1 into SCB contents.

The integration with the corrected baseline and normalization of the SCB distribution were done numerically. It is proposed in this work to use expressions similar to molar mass distributions based on moments to calculate C_N and C_W in average short chain contents similar to average molar masses, i.e.

$$C_N = \sum AiCi / \sum Ai \qquad \textbf{-----(1)}$$

$$C_W = \sum AiC_i^2 / \sum AiCi \qquad \textbf{-----(2)}$$

Where A_i is the slice area of SCB distribution; and C_i is the corresponding SCB evaluated from the calibration curve. The ration of C_W to C_N can serve as an indicator of the broadness of short chain branch distribution.

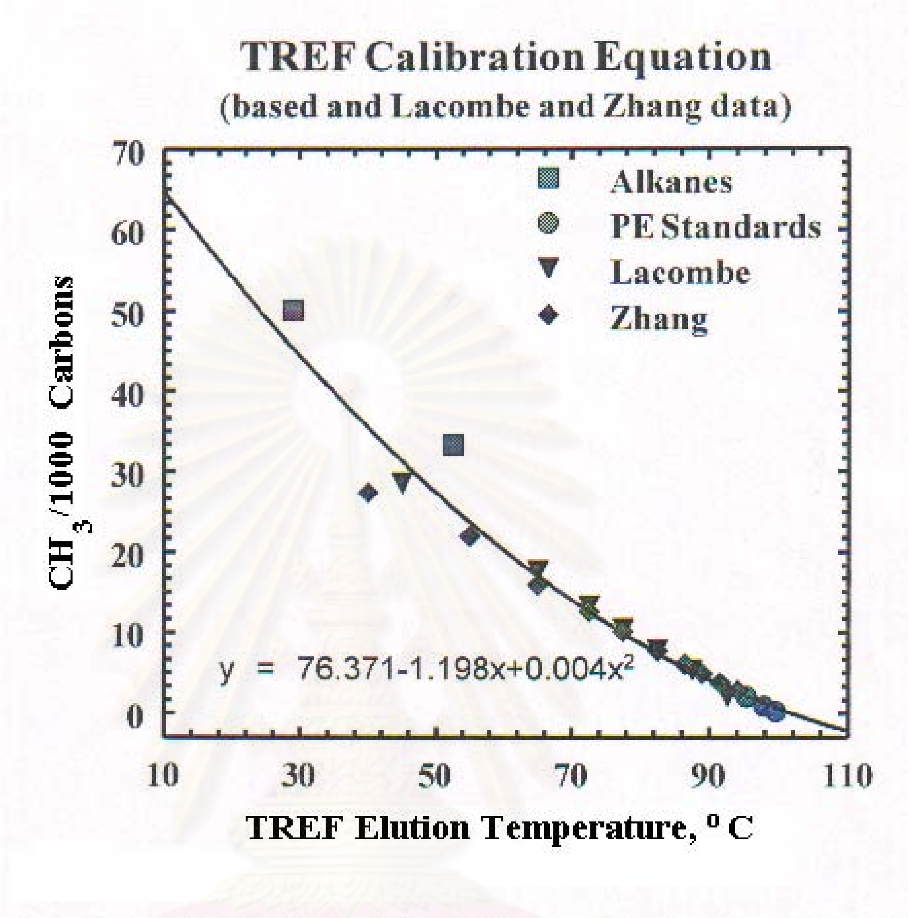

Figure C1. TREF calibration: short chain branch content as a function of elution temperature

All of the LLDPE samples obtained from gas-phase and slurry-phase polymerization were measured. The reproducibility of the Run 18 were chosen and shown in Figure C2. The run 8 shown in Figure C2 without removing the discontinuities were chosen to indicate that the multiple peak have very good in reproducibility.

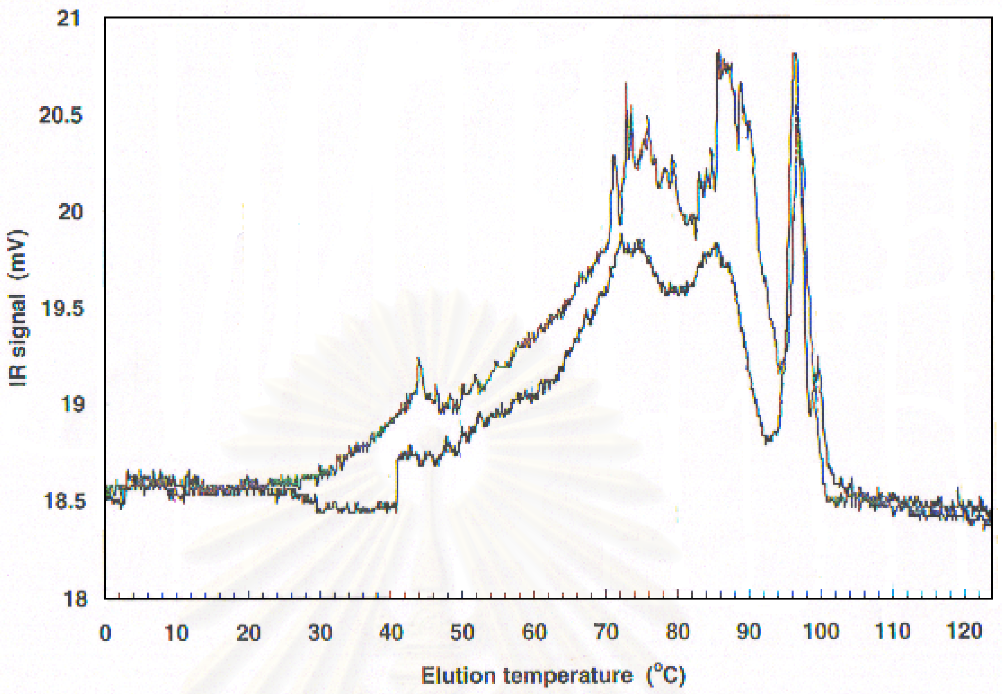

Figure C2. The reproducibility of TREF profiles for Run 18 (without removal the discontinuities)

VITA

Mr. Pornyoot Kumkaew was born in Bangkok, Thailand, on June 8, 1977. He received the degree of Bachelor of Engineering (Chemical Engineering) second-class honor from Rangsit University on May 1999. He continued in Doctoral degree of Engineering from the Department of Chemical Engineering, Chulalongkorn University on June 1999.

During his studying in Doctoral degree of Engineering, many activities were performed. At the beginning of his study, he had received the Royal Golden Jubilee Ph.D. research assistant fellowship from the Thailand Research Fund (TRF); this gave him the opportunity to carry out part of his Ph.D. research with his co-advisor, Prof. Dr. Sieghard E. Wanke, in Department of Chemical & Materials Engineering at the University of Alberta, Canada. In the second year of his study, he participated and presented some of his research results as a poster at the Bangkok International Conference on Heterogeneous Catalyst on the topic of “Effect of Pore Size on the Performance of Zirconocene Supported on Mesoporous Molecular Sieves during Ethylene Polymerization in Gas Phase”. A little later, he presented the poster paper on the occasion of the visit of Her Royal Highness Princess Maha Chakri Sirindhorn of Thailand to the University of Alberta on June 26, 2001. He found this very gratifying experience. On July and August 2002, he attended the Polymer Science and Technology Seminar and Nanocrystal, Catalyst, and Reaction Engineering Seminar established by Faculty of Science and Chemical Engineering at Chulalongkorn University, respectively, under Thailand Research Fund support. At the 52nd Canadian Chemical Engineering Conference, October 20-23, 2002, the oral presentation, based on his Ph.D. research, on the topic of ethylene/1-hexene copolymerization in the gas phase over supported (n-BuCp)$_2$ZrCl$_2$ catalyst was presented by Professor Sieghard E. Wanke. Finally, he also participated and presented his research in IUPAC Polymer Conference on the Mission and Challenges of Polymer Science and Technology (IUPAC-PC2002), December 2-5, 2002.

In addition, the version of his research has been accepted and/or submitted for three publications as described below.

(1) “Gas Phase Ethylene Polymerization Using Zirconocene Supported on Mesoporous Molecular Sieves” *Journal of Applied Polymer Science*, Vol. 87, 1161-1177 (2003).

(2) “Rates and Product Properties of Polyethylene Produced by Copolymerization of 1-Hexene and Ethylene in the Gas-Phase with (*n*-BuCp)$_2$ZrCl$_2$ on Supports with Different Pore Sizes” revised for publication in *Polymer*.

(3) “Slurry Ethylene Polymerization: Effect of Support Pore Size on Activity and Product Properties for (n-BuCp)2ZrCl2 Supported on MAO-Treated Mesoporous Silicas” submitted for publication in *Macromolecular Rapid Communications*.